Structural Volatility Modeling

DISSERTATION
of the University of St. Gallen,
School of Management,
Economics, Law, Social Sciences,
International Affairs and Computer Science,
to obtain the title of
Doctor of Philosophy in Economics and Finance

submitted by

Jeannine Polivka

from Basel (BS)

Supervisor:
Prof. Dr. Matthias R. Fengler

Co-Supervisor:
Prof. Dr. Luca Fanelli

Program Committee Member:
Prof. Dr. Francesco Audrino

Additional Member:
Prof. Dr. Lyudmila Grigoryeva

Acknowledgments

I would like to express my sincere gratitude to my supervisor Matthias Fengler for always providing valuable guidance, useful feedback and firm support for all my project endeavours – and for always having an open door for intense discussions of research matters. I would like to extend my thanks to Luca Fanelli for his continuing support, for always providing valuable comments on my projects and helpful strategical tips, and for giving me the opportunity to engage with the Bologna Econometrics group: Your questions pushed my projects further and the encouraging atmosphere was a psychological boost towards the end of my PhD.

I would also like to express my gratitude to Christian Brownlees for hosting me at UPF, for integrating me in all internal activities for Econometrics PhD students and for the lively discussions and the sincere feedback on my research ideas. I am indebted to the Mobi.Doc program of the University of St. Gallen for financial support of my research projects, and I thank the research committee for their assistance. Further thanks go to Lyudmila Grigoryeva for her helpful feedback on my job market paper and for agreeing to be my additional committee member and to Francesco Audrino for his valuable comments on my research proposal and seminar presentations in the course of my PhD.

In addition, I would like to thank my current and past colleagues at HSG and the Department of Mathematics and Statistics. I thoroughly enjoyed being part of the M+S and the Financial Econometrics group with its friendly and supportive atmosphere. Special thanks to Philipp for always being willing to discuss mathematical problems and for putting my theoretical set-up and analytical proofs through their paces. I also want to express my deepest appreciation to Ute for her proofreading assistance.

On a personal note, I would like to thank the swimming and running team at HSG – you were my social backbone, structured my week and gave me a new perspective of the hills and waters in and around St. Gallen. You have been inspiring and truly transformative company. Furthermore, I would like to express my deep gratitude to my friends who stuck and put up with me, especially through the last year of the PhD. Finally, I humbly thank my family and my partner: your love, encouragement and support gave me the necessary strength.

Summary

Multivariate volatility models provide insightful statistical descriptions of fluctuations in asset returns. However, as a drawback, they do not impart an intelligible interpretation of the shock system which drives returns. In contrast, structural models reflect the pertinent features of an economic system and provide an identified, interpretable shock system. Hence, they allow for spillover, counterfactual, business cycle and impulse response analyses. Applied to asset return systems and their second moments, they thus lend themselves to risk, asset management and financial stability investigations. This thesis, consisting of three complementary contributions, therefore innovatively combines volatility modeling with structural methods. While the empirical applications contribute to the socialization of macro-econometric concepts in financial econometrics, the contributions to identification theory are equally relevant to the structural VAR literature.

In the first paper (Fengler and Polivka, 2022a), we develop a structural multivariate GARCH model targeting the identification of shocks and volatility spillovers in a daily return system. In the spirit of the proxy-SVAR framework, we use external news-related data to identify the underlying shock system. Our identification strategy targets full identification. We obtain the entire shock system through a proxy-guided orthogonalization approach using Givens rotations. In an empirical application, we identify an equity, bond and currency shock and study the volatility spillovers implied by these shocks. Our analysis shows that symmetric spillover regimes are refutable.

The second paper (Fengler and Polivka, 2022b) makes three contributions to the volatility impulse response function (VIRF). First, we derive the law of the VIRF for MGARCH models of the BEKK type. Second, we present a structural embedding of the VIRF. Third, we show how to endow the VIRF with a causal interpretation. We illustrate the merits of a structural VIRF analysis by investigating the impacts of historical and out-of-sample shock scenarios on the U.S. equity, government bond and foreign exchange markets. Our findings suggest that it is vital to assess the statistical significance of VIRFs.

The third paper presents a framework to capture smoothly time-varying behavior in the impact of proxy-identified shocks. Through modification of the relevance condition, I obtain nonparametric structural estimates based on which I infer – targeting full identification – an optimal structural decomposition guaranteeing shock orthogonality. In an analysis of the dynamic impacts of financial and monetary policy uncertainty shocks on a structural MGARCH model of asset returns which are focal components of the green energy transition, the model delivers nuanced volatility spillover patterns. It indicates that it is crucial to account for time variation in structural transmission mechanisms for informed policy and stability analysis.

Zusammenfassung

Multivariate Volatilitätsmodelle liefern gute statistische Beschreibungen der Schwankungen von Renditen aber bieten keine verständliche Interpretation des Schocksystems, das die Renditen treibt. Fokussiert auf Modellschätzung und -fit scheitern sie an ökonomischen "Warum?" oder "Was-wäre-wenn?"-Fragen. Strukturelle Modelle hingegen spiegeln die statistischen Merkmale eines Systems wider und liefern ein identifiziertes, interpretierbares Schocksystem, das eine Analyse von Spillovereffekten, kontrafaktischen Schockereignissen, des Konjunkturzyklus und der Impulsantworten eines ökonomischen Systems ermöglicht. Angewendet auf Renditesysteme und deren zweite Momente eignen sie sich daher für Risiko- und Vermögensmanagements Anwendungen und finanzielle Stabilitätsanalysen. In dieser Dissertation, die in drei Beiträge gegliedert ist, kombiniere ich daher Modelle und Instrumente für die Analyse multivariater Volatilitätssysteme mit strukturellen Methoden. Während die empirischen Anwendungen zur Sozialisierung makroökonometrischer Methoden in der Finanzökonometrie beitragen, sind die theoretischen Beiträge zu Identifikationstechniken ebenso für die allgemeine strukturelle VAR-Literatur relevant.

In Fengler and Polivka (2022a) entwickeln wir ein strukturelles multivariates GARCH-Modell, das auf die Identifizierung von Schocks und Volatilitätsspillovers in einem täglichen Renditesystem abzielt. In Anlehnung an die Proxy-SVAR-Methode verwenden wir externe Nachrichtendaten, um das zugrunde liegende Schocksystem zu identifizieren. Unsere Strategie zielt auf eine vollständige Identifizierung ab. Wir erhalten das ganze System der Schocks durch ein proxy-geleitetes Orthogonalisierungsverfahren basierend auf Givens-Rotationen. In der empirischen Anwendung identifizieren wir einen Aktien-, Anleihen- und Währungsschock und untersuchen die Volatilitätsspillover durch diese Schocks. Unsere Analyse zeigt, dass symmetrische Spillover-Regimes nicht zutreffen.

Die zweite Abhandlung (Fengler and Polivka, 2022b) leistet drei Beiträge zu Volatilitätsimpulsantworten (VIRFs). Wir leiten die asymptotische Verteilung der VIRF für MGARCH-BEKK-Modelle her, stellen eine strukturelle Einbettung der VIRF vor und zeigen, wie man die VIRF mit einer kausalen Interpretation ausstattet. Wir illustrieren die Vorteile einer strukturellen VIRF-Analyse, indem wir die Auswirkungen von historischen und simulierten Schockszenarien auf die US-amerikanischen Aktien-, Staatsanleihen- und Devisenmärkte untersuchen. Unsere Ergebnisse zeigen, dass eine Betrachtung der statistischen Signifikanz von VIRFs essenziell ist für deren Auswertung.

Der dritte Beitrag stellt einen Modellierungsansatz für zeitliche Variationen in den Auswirkungen von Schocks, die via Proxys identifiziert wurden, vor. Durch Modifizierung der Relevanzbedingung erhalte ich nichtparametrische strukturelle Schätzer, auf deren Grundlage ich - mit dem Ziel einer vollständigen Identifizierung - eine optimale strukturelle Zerlegung ableiten kann, welche orthogonale Schocks garantiert. In einer Analyse der dynamischen Auswirkungen von finanz- und geldpolitischen Unsicherheitsschocks auf ein strukturelles MGARCH-Modell von Vermögensrenditen, welche zentral für die Energiewende sind, liefert das Modell nuancierte Volatilitäts-Spillover-Muster. Es zeigt, dass es für fundierte Politik- und Stabilitätsanalysen von entscheidender Bedeutung ist, die Zeitvariabilität in den Schockauswirkungen zu berücksichtigen.

Contents

List of Figures **viii**

List of Tables **x**

List of Abbreviations **xi**

1 Identifying structural shocks to volatility through a proxy-MGARCH model **1**

1.1 Introduction 3

1.2 Structural identification 6

1.2.1 Rotation invariance and identification problem 6

1.2.2 Identification by proxy 7

1.2.3 A general recurrence scheme for full identification 9

1.2.4 Estimation strategy 12

1.3 MGARCH model 17

1.4 An identified asset return system 18

1.4.1 Data 19

1.4.2 Structural model estimates 22

1.4.3 Volatility spillovers 27

1.5 Conclusion 29

Appendices **32**

1.A Rotation theory 32

1.B Illustrative example 33

1.C Implementation of recurrence scheme 34

1.D Tables 35

2 Structural volatility impulse response analysis **39**

2.1 Introduction 41

2.2 Volatility impulse response analysis 43

2.2.1 Modeling framework 43

2.2.2 Volatility impulse response functions 44

2.2.3 The VIRF in the BEKK(p, q) model 45

2.2.4 Asymptotic law of the VIRF 47

2.2.5 Structural VIRFs 48

2.2.6 Causality 49

2.3 Empirical Application 52

2.3.1 Structural volatility model 53

2.3.2 Structural volatility impulse response analysis 55

2.4 Conclusion 60

Appendices **67**

2.A Proofs 67

2.A.1 Notation and results from matrix algebra 67

2.A.2 Mathematical prerequisites for the VIRF 69

2.A.3 Asymptotic theory for VIRFs 71

2.A.4 Causality of the VIRF 74

3 Time-varying shock transmission in proxy-identified volatility models **75**

3.1 Introduction 77

3.2 Time-varying shock transmission 81

3.2.1 Modeling framework and identification 81

3.2.2 Identification by proxy 84

3.2.3 Dynamic structural shock transmission 86

3.3 Empirical Application 90

3.3.1 Data 90

3.3.2 Structural model 96

3.4 Conclusion 118

Appendices **130**

3.A Mathematical prerequisites 130

3.B Choice of proxy variables 131

3.B.1 Narrative corroboration 131

3.B.2 MPU versus MPS 135

3.B.3 Alternative proxy choices 135

3.C Robustness of estimation 137

References **151**

List of Figures

1.1 Demeaned daily log returns 19

1.2 ARMA filtered and standardized U.S. stock index and bond sentiment . . . 21

1.3 Volatility reception of the structural MGARCH model 30

1.4 Volatility transmission of the structural MGARCH model 31

2.1 Demeaned daily log returns 54

2.2 Historical VIRFs in response to the Dotcom bubble burst 62

2.3 Historical VIRFs in response to the Greenspan testimony 63

2.4 Historical VIRFs in response to the EU debt crisis 64

2.5 Scenario VIRFs in response to equity tail shocks 65

2.6 Scenario VIRFs in response to bond tail shocks 66

3.1 Demeaned daily log returns 91

3.2 Time series of the instruments 97

3.3 Covariance of the reduced form residual and instrument Z_1 120

3.4 Covariance of reduced form residual and instrument Z_2 121

3.5 Monetary policy divergence between the U.S. and the Eurozone 122

3.6 Time-varying rotation under the Procrustes approach 123

3.7 Time-varying rotation under the Givens approach 124

3.8 Time-varying shock transformation of a unit financial uncertainty shock . . 125

3.9 Time-varying shock transformation of a unit monetary policy uncertainty shock 126

3.10 Time-varying shock transformation of a unit monetary policy uncertainty shock (second view) 127

3.11 Volatility reception in the constant and time-varying proxy-MGARCH model under the Procrustes approach 128

3.12 Volatility reception in the constant and time-varying proxy-MGARCH model under the Givens approach 129

3.13 Autocorrelation of $\hat{u}_{1t}Z_{1t}$ and $\hat{u}_{2t}Z_{2t}$ 146

3.14 Estimators of β for different kernels 146

3.15 Time series of relevance parameters 147

3.16 Residuals of the nonparametric estimation of the covariance of $\hat{u}_t$ and Z_1t and their sample ACFs 148

3.17 Residuals of the nonparametric estimation of the covariance of $\hat{u}_t$ and Z_{2t} and their sample ACFs 149

3.18 Residuals of the nonparametric estimation of the covariance of $\hat{u}_t$ and Z_{2t} and their sample ACFs when removing outliers 150

List of Tables

1.1 Descriptive statistics of the log return system 20

1.2 Descriptive statistics of the standardized and filtered TRMI indices 21

1.3 QML parameter estimates of the unrestricted BEKK model 23

1.4 Estimation results of the structural MGARCH model 25

1.5 Descriptive statistics of the inferred structural shocks 26

1.6 Narrative corroboration of the equity shock 36

1.7 Narrative corroboration of the bond shock 37

1.8 Narrative corroboration of the currency shock 38

2.1 Estimation results of the structural MGARCH model 55

2.2 Structural shock vectors selected for the historical VIRF analysis with corresponding returns 56

3.1 Descriptive statistics of the log return system 92

3.2 Descriptive statistics of the standardized and filtered proxy variables 98

3.3 Quasi maximum likelihood (QML) parameter estimates of the unrestricted BEKK model 101

3.4 Estimation results of the constant structural MGARCH model using the proxy-guided Procrustes approach 103

3.5 Estimation results of the constant structural MGARCH model using the proxy-guided Givens approach 104

3.6 Long-run variance decomposition 105

3.7 Descriptive statistics of the inferred structural shocks under the Procrustes approach 106

3.8 Descriptive statistics of the inferred structural shocks under the Givens approach . . . 107

3.9 Correlations of the inferred structural shocks under the Givens approach . . 131

3.10 Narrative corroboration of the financial uncertainty shock 132

3.11 Narrative corroboration of the monetary policy shock 133

3.12 Narrative corroboration of the remainder shock 134

3.13 Estimation results of the constant structural MGARCH model identified using the MPU 136

3.14 Correlations of the inferred structural shocks identified using the MPU . . . 137

3.15 Estimation results of the constant structural MGARCH model identified using the MPU under the Givens approach 138

3.16 Correlations of the inferred structural shocks identified using the MPU under the Givens approach 139

3.17 Estimation results of the constant structural MGARCH model using the MPS140

3.18 Correlations of the inferred structural shocks identified using the MPS . . . 141

3.19 Estimation results of the constant structural MGARCH model using the MPS under the Givens approach 142

3.20 Correlations of the inferred structural shocks using the MPS under the Givens approach 143

3.21 Estimation results of the constant structural MGARCH model identified using EPU 144

3.22 Estimation results of the constant structural MGARCH model identified using GPR 145

3.23 Estimation results of the constant structural MGARCH model identified using gold 145

3.24 Estimation results of the constant structural MGARCH model when removing outliers 147

List of Abbreviations

ARMA	autoregressive moving average
BEKK	Baba, Engle, Kraft and Kroner
CBOE VIX	Chicago Board Options Exchange Volatility Index
CLT	central limit theorem
DCC	dynamic conditional correlation
ECB	European Central Bank
EPU	economic policy uncertainty
EUR	Euro
Fed	Federal Reserve
FEVD	forecast error variance decomposition
FFR	federal funds rate
FOMC	Federal Open Market Committee
FX	foreign exchange
GARCH	generalized autoregressive conditional heteroscedasticity
GFC	global financial crisis
GIRF	generalized IRF
GPR	geopolitical risk
iid	independent and identically distributed
IRF	impulse response function
LIBOR	London Interbank Offered Rate
LSAP	large-scale asset purchase program
MEP	Maturity Extension Program
MGARCH	multivariate generalized autoregressive conditional heteroscedasticity
MPS	monetary policy shocks
MPU	monetary policy uncertainty

MVM	multivariate volatility model
NASDAQ	National Association of Securities Dealers Automated Quotations
NYSE	New York Stock Exchange
QML	quasi maximum likelihood
QMLE	quasi maximum likelihood estimation
SUTVA	stable unit treatment value assumption
sVAR	structural VAR
SWN	strict white noise
TRMI	Thomson Reuters MarketPsych Indices
TVC	time-varying coefficient
TVP	time-varying parameter
USD	United States Dollar
USD Index	Finex U.S. Dollar Index
VAR	vector autoregressive
VARMA	vector ARMA
VEC	vectorized
VIRF	volatility impulse response function
VIX	Volatility Index
VMA	vector moving average
WLLN	weak law of large numbers
WN	white noise

Chapter 1

Identifying structural shocks to volatility through a proxy-MGARCH model*

Matthias R. Fengler†, Jeannine Polivka‡

*We are grateful for financial support by the Swiss National Science Foundation (SNF Grant No: 176684, Project "Structural Models of Volatility"). For constructive comments on previous versions of this article, the authors thank the conference participants of the NBER-NSF Time Series Conference, SoFiE, the 14th Annual Risk Management Conference of NUS RMI and the Conference of the Swiss Society of Economics and Statistics (SSES) 2021 and the research seminar participants of TU Dresden, University of Sussex, UCL and University of Bologna.

†School of Economics and Political Science, Department of Economics, University of St. Gallen, Bodanstrasse 6, 9000 St. Gallen, Switzerland. Email: matthias.fengler@unisg.ch.

‡School of Economics and Political Science, Department of Economics, University of St. Gallen, Bodanstrasse 6, 9000 St. Gallen, Switzerland. Email: jeannine.polivka@unisg.ch.

Abstract

We extend the classical multivariate GARCH (MGARCH) specification for volatility modeling by developing a structural MGARCH model targeting identification of shocks and volatility spillovers in a speculative return system of daily frequency. Similarly to the proxy-SVAR framework, we work with auxiliary proxy variables constructed from news-related measures to identify the underlying shock system. Our identification strategy targets full identification. We estimate the underlying structural rotation matrix by means of Givens rotations, which ensures orthogonality of the resulting shocks. In an empirical application, we identify an equity, bond and currency shock. We study the volatility spillovers implied by these labeled structural shocks. Our analysis shows that symmetric spillover regimes are rejected.

Keywords: Givens rotations, identification, news-based measures, proxy-MGARCH, shock labeling, structural innovations, volatility spillovers

JEL: C32, C51, C58, G10

"Knowing the main source of the decline in equity prices (and financial assets in general) may help policymakers understand its persistence and evaluate the policy response."
ECB Economic Bulletin, Issue 4/2020.

1.1 Introduction

A primary objective of multivariate volatility models is accurately describing the stylized facts of asset returns and their second-order moment dynamics. Much effort has therefore been devoted to precisely capturing the salient features of financial returns, such as fat tails, leverage effects and time-varying cross-asset dependencies (Andersen et al., 2009; Bauwens et al., 2012). While their widespread use is a vivid testimony to their success, extant multivariate volatility models do little in terms of offering an intelligible interpretation of the shock system which drives asset returns: they are merely reduced form models. This stands in sharp contrast to macroeconomics which has seen the development of structural models alongside reduced form models (Taylor and Uhlig, 2016). Besides reflecting the pertinent features of the modeled economic system, structural models at the same time identify the shock system. As a key advantage, they allow for counterfactual policy and business cycle analysis and an economic interpretation of shocks. In the extant literature on multivariate volatility models such a modeling framework is currently missing.

In this work, we make a first step towards extending reduced form multivariate volatility models of the GARCH form (MGARCH) to structural models in the macroeconometric sense. We achieve this goal by estimating a time-invariant rotation matrix, which transforms the vector of uncorrelated structural shocks into a correlated mixture of standardized reduced-form errors. The latter are subsequently multiplied with the principal matrix square root of the the time-varying covariance matrix and drive the speculative asset return system. The approach identifies the structural shocks because in the MGARCH model the multivariate variance process is fully identified and the estimation of the rotation matrix occurs conditionally on the initial choice of the matrix square root of the covariance matrix process. Thus, the set of structural parameters of interest are not the dynamic model parameters but the rotation matrix.

Necessarily, the estimation of the structural rotation requires identifying restrictions. While in the macroeconometric literature economic theory has furnished a valuable resource for identifying assumptions, it offers little guidance on establishing identifying restrictions in high-frequent speculative asset return systems. Indeed, the interconnectedness and fast-paced nature of financial markets seem to rule out the classical repertoire of identifying restrictions used in the macroeconomic SVAR literature (see Amisano and Giannini (2012) and Kilian and Lütkepohl (2017) for overviews) such as short- and long-run restrictions,

sign restrictions and exclusion or ordering restrictions imposed on the reduced form model.

For this reason, we follow ideas developed in the narrative identification approach of Romer and Romer (2010) and Mertens and Ravn (2013) and Stock and Watson (2012, 2016, 2018) and exploit information ingrained in external fundamental data to identify our shocks. As regards multivariate volatility models, we argue that the increasing availability of narrative records and news data at high frequency offers an untapped potential for proxy-based identification of reduced form volatility models. Our identification strategy allows for full identification of the rotation angles of the structural rotation by means of a general recurrence scheme using Givens rotations, which ensures orthogonality of the identified shocks. As a result, we obtain a structural decomposition of the multivariate volatility system and labeled structural shocks.

Using news data for identification in volatility models appears to be very natural given the notion of a link between information flows and volatility has been present in volatility modeling since its beginnings: consider the mixture of distributions hypothesis of Clark (1973), the news impact curve (Engle and Ng, 1993) and the reaction of financial markets to information at high frequency (Groß-Klußmann and Hautsch, 2011; Bollerslev et al., 2018; Boudoukh et al., 2018). Our identification strategy builds on the understanding that news items can represent novel public fundamental information which drives returns and volatility when prices respond to it.

Naturally, we are not the first to address identification in model specifications with heteroscedasticity. The class of VAR models with stochastic volatility initially suggested by Primiceri (2005) is however barely attractive for standard applications in empirical finance because daily return series typically feature large time dimensions and their (co)variances are assumed to be stationary. Moreover, heteroscedastic SVARs commonly deal with a different identification problem. For example, the identification by heteroscedasticity approach pioneered by Rigobon (2003) and further explored by Lanne et al. (2010), Weber (2010) and Lütkepohl and Schlaak (2021) assumes (conditionally) heteroscedastic structural shocks to infer a structural representation focusing on the dynamics of the mean equation with constant impact effects of structural shocks. In contrast, our identification approach acknowledges that for the purpose of asset return modeling, it is desirable to allow for complex dynamics in the covariance generating mechanisms of the reduced form innovations. By modeling the conditional covariance process of the reduced form errors by an MGARCH model while assuming white noise structural shocks, we permit such flexibility.

The identification problem in this context consists of finding a structural decomposition of the conditional covariance process to recover the structural shocks driving the multivariate volatility model. Hafner et al. (2022) tackle this in the tradition of independent component analysis which exploits the fact that under independence of the structural components at most one component can be Gaussian. However, statistical identification approaches do not necessarily deliver structural shocks which are economically meaningful. In contrast, our identification scheme delivers readily interpretable labeled shocks.

In our empirical application, we study a system of speculative asset returns of core interest to the U.S. economy: the S&P 500, the yield of the U.S. constant maturity 10 year treasury note and a USD index. As proxy variables, we use the Thomson Reuters news sentiment indicators of the U.S. stock and the U.S. bond market which allows us to uncover a fully identified daily asset return system, driven by an equity shock, a bond shock and a currency shock. To further corroborate these labels, we make the additional effort to trace the most extreme shock observations back to major financial and economic events. We find evidence that the volatility spillovers are clearly non-symmetric, which invalidates spectral decompositions, and change considerably over time and with the local and global economic state. For example, we discover that the share of impact of the equity shock on the S&P 500 returns has diminished from 1998 to 2012 – a trend starting long before the financial crisis of 2008 – with impact shifting to the treasury yield returns instead. This finding complements a strand of literature investigating the link between fixed income and equity markets (Rigobon and Sack, 2003; Ehrmann et al., 2011).

The remainder of the paper is structured as follows. In Section 1.2, we present the structural identification strategy using proxy variables. Section 1.3 lays out the MGARCH estimation underlying the identification. The results of the empirical application of our model are provided in Section 1.4. Section 1.5 concludes. The Appendix gives additional details on rotation theory and the recurrence scheme for identification.

1.2 Structural identification

1.2.1 Rotation invariance and identification problem

We consider the system of n speculative (log) returns given by

$$r_t = \mu + \varepsilon_t \quad (t \in I := \{1, \ldots, T\}) \tag{1.1}$$

where we set $\mu = 0$, as our focus is on volatility spillovers rather than mean dynamics. The n-dimensional reduced-form innovation vector ε_t satisfies

$$\begin{aligned} \mathrm{E}[\varepsilon_t | \mathcal{F}_{t-1}] &= 0 \\ \mathrm{E}[\varepsilon_t \varepsilon_t^\top | \mathcal{F}_{t-1}] &= H_t \ , \end{aligned} \tag{1.2}$$

where $\mathcal{F}_t$ is the σ-algebra generated by the returns up to and including time t. The conditional covariance matrix H_t is assumed to be positive definite and symmetric with probability one and can be allowed to display any MGARCH or DCC type dynamics.

The statistical innovations ε_t do not bear an economic interpretation. To endow the model with a structural meaning, let ε_t be generated according to

$$\varepsilon_t | \mathcal{F}_{t-1} \sim Q_t \xi_t \ , \tag{1.3}$$

where $(\xi_t)_{t \in I}$ is an n-dimensional vector of structural shocks with $\mathrm{E}[\xi_t] = 0$ and $\mathrm{E}[\xi_t \xi_t^\top] = I_n$, the n-dimensional identity matrix. Q_t denotes an a priori unknown structural matrix decomposition of H_t, which satisfies $Q_t Q_t^\top = H_t$, and represents the transmission mechanism which translates the structural shock ξ_t into the observable reduced-form innovation ε_t. For identification we assume that Q_t is positive definitive.[4] It is well-known that this matrix decomposition is unique up to an orthogonal transformation (Horn and Johnson, 2012, Theorem 7.3.11). Thus, if we can identify this transformation, we can determine the structural matrix decomposition underlying the asset return system, even when Q_t is time-varying. To see the identification problem more clearly, let $\tilde{Q}_t$ be any matrix decomposition such that $H_t = \tilde{Q}_t \tilde{Q}_t^\top$. One obtains another observationally equivalent decomposition by setting

$$H_t = \tilde{Q}_t \tilde{Q}_t^\top = \tilde{Q}_t R R^\top \tilde{Q}_t^\top = (\tilde{Q}_t R)(\tilde{Q}_t R)^\top \ , \tag{1.4}$$

[4] By $(-Q_t)\,(-Q_t)^\top = H_t$, Q_t could be taken to be negative definite, too.

where R is a real $(n \times n)$ rotation matrix satisfying

$$\begin{aligned} R^\top R = RR^\top = I_n \qquad & \text{(orthogonality)} \\ \det(R) = +1 \qquad & \text{(proper rotation).} \end{aligned} \tag{1.5}$$

Given an initial decomposition $\tilde{Q}_t$, identification of the true structural matrix decomposition Q_t amounts to identifying the unique rotation $\tilde{R}$ such that $\tilde{Q}_t\tilde{R} = Q_t$. The structural model parameters are thus given by the rotation matrix. Formulating identification problems in terms of rotations has become increasingly popular in recent years, especially in Bayesian frameworks (Giacomini et al., 2021; Arias et al., 2021) but also in frequentist models (Fisher and Huh, 2019; Hafner et al., 2022).
Because of non-identification, the choice of the matrix decomposition is often determined by an ad-hoc decision. For instance, popular choices are the principal square root, which is obtained from an eigenvalue decomposition of H_t, or the Cholesky factorization of H_t. While symmetric volatility spillovers as imposed through eigenvalue decompositions are undoubtly a strong assumption for financial return data, assuming a causal chain structure in economic shocks to daily speculative returns through a Cholesky decomposition may only be debatable for certain special asset systems and requires cogent economic justification. For this reason, we suggest employing additional external information about the economy to properly identify the structural rotation.

It is important to note that this identification problem differs from the one in the heteroscedastic SVAR case. When coupling economic identification with modeled heteroscedasticity, the SVAR literature models structural shocks by $w_t = B\epsilon_t$ and assumes w_t to be heteroscedastic such that $\mathrm{E}[\epsilon_t\epsilon_t^\top] = B^{-1}\Lambda_t B^{-1^\top}$ where Λ_t is the time-varying diagonal variance matrix of the structural shocks (Lütkepohl and Schlaak, 2021). It is clear that for the purpose of asset return modeling this assumption is very restrictive as it does not allow one to retain rich dynamics of the covariance generating process. Therefore the identification problem we are handling in the MGARCH case treats heteroscedastic reduced form innovations (returns) based on homoscedastic structural shocks.

1.2.2 Identification by proxy

Because the true structural relationship in (1.3) is unobserved, we consider the principal matrix square root $\tilde{Q}_t$ as initial decomposition of H_t. The reason is that the principal square

root[5] is known to be positive definite if and only if H_t is and positive definiteness of $\tilde{Q}_t$ ensures invertibility of all other matrix decompositions $\tilde{Q}_t R$: Indeed, the existence of an $(n \times n)$ matrix $\tilde{Q}_t^{-1}$ such that $\tilde{Q}_t^{-1}\tilde{Q}_t = I_n$ implies that, for any $(n \times n)$ rotation matrix R, there exists a matrix $B = (\tilde{Q}_t R)^{-1}$ such that $B(\tilde{Q}_t R) = R^{-1}\tilde{Q}_t^{-1}\tilde{Q}_t R = I_n$ because $\det(R) = +1$.

Given that H_t is $\mathcal{F}_{t-1}$-measurable, we define standardized residuals u_t by

$$\begin{aligned} \varepsilon_t &= Q_t \xi_t = \tilde{Q}_t \tilde{R} \xi_t \\ \Leftrightarrow \quad \tilde{R}\xi_t &= \left(\tilde{Q}_t\right)^{-1} \varepsilon_t =: u_t \end{aligned} \tag{1.6}$$

We decompose the $(n \times n)$ matrix $\tilde{R}$ into the vector $\tilde{R}_{\bullet 1}$ corresponding to the first column of $\tilde{R}$ and an $((n \times (n-1))$ remainder matrix $\tilde{R}^*$. Correspondingly, we split ξ_t into a shock of interest ξ_{1t}, which, without loss of generality, can be assumed to be the first vector entry, and a remainder ξ_t^{1*}. This decomposition yields:

$$u_t = \tilde{R}_{\bullet 1}\xi_{1t} + \tilde{R}^* \xi_t^{1*} \tag{1.7}$$

Hence, for partial identification of the model, we need an estimate of $\tilde{R}_{\bullet 1}$.

In many cases however, one is interested in full identification of the underlying structural model, i.e. an estimate of $\tilde{R}$. To this end, we build on ideas of Stock and Watson (2012) and Mertens and Ravn (2013). Assume there exists a centered $(n-1)$-dimensional instrument process $Z = (Z_t)_{t \in I}$ such that, for all $i = 1, \ldots, n-1$,

$$\mathrm{E}[\xi_{it} Z_{it}] = \phi_i \in \mathbb{R} \setminus \{0\} \qquad \text{(relevance)} \tag{1.8}$$

$$\mathrm{E}[\xi_t^{i*} Z_{it}] = \mathbf{0}_{(n-1)\times 1} \qquad \text{(exogeneity)} \tag{1.9}$$

where i relates to the i-th vector element and the product process $(\xi_t Z_{it})_{(t=1,\ldots,T)}$ is weakly stationary.[6] Using (1.7), (1.8) and (1.9), we have

$$\mathrm{E}[u_t Z_{1t}] = \mathrm{E}[\tilde{R}_{\bullet 1}\xi_{1t} Z_{1t} + \tilde{R}^* \xi_t^* Z_{1t}] = \tilde{R}_{\bullet 1}\, \mathrm{E}[\xi_{1t} Z_{1t}] = \tilde{R}_{\bullet 1}\phi_1\,, \tag{1.10}$$

[5] A real symmetric $(n \times n)$ matrix H can be factorized as $H = \Gamma \Lambda \Gamma^\top$; here, Γ is an orthogonal $(n \times n)$ matrix, with the normalized eigenvectors of H as columns, and Λ is a diagonal matrix of the eigenvalues. The principal square root of H is defined as $\Gamma \Lambda^{1/2} \Gamma^\top$ where $\Lambda^{1/2}$ denotes the diagonal matrix of the square root of the eigenvalues. It is the unique matrix square root which has non-negative eigenvalues, see Horn and Johnson (2012, Theorem 7.2.6).

[6] By assuming covariance stationarity instead of mean-stationarity we can apply non-restrictive weak laws of large numbers to show the consistency of our estimator.

which allows one to identify $\tilde{R}_{\bullet 1}$ up to an unknown scalar ϕ_1, i.e., up to scale and sign.

Similar to Lunsford (2015), we identify this scalar by exploiting the unit L^2-norm of the columns of the rotation matrix:

$$\mathrm{E}[Z_{1t}u_t^\top]\,\mathrm{E}[u_t Z_{1t}] = \phi_1 \tilde{R}_{\bullet 1}^\top \tilde{R}_{\bullet 1}\phi_1 = \phi_1^2 \tag{1.11}$$

Thus, by inserting (1.11) into (1.10), we obtain:

$$\tilde{R}_{\bullet 1} = \pm\,\mathrm{E}[u_t Z_{1t}]\left(\mathrm{E}[Z_{1t}u_t^\top]\,\mathrm{E}[u_t Z_{1t}]\right)^{-1/2}. \tag{1.12}$$

In (1.12), the sign is determined by the covariance of the instrumental variable and the structural shock of interest, i.e. by ϕ_1. By orthogonality of rotation matrices, we can infer the structural shock of interest as

$$(\tilde{R}_{\bullet 1})^\top u_t = \xi_{1t}. \tag{1.13}$$

Likewise, we can infer the first column $Q_{\bullet 1,t}$.

1.2.3 A general recurrence scheme for full identification

Due to (1.5), the entire rotation matrix of a bivariate system is identified with a single proxy variable. In order to identify the full rotation matrix in an n-dimensional system, one could proceed similar to the partial identification steps outlined above by simultaneously estimating all columns with $n-1$ instruments by means of (1.12). Instead, we suggest a scheme which exploits that n-dimensional rotations can be expressed as sequences of Givens rotations. The identification approach via Givens rotations guarantees orthogonality of the structural shocks. This is of importance, because it is a priori not clear which proxy variables deliver orthogonal shocks and the exogeneity assumption (1.9) is not testable in advance. In contrast to identification column-by-column, our approach delivers a parametrization of the rotation matrix which offers further insights in its own right: For instance, because one obtains a set of rotation angles, one may study the relations between pairs or subsets of structural shocks. As another important use case, one may combine the proxy-based identification with other restrictions (Fisher and Huh, 2019, see e.g.) to achieve full identification.[7] As a final asset, when aiming at partial identification in larger

[7]The use of Givens rotations has not been coupled with a proxy-based and full identification strategy to date. This is partly due to the fact that, if the structural shocks are correlated with several proxies, there still exists an identification problem, now on the level of the structural shocks, which requires additional restrictions (see Angelini and Fanelli, 2019; Arias et al., 2021, Jentsch and Lunsford, 2022 in the SVAR context).

dimensional systems, our strategy is well-defined even if one can identify only a subset of columns of $\tilde{R}$.

For the rotation theory underlying the identification approach we refer the reader to Appendix 1.A. In the following paragraphs, we present the recurrence scheme for full identification of the angles of a rotation matrix of order $n \in \mathbb{N}_{\geq 2}$. In this case, $\frac{n(n-1)}{2}$ restrictions are sufficient and necessary for identification, because every rotation in a n-dimensional space can be expressed as a composition of $\frac{n(n-1)}{2}$ elemental rotations. Let θ_{ij} denote the angle of rotation in the embedded plane in $\mathbb{R}^n$ spanned by the axes x_i, x_j ($i, j \in \{1, \ldots, n\}$, $i \neq j$). The elemental rotation in this plane can be expressed by the $(n \times n)$ rotation matrix R^{ij}:

$$R^{ij}(\theta_{ij}) = \{r_{k,l}\}_{(k,l=1,\ldots,n)} \text{ where } \begin{cases} r_{ii} & = \cos(\theta_{ij}) \\ r_{ij} & = -\sin(\theta_{ij}) \\ r_{ji} & = \sin(\theta_{ij}) \\ r_{jj} & = \cos(\theta_{ij}) \\ r_{kk} & = 1 \qquad\qquad (k \neq i, j) \\ r_{kl} & = 0 \qquad\qquad \text{(otherwise)}, \end{cases} \tag{1.14}$$

i.e., an elemental rotation holds all dimensions fixed apart from i, j.

Any rotation $\tilde{R}$ in $\mathbb{R}^n$ can be expressed as a continuous and differentiable composition of these elemental rotation matrices (Hoffman et al., 1972). For the present work, we specify this composition as

$$\tilde{R} = \prod_{i=1}^{n-1} \prod_{j=i+1}^{n} R^{ij}(\theta_{ij}). \tag{1.15}$$

Note that this is just one possible composition of elemental rotations because there is a multiplicity of combinations of angle values and products generating the same rotation outcome. As matrix multiplication is non-commutative, the order of the elemental rotations has to be predetermined to ensure uniqueness of the estimated rotation angles; in other words, it is an econometric identification condition. It has, however, no economic implications, because one always rotates through all two-dimensional mutually orthogonal subplanes. The ordering principle we adopt in (1.15) is prevalent in the time series literature (see e.g. Luati and Proietti, 2010) and ensures that the composition of the antecedent $\frac{m(m-1)}{2}$ elemental rotations forms an m-dimensional rotation ($m \in \mathbb{N}_{\leq n}$) which is attractive for computational reasons, see Appendix 1.B for an illustration. To outline the n-dimensional

case to infer unique rotation angles, denote the cosine (sine) evaluated at an angle θ_{ij} by c_{ij} (s_{ij}). We assemble the $\frac{n(n-1)}{2}$ angular parameters θ_{ij}, $(i = 1, \ldots, n-1, j = i+1, \ldots, n)$, in the angular parameter matrix Θ given by

$$\Theta = \begin{pmatrix} 0 & \theta_{12} & \theta_{13} & \ldots & \ldots & \theta_{1n} \\ \vdots & 0 & \theta_{23} & \theta_{24} & \ldots & \theta_{2n} \\ \vdots & \vdots & \ddots & \ddots & \ldots & \vdots \\ \vdots & \vdots & \ldots & \ddots & \ddots & \vdots \\ 0 & 0 & \ldots & \ldots & 0 & \theta_{n-1,n} \end{pmatrix} \tag{1.16}$$

The $\frac{n(n-1)}{2}$ angles θ_{ij}, $(i = 1, \ldots, n-1, j = i+1, \ldots, n)$ describing an n-dimensional rotation $\tilde{R}^{nD}$ with $n \in \mathbb{N}_{\geq 2}$ can be found by a recursive approach.

The following steps are for the purpose of illustration but we outline a numerically attractive implementation of the recurrence scheme in Appendix 1.C. For the angles θ_{ij}, with $i = 1, \ldots, n-2$ and $j = i+2, \ldots, n$, marked in (1.16) in red, it holds that

$$\begin{aligned} s_{in} &= \tilde{R}_{ni}^{((n-i+1)D)} \\ s_{ij} &= \tilde{R}_{ji}^{((n-i+1)D)} / \left(c_{i,(j+1)} \cdot \ldots \cdot c_{in} \right) \end{aligned} \tag{1.17}$$

where the angles are in $\left[-\frac{\pi}{2}, \frac{\pi}{2}\right)$; the remaining $(n-1)$ angles $\theta_{i,(i+1)}$, marked in blue have domain $[-\pi, \pi)$ and can be found from:[8]

$$\begin{aligned} s_{i,(i+1)} &= \tilde{R}_{i+1,i}^{((n-i+1)D)} / \left(c_{i,(i+2)} \cdot \ldots \cdot c_{in} \right) \\ c_{i,(i+1)} &= \tilde{R}_{ii}^{((n-i+1)D)} / \left(c_{i,(i+2)} \cdot \ldots \cdot c_{in} \right). \end{aligned} \tag{1.18}$$

If any angle $\theta_{i,k}$ in the denominator of (1.17) or (1.18) is equal to $-\frac{\pi}{2}$ all subsequent angles listed in this row of Θ can be chosen arbitrarily due to the loss of one degree of freedom in the angular parameters. At the parameter boundaries of the bluish angles with domains $[-\pi, \pi)$ we experience singularities where bijectivity and continuity of the map between the space of rotations and the angle parameter space fails.[9] While the existence of discontinuities in the Givens representation may seem troubling, the singularities can always be shifted by using a different angle parameterization scheme due to the cyclical

[8] For a derivation of the angular parameter domains, see Hoffman et al. (1972) but note that the ordering principle of the elemental rotations differs.

[9] For example, the inverse map from the space of two-dimensional rotations to $[-\pi, \pi)$ features a discontinuity at $F = \begin{pmatrix} -1 & 0 \\ 0 & -1 \end{pmatrix}$, because both $R^{12}(-\pi)$ and $\lim_{\theta \to \pi} R^{12}(\theta)$ converge to F.

property of rotations. More generally, instead of viewing the angle parameter space as an n-dimensional interval in the Euclidean space, it is more convenient to view it in a topology which results from "gluing" opposite faces of the n-dimensional interval where the singularities occur together. In this new topology, the singularities are thus removable.[10]

In summary, all $\frac{n(n-1)}{2}$ angles determining the n-dimensional rotation matrix can be identified if parts of the full rotation matrix as compositions of elemental rotations are known. Given either a rotation matrix or a set of rotations angles, we can reconstruct the corresponding angular or matrix representation. This implies that the availability of $(n-1)$ instruments allows for construction of the n-dimensional rotation matrix.

1.2.4 Estimation strategy

Let the asset system $(\varepsilon_t)_{t\in I}$ in $\mathbb{R}^n$ and assume that instruments $Z_{1t}, ..., Z_{n-1,t}$ are given for the first $(n-1)$ components of ξ_t. The estimation strategy is summarized in Algorithm 1:

Algorithm 1:

Result: full n-dimensional rotation matrix

Initialization:

1. Estimate sequence of n-dimensional conditional covariance matrices $(H_t)_{t\in I}$;
2. Compute principal square roots $(\tilde{Q}_t)_{t\in I}$ and standardized residuals $(u_t)_{t\in I}$;

for $(i = 1, \ldots, n-1)$: **do**

1. Estimate $\tilde{R}_{\bullet i}^{((n-i+1)D)}$ using Z_i;
2. Solve for $(n-i)$ rotation angles and obtain transition matrix D_{n-i+1};
3. Standardize $\tilde{R}^{((n-i+1)D)}$ with D_{n-i+1};

end

Use obtained angles to compute full n-dimensional rotation matrix.

We illustrate the algorithm for $i = 1$: We start by estimating $\tilde{R}_{\bullet 1}$. Knowledge of $\tilde{R}_{\bullet 1}$ provides us with the solutions to the first $(n-1)$ rotation angles, which are contained in the matrix D_n below:

$$\tilde{R}^{(nD)} = \underbrace{R^{12} \cdots R^{1n}}_{:=D_n} \cdot \underbrace{R^{23} \cdot \ldots \cdot R^{n-2,n-1} R^{n-2,n} R^{n-1,n}}_{:=\tilde{R}^{(n-1)D}}$$

[10] In reference to the example in footnote 9, this corresponds to connecting the limit points by bending the interval line into a circle.

Here, $\tilde{R}^{((n-1)D)}$ has the structure:

$$\tilde{R}^{((n-1)D)} = \begin{pmatrix} 1 & 0 & \cdots & 0 \\ 0 & * & \cdots & * \\ \vdots & \vdots & \cdots & \vdots \\ 0 & * & \cdots & * \end{pmatrix}$$

In case of a violation of (1.9), we observe a non-zero first entry in the second column of $\tilde{R}^{((n-1)D)}$. We estimate the second column of $\tilde{R}^{(nD)}$ using the second proxy variable. As a composition of elemental rotations, D_n is a rotation matrix and thus invertible, hence multiplication with the inverse of D_n yields

$$\Leftrightarrow D_n^{-1}\tilde{R}^{(nD)} = \underbrace{R^{23} \cdot \cdots \cdot R^{n-3,n} R^{n-2,n} R^{n-1,n}}_{:=\tilde{R}^{(n-1)D}} \tag{1.19}$$

Focusing on the second column, we obtain

$$D_n^{-1}\tilde{R}_{\bullet 2}^{(nD)} = \tilde{R}_{\bullet 2}^{((n-1)D)} = (0, *, \cdots, *)^\top$$

from which we infer the $(n-2)$ rotation angles θ_{ij} $(i = 2, j = i+1, \ldots, n)$. We iteratively continue these steps, until we arrive at the two-dimensional subsystem in the lower right corner, from which we derive the last angle $\theta_{n-1,n}$.

Estimation and consistency

Without loss of generality, we consider the estimation of the first column of an n-dimensional rotation matrix $\tilde{R}$. Let $\boldsymbol{z}_1 = (z_{11}, \ldots, z_{1T})^\top$ be the vector of the observed Z_1 and let $\hat{\boldsymbol{u}} = (\hat{u}_1, \ldots, \hat{u}_T)$ denote the matrix of estimated standardized residuals of the n-dimensional asset return system. In order to estimate $\tilde{R}_{\bullet 1}$, we define the estimators of (1.10) and (1.11) as

$$\hat{\psi}_1 := \widehat{\tilde{R}_{\bullet 1}\phi} = \frac{1}{T}\sum_{t=1}^{T} \hat{u}_t z_{1t} \tag{1.20}$$

and

$$\widehat{\phi^2} := \left(\frac{1}{T}\sum_{t=1}^{T} z_{1t}\hat{u}_t^\top\right)\left(\frac{1}{T}\sum_{t=1}^{T} \hat{u}_t z_{1t}\right) = \left(\hat{\psi}_1\right)^\top \hat{\psi}_1 \tag{1.21}$$

Then we obtain the estimator for $\tilde{R}_{\bullet 1}$ as

$$\widehat{\tilde{R}_{\bullet 1}} \pm \hat{\psi}_1 \left(\widehat{\phi^2}\right)^{-1/2} \tag{1.22}$$

The estimation procedure is repeated iteratively for all columns of the rotation matrix.

Let η denote the vector of parameters defining the dynamics of the conditional covariance matrix $H_t = H_t(\eta)$ and assume that H_t is a continuous function of the true parameter vector η_0. Let $\hat{\eta}$ denote the corresponding estimator. In order to establish consistency of $\widehat{\tilde{R}_{\bullet 1}}$ we adopt the following assumptions:

Assumption 1.2.1.

(a) $\hat{\eta} \xrightarrow{p} \eta_0$

(b) $\frac{1}{T}\sum_{t=1}^{T} \xi_t z_{1t} \xrightarrow{p} \mathrm{E}[\xi_t Z_{1t}]$

where $\xrightarrow{p}$ denotes convergence in probability.

Proposition 1.2.1. *Under Assumption 1.2.1, we have:* $\widehat{\tilde{R}_{\bullet 1}} \xrightarrow{p} \tilde{R}_{\bullet 1}$.

Proof. The continuous mapping theorem implies by (a) that $H_t(\hat{\eta}) \xrightarrow{p} H_t(\eta_0)$ as $T \to \infty$. Thus, the decomposition $\tilde{Q}_t(\hat{\eta})$ converges to $\tilde{Q}_t(\eta_0)$ because the usage of the unique positive definite principal square root as initial decomposition $\tilde{Q}_t$ represents a (uniformly) continuous operation in the space of positive definite matrices. By another application of the continuous mapping theorem we obtain $\hat{u}_t = \tilde{Q}_t(\hat{\eta})^{-1}\varepsilon_t \xrightarrow{p} \tilde{Q}_t(\eta_0)^{-1}\varepsilon_t = u_t$. As $u_t = \tilde{R}\xi_t$, it holds that $\frac{1}{T}\sum_{t=1}^{T} u_t z_{1t} = \frac{1}{T}\sum_{t=1}^{T} \tilde{R}\xi_t z_{1t} = \tilde{R}\frac{1}{T}\sum_{t=1}^{T} \xi_t z_{1t}$. By the continuous mapping theorem and assumption (b) $\frac{1}{T}\sum_{t=1}^{T} \hat{u}_t z_{1t}$ consistently estimates $\mathrm{E}[u_t Z_{1t}] = \tilde{R}_{\bullet 1}\phi$. Consistency of the estimators (1.21) and (1.22) follows by another application of the continuous mapping theorem. Note that assumption (b) does not require imposing an iid assumption but allows for a certain degree of serial correlation through the choice of a suitable weak law of large numbers (WLLN). For instance, we can choose a WLLN for weakly stationary correlated sequences with $\lim_{T\to\infty} \frac{1}{T}\sum_{i=0}^{T} \mathrm{cov}((\xi_t Z_{1t})(\xi_{t-i} Z_{1,t-i})) = 0$.[11] □

Given the estimates, we can uniquely infer the corresponding rotation angles. Recall that this map features discontinuities at certain angle domain boundaries. The continuous mapping theorem is still applicable by characterizing continuity in terms of preimages of open sets and considering the angular parameter space in a topological sense by gluing

[11] In the VAR literature it is common to impose $\mathrm{E}[Z_{1t} u_{t-j}] = 0$ $(j \neq 0)$. Should this condition not be satisfied, it can be recovered by regressing z_{1t} on u_t and using the residual of this regression as a proxy variable.

those interval faces at which we experience singularities (see the angular parameters marked in blue in (1.16)) together. This removes the discontinuities in the new topology.[12]

Testing

To justify the structural modeling approach, we develop a test for departures from symmetric volatility spillovers as implied by the usage of the (non-structural) principal square root. We suggest a Wald test based on the estimated rotation matrix. When the volatility spillovers between the assets are in fact asymmetric, the estimated rotation matrix departs from the identity matrix of no rotation postulated under the null hypothesis.

To build an inference framework, we follow ideas of Brüggemann et al. (2014, 2016) and Jentsch and Lunsford (2022). We adopt the following additional assumptions:

Assumption 1.2.2.

(1) Let $x_t := (u_t^\top, Z_t^\top)^\top$, such that the $(2n-1)$-dimensional process $(x_t)_{t\in\mathbb{Z}}$ consists of the n-dimensional standardized residual series and the $(n-1)$ dimensional instrument series, and assume that the product process $(u_t Z_t^\top)_{t\in\mathbb{Z}}$ is weakly stationary.

(2) Let $\alpha_x(h) = \sup_{A\in\mathcal{F}_{-\infty}^t,\, B\in\mathcal{F}_{t+h}^\infty,\, (t\in\mathbb{Z})} |P(A\cap B) - P(A)P(B)|$, $h \in \mathbb{N}$ denote the alpha-mixing coefficients of the process $(x_t)_{t\in\mathbb{Z}}$ where $\mathcal{F}_{-\infty}^t := \sigma(x_j : j \le t)$ and $\mathcal{F}_{t+h}^\infty := \sigma(x_j : j \ge t+h)$. Assume furthermore that $\sup_t \mathrm{E}\left[|x_t|_{2\beta}^{2\beta}\right] < \infty$ where $|M|_p = \left(\sum_{i,j} |m_{ij}|^p\right)^{1/p}$ for some matrix $M = (m_{ij})$ and let $\sum_{h\ge1} \alpha_x(h)^{1-\frac{2}{\beta}} < \infty$ for some $\beta > 2$.

(3) Define the $(n\times n)$ matrices $\tau_h = \mathrm{E}[(Z_{it}u_t)(Z_{i,t-h}u_{t-h})^\top]$ $(h\in\mathbb{Z})$ and assume that $V := \sum_{h=-\infty}^{+\infty} \left(\tau_h - \psi_i\psi_i^\top\right)$, where $\psi_i := \phi_i \tilde{R}_{\bullet i}$, exists and is positive definite.

The weak stationarity assumption (1) is needed to meet the relevance condition (1.8) and for the application of a suitable CLT. The summability condition in (2) ensures that $\alpha_x(h) \to 0$ as $h \to \infty$ such that the process $(x_t)_{t\in\mathbb{Z}}$ is said to be α-mixing. The mixing condition allows for general forms of serial dependence, for example for conditional heteroscedasticity. In particular, neither the standardized residuals nor the proxy variables must be iid. Assumption (3) guarantees the existence and positive definiteness of the

[12] For two-dimensional rotations this corresponds to interpreting the parameter interval as a circle; for three-dimensional rotations this corresponds to interpreting the parameter space as a cylinder; see e.g. Hemingway and O'Reilly (2018).

asymptotic variance of our estimator. Note that the summability condition and the moment condition in (2) are sufficient to prove the existence of V by Davidson (1994, Corollary 14.3).

Proposition 1.2.2. *Let $\psi_i := \phi_i \tilde{R}_{\bullet i}$ and define $\tilde{\psi}_i := \widetilde{\phi_i \tilde{R}_{\bullet i}} = \frac{1}{T}\sum_{t=1}^{T} u_t Z_{it}$. Under Assumption 1.2.2, we have*

$$\sqrt{T}(\tilde{\psi}_i - \psi_i) \xrightarrow{d} N(0, V)$$

where $\xrightarrow{d}$ denotes convergence in distribution.

Proof. To prove this CLT result under α-mixing assumptions on $(x_t)_{t\in\mathbb{Z}}$ we use the CLT of Herrndorf (1984) (see Francq and Zakoïan (2010, Theorem A.4)) generalized to random vectors by means of a Cramér-Wold device (see Davidson (1994, Theorem 25.5 & 25.6)). Let $\lambda \in \mathbb{R}^n$ such that $||\lambda|| = 1$ and define $\Lambda_{it} = \lambda^\top \iota_{it}$ where $\iota_{it} := u_t Z_{it} - \psi_i$. By the moment boundedness condition on $(x_t)_{t\in\mathbb{Z}}$ in (2), the univariate process $(\Lambda_{it})_{t\in\mathbb{Z}}$ satisfies $\sup_t \mathrm{E}[|\Lambda_{it}|^\beta] < \infty$ for some $\beta > 2$. Furthermore, Davidson (1994, Theorem 14.1) implies that the α-mixing coefficients $(\alpha_\Lambda(h), h \in \mathbb{N})$ of the process $(\Lambda_{it})_{t\in\mathbb{Z}}$ decay at the same rate as $(\alpha_x(h), h \in \mathbb{N})$ of the process $(x_t)_{t\in\mathbb{Z}}$, such that we have $\sum_{h\geq 1} \alpha_\Lambda(h)^{1-\frac{2}{\beta}} < \infty$ by the summability condition in Assumption 1.2.2. Together with the assumptions in (3) we can apply the CLT of Herrndorf (1984) in combination with the Cramér-Wold theorem. The limiting variance of $\sqrt{T}(\tilde{\psi}_i - \psi_i)$ is given by

$$\begin{aligned}\mathrm{Var}\left(\frac{1}{\sqrt{T}}\sum_{t=1}^{T}\iota_{it}\right) &= \frac{1}{T}\sum_{h=-(T-1)}^{T-1}\sum_{t=\max(1,1+h)}^{\min(T,T+h)}\mathrm{cov}(\iota_{it}, \iota_{i,t-h}) \\ &\to \sum_{h=-\infty}^{+\infty}\mathrm{cov}(Z_{it}u_t, Z_{i,t-h}u_{t-h}) = \sum_{h=-\infty}^{+\infty}\left(\tau_h - \psi_i\psi_i^\top\right)\end{aligned}$$

as $T \to \infty$ which completes the proof. □

To conduct the Wald test for departures from symmetric spillovers, we use Proposition 1.2.2 to derive the limiting distribution of the estimated rotation matrix in Corollary 1.2.1.

Corollary 1.2.1. *Under Assumption 1.2.2, we have:*

$$\sqrt{T}(\hat{\tilde{R}}_{\bullet i} - \tilde{R}_{\bullet i}) \xrightarrow{d} N(0, W)$$

where $W = M_\psi V M_\psi^\top$ and $M_\psi := -\psi_i(\psi_i^\top\psi_i)^{-\frac{3}{2}}\psi_i^\top + (\psi_i^\top\psi_i)^{-\frac{1}{2}} I_n$.

Proof. As $\tilde{R}_{\bullet i}$ is a smooth function of ψ_i, which is by assumption not the zero vector, we can apply the Delta method to obtain the asymptotic covariance matrix of the estimators of the rotation matrix. To derive M_ψ, rewrite the estimator as

$$\begin{aligned}\widetilde{\tilde{R}_{\bullet i}} &= \pm\left(\frac{1}{T}\sum_{t=1}^{T}\hat{u}_t z_{it}\right)\left[\left(\frac{1}{T}\sum_{t=1}^{T} z_{it}\hat{u}_t^\top\right)\left(\frac{1}{T}\sum_{t=1}^{T}\hat{u}_t z_{it}\right)\right]^{-1/2} \\ &= \pm\widetilde{\psi}_i\left(\widetilde{\psi}_i^\top\widetilde{\psi}_i\right)^{-\frac{1}{2}}\end{aligned}$$

Then M_ψ is given by:

$$\begin{aligned}M_\psi := \frac{\partial\tilde{R}_{\bullet i}}{\partial\psi_i^\top} &= \pm\left(-\frac{1}{2}\psi_i(\psi_i^\top\psi_i)^{-\frac{3}{2}}(\psi_i^\top(I_n+I_n)) + (\psi_i^\top\psi_i)^{-\frac{1}{2}}I_n\right) \\ &= \pm\left(-(\psi_i^\top\psi_i)^{-\frac{3}{2}}\psi_i\psi_i^\top + (\psi_i^\top\psi_i)^{-\frac{1}{2}}I_n\right).\end{aligned}$$

□

This result allows us to formulate a Wald test to check whether the estimated rotation matrix departs from the identity matrix by restricting the off-diagonal elements of the first $(n-1)$ columns of the rotation matrix to be zero.

Practically, the test is based on $\hat{u}_t$ rather than u_t. We therefore incur an additional error that is due to estimating η by the QML method. Unfortunately, it appears quite difficult to account for this additional sampling variation. However, our empirical evidence is sufficiently compelling to leave room for robustness under an inflated asymptotic variance due to sampling variability of the BEKK parameters. We estimate the asymptotic covariance matrix by means of a Newey-West heteroscedasticity and autocorrelation robust estimator with automatic lag length selection and thus account for heteroscedasticity and serial correlation of unknown forms.

1.3 MGARCH model

Let the process $(\xi_t)_{t\in\mathbb{Z}} \subseteq \mathbb{R}^n$ denote an n-dimensional real-valued strict white noise process with zero mean and unit covariance matrix, i.e. $\xi_t \sim SWN(0, I_n)$. The process $(\varepsilon_t)_{t\in\mathbb{Z}}$ follows a strong MGARCH process if it satisfies:

$$\varepsilon_t = H_t^{1/2}\xi_t \quad (t \in \mathbb{Z}). \tag{1.23}$$

Here, $H_t^{1/2} \in \mathbb{R}^{n\times n}$ denotes a decomposition of the form $H_t^{1/2}\left(H_t^{1/2}\right)^\top = H_t$ of the sequence of positive definite matrices $(H_t)_{t\in\mathbb{Z}}$. The process $(H_t)_{t\in\mathbb{Z}}$ is covariance stationary and measurable with respect to the filtration $\mathcal{F}_{t-1} = \sigma(\{\varepsilon_s : s \leq t-1\})$, $(\varepsilon_t)_{(t\in\mathbb{Z})}$ is a multivariate martingale difference with $\mathrm{E}[\varepsilon_t|\mathcal{F}_{t-1}] = 0$ ($\mathrm{E}[|\varepsilon_t|] < \infty$) and its conditional covariance matrix is given by $\mathrm{Var}[\varepsilon_t|\mathcal{F}_{t-1}] = H_t$. In order to specify the conditional dynamics of the process, various specifications have been proposed, among which the parametric VEC and BEKK GARCH models enjoy great popularity (Bauwens et al., 2006). The BEKK GARCH model of Engle and Kroner (1995) ensures positive definiteness of H_t by construction. The n-dimensional process $(\varepsilon_t)_{t\in\mathbb{Z}}$ admits a BEKK(p,q) specification if H_t satisfies for all $t \in \mathbb{Z}$:

$$H_t = CC^\top + \sum_{i=1}^{p} A_i^\top \varepsilon_{t-i}\varepsilon_{t-i}^\top A_i + \sum_{j=1}^{q} B_j^\top H_{t-j} B_j \quad (p,q \in \mathbb{N}) \tag{1.24}$$

where C is a lower triangular matrix and A_i and B_j are coefficient matrices in $\mathbb{R}^{n\times n}$. The intercept matrix $CC^\top$ is by construction symmetric and positive definite if C has full rank. The latter ensures positive definiteness of $(H_t)_{t\in\mathbb{Z}}$. Boussama et al. (2011, Theorem 2.4) show that under weak regularity conditions on $(\xi_t)_{(t\in\mathbb{Z})}$, the MGARCH process is ergodic, strictly and weakly stationary and invertible if the eigenvalues of $\sum_{i=1}^{p} A_i \otimes A_i + \sum_{j=1}^{q} B_j \otimes B_j$ are less than one in modulus. Hafner and Preminger (2009) provide conditions to establish consistency as well as asymptotic normality of the QML estimator assuming i.a. existence of second-order moments of $(\xi_t)_{(t\in\mathbb{Z})}$ and finite sixth-order moments of $(\varepsilon_t)_{t\in\mathbb{Z}}$. The MGARCH model thus fulfills the requirements for identification postulated in Section 1.2.4. Due to the quadratic structure of the BEKK(p,q) model, the parameter matrices are only identified up to sign. The BEKK$(1,1)$ model is uniquely identified if we assume the diagonal elements of C and the first matrix entries of A_1, $a_{11(1)}$, and B_1, $b_{11(1)}$, to be positive.

1.4 An identified asset return system

In this section, we illustrate the structural proxy-MGARCH approach by analyzing a system of daily returns covering three major asset classes: equity, fixed income and the foreign exchange markets. These are the most important asset classes for portfolio optimization and the key ingredients of the composite indicator of systemic stress in the financial system employed by the European Central Bank (ECB) (Kremer et al., 2012).

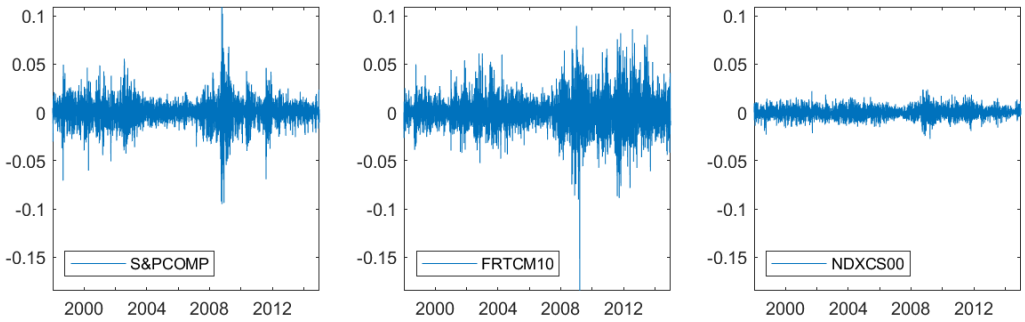

Figure 1.1: Demeaned daily log returns of the S&P 500 Composite Index (SP500), the yield of the U.S. constant maturity 10 year treasury note (FRTCM10) and the Finex U.S. Dollar Index (NDXCS00) from 1/1/1998 to 12/31/2014.

1.4.1 Data

We study daily price data ranging from 1/1/1998 to 12/31/2014 taken from Bloomberg. Our asset triple consists of the S&P 500 Composite Index (SP500), the yield of the U.S. constant maturity 10 year treasury note (FRTCM10) and the Finex U.S. Dollar Index (NDXCS00). The Finex is a measure of the value of the U.S. Dollar relative to a currency basket of major U.S. trade partners. It increases when the U.S. Dollar gains value compared to the other currencies. We compute daily log returns r_t for each asset; see Figure 1.1. All series exhibit the typical features of daily return data, such as heteroscedasticity and volatility clustering (see also the summary statistics in Table 1.1).

News data to proxy for the underlying structural shocks are taken from Thomson Reuters MarketPsych Indices (TRMI). Thomson Reuters process news and social media in real-time to construct economic indicators, among them sentiment indicators. The indicators are available for individual companies, economic sectors, geographical regions, countries, country markets, commodities and energy topics, indices as well as currencies. We use TRMIs for the U.S. as a geographical and political entity as well as the U.S. as an economic and financial marketplace. The TRMIs are available on a daily level. Only news items published until 3:30 pm Eastern time are taken into account by Thomson Reuters for the computation of the daily index values. This time window is not perfectly aligned with the end of the core trading session of the NYSE at 4:00 pm Eastern time, which determines the closing price. As the news measurement window ends thirty minutes before market close, we may miss information inherent to important news items published during the last thirty minutes of the core trading session, which may weaken our proxy. However,

Statistic	SP500	FRTCM10	NDXCS00
Minimum	-0.0950	-0.1847	-0.0275
Maximum	0.1093	0.0895	0.0236
Mean	-0.0001	0.0000	-0.0000
Median	-0.0000	0.0002	-0.0000
Std. Dev.	0.0125	0.0176	0.0052
Skewness	-0.2033	-0.1360	-0.0343
Kurtosis	10.9287	8.4542	4.4914

Table 1.1: Descriptive statistics of the demeaned daily log returns of the S&P 500 Composite Index (SP500), the yield of the U.S. constant maturity 10 year treasury note (FRTCM10) and the Finex U.S. Dollar Index (NDXCS00) from 1/1/1998 to 12/31/2014; $N = 4435$ observations.

the misalignment precludes a forward-looking bias of our proxy variables.

With regard to proxy variable selection, natural candidates are the U.S. stock index sentiment and the U.S. bond sentiment. The U.S. stock index sentiment is likely to reflect unexpected economic and political news concerning the S&P 500 and is thus expected to proxy for an equity market shock. Similarly, the bond market sentiment captures the perception of news about government bond markets and may thus proxy for a bond market shock. As bond prices move in opposite direction to bond yields, a structural shock identified by means of the bond market sentiment is expected to be connected to the treasury yield with inverted sign. It is vital to realize that the exogeneity condition imposed on proxies and structural shocks does not preclude that e.g. bond market news affect equity returns. While the structural rotation categorizes the standardized residuals into identified structural shocks, the matrix square root of the conditional covariance matrix determines the mix of these shocks which makes up the individual asset returns.

With regard to the range of the TRMIs, a value of zero is interpreted as a neutral signal, negative values convey a negative signal and positive values a positive one. As our proxy variables are high-frequent, we do not face the difficulties stemming from proxy variables being censored at zero as is common in the proxy-SVAR literature. We fit flexible ARMA models to the series to distill the unexpected innovations to the proxy series. Table 1.2 shows statistical summary measures of the resulting indicators. Figure 1.2 shows the

Statistic	stock index sentiment	bond sentiment
Minimum	-3.1342	-4.8296
Maximum	3.3754	5.5997
Mean	-0.0000	0.0000
Median	-0.0097	-0.0469
Std. Dev.	1.0000	1.0000
Skewness	0.0564	0.2383
Kurtosis	2.5325	4.2307

Table 1.2: Descriptive statistics for the standardized and filtered TRMI indices on trading days from 1/1/1998 to 12/31/2014; $N = 4435$ observations.

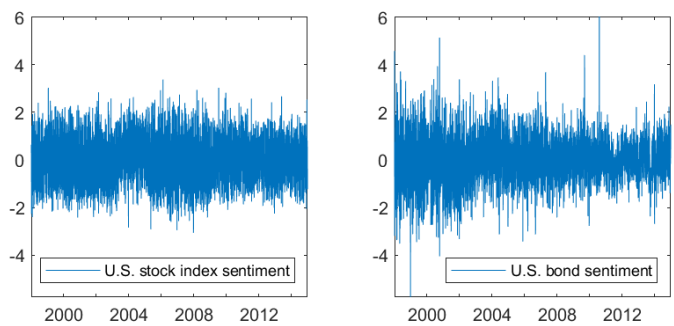

Figure 1.2: ARMA filtered and standardized U.S. stock index and bond sentiment on trading days from 1/1/1998 to 12/31/2014.

filtered and standardized proxy time series.

1.4.2 Structural model estimates

Table 1.3 documents the results of the QMLE of the full BEKK on the asset return system. By using the values of a diagonal BEKK model as starting values combined with a randomization strategy for the off-diagonal elements of the coefficient matrices, we verify that the resulting estimates correspond to a maximum of the loglikelihood function. We optimize the loglikelihood numerically using the analytical derivatives provided in Hafner and Herwartz (2008), while monitoring the spectral radius. Inference with regard to the coefficient matrices of the BEKK model is based on t-statistics derived from the analytical derivatives. The diagonal parameters and selected off-diagonal parameters of the coefficient matrices turn out to be statistically significant at conventional levels. The Akaike criterion speaks in favor of the full BEKK specification (see Table 1.3) such that we base our further analysis on the latter model.

The analysis of the proxy variables reveals that the stock market index and bond market sentiment seem to be relevant instruments; see Table 1.4. The inferred rotation angles lie in the interior of the angular parameter space. They are clearly different from zero causing the structural rotation matrix to depart from the identity matrix. This indicates that spectral decompositions imposing symmetric spillover mechanisms are not applicable. The Wald test confirms this finding; see Table 1.4. The correlation matrix of the inferred structural shocks with the proxy variables shows a diagonal structure in agreement with the relevance (1.8) and the exogeneity condition (1.9) with p-values of zero indicating the statistical significance of the relation of the structural shocks of interest and their respective proxy variables. The inferred structural shocks are mutually and serially uncorrelated and seem to exhibit white noise properties (see Table 1.5).

$\hat{C}$			$\hat{A}$			$\hat{B}$		
0.0011	$3.04 \times 1e^{-6}$	$-2.98 \times 1e^{-6}$	0.2677	0.0169	-0.0108	0.9580	-0.0029	0.0029
–	$8.92 \times 1e^{-4}$	$1.04 \times 1e^{-4}$	0.0003	0.2170	0.0036	0.0014	0.9752	-0.0008
–	–	$2.89 \times 1e^{-4}$	0.0631	-0.0534	0.1430	-0.0120	0.0102	0.9883
(3.8683)	(0.0027)	(-0.0195)	(4.7720)	(0.1861)	(-0.8522)	(50.322)	(-0.0840)	(1.1631)
–	(2.9861)	(2.1167)	(0.0209)	(7.6499)	(1.3591)	(0.2268)	(195.32)	(-1.6027)
–	–	(6.0328)	(1.3258)	(-1.0422)	(13.169)	(-0.6507)	(1.1362)	(677.01)
Spectral radius: 0.9985								
Akaike criterion								
full BEKK: -88661			DBEKK: -88639					

Table 1.3: Quasi maximum likelihood (QML) parameter estimates of the unrestricted BEKK model of the demeaned daily log returns of the S&P 500 Composite Index (SP500), the yield of the U.S. constant maturity 10 year treasury note (FRTCM10) and the Finex U.S. Dollar Index (NDXCS00) over the time period from 1/1/1998 to 12/31/2014. Entries in parentheses are the robust QML t-ratios determined by means of the analytical derivatives as provided by Hafner and Herwartz (2008).

To substantiate the claim that our inferred model is indeed structural, we narratively corroborate the lower (upper)[13] 1%-quantiles of the structural shocks by extracting the major financial news of these days. The results are tabulated in Tables 1.6, 1.7 and 1.8 which are provided in Appendix 1.D. We can connect each structural shock to specific economic and financial turmoil events reported in the news. As Tables 1.6, 1.7 and 1.8 show, the structural shocks are associated with distinct categories of news. ξ_1 captures news related to global economic and political uncertainty affecting equity markets as well as the impact of unexpected events such as terrorist attacks. Moreover, it comprises news regarding the current and prospective financial solidity of big U.S. companies and sectors and reflects the outlook on U.S. economic activity. In addition, we find news items which debate the potential impact of interest rate changes on equity markets. Importantly, ξ_1 captures shocks related to the financial crisis of 2008 and the European debt crisis and, related to this, fiscal shocks such as sovereign rating changes.

The second structural market shock is driven almost exclusively by Fed announcements, inflation data and employment reports with a smaller part of news related to economic turmoil events threatening global economic prospects. It thus carries the flavor of a monetary policy and macroeconomic shock. The third shock vector captures all events relevant to the system which are not covered by the first two structural shocks. Whereas it does not have a structural interpretation a priori, our narrative corroboration reveals that the third shock does indeed reflect a certain category of news, namely events related to movements in the foreign exchange markets. While currency topics seem to dominate, we also observe connections to the gold price, energy and trade balance matters. Concretely, the upper 1%-quantile of the shock vector coincides largely with USD dips and oil or gold rallies, whereas the lower 1%-quantile correspondingly reflects jumps in the USD and USD strength especially against the EUR. Summarizing the discussion, we thus conclude that we identify ξ_1 as equity shock, ξ_2 as bond market shock and refer to ξ_3 as currency shock.

[13] Note that for the second and third shock the analysis is based on the upper 1%-quantile. This is due to the inverse relationship of bond prices and yields which implies a reversed sign in the associated structural shock vector. The sign of the last shock vector is a priori undetermined but can be inferred from the financial context for interpretation.

		proxy-MGARCH model		
$(\hat{\theta}_{12}, \hat{\theta}_{13}, \hat{\theta}_{23})^\top$		0.3811	−0.1885	−2.9164
$\hat{\hat{R}}$		0.9118	0.3238	−0.2526
		0.3654	−0.9204	0.1393
		−0.1874	−0.2193	−0.9575
		ξ_1	ξ_2	ξ_3
correlations	Z_1	0.3347	0.0000	−0.0000
	Z_2	0.0052	0.1936	0.0000
t-statistics	Z_1	23.6478	0.0000	−0.0000
	Z_2	0.3469	13.1349	0.0000
p-values	Z_1	0	1.0000	1.0000
	Z_2	0.7286	0	1.0000
Wald test	distribution	statistic	critical value	p-value
symmetric spillovers	$\chi^2_{(4)}$	107.85	9.4877	0.0000

Table 1.4: Estimation results of the structural MGARCH model of the demeaned daily log returns of the S&P 500 Composite Index (SP500), the yield of the U.S. constant maturity 10 year treasury note (FRTCM10) and the Finex U.S. Dollar Index (NDXCS00) from 1/1/1998 to 12/31/2014 when using the stock market index (Z_1) and bond market sentiment (Z_2) TRMIs as proxy variables. The table shows, from top to bottom, the estimated rotation angles, the estimated rotation matrix and the correlations of the proxies with the inferred structural shocks ξ_1, ξ_2 and ξ_3 including Wald test for symmetry of volatility spillovers.

	proxy-MGARCH model		
Statistic	ξ_1	ξ_2	ξ_3
Mean	-0.0106	0.0023	0.0077
Median	0.0224	-0.0022	0.0117
Minimum	-7.2849	-4.6486	-4.3832
Maximum	3.6610	7.3030	5.4038
Std. Dev.	0.9903	1.0027	1.0006
Skewness	-0.4683	-0.0190	0.1615
Kurtosis	4.7569	5.0415	4.0728
	Ljung-Box test for serial correlation		
Lag order	p-value ξ_1	p-value ξ_2	p-value ξ_3
$l = 5$	0.1631	0.0868	0.0769
$l = 10$	0.2133	0.1756	0.3679
$l = 15$	0.2607	0.1660	0.3881
	Correlation		
	ξ_1	ξ_2	ξ_3
ξ_1	1.0000	0.0179	0.0171
ξ_2	0.0179	1.0000	-0.0242
ξ_3	0.0171	-0.0242	1.0000
p-values ξ_1	0	0.2331	0.2544
p-values ξ_2	0.2331	0	0.1068
p-values ξ_3	0.2544	0.1068	0

Table 1.5: Descriptive statistics of the inferred structural shocks of the structural MGARCH model of the demeaned daily log returns of the S&P 500 Composite Index (SP500), the yield of the U.S. constant maturity 10 year treasury note (FRTCM10) and the Finex U.S. Dollar Index (NDXCS00) from 1/1/1998 to 12/31/2014 using the stock market index and bond market sentiment as proxy variables.

1.4.3 Volatility spillovers

One of the most important application of MGARCH models is the analysis of volatility transmission mechanisms between several markets (Bauwens et al., 2006). Given the identified labeled structural shocks, we now analyze the volatility spillovers implied by these economically interpretable shocks. To this end, we define the following two measures for volatility reception and transmission. Let $i, j \in \{1, \ldots, n\}$. Then volatility reception and transmission between i and j is measured by

$$VR_{t,i\leftarrow j} = \frac{q_{t,ij}^2}{\sum_{l=1}^{k} q_{t,il}^2} \quad \text{(volatility reception)} \tag{1.25}$$

$$VT_{t,i\rightarrow j} = \frac{q_{t,ij}^2}{\sum_{l=1}^{k} q_{t,lj}^2} \quad \text{(volatility transmission)} \tag{1.26}$$

where $q_{t,ij}$ denote the matrix entries of the identified Q_t. Volatility reception measures the share of the impact of the j-th structural shock on the i-th return in relation to the impact of all other shocks on this component. Volatility transmission measures the share of the impact of the i-th structural shock on the j-th return component in relation to its impact on all return components in the system. This definition follows a similar concept as the spillover measures defined by Diebold and Yilmaz (2012) and Fengler and Herwartz (2018) and can be understood as a 0-order forecast error variance decomposition.

Figures 1.3 and 1.4 show the volatility reception and transmission mechanisms implied by the structural model. We focus first on the reception mechanisms in Figure 1.3. Understandably, the equity shock contributes the most to S&P 500 return fluctuations, about 80% (see Figure 1.3a). The dominance becomes stronger since the financial crisis (2008) and remains elevated in the subsequent five years where the contribution amounts to up to 100%. While the equity shock accounts for the largest share in S&P 500 return fluctuations, the bond market shock shows notable contributions especially during calm market periods (see Figure 1.3b). This aligns well with Boyd et al. (2005), who finds evidence of strong responses of the U.S. equity market to macroeconomic news dependent on the economic conditions. With regard to the relative influence of the currency shock on the S&P 500 returns, there seems to exist a relatively stable base level of volatility reception of around 7% paired with an absence of volatility reception during the quantitative easing efforts of the Fed (see Figure 1.3c).

Turning to the second row in Figure 1.3, we see that the return on the yield shows a comparably lower but pronounced volatility reception of on average if 20% coming from

the equity shock (see Figure 1.3d). This reception strength increases in the course of the DotCom crisis from 2000 to 2003 from a level close to zero to almost 60%, before dropping to about 15% in 2003 and remaining stable until 2007. Subsequently, the link becomes strong again during the financial crisis (2007 - 2008) and the Euro zone crisis (2009 - 2014). Naturally, the bond market shock contributes the most to movements in the yield (see Figure 1.3e), whereas the currency shock exhibits almost no influence (see Figure 1.3f) on yield variations. The observation that currency shocks contribute little to the volatility of equity and bond returns aligns well with the findings, e.g., of Cenedese and Mallucci (2016).

Finally, the third row of Figure 1.3 depicts the volatility reception of the Finex return from the structural shocks. While the contribution of the equity shock to movements in the index returns is close to zero from 1998 to 2008, from the end of September 2008 to the end of May 2013 we observe a sudden surge in volatility reception to levels of 20% and more from the equity shock (see Figure 1.3g). The latter time span corresponds to a period of low interest rates reflecting the quantitative easing measures of the Fed and consequential depreciations of the USD. Figure 1.3h documents a relatively strong influence of the bond market shock on the Finex return which is in line with the finding by Andersen et al. (2003) that U.S. macroeconomic news has a significant effect on the USD - EUR exchange rate. According to Figure 1.3i the currency shock contributes the most to movements in the returns. However, it seems to lose in terms of relative importance over the sample period with its contribution dropping from a level of close to 100% to around 80%.

Figure 1.4 documents the volatility transmission mechanisms. As a most striking observation we observe secular trends in volatility transmission between equity and fixed income markets (see Figures 1.4a and Figures 1.4d): The relative importance of the equity shock on the S&P 500 return decreases in relation to its impact on all return components in the system from approximately 80% to 50%, whereas the relative importance of the equity shock on the treasury yield increases simultaneously from 20% to a level around 50%. While we may find such observations natural in light of quantitative easing measures of the Fed, our analysis reveals that this trend started much before the financial crisis in 2008. This finding complements a strand of literature suggesting a strong link between fixed income and equity markets (Rigobon and Sack, 2003; Ehrmann et al., 2011).

The transmission mechanism from the bond market shock to the S&P 500 return weakens over time, decreasing from levels of around 10% at the turn of the millennium to close to zero by 2008; see Figure 1.4b. Figure 1.4e shows that this shift is mirrored in a stronger

transmission of the bond market shock to the treasury yield return over time.

Finally, the currency shock exhibits a distinct volatility transmission pattern on each return component. We observe the strongest total shock contribution in Figure 1.4i. The transmission strength on the Finex return seems to fluctuate around a stable mean level of 70%. In contrast, we observe surges in transmission strength to the S&P 500 return from 1998 to 2004 and from 2006 to 2009. While the transmission level to the treasury yield returns is generally low at levels below 20%, it increases in the aftermath of the financial crisis, reaching a maximum of 60% during the Euro zone crisis in 2012. These observations support the interpretation of the third shock as a currency shock.

1.5 Conclusion

We have introduced a proxy-based structural MGARCH model which extends the reduced form MGARCH model to a structural model in the macroeconometric sense. It guarantees flexible modeling of the multivariate volatility dynamics of daily returns and simultaneously identifies the underlying shock system and the shock propagation channels by delivering labeled structural shocks. Indeed, it is even possible to connect each shock component to specific news items and financial market events. Our identification strategy allows for full identification of the rotation angles of the structural rotation by means of a general recurrence scheme using Givens rotations which ensures orthogonality of the resulting shocks. In an empirical application to a system of equity, bond and foreign exchange returns, we obtain readily interpretable structural shocks and can reveal structural volatility reception and transmission patterns between the three markets. In particular, the volatility spillover mechanism departs from symmetric spillovers as implied by spectral decompositions as a typical ad hoc solution of the identification problem. The interpretation of the model-implied structural shocks can be narratively corroborated.

Our structural approach to multivariate volatility modeling opens multiple pathways to further research. For example, it could be appealing to allow for time variation in the rotation matrix to reflect secular trends in the economy. Future research may also consider embedding our approach in a large-dimensional MGARCH system which is driven by a small set of proxy-identified factors.

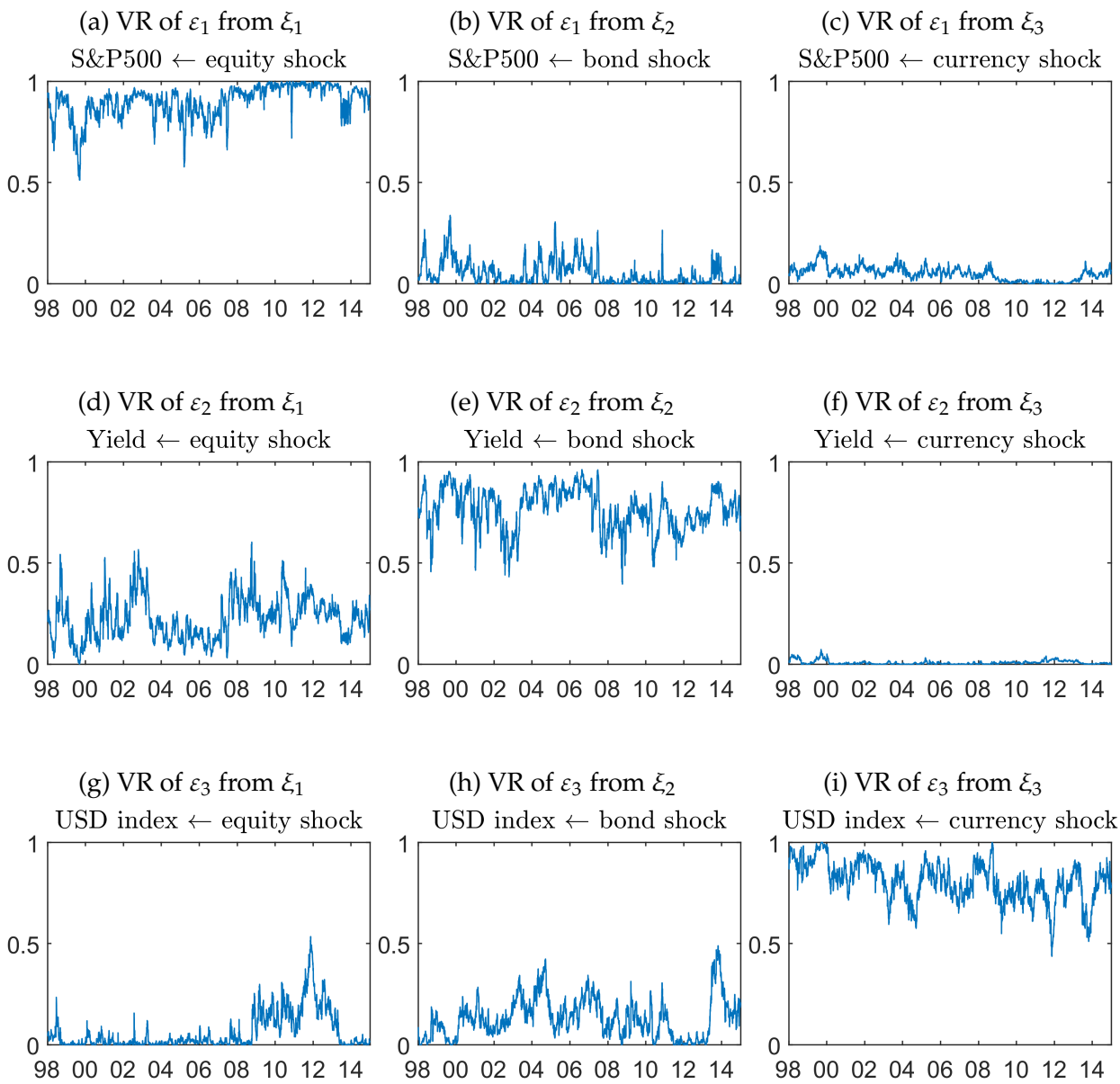

Figure 1.3: Volatility reception of the structural MGARCH model of the demeaned daily log returns of the S&P 500 Composite Index (SP500), the yield of the U.S. constant maturity 10 year treasury note (FRTCM10) and the Finex U.S. Dollar Index (NDXCS00) from 1/1/1998 to 12/31/2014 when using the stock market index (Z_1) and bond market sentiment (Z_2) TRMIs as proxy variables.

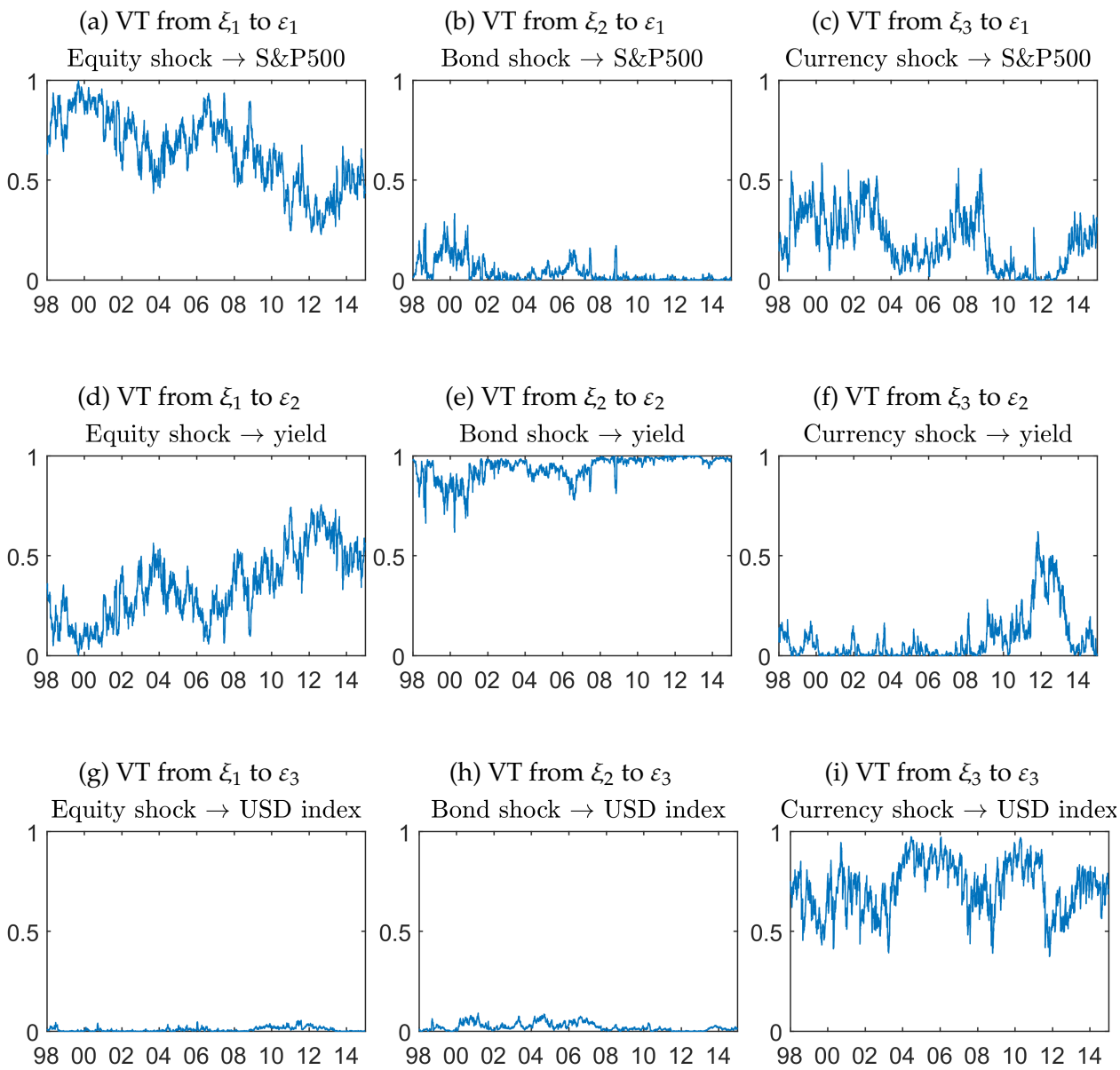

Figure 1.4: Volatility transmission of the structural MGARCH model of the demeaned daily log returns of the S&P 500 Composite Index (SP500), the yield of the U.S. constant maturity 10 year treasury note (FRTCM10) and the Finex U.S. Dollar Index (NDXCS00) from 1/1/1998 to 12/31/2014 when using the stock market index (Z_1) and bond market sentiment (Z_2) TRMIs as proxy variables.

1.A Rotation theory

Rotation matrices provide an algebraic description of rotations performed about the origin in Euclidean spaces. They can be characterized as orthogonal matrices with determinant equal to one. The set of all n-dimensional matrices fulfilling these properties is known as the special orthogonal group $SO(n) = \{R \in \mathbb{R}^{n\times n},\ R^{-1} = R^\top,\ \det(R) = +1\}$, which is non-abelian for $n > 2$, i.e. the multiplication of rotation matrices is not commutative. Multiplication of rotation matrices corresponds to compositions of rotations. Every rotation in an n-dimensional space can be expressed as a composition of $\frac{n(n-1)}{2}$ elemental rotations. Geometrically, these elemental rotations, called Givens rotations (Givens, 1958), correspond to sequences of rotations taking place in two-dimensional planes that are embedded in the n-dimensional space. The $\binom{n}{2}$ ways to position two-dimensional planes in $\mathbb{R}^n$ correspond to the postulated $\frac{n(n-1)}{2}$ elemental rotations. Let θ_{ij} denote the angle of rotation in direction of axis x_j in the embedded plane in $\mathbb{R}^n$ spanned by the axes x_i, x_j ($i, j \in \{1, \dots, n\}$, $i \neq j$). Then the elemental rotation R^{ij} holds all dimensions – apart from i, j – fixed through an underlying identity matrix scheme. Premultiplication of an n-dimensional vector by $R^{ij}(\theta_{ij})$ corresponds to a rotation by θ_{ij} radians in the plane spanned by coordinate axes i and j as (27) illustrates (zero entries are omitted).

$$R^{ij}(\theta_{ij}) = \begin{array}{c} \\ \\ \\ i \\ \\ \\ \\ j \\ \\ \\ \\ \end{array} \begin{array}{c} \begin{array}{ccccccccccc} & & & i & & & & j & & & \end{array} \\ \begin{pmatrix} 1 & & & & & & & & & & \\ & \ddots & & & & & & & & & \\ & & 1 & & & & & & & & \\ & & & \cos(\theta_{ij}) & & & & -\sin(\theta_{ij}) & & & \\ & & & & 1 & & & & & & \\ & & & & & \ddots & & & & & \\ & & & & & & 1 & & & & \\ & & & \sin(\theta_{ij}) & & & & \cos(\theta_{ij}) & & & \\ & & & & & & & & 1 & & \\ & & & & & & & & & \ddots & \\ & & & & & & & & & & 1 \end{pmatrix} \end{array} \tag{27}$$

The convention of each angle representing a rotation about a distinct fixed axis is commonly referred to as a Tait-Bryan system. It makes our calculations tractable as we always keep at least one dimension fixed. A rotation of a vector around one specific fixed axis, requires $n - 1$ elemental rotations. Keeping our coordinate system fixed and rotating the vector instead of proceeding vice versa, we perform so-called active or extrinsic rotations. This choice appears most reasonable in an economic setting for comparison reasons because it

keeps the initial reference frame fixed. For a positive angle $\theta_{ij} > 0$, the elemental rotation occurs counterclockwise in a right-handed coordinate system. Intuitively, the inverse of the corresponding rotation matrix corresponds to a clockwise rotation in the plane by the same angle. We perform rotations both in counterclockwise and clockwise directions, when facing the positive direction of an axis, such that all rotation angles can be positive and negative. This is especially convenient in an economic application as it allows the rotation matrix to deviate in both angle directions from the identity matrix as an initial state where volatility transmission and reception between assets are symmetric.

1.B Illustrative example

For illustration, we give here the rotation matrix and its decomposition into elemental matrices in the four-dimensional case explicitly. As explained in Appendix 1.A, a four-dimensional rotation can be decomposed into six elemental rotations. According to (1.15), the four-dimensional rotation is described by

$$\tilde{R}^{(4D)} = \prod_{i=1}^{3} \prod_{j=i+1}^{4} R^{ij}(\theta_{ij}) = \underbrace{R^{12}R^{13}R^{14}\,\underbrace{R^{23}R^{24}\,\underbrace{R^{34}}_{=\tilde{R}^{(2D)}}}_{=\tilde{R}^{(3D)}}}_{=\tilde{R}^{(4D)}} \tag{28}$$

such that it nests all lower-dimensional rotations in descending order. Holding for example the first coordinate axis fixed, only a three-dimensional rotation composed by the three elemental rotations $R^{23}R^{24}R^{34}$ remains. The four-dimensional rotation is given explicitly by:

$$\begin{aligned}
\tilde{R}^{(4D)} &= R^{12}R^{13}R^{14}R^{23}R^{24}R^{34} \\
&= \begin{pmatrix} c_{12} & -s_{12} & 0 & 0 \\ s_{12} & c_{12} & 0 & 0 \\ 0 & 0 & 1 & 0 \\ 0 & 0 & 0 & 1 \end{pmatrix} \begin{pmatrix} c_{13} & 0 & -s_{13} & 0 \\ 0 & 1 & 0 & 0 \\ s_{13} & 0 & c_{13} & 0 \\ 0 & 0 & 0 & 1 \end{pmatrix} \begin{pmatrix} c_{14} & 0 & 0 & -s_{14} \\ 0 & 1 & 0 & 0 \\ 0 & 0 & 1 & 0 \\ s_{14} & 0 & 0 & c_{14} \end{pmatrix} \\
&\quad \begin{pmatrix} 1 & 0 & 0 & 0 \\ 0 & c_{23} & -s_{23} & 0 \\ 0 & s_{23} & c_{23} & 0 \\ 0 & 0 & 0 & 1 \end{pmatrix} \begin{pmatrix} 1 & 0 & 0 & 0 \\ 0 & c_{24} & 0 & -s_{24} \\ 0 & 0 & 1 & 0 \\ 0 & s_{24} & 0 & c_{24} \end{pmatrix} \begin{pmatrix} 1 & 0 & 0 & 0 \\ 0 & 1 & 0 & 0 \\ 0 & 0 & c_{34} & -s_{34} \\ 0 & 0 & s_{34} & c_{34} \end{pmatrix}
\end{aligned}$$

$$
\begin{aligned}
&= R^{12}R^{13}R^{14}\begin{pmatrix} 1 & 0 & 0 & 0 \\ 0 & c_{23}c_{24} & -c_{34}s_{23}-c_{23}s_{24}s_{34} & -c_{23}c_{34}s_{24}+s_{23}s_{34} \\ 0 & c_{24}s_{23} & c_{23}c_{34}-s_{23}s_{24}s_{34} & -c_{34}s_{23}s_{24}-c_{23}s_{34} \\ 0 & s_{24} & c_{24}s_{34} & c_{24}c_{34} \end{pmatrix} \\
&= \begin{pmatrix} c_{12}c_{13}c_{14} & * & * & * \\ c_{13}c_{14}s_{12} & * & * & * \\ c_{14}s_{13} & * & * & * \\ s_{14} & c_{14}s_{24} & c_{14}c_{24}s_{34} & c_{14}c_{24}c_{34} \end{pmatrix}
\end{aligned} \tag{29}
$$

where we keep those entries which allow for the straightforward identification of the angle parameters associated with the first column of the rotation matrix.[14] The domains of $\theta_{12}, \theta_{23}, \theta_{34}$ are $[-\pi, \pi)$ and $[-\frac{\pi}{2}, \frac{\pi}{2})$ for all others. Clearly, knowing the first column of the rotation matrix, $\tilde{R}^{(4D)}_{\bullet 1}$, allows one to infer θ_{12}, θ_{13} and θ_{14} through a recursive scheme described in Appendix 1.C. Having identified these angles and holding the associated first coordinate axis fixed, see the entries marked in yellow, the same recursive scheme can be applied to the three-dimensional sub-rotation etc.

1.C Implementation of recurrence scheme

In case a two-argument arctan function, which returns values lying in the specified angle domains and takes into account signs, is available,[15] the following recursive identification scheme is numerically preferable to solving equations (1.17) and (1.18): The angles $\theta_{i,(i+1)}$ $(i = 1, \ldots, n-1)$ $(\theta_{i,(i+1)} \in [-\pi, \pi)$ are recovered from

$$
\begin{aligned}
\tan(\theta_{i,(i+1)}) &= \tilde{R}^{(n-i+1)D}_{i+1,i} / \tilde{R}^{(n-i+1)D}_{ii} \\
\operatorname{sign}(s_{i,(i+1)}) &= \operatorname{sign}\left(\tilde{R}^{(n-i+1)D}_{i+1,i}\right) \\
\operatorname{sign}(c_{i,(i+1)}) &= \operatorname{sign}\left(\tilde{R}^{(n-i+1)D}_{ii}\right)
\end{aligned} \tag{30}
$$

and $\theta_{ij} \in \left[-\frac{\pi}{2}, \frac{\pi}{2}\right)$ with $i = 1, \ldots, n-1$ and $j = i+2, \ldots, n$ follow from

$$
\begin{aligned}
\tan(\theta_{ij}) &= \left(\tilde{R}^{(n-i+1)D}_{ji} s_{i,(j-1)}\right) / \tilde{R}^{(n-i+1)D}_{(j-1),i} \\
\operatorname{sign}(s_{ij}) &= \operatorname{sign}\left(\tilde{R}^{(n-i+1)D}_{ji}\right).
\end{aligned} \tag{31}
$$

[14] The remaining columns become arbitrarily complex analytic forms of trigonometric functions with increasing dimensionality.

[15] Such a function is available in Matlab under the name "atan2."

Similarly to the previous setting, if any term $s_{i,(j-1)}$ should be equal to $\tilde{R}^{(n-i+1)D}_{(j-1),i}$ all subsequent entries $\tilde{R}^{(n-i+1)D}_{k,i}$, $k = j, \ldots, n$ cannot be determined and the remaining angles θ_{ik} in this row of Θ are set to zero.

1.D Tables

Structural shocks to the stock market		
Date	Shock	Event
04-Aug-1998	-2.9618	U.S. stock markets decline amid growing concerns over Asian economic pressures and political uncertainty around the impeachment of Clinton.
27-Aug-1998	-3.7164	U.S. stock markets decline amid concerns over a global economic downturn due to Russian market turmoil and ruble slide.
31-Aug-1998	-4.4438	U.S. stock markets decline amid uncertainty over the political and economic future of Russia and signs of an economic slow down in the U.S.
19-Apr-1999	-2.7502	U.S. stock markets decline amid investor flight from technology stocks.
23-Sep-1999	-3.0031	U.S. stock markets decline amid weakening dollar and growing concerns that the Fed may raise interest rates at next meeting.
15-Oct-1999	-2.5433	U.S. stock markets decline amid news of ising wholesale inflation and a warning by Greenspan.
04-Jan-2000	-5.8713	U.S. stock markets decline amid Fed rate hike fears.
24-Jan-2000	-3.2366	U.S. stock markets decline amid Fed rate hike fears.
18-Feb-2000	-2.8143	U.S. stock markets decline amid Fed rate hike fears despite tame inflation news after Greenspan's semi-annual Humphrey-Hawkins testimony; Double witching adds to volatility.
07-Mar-2000	-1.9049	U.S. stock markets decline amid a surprise profit warning from a big blue chip prompting investors to sell-off old economy stocks.
14-Apr-2000	-4.4173	NASDAQ crash and Dot-Com crisis until March 2003; Activation of circuit breakers at the NYSE due to fear sales because of rising inflation and overvalued tech companies.
02-Jan-2001	-2.8476	U.S. stock markets decline amid growing concerns about falling index of manufacturing prompting technology and industry stocks to plunge.
12-Mar-2001	-3.9358	U.S. stock markets decline amid number of factors, including inflated stock prices and weak corporate profits.
08-Aug-2001	-2.8189	Black Monday; U.S. and global stock market crash following the credit rating downgrade of the U.S. souvereign debt by S&P.
17-Sep-2001	-3.3468	U.S. stock markets decline as trading resumes following 9/11 terrorist attacks; Dow Jones industrial average suffers its worst point-loss in history.
29-Jan-2002	-3.4876	U.S. stock markets decline after Tyco International sparkes worries that more companies will downwardly restate financial results like Enron before going bankrupt. Recent bankruptcies of Enron, Kmart and Global Crossing.
15-Apr-2005	-2.8127	U.S. stock markets decline amid weak New York Empire State index, weak Consumer Sentiment index and IBM's earnings miss.
20-Jan-2006	-2.7175	U.S. stock markets decline amid earnings jitters and rising oil prices due to Iran's nuclear ambitions; Dow and S&P post biggest one day drop in nearly 3 years.
27-Feb-2007	-7.2849	Federal Home Loan Mortgage Corporation (Freddie Mac) announces that it will no longer buy the most risky subprime mortgages and mortgage-related securities.
26-Jul-2007	-2.7547	U.S. stock markets decline amid concerns about credit, housing markets and energy prices; Homebuilding companies D.R. Horton and Pulte Homes post huge losses; Commerce Department reports sharp drop in new home sales in June.
19-Oct-2007	-3.2562	U.S. stock markets decline amid fears about credit and housing sector, earnings, record-high oil prices and the slide in the USD; Wachovias earnings fall beyond forecasts due to credit market turmoil.
01-Nov-2007	-2.8839	Citigroup downgrade by CIBC analyst reignites credit concerns fueling fears that other major financial players were harder hit by this summer's subprime crisis than originally anticipated.
05-Feb-2008	-2.8107	U.S. stock markets decline amid ISM services index showing business activity falling in January for the first time in five years. Comments by Richmond Fed President Jeffrey Lacker suggest risks of a recession (stagflation).
06-Jun-2008	-2.8459	Crude prices' largest one-day advance ever (oil price shock) and the biggest one-month surge in over 20 years in the unemployment rate.
04-Sep-2008	-3.1129	U.S. stock markets decline amid mixed retail sales reports, weak job market news and an oil price slide magnifying fears about a global slowdown.
15-Sep-2008	-3.7002	Lehman Brothers Holdings Inc. bankruptcy. Bank of America announces its intent to purchase Merrill Lynch & Co.
29-Sep-2008	-4.3746	U.S. House of Representatives rejects the Emergency Economic Stabilization Act of 2008 (bailout plan); Stock market crash.
20-Jan-2009	-2.8270	Financial shares decline among weak earnings and after Royal Bank of Scotland (RBS) warned that it may report a loss of USD 41.3 billion – the biggest loss in British corporate history – on Monday.
01-Oct-2009	-2.9322	U.S. stock markets decline amid Supply Management's September ISM index unexpected fall and weekly jobless claims jumping more than expected.
04-Feb-2010	-3.2186	U.S. stock markets decline amid China curbing lending and sovereign debt issues in Greece, Portugal and Spain.
27-Apr-2010	-3.5608	Global stock markets decline after Greece's sovereign credit rating downgrade by S&P to junk four days after the activation of an EU-IMF bailout; EUR declines. European sovereign debt crisis severes.
06-May-2010	-2.8691	Flash Crash of 2010.
11-Aug-2010	-2.8398	U.S. stock markets decline after Fed announcement of QE2 the previous day; VIX spike.
28-Jan-2011	-2.9663	U.S. and Japan receive sharp warnings from IMF and rating agencies to tackle their budget deficits; Economic indicators below expectations.
22-Feb-2011	-3.2615	Global stock markets decline amid tensions in the Middle East and North Africa (Lybia) sending oil and gold prices soaring.
01-Jun-2011	-3.3788	U.S. stock markets decline after Moody's cut Greece's bond rating by three notches to Caa1 in even lower junk level.
02-Aug-2011	-2.7311	U.S. stock markets decline after fiscal cliff and worries about the U.S. economy.
04-Aug-2011	-4.3829	Global stock markets decline due to continuing high foreclosure rates in the U.S and the European debt crisis (Italy, Spain); Vix spike (uncertainty shock).
08-Aug-2011	-4.1879	Global stock markets decline due to the widening eurozone government debt crisis and Friday's U.S. rating downgrade.
07-Nov-2012	-2.9667	Global stock markets decline amid U.S. fiscal cliff and weak economic outlook for economic growth in Europe; Mario Draghi warns of an economic slowdown in Germany in the course of European debt crisis.
25-Feb-2013	-2.7030	U.S. stock markets decline amid political uncertainty in Italy connected to the European debt crisis. Vix spike (uncertainty shock).
15-Apr-2013	-3.2814	Global stock markets decline amid report of Boston explosions; China reports economic growth slow down in Q1; Gold price plunges.
24-Jan-2014	-3.1215	Global stock markets decline amid emerging market bond and currency turmoil surrounding the fragile five (Brazil, India, Indonesia, SA and Turkey).
31-Jul-2014	-3.1547	Global stock markets decline amid Argentinian debt crisis.
25-Sep-2014	-2.9306	U.S. stock markets decline amid worries about global growth (economic slowdown in Europe, no more stimulus measures in China) and geopolitical tension (Ukraine conflict); VIX spikes.

Table 1.6: Narrative corroboration of the lower 1%-quantile of the equity shock of the unrestricted BEKK model of the system of daily log returns of the S&P 500 Composite Index (SP500), the yield of the U.S. constant maturity 10 year treasury note (FRTCM10) and the Finex U.S. Dollar Index (NDXCS00) from 1/1/1998 to 12/31/2014 when using the stock market index (Z_1) and bond market sentiment (Z_2) TRMIs as proxy variables. News items are extracted from market reports on money.cnn.com and news articles from the Wall Street Journal news archive on wsj.com.

Structural shocks to the bond market		
Date	Shock	Event
30-Apr-1998	2.5518	Inflation and unemployment data quell fears of a Fed interest rate hike.
27-Aug-1998	2.4515	U.S. stock markets decline amid russian ruble crisis causing investors to flock to the relative safety of government securities.
10-Sep-1998	4.0574	Economic and political uncertainty over emerging markets, Russia's economic restructuring and U.S. President Bill Clinton's grip on power.
05-Oct-1998	2.5082	Global economic meltdown over emerging market turmoil (Asia, Russia, Brazil).
03-Feb-2000	2.4631	Fed decision to rise interest rates and expected outlook of interest rate hike. Fed announcement of cut back of issuance of long-term debt causes inversion of the yield curve.
22-Feb-2000	2.6358	Inflation data causes treasury bond rally.
20-Jul-2000	3.0104	Fed Monetary Policy report and economic testimony to Congress by Alan Greenspan; U.S. stock market declines amid profit and rate concerns.
05-Dec-2000	3.7927	Greenspan Speech to America's Community Bankers proffering the possibility of interest cuts next year due to economic cool-down; Resolution of presidential election.
02-Jan-2001	3.2043	U.S. stock markets decline amid growing concerns about falling index of manufacturing activity.
18-Apr-2001	2.5140	Fed surprise announcement to cut short-term interest rates by an aggressive half-percentage point to avert a recession.
08-Aug-2001	3.3438	Fed Beige Book Report and better-than-expected auction of new 10-year notes.
13-Sep-2001	3.8082	First day of official trading after 9/11 pushing treasury yields to historic lows.
26-Jun-2002	2.5152	Fed interest rate announcement. WorldCom Inc. accounting scandal and SEC investigations among big companies causing investors to flock to the relative safety of government securities.
31-Jul-2002	2.7118	Fed Beige Book Report shows worse-than-expected economic reports. U.S. stock markets decline amid profit warnings in the chip and retail sectors.
07-Nov-2002	2.7725	U.S. stock markets decline in a sell-off after a months rally. Previous day's Fed decision to cut interest rates surprisingly sharply signals concerns with weakening U.S. economy.
06-May-2003	2.4345	Fed decision to leave interest rates unchanged; Warning about the risks of continued economic weakness.
05-Mar-2004	3.8268	U.S. payroll and unemployment data showing slowest pace in wage growth in 18 years and persistent unemployment.
15-Jun-2004	3.3906	Greenspan testimony suggesting that inflation was likely to be contained enough to allow for measured rate hike.
06-Aug-2004	2.6565	U.S. payroll and employment data below estimates and concern about oil supply around Yukos woes causing surge in oil prices.
03-Dec-2004	2.7216	U.S. payroll and employment data below estimates.
04-Feb-2005	2.6553	U.S. payroll and employment data below estimates.
31-Aug-2005	3.6312	Hurricane Katrina raises concerns about the mounting pressures on the U.S. economy from rising energy prices. Prospect of a flat or inverted treasury yield curve.
02-Jun-2006	2.5729	U.S. payroll data below estimates; Data on home prices and manufacturing activity signal economic cool-down.
26-Nov-2007	3.2121	U.S. stock markets slide into correction amid investor concerns that the financial and housing market crisis could send the economy into a recession causing investors to flock to the relative safety of government securities.
15-Sep-2008	3.5972	Lehman Brothers Holdings, Inc. files for Chapter 11 bankruptcy protection and Bank of America announces its intent to purchase Merrill Lynch & Co. for USD 50 billion causing investors to flock to the relative safety of government securities.
04-Nov-2008	2.4869	U.S. presidential election day with Obama as prospective winner. Efforts of U.S. and world governments to stimulate cash flowing to the economy.
25-Nov-2008	3.2765	Fed announcement of QE1
16-Dec-2008	3.8105	Fed decision for aggressive rate cut. Longer-term treasury notes rise amid uncertainty about the bailout of the auto industry. U.S. and European stock markets decline. Prospects of Fed using unconventional tools, e.g. buying longer-dated treasury debt to keep cash flowing to the economy as official lending rates fall toward zero. Regional manufacturing data below estimates and inflation data leading to deflation concerns.
18-Mar-2009	7.3030	Fed's USD 300B pledge to purchase long-term Treasurys over the next six months.
29-May-2009	2.4599	Business activity data in the Midwest below estimates and drop in ISM-Chicago Purchasing Managers Index signals economic cool-down. Upwards correction at U.S. government market after wave of heavy selling Wednesday as mortgage investors shed Treasurys to hedge against rising rates.
10-Sep-2009	2.4555	Fed Beige Book Report raises new concern about consumer spending. Fed statement that rapid rate hike improbable given weakness of global economy.
16-Nov-2009	2.5876	Fed chairman Ben Bernanke speech to the Economic Club of New York stating that economic headwinds will restrain the pace of the U.S. recovery and that reduced bank lending and a weak labour market continue to justify low interest rates.
16-Aug-2010	2.7043	Growing concerns about the global economic outlook (Japan) cause investors to flock to the relative safety of government securities.
13-Sep-2010	2.4036	Fed purchase of USD 3.4 billion in treasury debt as part of the Fed's plan to reinvest cash back into the bond market to help the economic recovery and correction on U.S. government bond markets.
04-Nov-2010	3.8146	Fed announcement of QE2 on 03-Nov-2010 causes yields on U.S. governments bonds to fall.
08-Jul-2011	2.6512	U.S. job data for June below estimates.
29-Jul-2011	3.4123	American Debt Crisis and Q2 GDP report below estimates.
09-Aug-2011	6.3727	Fed statement to keep interest rates exceptionally low until at least 2013.
25-Jan-2012	2.5402	Fed statement to keep interest rates near historic lows through late 2014. Fed chief Ben Bernanke leaves the door wide open to QE3.
06-Apr-2012	2.5742	U.S. payroll and employment data below estimates rekindling doubts about strength of recovery. U.S. jobs report well below estimates raises concerns about the pace of the economic growth causing investors to flock to the relative safety of government securities.
30-May-2012	2.5846	European Debt Crisis (Spanish banking system) causes investors to flock to the relative safety of U.S. government securities.
22-Aug-2012	2.5062	Fed appears ready to take action e.g. by bond buying to stimulate the economy according to FOMC minutes.
18-Sep-2013	3.9394	Fed surprise announcement not to slow down the pace of its bond purchases yet.
14-Oct-2014	3.0677	Global stock market decline amid fears of a global economic slowdown, fighting in the Middle East, gepolitical tensions between West and Russia and the spread of the Ebola virus cause investors to flock to the relative safety of government securities.

Table 1.7: Narrative corroboration of the upper 1%-quantile of the bond shock of the unrestricted BEKK model of the system of daily log returns of the S&P 500 Composite Index (SP500), the yield of the U.S. constant maturity 10 year treasury note (FRTCM10) and the Finex U.S. Dollar Index (NDXCS00) from 1/1/1998 to 12/31/2014 when using the stock market index (Z_1) and bond market sentiment (Z_2) TRMIs as proxy variables. News items are extracted from market reports on money.cnn.com and news articles from the Wall Street Journal news archive on wsj.com.

Structural shocks to the fx market		
Date	Shock	Event
23-Jan-1998	3.0030	Asian financial and fx markets crisis, plunge in Asian currencies.
08-Apr-1998	2.5871	The USD loses over one Yen on talk of Japanese tax cut; stock prices slide on more worries about tech sector.
28-Aug-1998	4.4628	Russian tremors on Wall Street. The USD fell against the Japanese Yen after Tokyo stock market slide and against the German mark.
07-Oct-1998	5.4038	Yen's spectacular climb against the dollar continues. USD plunge against the Japanese Yen.
08-Jun-1999	3.2069	Comments from OPEC spur rally in oil futures. Gold falls.
06-Dec-1999	2.8206	White House has no plans to tap oil reserves to offset high prices. Gold falls. The USD weakens against Yen, the EUR slides to parity with the USD. Worries about rising rates evaporate over positive employment data.
03-Jan-2000	3.6997	The USD is lower against the Yen and the EUR.
12-May-2000	3.4002	Crude oil hits USD 30. USD gains on EUR, but slides against Yen. Stocks rally on U.S. gains. ECB interest rate decision.
03-Apr-2001	2.9949	Dollar soars against Yen as Japan outlook worsens. Crude-Oil futures hit lowest level of the year.
17-Sep-2001	5.3010	Trading resumed for the first time after 9/11. Markets are down and gold and oil rally. The dollar finished little changed against the EUR and Yen.
07-Mar-2002	3.3575	Shares tumble on rate jitters amidst Fed Greenspan testimony. USD sinks against the Yen and the EUR.
17-May-2002	2.8494	Tech stocks gain and Gold prices on the rise.
20-Jun-2002	2.5645	Jump in Oil prices sends trade gap to record level.
08-Jul-2002	2.6248	USD drops against Yen and EUR, Gold stocks continue to soar. Technology stocks dropped.
05-Jun-2003	3.0461	USD plummets against EUR on ECB cut. Weak U.S. job data.
22-Sep-2003	2.9737	Techs drop amid USD weakness. G-7 endorsement of flexible exchange rates lifts Asian currencies.
18-Nov-2003	2.8640	Strong Euro.
30-Sep-2004	2.7684	Dollar weakens against Yen. Tech stocks inch higher, oil price rally.
05-Nov-2004	2.7029	Gold vaults higher on weak USD, oil prices drive ECB to consider a rate increase. China may be ready to loosen Yuan peg.
22-Feb-2005	3.2807	Techs drop amid rising oil prices.
12-Jul-2005	2.6037	USD suffers broad decline, China reports surge in trade surplus.
01-Sep-2005	3.0657	U.S. releases oil from reserve to ease crunch in the aftermath of hurricance Katrina. USD falls on oil impact.
06-Oct-2005	3.5692	Stocks fall despite oil slide, Tech shares fall ahead of earnings season.
25-Oct-2005	2.7736	Cold front causing energy prices to jump and stocks to slide. USD slips after Bernanke news.
28-Nov-2005	2.5890	Gold price on the rise, Gold tops USD 500 in after-hours trade.
30-Mar-2006	2.7642	USD declines on Yen and EUR. U.S. officials urge China on markets, Yuan.
30-May-2006	3.2148	Major markets sink amid rising oil prices and sliding U.S. consumer confidence. Paulson appointed Treasury secretary.
24-Nov-2006	2.5682	Stocks fall on weaker USD. Rally in commodities markets.
03-Aug-2007	2.5689	Markets down among credit market fears and Bear Stearns debt rating downgrade. USD falls against the EUR and the Yen.
20-Sep-2007	4.8135	USD dips at an all-time low against the EUR, oil boils, metals shine.
07-Nov-2007	3.2403	Weakening USD, Gold trading higher, Crude oil nears USD100 a barrel.
24-Jan-2008	2.9601	Nasdaq advances on Tech earnings, USD falls versus the Yen and EUR. Gold rallies.
12-Sep-2008	3.0098	Dollar weak, commodity prices down, VIX soaring. Lehman Slides 42%. Euro Rallies on Weak U.S. Data. Fixed-Rate 30-Year Mortgages fall below 6% on bailout news.
17-Sep-2008	3.3380	Gold staged its biggest one-day move ever Wednesday, with investors flocking to the metal amid a tidal wave of stock market uncertainty.
		USD dropped Wednesday against the EUR and against the Yen, after news that the Fed would bail out AIG.
22-Sep-2008	3.3505	Oil: Biggest one-day gain ever. USD gets biggest hit in seven years from treasury plan. Commodities gain across the board as the dollar tumbles.
29-Oct-2008	2.7490	Credit crunch hits trade. USD and EUR rise sharply on Yen. Stocks succumb to bleak Fed outlook. Weaking USD propels dollar-traded commodities.
19-Mar-2009	2.8385	Dollar dips due to Fed statement to buy long-term Treasuries. Fed's announcement dampened the dollar's safe-haven appeal, knocking it down from a three-year peak hit against a basket of currencies earlier in the month.
21-Oct-2009	2.7399	The prospect of U.S. interest rates staying at exceptionally low levels for longer than most other major countries sent the greenback sliding. In turn crude oil and other commodities continued their march higher. VIX falls.
20-May-2010	3.3361	The US dollar rose against a basket of major currencies, while oil fell below USD 69 a barrel. Spot gold prices rose.
01-Jul-2010	3.0012	Gold prices plunge over 3%. EUR recovery: short euro/long gold trade appears to be unwinding.
08-Aug-2011	2.7772	Gold soars to record after U.S. downgrade.
29-Jun-2012	2.7401	EU moves boost EUR. Crude Prices Jump 9.4% buoyed by EU summit and renewed anxiety on Iran. Silver Soars 5.1%, Gold Up 3.5%. Risk currencies also got a boost and the USD weakened. Yuan had its biggest quarterly drop ever.
10-Jan-2013	3.0327	Oil rises on Saudi cutback, explosion in Yemen that halted most of the country's oil exports and bullish Chinese trade data. Signs that the ECB will not cut interest rates any time soon boosted bullion buying.
		EUR shoots to 18-month high vs. Yen and hit a one-week peak against the USD.
15-Aug-2013	2.9833	Gold prices settle 2% higher on Mideast tensions and violence in Egypt, home to the strategically important Suez Canal and the Sumed pipeline. USD falls in volatile trade after mixed signals from economic data.

Table 1.8: Narrative corroboration of the upper 1%-quantile of the currency shock of the unrestricted BEKK model of the system of daily log returns of the S&P 500 Composite Index (SP500), the yield of the U.S. constant maturity 10 year treasury note (FRTCM10) and the Finex U.S. Dollar Index (NDXCS00) from 1/1/1998 to 12/31/2014 when using the stock market index (Z_1) and bond market sentiment (Z_2) TRMIs as proxy variables. News items are extracted from market reports on money.cnn.com and news articles from the Wall Street Journal news archive on wsj.com.

Chapter 2

Structural volatility impulse response analysis*

Matthias R. Fengler†, Jeannine Polivka‡

*We are grateful for financial support by the Swiss National Science Foundation (SNF Grant No: 176684, Project "Structural Models of Volatility").

†School of Economics and Political Science, Department of Economics, University of St. Gallen, Bodanstrasse 6, 9000 St. Gallen, Switzerland. Email: matthias.fengler@unisg.ch.

‡School of Economics and Political Science, Department of Economics, University of St. Gallen, Bodanstrasse 6, 9000 St. Gallen, Switzerland. Email: jeannine.polivka@unisg.ch.

Abstract

In this paper, we make three contributions to the volatility impulse response function (VIRF) developed by Hafner and Herwartz (2006), the most widely applied impulse response function in the context of multivariate volatility models. First, we derive its law for multivariate generalized autoregressive conditional heteroscedasticity (MGARCH) models of the BEKK type. Second, we present a structural embedding of the VIRF by relying on recent developments concerning identification of MGARCH models. This broadens the use cases of the VIRF, which has previously been limited to historical analyses, by allowing for counterfactual and out-of-sample scenario analyses of volatility responses. Third, we show how to endow the VIRF with a causal interpretation. We illustrate the merits of a structural VIRF analysis by investigating the impacts of historical shock events as well as the consequences of well-defined future shock scenarios on the U.S. equity, government bond and foreign exchange markets. Our findings suggest that it is vital to be able to assess the statistical significance of volatility impulse responses.

Keywords: causality in volatility, multivariate GARCH models, proxy identification, structural identification, volatility impulse response functions

JEL Codes: C32, C58, G17

2.1 Introduction

The impulse response function (IRF) is the tool of choice for analyzing how dynamic multivariate systems respond to shocks. It shows how an unanticipated perturbation impacts the modeled variables and exhibits how the sign, magnitude and persistence of the response evolve over time. In its standard use case in vector autoregressions, the focus of IRF analysis rests on learning about the feedback in the mean process (Inoue and Kilian, 2013; Lütkepohl, 2010). By contrast, in volatility models of high-frequent speculative asset returns, where the mean equation is often mundane, it is the second-order response that is of commanding interest. For example, a mutual fund manager may be concerned about how the variance matrix of certain asset classes may react to an unforeseen monetary policy shock. In this situation, the volatility impulse response function (VIRF) can afford the relevant insights.

The VIRF, as first conceptualized by Hafner and Herwartz (2006), extends the ideas of the generalized IRF (GIRF) developed by Koop et al. (1996) to second-order moments. It conditions on past information and an exogenous shock component and traces the nonlinear effects of the shocks on volatility dynamics. Among the extant VIRF specifications, the VIRF of Hafner and Herwartz (2006) is especially attractive because it allows a closed-form expression for one of the most general multivariate generalized autoregressive conditional heteroskedasticity (MGARCH) models, the Baba, Engle, Kraft and Kroner or BEKK(p, q) model (Engle and Kroner, 1995), and is also available for the Markov-switching MGARCH (Cavicchioli, 2019). In this work, we take a fresh look at the VIRF and add to the extant literature in three ways: First, we derive the asymptotic distribution of the VIRF in the BEKK model, which is the most frequently applied form in the empirical VIRF literature. More specifically, we show that, like the VIRF, its asymptotic variance matrix can be written as a function of the forecast horizon in a compact recursive form. This allows for an efficient numerical evaluation of confidence intervals, which until now could only be obtained by time-consuming simulation techniques, such as the bootstrap method. Importantly, our empirical analysis suggests that the interpretation of VIRFs without taking into account statistical significance may lead researchers astray because seemingly long-term impacts can be of much shorter-lived significance than one may be tempted to expect.

As a second contribution, we endow the VIRF with a structural interpretation by relying on recent advances regarding identification in MGARCH models (Fengler and Polivka,

2022a; Hafner et al., 2022). This new interpretation materially broadens the use cases of the VIRF, which has previously been limited to historical analyses. A structural volatility model featuring identified and labeled structural shocks raises the curtain for proper scenario analyses, as is common in structural vector autoregressive (VAR) analyses of the mean equation (Amisano and Giannini, 2012; Kilian, 2013). It allows one, e.g., to define counterfactual scenarios and to obtain insights into the average volatility impact of certain families of well-defined shock scenarios. We coin the term "scenario VIRF" for this novel use case. Our third contribution is to empower the VIRF with a causal interpretation. To this end, we build on recent advances on causal inference in the time series context by Rambachan and Shephard (2020, 2021). This allows us to use the microeconometricians' notion of causality when analyzing scenarios relevant for risk management purposes, e.g., the causal effects of tail events in a specific financial market on the asset return system.

Identifying the impact of structural shocks on financial volatility is crucial for models designed for asset price dynamics, risk management and portfolio optimization, and has been investigated by, among others, Gallant et al. (1993), Lin (1997), Hafner and Herwartz (2006) and more recently by Liu (2018) and Cavicchioli (2019). However, despite this long history, structural advances in volatility impulse response analysis have remained in their infancies. The conditional moment profile developed by Gallant et al. (1993) suffers from difficulties in choosing realistic shocks and a useful baseline for setting the conditional volatility profile into context, because it defines the news to appear in the conditionally heteroskedastic errors. Lin (1997) bases his univariate volatility impulse response analysis on reduced-form GARCH models with the result that the shocks lack a structural interpretation. Hafner and Herwartz (2006) tackle the issues of Gallant et al. (1993) by developing a VIRF concept in the spirit of the GIRF devised by Koop et al. (1996). However, their shock identification strategy – while not building on a reduced form model approach as in Lin (1997) – relies on statistical concepts, which does not offer economic interpretability. Its ambit is therefore limited to retrospective historical analyses with model-implied past shocks. Moreover, the majority of the aforementioned studies do not provide asymptotic properties for the statistical inference of their VIRFs. As an initial step toward inferential statistics, Liu (2018) derives confidence intervals for an alternative VIRF definition based on the dynamic conditional correlation (DCC) model. However, he applies his VIRF to shocks which are identified statistically via time-varying heteroskedasticity and thus still do not provide a direct economic interpretation.

The remainder of this paper is structured as follows. Section 2.2 presents the concept of the

VIRF, including rigorous mathematical derivations, derives its asymptotic distribution and establishes the connections to structural and causal modeling. Section 2.3 briefly presents the structural model we use for the identification of the asset return system covering equity, fixed income and foreign exchange markets. It then showcases historical as well as out-of-sample scenario VIRFs for well-defined risk scenarios. Section 2.4 concludes this work. Appendix 2.A provides an overview of the definitions and mathematical prerequisites as well as featuring all the proofs.

2.2 Volatility impulse response analysis

2.2.1 Modeling framework

We consider the system of n speculative (log) returns given by

$$r_t = \mu_t + \varepsilon_t \quad (t \in \mathbb{Z}) \tag{2.1}$$

where $\mu_t = \mathrm{E}[r_t|\mathcal{F}_{t-1}]$ and $\mathcal{F}_t = \sigma(\{\varepsilon_s : s \leq t\})$ denotes the information available up to time t, generating the filtration $\{\mathcal{F}_t\}$. The n-dimensional innovation vector ε_t is assumed to be square-integrable, satisfies $\mathrm{E}[\varepsilon_t|\mathcal{F}_{t-1}] = 0$ ($\mathrm{E}[|\varepsilon_t|] < \infty$) and has the conditional covariance matrix $\mathrm{Var}[\varepsilon_t|\mathcal{F}_{t-1}] = H_t$. The process $(H_t)_{t\in\mathbb{Z}}$ is assumed to be almost surely symmetric, positive definite for all t and covariance stationary, and is by definition $\mathcal{F}$-adapted. We denote by $H_t^{1/2} \in \mathbb{R}^{n\times n}$ the principal matrix square root (see Definition D.1) of H_t which exists for all t and is uniquely defined. Furthermore, we define $\tilde{R}$ to be a structural rotation matrix (see Definition D.2) and $\xi = (\xi_t)_{t\in\mathbb{Z}}$ is an n-dimensional real-valued white noise process of structural shocks with zero mean and identity covariance matrix, i.e., $\xi_t \sim WN(0, I_n)$.

Definition 2.2.1. The process $(\varepsilon_t)_{t\in\mathbb{Z}}$ follows a structural multivariate GARCH process if it satisfies:

$$\varepsilon_t = H_t^{1/2}\tilde{R}\xi_t. \tag{2.2}$$

If $\xi_t \sim SWN(0, I_n)$, $(\varepsilon_t)_{t\in\mathbb{Z}}$ is said to follow a strong structural multivariate GARCH process (Fengler and Polivka, 2022a; Hafner et al., 2022).

The structural rotation matrix $\tilde{R}$ in (2.2) endows the model with a structural interpretation and specifies the propagation channels of the structural shocks. For example, choosing $\tilde{R}$

as the identity matrix implies a symmetric volatility spillover mechanism, as the principal matrix square root preserves the positive definiteness as well as the symmetry of H_t. In contrast, if one chooses the rotation which transforms the principal matrix square root into, e.g., a Cholesky decomposition, the volatility spillovers obey a recursive ordering principle imposed through the triangular structure of the decomposition. Although both are popular ad hoc decompositions, neither specification for $\tilde{R}$ rests on solid economic grounds for asset return systems. Potential avenues for the identification of $\tilde{R}$ include the identification by non-Gaussianity developed by Hafner et al. (2022) and the proxy-based scheme devised by Fengler and Polivka (2022a) which may additionally allow for shock labeling. We sketch the latter identification scheme in Section 2.3.1.

2.2.2 Volatility impulse response functions

In order to assess the impact of a shock ξ_t on volatility given $\mathcal{F}_{t-1}$, Hafner and Herwartz (2006) define the h-step ahead VIRF as the difference between the expected h-step-ahead covariance conditioning on the shock and past information and the expected h-step-ahead covariance conditioning on past information only. This choice of conditioning sets is in the tradition of the GIRF developed by Koop et al. (1996) to address the problems of history, shock and compositional dependence of impulse responses in nonlinear multivariate models (see the discussion at the end of this section).

Definition 2.2.2. We denote by $\tilde{\mathcal{F}}_t = \sigma(\{\xi_t, \varepsilon_s, s \leq t-1\})$, i.e., $\mathcal{F}_{t-1}$ augmented by the structural shock information. Let $h \in \mathbb{N}$. The h-step ahead VIRF is given by:

$$\mathrm{V}_{t+h}(\xi_t) := \mathrm{E}[\mathrm{vech}(H_{t+h})|\tilde{\mathcal{F}}_t] - \mathrm{E}[\mathrm{vech}(H_{t+h})|\mathcal{F}_{t-1}]. \tag{2.3}$$

where the vech operator is defined in Definition D.4. Thus, $\mathrm{V}_{t+h}(\xi_t)$ is an n^*-dimensional vector of impulse responses of the conditional (co-)variances with $n^* = \frac{n(n+1)}{2}$. Note that despite referring to "volatility," the VIRF is in fact a (co-)variance IRF. The definition of the VIRF based on $\tilde{\mathcal{F}}_t$ and $\mathcal{F}_{t-1}$ is motivated by the fact that, in contrast to IRFs for conditional means, there is no natural baseline for volatility based on a fixed return vector. In IRFs for conditional means, a baseline ε_t^0 corresponding to the long-run mean of the process is economically natural. A fixed return baseline, however, cannot represent the steady state of volatility, because $\varepsilon_t^0 \varepsilon_t^{0\top}$ has rank one with probability one. Thus, it cannot coincide with the average volatility state. Hence, instead of artificially adding a shock δ to an arbitrarily chosen baseline level of volatility to generate impulse responses as proposed by Gallant

et al. (1993), Hafner and Herwartz (2006) consider responses to shocks ξ_t.

The VIRF in (2.3) is attractive for two further reasons. On the one hand, for the analysis of responses of volatility to historical shocks, it is sufficient to employ the principal square root of H_t, because the VIRF as a quadratic form is independent of the underlying structural model.[4] This invariance allows one to infer past shocks quickly and efficiently and to calculate corresponding historical VIRFs by means of (2.2) and (2.3) using $\tilde{R} = I_n$; this makes any additional computational effort related to structural modeling redundant in the historical set-up. On the other hand, however, in a scenario analysis, constructing VIRFs based on structural shocks is highly appealing. To begin with, employing a structural model solves the so-called "composition effect" problem (Koop et al., 1996): first, in multivariate models, it is a priori not clear how a shock of interest should be chosen, as it will often have contemporaneous effects on several outcome variables; second, it is unrealistic to observe perturbations in solely one shock while keeping the others fixed, because impulse responses generally depend on compositions of shocks. A structural volatility model, in a similar manner to structural VAR models (see, e.g., Kilian, 2013), specifies the shock composition mechanism and provides an economically meaningful multivariate shock time series. This solves the composition effect problem and allows one to investigate the impacts of specific future market scenarios defined by the labeled structural shocks. Such investigations using scenario VIRFs have not been possible to date, as they critically hinge on the interpretability of the shocks. We stress this aspect further in Section 2.2.5.

2.2.3 The VIRF in the BEKK(p, q) model

To derive closed-form expressions for structural VIRFs, we need to choose a model for the dynamics of the conditional covariance matrix process. Amongst these, the parametric BEKK GARCH models enjoy great popularity (Bauwens et al., 2006) and are most frequently employed in the applied VIRF literature (see, e.g., Jin et al., 2012 and Olson et al., 2014). The n-dimensional process $(\varepsilon_t)_{t\in\mathbb{Z}}$ admits a BEKK(p, q) specification (Engle and

[4]The VIRF traces the effects of shocks on the covariance matrix H_t and not on its structural decomposition $H_t^{1/2}\tilde{R}$. When considering the square of the matrix decomposition, the effect of the structural model vanishes (compare Section 2.2.5).

Kroner, 1995) if H_t satisfies for all $t \in \mathbb{Z}$:

$$H_t = CC^\top + \sum_{i=1}^{p} A_i^\top \varepsilon_{t-i}\varepsilon_{t-i}^\top A_i + \sum_{j=1}^{q} B_j^\top H_{t-j} B_j \quad (p, q \in \mathbb{N}) \tag{2.4}$$

where C is a lower triangular matrix and A_i and B_j are coefficient matrices in $\mathbb{R}^{n\times n}$. The intercept matrix $CC^\top$ is symmetric and positive semi-definite by construction, and strictly positive definite if C has full rank. The latter property ensures the positive definiteness of $(H_t)_{t\in\mathbb{Z}}$. Boussama et al. (2011, Theorem 2.4) show that under weak regularity conditions on $(\xi_t)_{t\in\mathbb{Z}}$, the multivariate BEKK GARCH process is ergodic, strictly and weakly stationary and invertible if the eigenvalues of $\sum_{i=1}^{p} A_i \otimes A_i + \sum_{j=1}^{q} B_j \otimes B_j$ are less than one in modulus. Hafner and Preminger (2009) provide conditions to establish the consistency as well as asymptotic normality of the quasi-maximum likelihood (QML) estimator, assuming inter alia the existence of second-order moments of $(\xi_t)_{(t\in\mathbb{Z})}$ and finite sixth-order moments of $(\varepsilon_t)_{t\in\mathbb{Z}}$. Due to the quadratic structure of the BEKK(p, q) model, the parameter matrices are only identified up to the sign. For the BEKK$(1, 1)$, the model is uniquely identified if one assumes the diagonal elements of C and the first matrix entries of A_1, $a_{11(1)}$, and B_1, $b_{11(1)}$, to be positive.

For the BEKK(p, q) model, a closed-form expression exists for the h-step ahead VIRF (Hafner and Herwartz, 2006). For the sake of completeness, we provide a rigorous derivation in the appendix, which we adapted to the case of a structural model of type (2.2) and which will be of further value in Section 2.2.4.

Proposition 2.2.1. *Assume H_t has the BEKK(p, q) representation given in (2.2) with parameter vector $\eta = \left(\mathrm{vec}(C)^\top, \mathrm{vec}(A_i)^\top, \mathrm{vec}(B_j)^\top\right)^\top$, $(i = 1, \ldots, p;\ j = 1, \ldots, q;\ p, q \in \mathbb{N})$, see D.3 for a definition of $\mathrm{vec}(\cdot)$, and with a VMA(∞) representation with coefficients $(\Psi_i)_{i\in\mathbb{N}}$ as provided in Proposition 2.A.1. Then the h-step ahead VIRF given a structural shock ξ_t is*

$$\mathrm{V}_{t+h}(\xi_t, \eta) = \Psi_h\, D_n^+ \left(H_t^{1/2} \otimes H_t^{1/2}\right) D_n \left(\mathrm{vech}(\tilde{R}\xi_t\xi_t^\top \tilde{R}^\top - I_n)\right) \tag{2.5}$$

where D_n denotes the duplication matrix and D_n^+ its Moore-Penrose inverse (see Definition D.6).

Proof. See Proof (2.1) in Appendix 2.A.2. □

Notably, the IRF is a nonlinear, but even function of the structural shock. As the conditional volatility at the time of the shock occurrence enters the VIRF, it is an $\tilde{\mathcal{F}}_t$-adapted process. The persistence of a shock to volatility is governed by the moving average matrices Ψ_h.

Remark. For the BEKK(1, 1) model with parameter vector η and with VMA(∞) coefficients $\Psi_0 = I_{n^*}$, $\Psi_1 = \tilde{A}_1$ and $\Psi_i = \left(\tilde{A}_1 + \tilde{B}_1\right)\Psi_{i-1} = \left(\tilde{A}_1 + \tilde{B}_1\right)^{i-1}\tilde{A}_1$ $(i \geq 2)$, the VIRF given an initial shock ξ_t and a corresponding variance level H_t reduces to the recursion (Hafner and Herwartz, 2006):

$$\begin{aligned} &\mathrm{V}_{t+h}(\xi_t, \eta) = \left(\tilde{A}_1 + \tilde{B}_1\right)^{h-1} \tilde{A}_1 D_n^+ \left(H_t^{1/2} \otimes H_t^{1/2}\right) D_n \operatorname{vech}(\tilde{R}\xi_t\xi_t^\top \tilde{R}^\top - I_n) \quad (h \geq 1) \\ \Rightarrow\ &\mathrm{V}_{t+h}(\xi_t, \eta) = \left(\tilde{A}_1 + \tilde{B}_1\right) V_{t+h-1}(\xi_t) \quad (h \geq 2). \end{aligned} \tag{2.6}$$

This can be shown by deriving the vech form of the BEKK(1, 1) model, as in Proposition 2.A.1, Equation (A.35), and inserting the VMA(∞) coefficients in (2.5).

2.2.4 Asymptotic law of the VIRF

As our first central contribution, we now complete the notion of the VIRF by providing the asymptotic theory.

Consistency of the VIRF

Proposition 2.2.2. *Let $h \in \mathbb{N}$ and $\xi_t \in \mathbb{R}^n$ arbitrary but fixed. Under the regularity conditions of Hafner and Preminger (2009) and if the VIRF is a continuous function of the parameter vector η of the MGARCH model, $\mathrm{V}_{t+h}(\xi_t, \eta)$ can be estimated consistently by replacing η with its QMLE $\hat{\eta}$.*

$$\mathrm{V}_{t+h}(\xi_t, \hat{\eta}) \xrightarrow{p} \mathrm{V}_{t+h}(\xi_t, \eta) \quad (h \in \mathbb{N}) \tag{2.7}$$

Proof. By continuity and the continuous mapping theorem. □

Remark. The BEKK(p, q) model is continuous in η and therefore the BEKK-VIRF.

Asymptotics of the BEKK-VIRF

Theorem 1. *Let $h \in \mathbb{N}$. Under the regularity conditions of Hafner and Preminger (2009)*[5] *and given continuous differentiability of the BEKK-VIRF as function of $\eta \in \mathbb{R}^m$, we have:*

$$\sqrt{T}\left(\mathrm{V}_{t+h}(\xi_t, \hat{\eta}) - \mathrm{V}_{t+h}(\xi_t, \eta)\right) \xrightarrow{d} N(0, \boldsymbol{V}_\eta(\mathrm{E}[\boldsymbol{\mathcal{H}}(\eta)])^{-1}\boldsymbol{\mathcal{I}}(\mathrm{E}[\boldsymbol{\mathcal{H}}(\eta)])^{-1}\boldsymbol{V}_\eta^\top) \tag{2.8}$$

[5] In particular, assuming that the true parameter η lies inside the compact parameter space $\mathcal{E}$.

where $\boldsymbol{V}_\eta = \frac{\partial \mathrm{V}_{t+h}(\xi_t,\eta)}{\partial \eta^\top}$ *denotes the* $n^* \times m$ *Jacobian matrix of the VIRF with respect to the m-dimensional parameter vector* η*;* $\boldsymbol{\mathcal{H}}(\eta) = \frac{\partial^2 \log(l_t(\eta))}{\partial\eta\partial\eta^\top}$ *is the Hessian matrix of the log-likelihood contribution* $\log(l_t)$ *and* $\boldsymbol{\mathcal{I}} = \mathrm{E}\left[\left(\frac{\partial \log(l_t(\eta))}{\partial\eta}\right)\left(\frac{\partial \log(l_t(\eta))}{\partial\eta^\top}\right)\right]$ *the Fisher information matrix. The* $(n^* \times m)$ *Jacobian of the VIRF with respect to* $\eta \in \mathbb{R}^m$ *is given by*

$$\frac{\partial \mathrm{V}_{t+h}(\xi_t,\eta)}{\partial\eta^\top} = \left(\mathrm{V}_t^\top \otimes I_{\frac{n(n+1)}{2}}\right)\frac{\mathrm{vec}(\Psi_h)}{\partial\eta^\top} + \left(I_{\frac{n(n+1)}{2}} \otimes \Psi_h\right)\frac{\partial \mathrm{V}_t}{\partial\eta^\top} \tag{2.9}$$

where

$$\begin{aligned}\frac{\partial \mathrm{V}_t(\xi_t,\eta)}{\partial\eta^\top} = D^+\Bigg[&\left(\left(H_t^{1/2}\tilde{R}\xi_t\xi_t^\top\tilde{R}^\top \otimes I_n\right) + \left(I_n \otimes H_t^{1/2}\tilde{R}\xi_t\xi_t^\top\tilde{R}^\top\right)\right)\\ &\times\left[\left(H_t^{1/2}\otimes I_n\right) + \left(I_n \otimes H_t^{1/2}\right)\right]^{-1} - I_{n^2}\Bigg]\frac{\partial\,\mathrm{vec}(H_t)}{\partial\eta^\top}\end{aligned} \tag{2.10}$$

and $(\Psi_i)_{i\in\mathbb{N}}$ *denote the coefficients of the VMA(*∞*) representation of the BEKK(*p,q*) model.*

For the BEKK($1,1$*) model the expression*

$$\frac{\partial \mathrm{V}_{t+h}(\xi_t,\eta)}{\partial\eta^\top} = \left(\mathrm{V}_{t+h-1}^\top \otimes I_{n^*}\right)\frac{\partial\,\mathrm{vec}(\tilde{A} + \tilde{B}\mathbb{1}_{\{h>1\}})}{\partial\eta^\top} + \left(\tilde{A} + \tilde{B}\mathbb{1}_{\{h>1\}}\right)\frac{\partial \mathrm{V}_{t+h-1}}{\partial\eta^\top} \tag{2.11}$$

is available where $\mathbb{1}_{\{\cdot\}}$ *denotes the indicator function which is equal to one if the condition in the subscript is satisfied and zero otherwise.*

Proof. See Appendix 2.A.3. □

The asymptotic distribution of the structural VIRF estimator allows us to construct simultaneous confidence intervals for the impulse responses of individual asset returns to structural shocks. For our application, we choose the χ^2-approximation to Hotelling's T^2 statistic to compute simultaneous confidence intervals for all components of the VIRF for a given significance level α (see, e.g., Sims and Zha, 1999, and Lütkepohl et al., 2015, for discussions regarding confidence interval construction for impulse responses). This enables us to assess the statistical significance of the responses of the (co-)variances of all assets in our speculative return system to a structural shock.

2.2.5 Structural VIRFs

In unidentified MGARCH models, volatility impulse response analysis is limited to a retrospective inspection of past financial, economic, or political events. We accordingly

refer to this approach as historical VIRF analysis. By taking the estimated residual $\hat{\varepsilon}_t$ and the volatility state $\hat{H}_t$ at the time of the shock occurrence, Hafner and Herwartz (2006) define their structural shocks $\hat{\xi}_t = \hat{H}_t^{-1/2}\hat{\varepsilon}_t$ using the principal square root, an approach which to the best of our knowledge has not been questioned so far. Hafner et al. (2022) and Fengler and Polivka (2022a), however, provide evidence that the principal matrix square root and its associated shocks do not comply with empirical results on asymmetry of volatility spillovers and suggest alternative matrix decompositions for H_t.

Nonetheless, the VIRF is unaffected by this identification problem because it is invariant to rotations in the historical context such that the results are independent of the structural model. To see this more clearly, let $Q_t = H_t^{1/2}\tilde{R}$ denote a structural decomposition of H_t. Given the return realized on the day of interest t, the h-step ahead VIRF is:

$$\begin{aligned} V_{t+h}(\xi_t) &= \Psi_h \left(\operatorname{vech}(Q_t(\xi_t\xi_t^\top - I_k)Q_t^\top)\right) \\ &= \Psi_h \left(\operatorname{vech}\left(H_t^{1/2}\tilde{R}\left(\tilde{R}^\top H_t^{-1/2}\varepsilon_t\varepsilon_t^\top H_t^{-1/2}\tilde{R} - I_k\right)\tilde{R}^\top H_t^{1/2}\right)\right) \\ &= \Psi_h \operatorname{vech}(\varepsilon_t\varepsilon_t^\top - H_t) \end{aligned} \tag{2.12}$$

Thus, when ε_t is known, at least in retrospect, this expression is independent of the structural mechanism decoded by $\tilde{R}$.

However, structural volatility models stimulate new usages of VIRFs. First, in out of sample settings, structural decompositions allow one to process responses to synthetic but economically meaningful structural shocks. Second, structural VIRFs allow for conducting counterfactual analyses by defining specific shock scenarios. We coin the term "scenario VIRF" for this new application framework and illustrate its merits in Section 2.3.

2.2.6 Causality

Our volatility impulse response analysis connects well to recent advances on causality in times series where changes in model outcomes are interpreted as the result of changes in structural shocks, which are regarded as treatment variables. This notion of causality (see Lechner (2010) for an overview of the different causality concepts in econometrics) differs from the one usually employed in time series analysis, the Granger-Sims causality (Granger, 1969; Sims, 1972). The absence of Granger causality means non-predictability, whereas here we compare different states of the world, which are identified with different values of the causing variable. Therefore, in absence of causation, the outcomes would

be the same whatever the state of the causing variable. This interpretation requires additional identifying assumptions that allow one to relate the observed data to the distribution of the potential outcome variables allowing the researcher to infer the causal effect from observed data. In their recent advances, Rambachan and Shephard (2020, 2021) provide conditions how the GIRF of Koop et al. (1996) can be endowed with this causal interpretation. In contrast to the GIRF, the VIRF does not trace the dynamic effects of a shock to the conditional mean but to the conditional covariance matrix. It does not have a causal content a priori, as it is the difference of two conditional expectations. In contrast, a causal effect traces the effects of changes in treatments. To show that the VIRF can be endowed with a causal interpretation as well, we adapt the assumptions of Rambachan and Shephard (2020, 2021) to model (2.2). We start by rephrasing our variables of interest with terms stemming from causal inference:

Definition 2.2.3. Let $\xi := (\xi_t)_{t\in I}$, $(I = \{1, \dots, T\})$, denote a stochastic treatment path with realizations $\bar{\xi}_t \in \mathcal{W} \subseteq \mathbb{R}^n$ and let the potential outcome path for any deterministic trajectory $\bar{\xi} := (\bar{\xi}_t)_{t\in I}$ be given by $X := X_t(\bar{\xi})_{t\in I} = (X_1(\bar{\xi}), X_2(\bar{\xi}), \dots, X_T(\bar{\xi}))$ where $X_t := \text{vech}(\varepsilon_t\varepsilon_t^\top)$ and define $\mathcal{G}_t := \sigma(\{X_s, \xi_s \ (s \leq t)\})$.

The demeaned return vectors, and their respective outer products, are the observable, continuously valued, multidimensional outcomes, for which the VMA(∞) representation of the BEKK model is available. Thus, our treatment variable features continuous parameter values as opposed to the classical setting with a binary or finitely discrete treatment variable. We observe only one realization of the stochastic treatment path. Note that $\mathcal{G}_t \subseteq \sigma(\varepsilon_s, \xi_s, s \leq t\})$ as the outer product of two random vectors is a Borel measurable function. Due to the predictability of H_t, the measurability of the principal matrix square root operator and the fact that $\tilde{R}$ is treated as deterministic, it even holds that $\mathcal{G}_t = \tilde{\mathcal{F}}_t$ (see Definition 2.2.2). To define subsequences of entire time series, we use the notation $\xi_{s:t}$ to indicate the start s and end point t of the subseries in time. Furthermore, let ξ and X satisfy the following assumptions:

Assumption 2.2.1 (Time series non-interference)**.** For each $t \in I$ and all deterministic $(\bar{\xi}_t)_{t\in I}$, $(\bar{\xi}'_t)_{t\in I}$ with $\bar{\xi}_t, \bar{\xi}'_t \in \mathcal{W}$:

$$X_t(\bar{\xi}_{1:t}, \bar{\xi}_{t+1:T}) = X_t(\bar{\xi}_{1:t}, \bar{\xi}'_{t+1:T}) \text{ almost surely.}$$

Assumption 2.2.1 allows the potential outcomes to depend on past and contemporaneous treatments but excludes dependence on future treatments. It links the potential outcomes and treatments such that $X_t(\bar{\xi})_{t\in I} = (X_1(\xi_1), X_2(\xi_{1:2}), \dots, X_T(\xi_{1:T}))^\top$ and acts as the time

series analogon of the stable unit treatment value assumption (SUTVA) (Cox, 1958; Rubin, 1980). Our outcome series satisfies Assumption 2.2.1, which follows from the definition $\varepsilon_t = Q_t \xi_t$, where $Q_t = H_t^{1/2}\tilde{R}$ is $\mathcal{G}_{t-1}$-measurable, and the fact that the sequence of structural shocks ξ is assumed to be strict white noise.

Assumption 2.2.2 (Time series unconfoundedness)**.** For each $t \in I$ and all $h > 0$:

$$\xi_t \perp\!\!\!\perp (\xi_{t+1:t+h}, \{X_{t+h}(\bar{\xi}_{1:t-1}, (\bar{\xi}_s)_{t \leq s \leq t+h}) : \bar{\xi}_s \in \mathcal{W}\}) \,|\mathcal{G}_{t-1}$$

Assumption 2.2.2 defines non-anticipating treatment paths conditional on the information available up to time $t-1$. With ξ_t being independent and identically distributed, Assumption 2.2.2 is fulfilled due to the serial independence of the structural shocks and the predictability of the conditional covariance matrix in the MGARCH model given the past information contained in the returns. This guarantees the independence of the treatment ξ_t of future treatments and the associated potential outcomes. Indeed, going even further than non-anticipation, Francq and Zakoïan (2010, Thm 11.5) provide the conditions for the MGARCH model to admit a strictly stationary and non-anticipative solution.[6]

Assumption 2.2.3 (Sequential overlap)**.** Let $\mathcal{T} \subset \mathcal{W}$ be a Borel set with positive measure. For each $t \in \mathbb{Z}$ the stochastic treatment path satisfies

$$0 < \Pr(\xi_t \in \mathcal{T}) < 1$$

almost surely for all $\mathcal{T} \subset \mathcal{W}$.

Assumption 2.2.3 mirrors the overlap assumption of cross-sectional causality analyses in the time series setting and is essential for proving Corollary 2.2.1. As we are handling a continuous treatment variable, the overlap assumption is stated for Borel sets which can be chosen as ϵ-neighborhoods of the structural shock of interest $\bar{\xi}_t$: $\mathcal{T}_t = \{\tilde{\xi} \in \mathcal{W} : d(\bar{\xi}_t, \tilde{\xi}) < \epsilon\}$ for some metric d on $\mathbb{R}^n$ and $\epsilon > 0$, which can be arbitrarily small. In empirical practice, the set-based definition aligns well with the concept of scenario and sensitivity analysis where a wide range of potential scenario settings is considered. As the BEKK model and thus the BEKK-VIRF are continuous in the structural shock, applying them to a set $\mathcal{T}_t$ results in connected Borel sets of conditional covariance matrices $H_{t+h}(\mathcal{T}_t) = \mathcal{H}_{t+h}$, outer return products $X_{t+h}(\mathcal{T}_t) = \mathcal{X}_{t+h}$ and VIRF vectors $V_{t+h}(\mathcal{T}_t)$.

[6] A non-anticipative solution is defined as a process $(\varepsilon_t)_{t\in\mathbb{Z}}$ such that ε_t is a measurable function of ξ_{t-s} $(s \geq 0)$ with $H_t^{1/2} \perp\!\!\!\perp \sigma(\xi_{t+h}, h \geq 0)$ and $\varepsilon_t \perp\!\!\!\perp \sigma(\xi_{t+h}, h > 0)$.

Based on these assumptions, we can show that the VIRF applied to an ϵ-neighborhood $\mathcal{T}_t$ of a structural shock of interest $\bar{\xi}_t$ can be decomposed into a filtered treatment effect, i.e., a filtered causal volatility impulse response, and a selection bias term which vanishes under time series unconfoundedness.

Corollary 2.2.1. *Let Assumptions 2.2.1 – 2.2.3 hold, let $h \geq 0$ and assume that for any deterministic $\bar{\xi}_t \in \mathcal{W}$ and any $\tilde{\xi}_t \in \mathcal{T}_t = \{\tilde{\xi} \in \mathcal{W} : d(\bar{\xi}_t, \tilde{\xi}) < \epsilon\}$ for some metric d on $\mathbb{R}^n$ and $\epsilon > 0$: $\mathrm{E}[X_{t+h}(\tilde{\xi}_t) - X_{t+h}|\tilde{\mathcal{F}}_{t-1}] < \infty$. Then it holds for the resulting set of VIRFs:*

$$\mathrm{V}_{t+h}(\mathcal{T}_t) = \mathrm{E}[\mathcal{X}_{t+h} - X_{t+h}|\tilde{\mathcal{F}}_{t-1}] + \Delta_{t+h}(\mathcal{T}_t|\tilde{\mathcal{F}}_{t-1})$$

where $\Delta_{t+h}(\mathcal{T}_t|\tilde{\mathcal{F}}_{t-1}) = \frac{\mathrm{cov}\left[\mathrm{vech}(\mathcal{X}_{t+h}), \mathbb{1}_{\{\xi_t \in \mathcal{T}_t\}}|\tilde{\mathcal{F}}_{t-1}\right]}{\mathrm{E}\left[\mathbb{1}_{\{\xi_t \in \mathcal{T}_t\}}\right]}$ is a selection bias which vanishes under Assumption 2.2.2.

Proof. The proof is given in (1.1). □

Remark. The filtered treatment effect is closely related to the causal response function defined by Rambachan and Shephard (2020), which compares the effects of two finitely discrete treatments $\bar{\xi}_t$ and $\bar{\xi}_t^*$ given past information. In the VIRF, the occurrence of the shock $\bar{\xi}_t$ given past information is however contrasted with the model results given only the past information instead of conditioning on an artificial base shock $\bar{\xi}_t^*$.[7] By integrating out the effect of the shock $\bar{\xi}_t^*$, where the expectation is calculated from the law of the structural shocks, the integrated causal response function coincides with the VIRF. This gives a causal meaning to the VIRF as a vectorized integrated causal response function applied to the outer product of returns.

In summary, the VIRF allows one not only to investigate the effects of structural shocks, but to assess the causal impacts of these interpretable structural "treatment" shocks on volatility.

2.3 Empirical Application

We illustrate the merits of the structural VIRF approach by analyzing a system of daily asset returns. It comprises three asset classes which are among the most important for

[7]The VIRF also allows one to compare the causal impacts of two specific shock scenarios. This amounts to calculating the difference of the two respective VIRFs.

portfolio optimization as well as key ingredients in financial stress scenarios mandated by the European Central Bank (Kremer et al., 2012): equity, fixed income and the foreign exchange markets. To obtain an economically interpretable structural model, we employ the structural proxy-MGARCH approach of Fengler and Polivka (2022a).

2.3.1 Structural volatility model

The structural proxy-MGARCH model of Fengler and Polivka (2022a) derives the structural rotation matrix by means of a proxy variable scheme (see also Stock and Watson, 2012, and Mertens and Ravn, 2013). Assume there exists a centered $(n-1)$-dimensional instrument process $Z = (Z_t)_{t \in I}$ such that, for all $i = 1, \ldots, n-1$,

$$\mathrm{E}[\xi_{it} Z_{it}] = \phi_i \in \mathbb{R} \setminus \{0\} \qquad \text{(relevance)} \tag{2.13}$$

$$\mathrm{E}[\xi_t^{i*} Z_{it}] = \mathbf{0}_{(n-1)\times 1} \qquad \text{(exogeneity)} \tag{2.14}$$

where the product process $(\xi_t Z_{it})_{(t=1,\ldots,T)}$ is weakly stationary and the index i relates to the i-th vector element, the superscript $i*$ denotes all vector elements apart from the i-th element. Based on these assumptions, the columns of the rotation matrix are given by

$$\tilde{R}_{\bullet i} = \pm \mathrm{E}[u_t Z_{it}] \left(\mathrm{E}[Z_{it} u_t^\top] \, \mathrm{E}[u_t Z_{it}] \right)^{-1/2}. \tag{2.15}$$

where $u_t = H_t^{-1/2} \varepsilon_t$ denotes the standardized residual, i.e., the return standardized with the principal matrix square root of H_t. One can estimate the full rotation matrix by means of a proxy-guided Givens orthogonalization scheme (Fengler and Polivka, 2022a).

Consistent estimation of the rotation matrix and asymptotic inference is possible by replacing expectations with their sample mean analogues (Fengler and Polivka, 2022a).

We borrow the empirical analysis from Fengler and Polivka (2022a) and study daily price data ranging from 1/1/1998 to 12/31/2014 taken from Bloomberg. The three assets consist of the Standard and Poor's (S&P) 500 Composite Index (SP500), the yield of the US constant maturity 10-year treasury note (FRTCM10) and the Finex US Dollar Index (NDXCS00). The daily log returns r_t for each asset are displayed in Figure 2.1.

With the aim of identifying an equity market and a bond market shock, we use two series of news data taken from Thomson Reuters MarketPsych Indices (TRMI) to proxy for the underlying structural shocks: the US stock index news sentiment and the US bond news

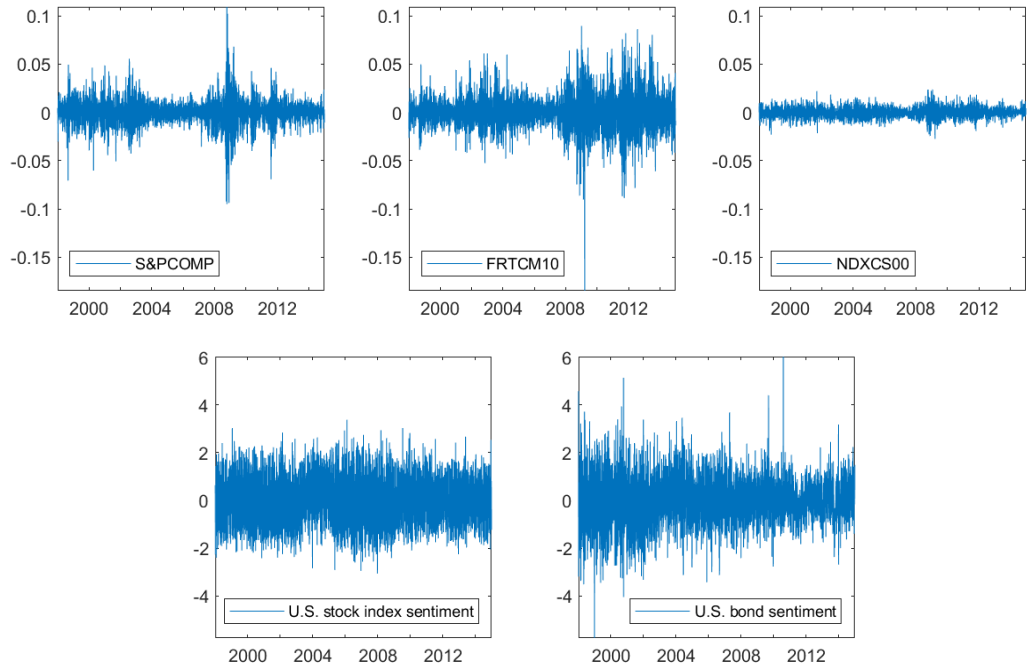

Figure 2.1: Demeaned daily log returns of the S&P 500 Composite Index (SP500), the yield of the US constant maturity 10-year treasury note (FRTCM10) and the Finex US Dollar Index (NDXCS00) from 1/1/1998 to 12/31/2014.

sentiment. The data are provided on a daily frequency, and we fit flexible autoregressive moving average (ARMA) models to them to distill the unexpected innovations. Our choice of these proxy variables is motivated by the well-documented link between news and salient intraday stock returns (see, e.g., Jeon et al., 2021).

Following Fengler and Polivka (2022a), we estimate the structural model using a BEKK(1, 1) specification. Table 2.1 shows that the rotation differs from the identity matrix. This suggests a deviation from the volatility spillover symmetry imposed by the spectral decomposition $H_t^{1/2}$ obtained when $\tilde{R} = I_n$. This can be nicely seen, as the structural model shifts mass from the unit diagonal entries of the identity matrix of no rotation in an asymmetric fashion to the off-diagonal matrix elements of the rotation matrix in Table 2.1. Furthermore, the second section of Table 2.1 shows that the stock market index Z_1 and bond market sentiment Z_2 are relevant instruments. Fengler and Polivka (2022a, Tables 6-8) conduct a narrative corroboration of the first percentiles of the structural shocks by studying the extent to which large shocks can be related to major financial market news referring to the day of the shock occurrence. Because they can connect each structural shock to specific economic and financial turmoil events, they identify ξ_1 as equity shock,

ξ_2 as bond market shock and refer to ξ_3 as currency shock.

		proxy-MGARCH model		
$\hat{\hat{R}}$		0.9118	0.3238	−0.2526
		0.3654	−0.9204	0.1393
		−0.1874	−0.2193	−0.9575
		ξ_1	ξ_2	ξ_3
correlations	Z_1	0.3347	0.0000	−0.0000
	Z_2	0.0052	0.1936	0.0000

Table 2.1: Estimation results of the structural MGARCH model of the demeaned daily log returns of the S&P 500 Composite Index (SP500), the yield of the US constant maturity 10-year treasury note (FRTCM10) and the Finex US Dollar Index (NDXCS00) from 1/1/1998 to 12/31/2014 when using the stock market index (Z_1) and bond market sentiment (Z_2) TRMIs as proxy variables.

2.3.2 Structural volatility impulse response analysis

One of the most important applications of MGARCH models is the analysis of responses of volatility to shocks (Bauwens et al., 2006). With identified and labeled structural shocks at hand, we turn to an analysis of the structural VIRFs implied by our model starting with historical VIRFs followed by scenario VIRFs.

Historical VIRFs

We showcase three historical key events in our sample: First, as an example of a structural 1% marginal equity tail shock, we consider the NASDAQ crash on April 14, 2000, which accompanied the burst of the Dotcom bubble. Second, we consider the semiannual monetary policy report of the chairman of the Federal Reserve Board, Alan Greenspan, given to the US Senate on March 7, 2002. This is an example of a 1% marginal currency tail and bond market tail shock. Third, we examine the concerns in the US equity markets over the European debt crisis on August 4, 2011, as another example of an equity shock.

	Event		
Shock vector component	Dotcom crisis 04/14/2000	Greenspan speech 03/07/2002	EU debt crisis 08/04/2011
Equity	-4.4173	0.7168	-4.3829
Bond	0.0050	-2.5834	0.6824
Currency	1.5779	3.3575	-0.7705
Return vector	Dotcom crisis	Greenspan speech	EU debt crisis
S&P 500	-0.0603	-0.0048	-0.0493
Yield	-0.015	0.0314	-0.0663
USD Index	-0.0044	-0.0101	0.0155

Table 2.2: Structural shock vectors selected for the historical VIRF analysis with corresponding returns.

The corresponding shock vectors are documented in Table 2.2 and the resulting VIRFs are displayed in Figures 2.2 to 2.4. The 5% critical values for the simultaneous confidence intervals are obtained from the $\chi^2(3)$.

The structural shock of the NASDAQ crash on 04/14/2000 leads to a strong positive response in the predicted variance of the S&P 500 which is statistically significant at the 5% level (see Figure 2.2). The increase in the level of volatility of the S&P 500 is significant up to a duration of approximately 75 days. Although there is a strong economic reaction in the covariance of the S&P 500 and the 10-year treasury yield as well, this impulse response appears to be insignificant. Overall, the structural model indicates that the NASDAQ crash on 04/14/2000 has a strong medium-term impact on the level of volatility of the equity market with other (co-)volatilities being largely unaffected. Indeed, our MGARCH model displays elevated equity volatility levels after the NASDAQ crash, as also found by Sornette et al. (2018).

On 03/07/2002, the chair of the Federal Reserve Board, Alan Greenspan, made an unusual appearance in Congress, which took markets by surprise: He offered a much more upbeat discussion of the economic outlook in his speech to the Senate than in his testimony to the House of Representatives only seven days before. The structural shock associated with

this event exhibits a complex set of different impacts on the volatilities of the return system (see Figure 2.3). First of all, even though the equity component of the shock is close to zero, we observe a small but statistically significant decrease in the predicted variance of the S&P 500. This effect lasts for almost 60 days before turning insignificant and converging to zero. Thus, the news of the accelerated recovery of the US economy forecast a calming effect on equity markets according to the VIRF.

At the same time, the strong negative shock to the bond market[8] leads to a high-magnitude short-term increase in the predicted yield volatility, which stays significantly different from zero for almost 30 days. The negative bond market shock may reflect markets' anticipations of rate hikes. The reaction of treasury yields and their rising volatility in response to Federal Open Market Committee (FOMC) announcements and monetary policy reports has been studied extensively in the literature (see, e.g., Jones et al., 1998, Bomfim, 2003, Rosa, 2013, and the references therein). Remarkably, without taking into account the confidence intervals, the VIRF plot could give the misleading impression of a long-term positive effect on the yield variance.

The predicted covariance impulse responses of the S&P 500 with the yield and of the S&P 500 with the USD Index are both insignificant. In contrast, the structural shock has a significant impact on the predicted covariance of the USD Index with the yield and on the predicted variance of the USD Index itself. In the identified system, positive currency shocks, as present in the structural shock vector of 03/07/2002, tend to be related to news of a weakening USD (Fengler and Polivka, 2022a). Greenspan's announcement was no exception: On the day of his testimony, the USD sank against the Yen and the Euro (see Table 2.2). In contrast, the yield return spiked in response to the negative bond market shock. This negative association gives rise to an immediate and long-lasting decrease in the predicted covariance of the USD Index and the yield in our model. The decrease may seem puzzling at first sight because standard exchange rate models may suggest a positive association between yields and the domestic currency (Hofmann et al., 2020), but the VIRF does not allow for conclusions regarding the levels of (co-)volatilities. However, an inspection of the MGARCH model indicates that the estimated covariance of the yield and the USD index is indeed positive and above the long term mean on the preceding day as well as on the day of the shock occurrence. Thus, the structural shock merely lowers this level rather than strengthening the association further. Finally, we observe a strong positive response of the predicted variance of the USD index to the structural shock, which

[8] A negative bond market shock leads to decreases in bond prices and increases in bond yields.

lasts over a horizon of almost 100 days. Mueller et al. (2017) provide empirical findings on higher foreign exchange volatility upon FOMC news in the short term. For this event, the VIRF signals an increased forex (FX) volatility in response to Greenspan's speech even over a long-term period.

Turning to the structural shock of the European debt crisis (see Figure 2.4), one observes an immediate, large positive impact on the predicted variance of the S&P 500 lasting for approximately 30 days. The predicted elevated level of volatility is consistent with heightened market fears of European debt defaults. With the exception of the equity market shock, the other components of the structural shock on 08/04/2011 are well within one standard deviation around the zero mean (see Table 2.2). However, the shock has strong, statistically significant effects on the predicted (co-)variances of all asset return components: The historical VIRF of the 10-year treasury yield is significantly different from zero for a time period of approximately 45 days. The other VIRFs display medium- to long-term impacts of between 70 and 90 days. The sources for these large significant responses can be found in the data: On the day of the shock occurrence, the covariance of the yield with the S&P 500 and the variance of the yield itself are well above the long-term mean. The covariances of the USD Index with the other assets are well below their long-term means. Hence, the comparably small shock components are strongly magnified through the large entries in the structural transmission matrix $H_t^{1/2}\tilde{R}$ – resulting in significant volatility responses for all assets. The upward jump in the predicted variance of the yield and in its forecasted covariance with the S&P 500 may mirror movements in US treasuries due to flight-to-safety investments in view of the falling equity markets and the European debt crisis. Furthermore, the VIRF suggests a significant and strong decrease in the predicted covariance of the S&P 500 and the USD index. This finding is consistent with the literature documenting that volatility spillover effects between equity and foreign exchange markets are small in normal market times but strong in periods preceding crises (see, e.g., Grobys, 2015, or Cenedese and Mallucci, 2016). The even stronger drop in the predicted covariance of the USD Index and the 10-year treasury yield mirrors two effects: a surge of the USD relative to the Euro, which is indeed reflected in the positive USD Index return at the shock date (see Table 2.2), and a decrease in the yield, potentially through a higher demand for safe-haven investments. Finally, the predicted increase in the USD Index volatility in the wake of the European debt crisis is consistent with potentially higher levels of uncertainty in foreign exchange markets. This uncertainty manifests itself in our data through an increase in the conditional variance of the USD Index in the subsequent quarter. Overall, our historical VIRF analysis emphasizes the importance of considering

confidence intervals to be able to appreciate volatility impulse responses. Moreover, our discussion highlights the benefits of using structural shocks for their interpretation. To the practitioner, employing structural VIRFs has immediate benefits in asset allocation and risk management. While an asset manager may, e.g., use a reduced-form volatility model for portfolio diversification, a structural model allows for understanding whether and to what extent these assets were historically affected by the same economic shocks. Thus, the structural VIRF grants a deeper understanding of the risk to which a portfolio is exposed.

Causal scenario VIRFs

Historical VIRFs are useful for understanding volatility events in hindsight, but beyond that are of limited value because certain events, such as those singled out in Section 2.3.2, will never occur again. With the help of a structural model, however, the causal effects of meaningful shock scenarios – in an out-of-sample context or as counterfactuals – can be considered. A portfolio manager might, for instance, be interested in understanding the instant volatility impact on her portfolio resulting from certain tail events of FOMC decision days. A manifold of other scenarios is conceivable.

For illustration, here we adopt a risk manager's perspective and investigate the VIRFs of (a) a scenario associated with 1% marginal tail equity shocks; and (b) a scenario associated with marginal 1% tail bond shocks on the out-of-sample date 01/02/2015. Because our causality concept in Section 2.2.6 involves sets of structural shocks, we estimate the multivariate density of the structural shocks. This allows us to draw observations from the intervals of interest. To model multivariate dependence, we initially experimented with a t-copula, but found only very mild departures from independence. For the sake of simplicity, we therefore decided to proceed with the independence copula. The marginal distributions are fitted nonparametrically with Gaussian kernel density estimators. Subsequently, we independently draw for each scenario $10,000$ observations from the 1% fitted quantile of the shock component of interest and from the full distributional range of the other components to create marginal tail risk scenarios. This means that while sampling from the estimated marginal quantile of one shock component we do not set the other structural shock components artificially to zero. To illustrate the responses to the set of structural shocks, we compute the pointwise median VIRFs and the pointwise 25% and 75% quantile VIRFs at every forecast horizon h. To visualize the parameter estimation uncertainty, we add the analytical confidence intervals of the median target VIRF which

we calculate following Fry and Pagan (2011).

Figure 2.5 displays the VIRFs resulting from shock scenario (a). According to our analysis in Section 2.2.6, we can interpret these responses as the causal effects associated with the 1% marginal equity shock quantile. We detect a pronounced positive median impact on the forecasted conditional (co-)variance of the S&P 500 and the treasury yield and the variance of the USD Index. Judged by the impact of the median target VIRF, the effect on the S&P 500 is statistically significant at the 5% level for approximately 70 days, the effect on the yield and on its covariance with the S&P 500 is statistically significant for approximately 100 respectively 35 days. The covariance impulse responses of the Finex US Dollar Index to the equity tail events do not exhibit a clear sign, nor do they indicate a clear form of possible outcome paths. The confidence intervals of the median target VIRFs of the predicted covariance of the USD Index with the yield and the predicted variance of the USD Index itself, however, indicate a slight negative impact. To summarize, the shock causes an increase in uncertainty levels and in correlations between equity and fixed income markets over the upcoming medium term.

In contrast, in Figure 2.6, the sampled 1% quantile bond shocks of scenario (b) exhibit only a very small impact on the predicted conditional covariance of the treasury yield and the S&P 500 and almost none on the forecasted conditional variance of the S&P 500. Remarkably, there seems to be a strong positive effect on the predicted variance of the yield which is, however, statistically not significant. In contrast, the effect on the predicted conditional covariance with the Finex US Dollar Index is statistically significant for the median target VIRF over a period of almost 25 days. Thus, the increase in covariance between fixed income and fx markets caused by the shock may be of primary concern for risk assessment. In summary, Figures 2.5 and 2.6 provide, depending on the shock scenario, very different predictions regarding (co-)variance levels in the asset return system can be expected to rise and to what extent – thus allowing for differential risk managerial precautions.

2.4 Conclusion

In this paper, we made a fresh examination of the VIRF of Hafner and Herwartz (2006), which is a valuable device for analyzing the impact of shocks on conditional variance matrices in MGARCH models. By deriving the asymptotic law of the VIRF in the BEKK

model, we refine the VIRF analysis by providing asymptotic confidence intervals. We show that the asymptotic variance matrix can, like the VIRF, be written as a function of the forecast horizon in a compact recursive form, which allows for an efficient numerical evaluation. Building on recent advances for identification in MGARCH models, we extend the VIRF to benefit from the advantages of structural volatility models: interpretable, labeled shocks and specified structural propagation channels allow us to broaden the use case of the VIRF to counterfactual and out-of-sample scenario analyses. Moving beyond a structural interpretation, we show how to endow the VIRF with a causal interpretation which allows one to use the microeconometricians' notion of causality when analyzing the impact of well-defined shock scenarios. In an empirical application to an identified system of equity, government bond and foreign exchange returns, we discuss two obvious use cases of the structural VIRF. All our applications demonstrate that it is vital to be able to assess the statistical significance of volatility impulse responses.

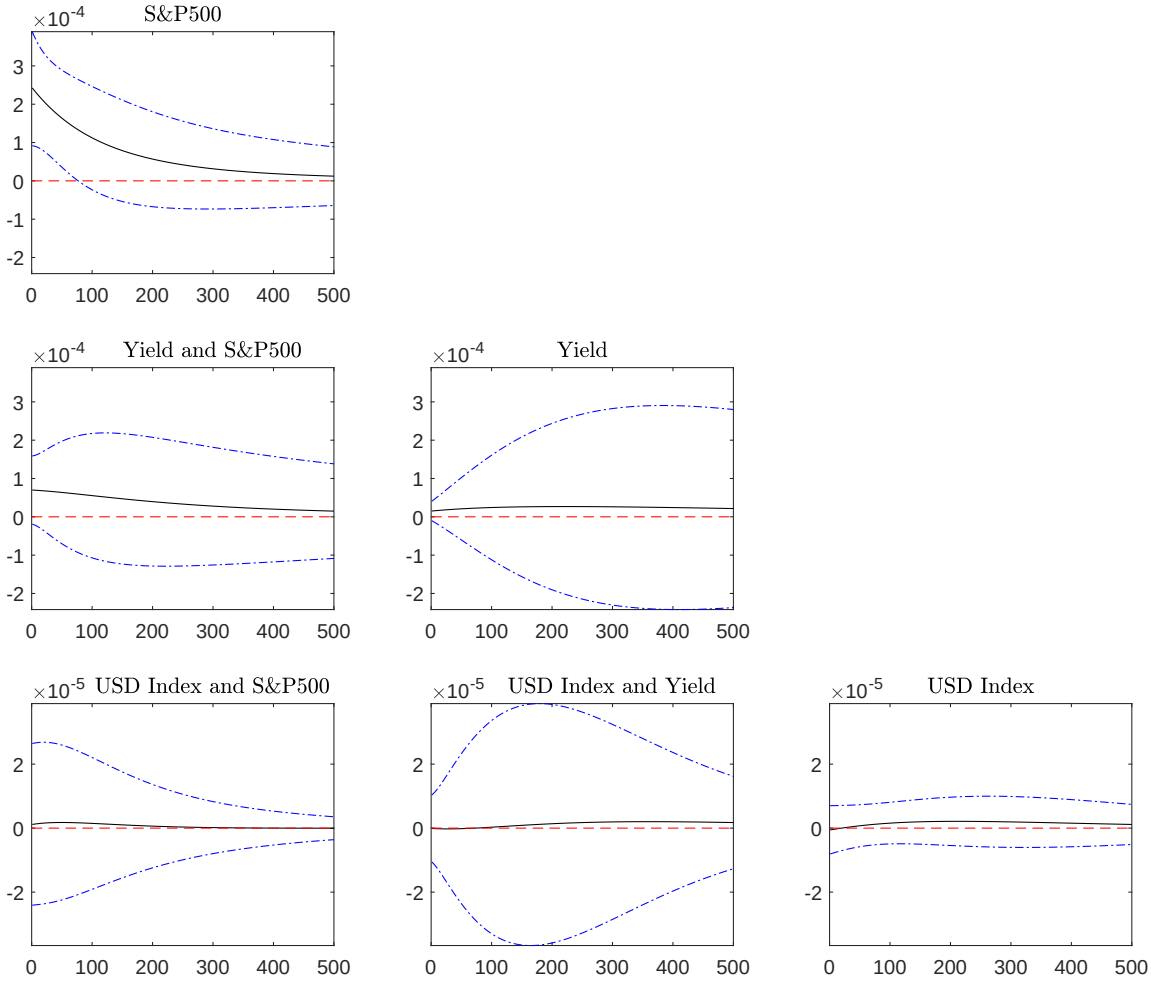

Figure 2.2: Historical VIRFs in response to the Dotcom bubble burst.

The predicted 500-step ahead VIRFs (black) with 95% confidence intervals (blue) are driven by the structural shock on 04/14/2000, see Table 2.2. The return system consists of the S&P 500 Composite Index (S&P500), the yield of the US constant maturity 10-year treasury note (Yield) and the Finex US Dollar Index (USD Index).

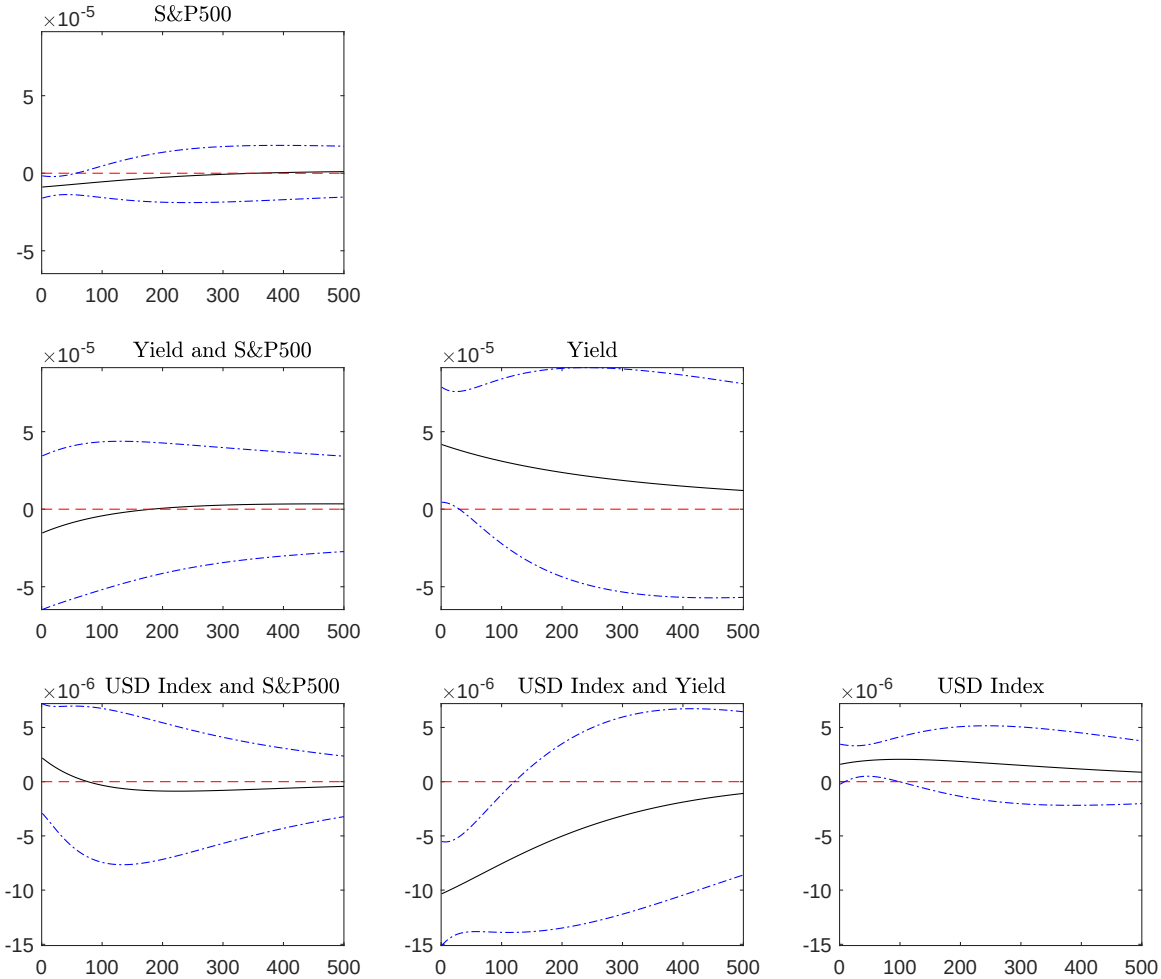

Figure 2.3: Historical VIRFs in response to the Greenspan testimony.

The predicted 500-step ahead VIRFs (black) with 95% confidence intervals (blue) are driven by the structural shock on 03/07/2002, see Table 2.2. The return system consists of the S&P 500 Composite Index (S&P500), the yield of the US constant maturity 10-year treasury note (Yield) and the Finex US Dollar Index (USD Index).

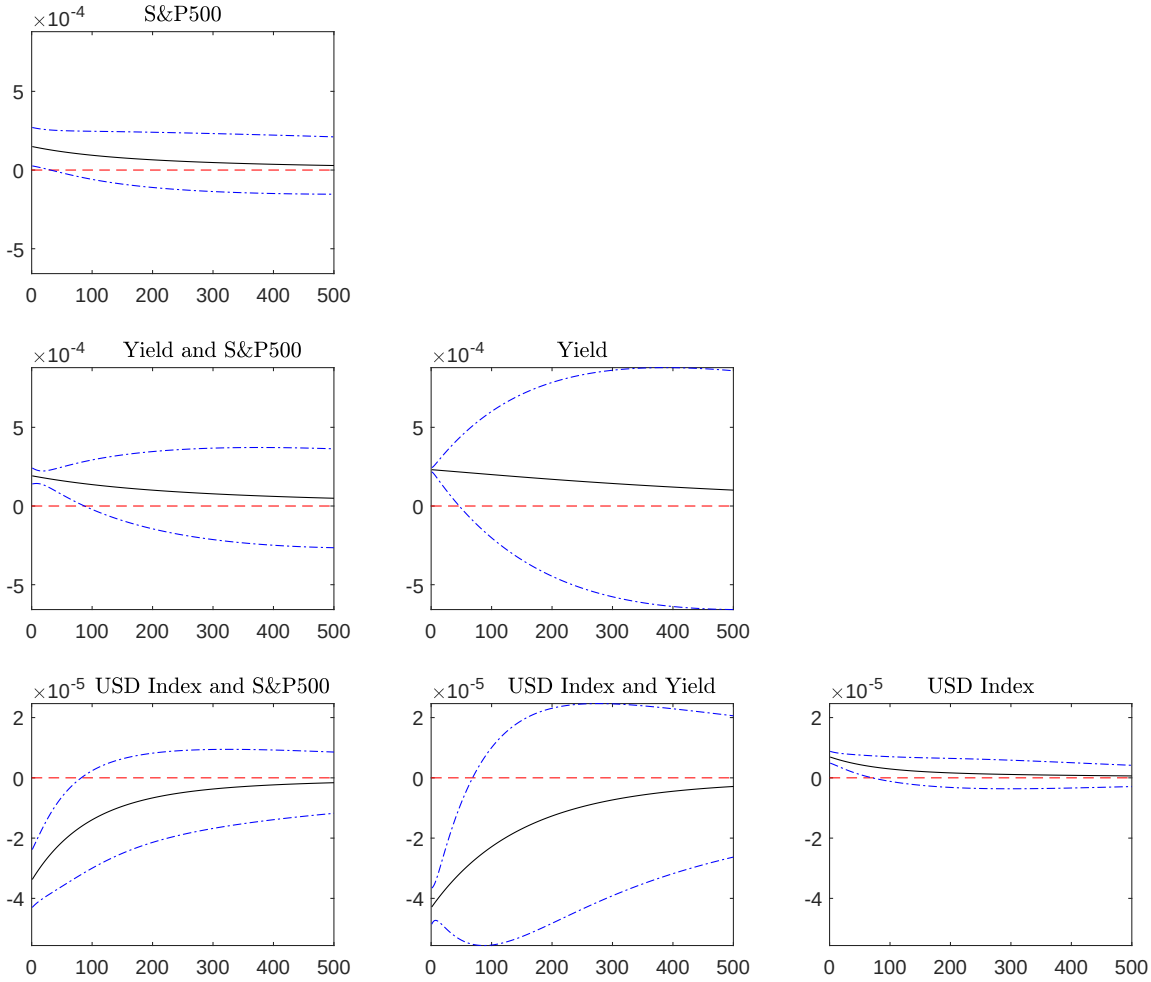

Figure 2.4: Historical VIRFs in response to the EU debt crisis.

The predicted 500-step ahead VIRFs (black) with 95% confidence intervals (blue) are driven by the structural shock on 08/04/2011, see Table 2.2. The return system consists of the S&P 500 Composite Index (S&P500), the yield of the US constant maturity 10-year treasury note (Yield) and the Finex US Dollar Index (USD Index).

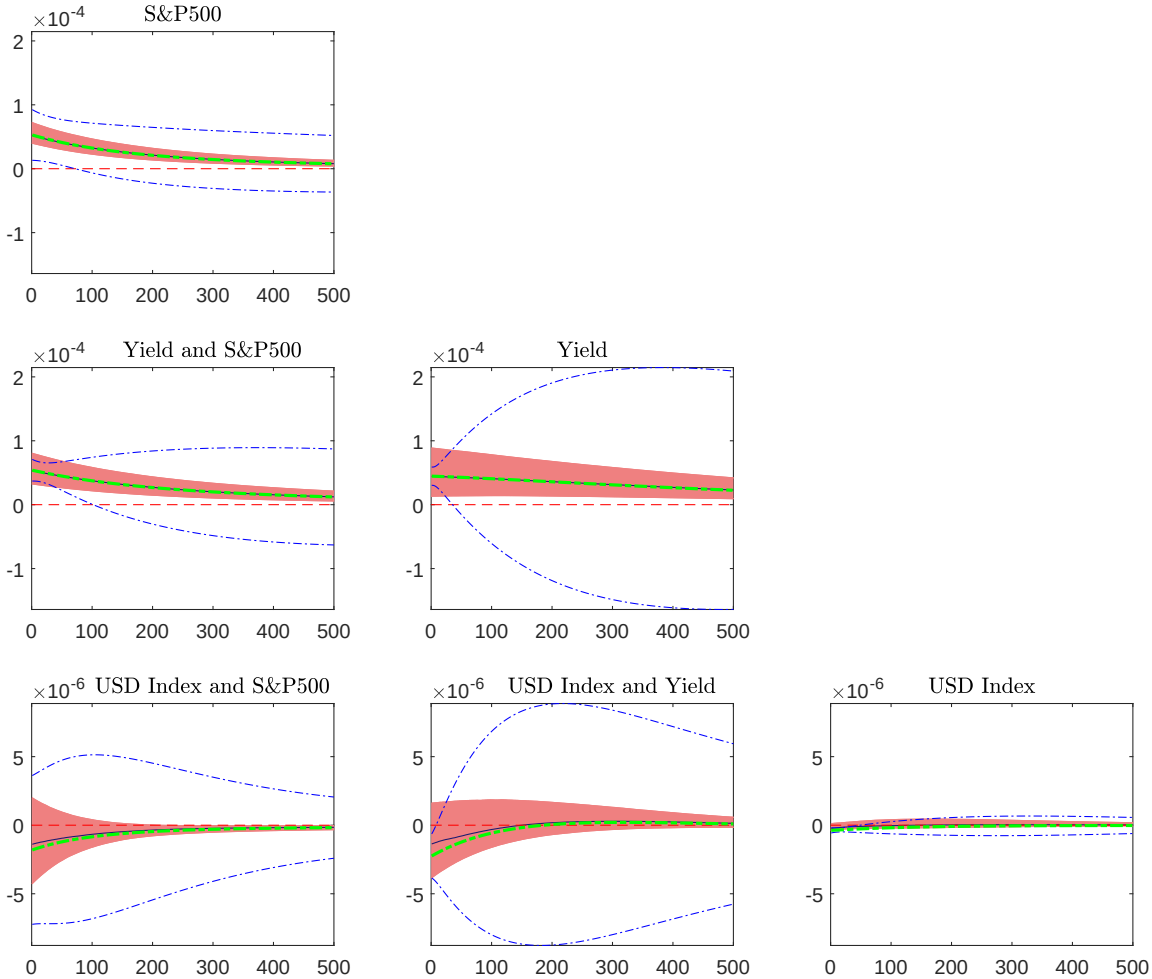

Figure 2.5: Scenario VIRFs in response to equity tail shocks.

Predicted 500-step ahead VIRFs in response to a scenario family of 1% structural equity tail shocks on the out-of-sample date 01/02/2015: median scenario VIRF (black) with pointwise 25% and 75% quantiles (salmon) and corresponding median target VIRF (green) with analytical confidence intervals (blue). The return system consists of the S&P 500 Composite Index (S&P500), the yield of the US constant maturity 10-year treasury note (Yield) and the Finex US Dollar Index (USD Index).

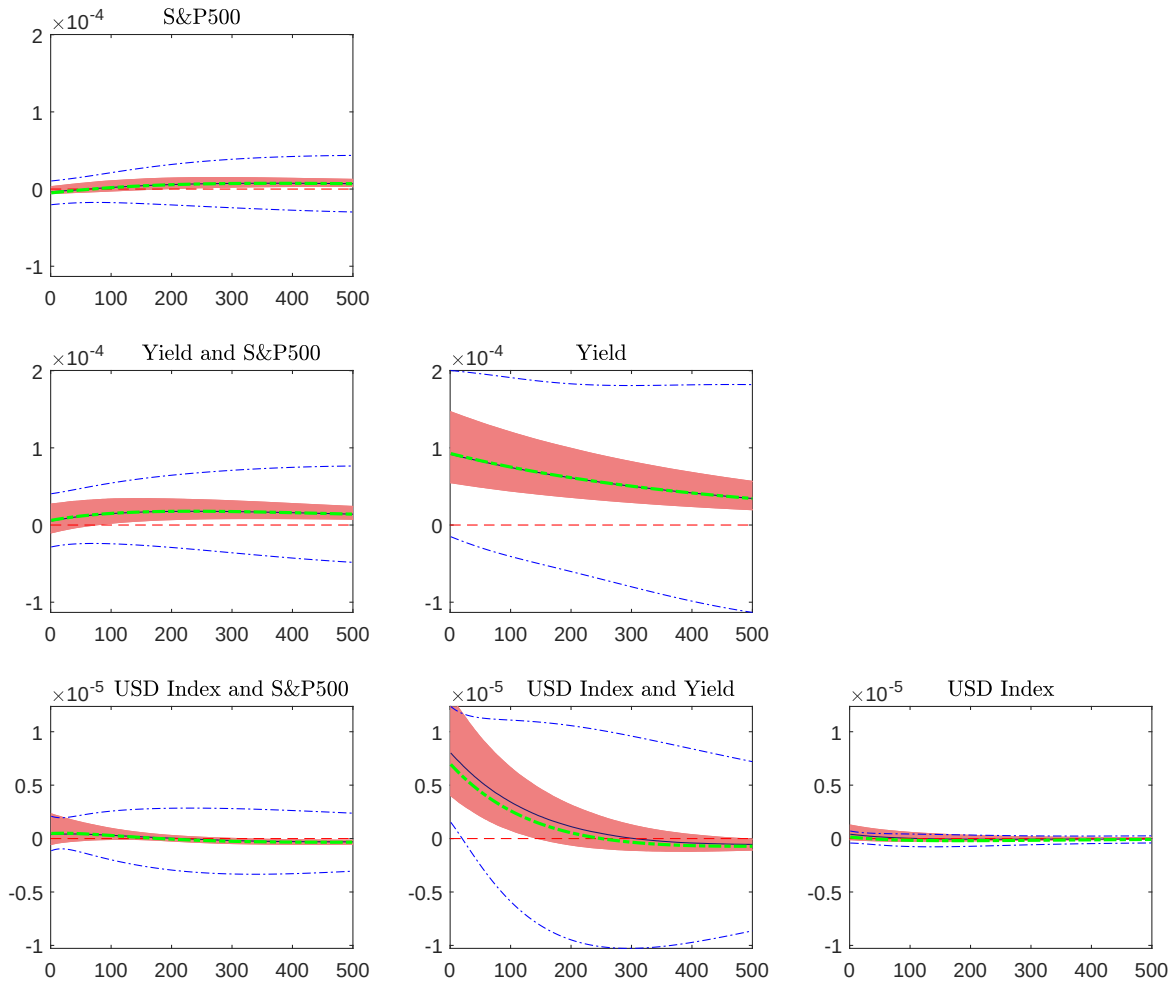

Figure 2.6: Scenario VIRFs in response to bond tail shocks.

Predicted 500-step ahead VIRFs in response to a scenario family of 1% structural bond tail event shocks on the out-of-sample date 01/02/2015: median scenario VIRF (black) with pointwise 25% and 75% quantiles (salmon) and corresponding median target VIRF (green) with analytical confidence intervals (blue). The return system consists of the S&P 500 Composite Index (S&P500), the yield of the US constant maturity 10-year treasury note (Yield) and the Finex US Dollar Index (USD Index).

2.A Proofs

2.A.1 Notation and results from matrix algebra

Definition D.1. Principal matrix square root. Any real symmetric $(n \times n)$ matrix M can be factorized as $M = \Gamma\Lambda\Gamma^\top$ where Γ is an orthogonal $(n \times n)$ matrix with the normalized eigenvectors of M as columns and Λ the diagonal matrix of the eigenvalues. The principal matrix square root of M is defined as $\Gamma\Lambda^{1/2}\Gamma^\top$ where $\Lambda^{1/2}$ denotes the diagonal matrix of the square root of the eigenvalues of M. It is the unique matrix square root which has non-negative eigenvalues, see Horn and Johnson (2012, Theorem 7.2.6).

Definition D.2. Rotation matrix. A rotation matrix R is a real $(n \times n)$ matrix satisfying $R^\top R = RR^\top = I_n$ and $\det(R) = +1$.

Definition D.3. $\mathrm{vec}(\cdot)$ operator. The $\mathrm{vec}(\cdot)$ operator stacks, starting with the first column, the columns of an $(n \times n)$ matrix M in an n^2-dimensional vector. It is a linear operator.

Definition D.4. $\mathrm{vech}(\cdot)$ operator. The $\mathrm{vech}(\cdot)$ operator stacks, starting with the first column, the lower triangular part of a (symmetric) $(n \times n)$ matrix M in an n^*-dimensional vector where $n^* = \frac{n(n+1)}{2}$.

Definition D.5. Moore-Penrose inverse. The Moore-Penrose inverse of an $(m \times n)$ matrix M with $M^\top M$ non-singular is defined as

$$M^+ = (M^\top M)^{-1} M^\top. \tag{A.16}$$

Definition D.6. Duplication matrix. For any symmetric $(n \times n)$ matrix M, the duplication matrix D_n denotes the unique $\left(n^2 \times \frac{n(n+1)}{2}\right)$ matrix such that

$$\mathrm{vec}(M) = D_n \,\mathrm{vech}(M). \tag{A.17}$$

The Moore-Penrose inverse of the duplication matrix is denoted by D_n^+.

Definition D.7. Commution matrix. For every $(m \times n)$ matrix M, the $(mn \times mn)$ commutation matrix K_{mn} is defined by

$$K \,\mathrm{vec}(M) = \mathrm{vec}(M^\top). \tag{A.18}$$

For $n = m$ we abbreviate $K_{nn} = K_n$.

Result R.1. $\mathrm{vec}(\cdot)$ operations. For appropriately defined matrices A, B and C and for some $(n \times n)$ matrices M, P:

$$\mathrm{vec}(ABC) = \left(C^\top \otimes A\right) \mathrm{vec}(B). \tag{A.19}$$

$$\mathrm{vec}(A^\top \otimes A^\top) = \mathrm{vec}((A \otimes A)^\top) \tag{A.20}$$

$$\mathrm{vec}(M \otimes P) = (I_n \otimes K_n \otimes I_n)\left[\mathrm{vec}(M) \otimes \mathrm{vec}(P)\right] \tag{A.21}$$

see (Magnus and Neudecker, 1988, Theorem 3.10) for a proof of (A.21).

Result R.2. Matrix derivatives results.

(1) For $n \times n$ matrices X and Z, Z symmetric, it holds:

$$\frac{\partial\, \mathrm{vec}(XZX)}{\partial\, \mathrm{vec}(X)^\top} = (XZ \otimes I_n) + (I_n \otimes XZ) \tag{A.22}$$

by an application of the chain rule (see Magnus and Neudecker, 1988, Theorem 5.12) in conjunction with two applications of (A.19).

(2) For any symmetric, positive semidefinite $n \times n$ matrix H with principal square root $H^{1/2}$, it holds:

$$\frac{\partial\, \mathrm{vec}(H^{1/2})}{\partial\, \mathrm{vec}(H)^\top} = \left[\left(I_n \otimes H^{1/2}\right) + (H^{1/2} \otimes I_n)\right]^{-1} \tag{A.23}$$

which can be derived by solving a Sylvester type equation for the differential.

(3) For any $(n \times n)$ matrices M and P, it holds:

$$\frac{\partial\, \mathrm{vec}(M) \otimes \mathrm{vec}(P)}{\partial\, \mathrm{vec}(M)^\top} = I_n \otimes \mathrm{vec}(P). \tag{A.24}$$

(4) For any $(n \times n)$ matrix M:

$$\frac{\partial\, (\mathrm{vec}(M) \otimes \mathrm{vec}(M))}{\partial\, \mathrm{vec}(M)^\top} = (I_n \otimes \mathrm{vec}(M)) + (\mathrm{vec}(M) \otimes I_n) \tag{A.25}$$

by (A.24) and the product rule.

(5) For any $(n \times n)$ matrix M:

$$\frac{\partial\, \mathrm{vec}(M^\top)}{\partial\, \mathrm{vec}(M)^\top} = K_n. \tag{A.26}$$

2.A.2 Mathematical prerequisites for the VIRF

Corollary 2.A.1. *Let $(Y_t)_{(t\in\mathbb{N}_0)}$ be a sequence of integrable random vectors in $\mathbb{R}^k$ defined on a probability space $(\Omega, \mathcal{F}, \mathrm{P})$, let $\tilde{\mathcal{F}}$ be a σ-algebra on Ω with $\tilde{\mathcal{F}} \subset \mathcal{F}$ and let $(\phi_i)_{(i\in\mathbb{N}_0)}$ be a sequence of absolutely summable matrices in $\mathbb{R}^{k\times k}$. Then $\sum_{i=0}^{\infty} \phi_i Y_{t-i}(\omega)$ exists and $\mathrm{E}[\sum_{i=0}^{\infty} \phi_i Y_{t-i}|\tilde{\mathcal{F}}] = \sum_{i=0}^{\infty} \phi_i \mathrm{E}[Y_{t-i}|\tilde{\mathcal{F}}]$. Thus we can interchange infinite summation and conditional expectation.*

Proof. The proof is available from the authors on request. □

Proof of Proposition 2.2.1. Let $X_t = \mathrm{vech}(\varepsilon_t\varepsilon_t^\top)$ and $Y_t = X_t - \mathrm{vech}(H_t)$ and $h \geq 1$. Then we have

$$\mathrm{E}[\mathrm{vech}(H_{t+h})|\mathcal{F}_{t-1}] = \mathrm{E}[\mathrm{E}[X_{t+h}|\mathcal{F}_{t+h-1}]|\mathcal{F}_{t-1}] = \mathrm{E}[X_{t+h}|\mathcal{F}_{t-1}]. \tag{A.27}$$

Together with the VMA(∞) representation we obtain for the VIRF in (2.3)

$$\mathrm{V}_{t+h}(\xi_t;\eta) = \mathrm{E}\left[\sum_{i=0}^{\infty} \Psi_i Y_{t+h-i}|\tilde{\mathcal{F}}_t\right] - \mathrm{E}\left[\sum_{i=0}^{\infty} \Psi_i Y_{t+h-i}|\mathcal{F}_{t-1}\right]. \tag{A.28}$$

By square integrability of $(\varepsilon_t)_{t\in\mathbb{Z}}$, $(X_t)_{t\in\mathbb{Z}}$ is a sequence of integrable random variables, and because the series $\mathrm{vech}(H_t)_{t\in\mathbb{Z}}$ is integrable by the square integrability of ε_t, so is $(Y_t)_{t\in\mathbb{Z}}$. Because $\mathrm{Var}(Y_t) = H_Y < \infty$, the absolute moments of Y_t are uniformly bounded. Hence, by Corollary 2.A.1, we can interchange infinite summation and conditional expectation:

$$\begin{aligned}\mathrm{V}_{t+h}(\xi_t;\eta) &= \sum_{i=0}^{\infty} \Psi_i \left(\mathrm{E}\left[Y_{t+h-i}|\tilde{\mathcal{F}}_t\right] - \mathrm{E}[Y_{t+h-i}|\mathcal{F}_{t-1}]\right) \\ &= \Psi_h \left(\mathrm{E}\left[Y_t|\tilde{\mathcal{F}}_t\right] - \mathrm{E}[Y_t|\mathcal{F}_{t-1}]\right).\end{aligned} \tag{A.29}$$

This follows from $\mathrm{E}\left[Y_{t+h-i}|\tilde{\mathcal{F}}_t\right] - \mathrm{E}[Y_{t+h-i}|\mathcal{F}_{t-1}] = 0$ for all $(t+h-i) \leq t-1$ due to measurability given $\mathcal{F}_{t-1}$ and $\mathrm{E}\left[Y_{t+h-i}|\tilde{\mathcal{F}}_t\right] - \mathrm{E}[Y_{t+h-i}|\mathcal{F}_{t-1}] = 0$ for all $(t+h-i) \geq t+1$ by the tower property. Similarly, using the tower property and the independence of ξ_{t+h-i} of $\mathcal{F}_{t-1}$ and ξ_t, $\mathrm{E}[Y_{t+h-i}|\tilde{\mathcal{F}}_t] = 0$. Using predictability[9] and tower property arguments and

[9]Note that $H_t^{1/2}$ is $\mathcal{F}_{t-1}$-measurable. The measurability follows from the $\mathcal{F}_{t-1}$-measurability of H_t and because the principal square root is a (uniformly) continuous operator in the space of positive definite matrices. Matrix multiplication with $\tilde{R}$ preserves measurability.

inserting the structural model (2.2), we obtain:

$$\begin{aligned}
\mathrm{V}_{t+h}(\xi_t;\eta) &= \Psi_h \left(\mathrm{E}\left[X_t - \mathrm{vech}(H_t)|\tilde{\mathcal{F}}_t\right] - \mathrm{E}[X_t - \mathrm{vech}(H_t)|\mathcal{F}_{t-1}]\right) \\
&= \Psi_h \left(\mathrm{E}\left[\mathrm{vech}(\varepsilon_t\varepsilon_t^\top)|\tilde{\mathcal{F}}_t\right] - \mathrm{E}\left[\mathrm{vech}(\varepsilon_t\varepsilon_t^\top)|\mathcal{F}_{t-1}\right]\right) \\
&= \Psi_h \left(\mathrm{E}\left[\mathrm{vech}\left(H_t^{1/2}\tilde{R}\xi_t\xi_t^\top\tilde{R}^\top H_t^{1/2^\top}\right)|\tilde{\mathcal{F}}_t\right] - \mathrm{E}\left[\mathrm{vech}(H_t)|\mathcal{F}_{t-1}\right]\right) \\
&= \Psi_h \left(\mathrm{vech}\left(H_t^{1/2}\tilde{R}\xi_t\xi_t^\top\tilde{R}^\top H_t^{1/2^\top}\right) - \mathrm{vech}\left(H_t^{1/2}\tilde{R}\tilde{R}^\top H_t^{1/2^\top}\right)\right) \\
&= \Psi_h \left(\mathrm{vech}\left(H_t^{1/2}(\tilde{R}\xi_t\xi_t^\top\tilde{R}^\top - I_n)H_t^{1/2^\top}\right)\right).
\end{aligned} \tag{A.30}$$

By the symmetry of $(\tilde{R}\xi_t\xi_t^\top\tilde{R}^\top - I_n)$ and (A.19):

$$\mathrm{V}_{t+h}(\xi_t;\eta) = \Psi_h\, D_n^+ \left(H_t^{1/2} \otimes H_t^{1/2}\right) D_n \left(\mathrm{vech}(\tilde{R}\xi_t\xi_t^\top\tilde{R}^\top - I_n)\right). \tag{A.31}$$

□

Proposition 2.A.1. *The VMA(∞) representation of the BEKK(p, q) model (2.4) is given by*

$$X_t = \mathrm{vech}(H) + \sum_{i=0}^{\infty} \Psi_i Y_{t-i} \tag{A.32}$$

where $\mathrm{vech}(H) = \Phi(1)^{-1}c$ *denotes the long-run covariance matrix with* $c = \mathrm{vech}(CC^\top)$ *and the* $(n^* \times n^*)$ *coefficient matrices* Ψ_i *are given by* $\Psi_0 = I_{n^*}$ *and* $\Psi_i = -\tilde{B}_i + \sum_{j=1}^{i}\left(\tilde{A}_j + \tilde{B}_j\right)\Psi_{i-j}$ *(*$i = 1, 2, \ldots$*) where* $\tilde{A}_j = D_n^+\left(A_i \otimes A_i\right)^\top D_n$ *and* $\tilde{B}_j = D_n^+\left(B_j \otimes B_j\right)^\top D_n$*.*

For the BEKK(1, 1) model, these expressions simplify to: $\Psi_0 = I_{n^*}$, $\Psi_1 = \tilde{A}_1$ *and* $\Psi_i = \left(\tilde{A}_1 + \tilde{B}_1\right)\Psi_{i-1} = \left(\tilde{A}_1 + \tilde{B}_1\right)^{i-1}\tilde{A}_1$ *(*$i \geq 2$*).*

Proof. Transform (2.4) into its equivalent VEC representation:

$$\mathrm{vec}(H_t) = \mathrm{vec}(CC^\top) + \sum_{i=1}^{p}\mathrm{vec}(A_i^\top\varepsilon_{t-i}\varepsilon_{t-i}^\top A_i) + \sum_{j=1}^{q}\mathrm{vec}(B_j^\top H_{t-j}B_j). \tag{A.33}$$

Using (A.19) and exploiting (A.17) we get:

$$\begin{aligned}
D_n\,\mathrm{vech}(H_t) = D_n\,\mathrm{vech}(CC^\top) &+ \sum_{i=1}^{p}\left(A_i \otimes A_i\right)^\top D_n\,\mathrm{vech}(\varepsilon_{t-i}\varepsilon_{t-i}^\top) \\
&+ \sum_{j=1}^{q}\left(B_j \otimes B_j\right)^\top D_n\,\mathrm{vech}(H_{t-j}).
\end{aligned} \tag{A.34}$$

Multiplication with the Moore-Penrose inverse D_n^+ of the duplication matrix results in:

$$\begin{aligned}\operatorname{vech}(H_t) = \underbrace{\operatorname{vech}(CC^\top)}_{=:c} + \sum_{i=1}^{p} \underbrace{D_n^+ \left(A_i \otimes A_i\right)^\top D_n}_{=:\tilde{A}_i} \operatorname{vech}(\varepsilon_{t-i}\varepsilon_{t-i}^\top) \\ + \sum_{j=1}^{q} \underbrace{D_n^+ \left(B_j \otimes B_j\right)^\top D_n}_{=:\tilde{B}_j} \operatorname{vech}(H_{t-j})\end{aligned} \tag{A.35}$$

To derive the equivalent VARMA($\max(p,q), q$) representation as in Hafner and Herwartz (2006), set $X_t := \operatorname{vech}(\varepsilon_t\varepsilon_t^\top)$ and $Y_t := X_t - \operatorname{vech}(H_t)$. Y_t is a weak white noise process with $\mathrm{E}[Y_t] = 0$, $\mathrm{Var}(Y_t) = H_Y$ and $\mathrm{E}[Y_t Y_s^\top] = 0$ $(t \neq s)$. Rearranging (A.35) yields:

$$X_t = c + \sum_{i=1}^{\max(p,q)} \left(\tilde{A}_i + \tilde{B}_i\right) X_{t-i} - \sum_{j=1}^{q} \tilde{B}_j Y_{t-j} + Y_t \tag{A.36}$$

where $\tilde{A}_i = 0$ for $i > p$ and $\tilde{B}_i = 0$ for $i > q$. By stationarity of (2.4), this can be rewritten in VMA(∞) form using the lag operator L:

$$\begin{aligned}\underbrace{\left(I_{n^*} - \sum_{i=1}^{\max(p,q)} \left(\tilde{A}_i + \tilde{B}_i\right) L^i\right)}_{=:\Phi(L)} X_t &= c + \underbrace{\left(I_{n^*} - \sum_{j=1}^{q} \tilde{B}_j L^j\right)}_{=:\Theta(L)} Y_t \\ \Leftrightarrow X_t &= \Phi(1)^{-1}c + \underbrace{\Phi(L)^{-1}\Theta(L)}_{=:\Psi(L)} Y_t \\ &= \operatorname{vech}(H) + \sum_{i=0}^{\infty} \Psi_i Y_{t-i}.\end{aligned} \tag{A.37}$$

The $(n^* \times n^*)$ coefficient matrices Ψ_i are determined recursively by coefficient matching (Lütkepohl, 2005). □

2.A.3 Asymptotic theory for VIRFs

Proof of Theorem 1. The result follows by an application of the Delta method together with the asymptotic normality of the QML estimator. The Jacobian can be derived as follows: Let $\eta \in \mathbb{R}^m$ denote the vector of stacked parameters of the BEKK(p,q) model: $\eta = \left(\operatorname{vec}(C)^\top, \operatorname{vec}(A_1)^\top, \ldots, \operatorname{vec}(A_p)^\top, \operatorname{vec}(B_1)^\top, \ldots, \operatorname{vec}(B_q)^\top\right)^\top$. Starting with the definition of the VIRF for BEKK(p,q) models, we have:

$$\mathrm{V}_{t+h}(\xi_t;\eta) = \Psi_h D_n^+ \left(\operatorname{vec}(H_t^{1/2}\tilde{R}\xi_t\xi_t^\top\tilde{R}^\top(H_t^{1/2})^\top) - \operatorname{vec}(H_t)\right) \tag{A.38}$$

where $(\Psi_h)_{h\in\mathbb{N}}$ are given in Proposition 2.A.1. To calculate the derivative of the VIRF with respect to η we make use of (A.22) and (A.23). Moreover, the derivatives of the BEKK model with regard to its parameters, i.e., $\frac{\partial \operatorname{vec}(H_t)}{\partial \eta^\top}$ can be found in Hafner and Herwartz (2008), such that $\frac{\partial \operatorname{vec}(H_t)}{\partial \eta^\top}$ is known. Then, for the VIRF at time $h = 0$:

$$\begin{aligned}
\frac{\partial \mathrm{V}_t(\xi_t;\eta)}{\partial \eta^\top} &= D_n^+ \left[\frac{\partial \operatorname{vec}\left(H_t^{1/2}\tilde{R}\xi_t\xi_t^\top\tilde{R}^\top H_t^{1/2}\right)}{\partial \operatorname{vec}\left(H_t^{1/2}\right)^\top} \frac{\partial \operatorname{vec}\left(H_t^{1/2}\right)}{\partial \operatorname{vec}\left(H_t\right)^\top} \frac{\partial \operatorname{vec}(H_t)}{\partial \eta^\top} - \frac{\partial \operatorname{vec}(H_t)}{\partial \eta^\top} \right] \\
&\quad \times \left[\left(H_t^{1/2}\otimes I_n\right) + \left(I_n \otimes H_t^{1/2}\right)\right]^{-1} \frac{\partial \operatorname{vec}(H_t)}{\partial \eta^\top} - \frac{\partial \operatorname{vec}(H_t)}{\partial \eta^\top} \Bigg] \\
&= D_n^+ \Bigg[\left(\left(H_t^{1/2}\tilde{R}\xi_t\xi_t^\top\tilde{R}^\top \otimes I_n\right) + \left(I_n \otimes H_t^{1/2}\tilde{R}\xi_t\xi_t^\top\tilde{R}^\top\right)\right) \\
&\quad \times \left[\left(H_t^{1/2}\otimes I_n\right) + \left(I_n \otimes H_t^{1/2}\right)\right]^{-1} - I_{n^2} \Bigg] \frac{\partial \operatorname{vec}(H_t)}{\partial \eta^\top}.
\end{aligned}$$

Now let $h \in \mathbb{N}$. Exploiting the fact that the VMA coefficients Ψ_i, $i = 1, \ldots, h$ are recursively defined, the derivative of the BEKK(p, q) VIRF can be derived building on the product rule (Magnus and Neudecker, 1988, Theorem 5.12):

$$\frac{\partial \mathrm{V}_{t+h}(\xi_t;\eta)}{\partial \eta^\top} = \left(\mathrm{V}_t^\top \otimes I_{\frac{n(n+1)}{2}}\right) \frac{\partial \operatorname{vec}(\Psi_h)}{\partial \eta^\top} + \left(I_{\frac{n(n+1)}{2}} \otimes \Psi_h\right) \frac{\partial \mathrm{V}_t(\xi_t;\eta)}{\partial \eta^\top}$$

Moreover, we can establish the recursion

$$\begin{aligned}
\frac{\partial \operatorname{vec}(\Psi_h)}{\partial \eta^\top} &= \frac{\partial \operatorname{vec}(-\tilde{B}_h)}{\partial \eta^\top} + \sum_{j=1}^{h} \frac{\partial \operatorname{vec}\left(\left(\tilde{A}_j + \tilde{B}_j\right)\Psi_{h-j}\right)}{\partial \eta^\top} \\
&= \frac{\partial \operatorname{vec}(-\tilde{B}_h)}{\partial \eta^\top} + \sum_{j=1}^{h} \left(\Psi_{h-j}^\top \otimes I_{n^*}\right) \frac{\partial \operatorname{vec}\left(\tilde{A}_j + \tilde{B}_j\right)}{\partial \eta^\top} \\
&\quad + \left(I_{n^*} \otimes \left(\tilde{A}_j + \tilde{B}_j\right)\right) \frac{\partial \operatorname{vec}\left(\Psi_{h-j}\right)}{\partial \eta^\top}.
\end{aligned}$$

To evaluate this expression, we derive $\frac{\partial \operatorname{vec}\left(\tilde{A}_j\right)}{\partial \eta^\top}$, $(j = 1, \ldots, h)$. The derivations for $\tilde{B}_j$ follow analogously. To this end, we insert the definition of $\tilde{A}_j$ and make use of (A.19),

(A.20) and (A.21) to make the following transformations:

$$\begin{aligned}
\frac{\partial \operatorname{vec}\left(\tilde{A}_j\right)}{\eta^\top} &= \frac{\partial \operatorname{vec}\left(D_n^+ \left(A_j \otimes A_j\right)^\top D_n\right)}{\partial \eta^\top} \\
&= \frac{(D_n^\top \otimes D_n^+)\partial \operatorname{vec}\left(A_j \otimes A_j\right)^\top}{\partial \eta^\top} \\
&= \frac{(D_n^\top \otimes D_n^+)\partial \operatorname{vec}\left(A_j^\top \otimes A_j^\top\right)}{\partial \eta^\top} \\
&= \left(D_n^\top \otimes D_n^+\right)\left(I_n \otimes K_n \otimes I_n\right) \frac{\partial \left(\operatorname{vec}(A_j^\top) \otimes \operatorname{vec}(A_j^\top)\right)}{\partial \eta^\top}.
\end{aligned}$$

Finally, by an application of (A.25) and (A.26) it holds:

$$\frac{\partial \left(\operatorname{vec}(A_j^\top) \otimes \operatorname{vec}(A_j^\top)\right)}{\partial \eta^\top} = \left(K_n \otimes \operatorname{vec}(A^\top)\right) + \left(\operatorname{vec}(A^\top) \otimes K_n\right) \tag{A.39}$$

Thus, the formula for the derivative of the BEKK(p, q) VIRF can be implemented recursively.

For the BEKK$(1, 1)$ model, we can derive a more compact recursive formula for $\frac{\partial \mathrm{V}_{t+h}(\eta)}{\partial \eta^\top}$ based on (2.6). Let $h \in \mathbb{N}$. By an application of the product rule it holds:

$$\begin{aligned}
\frac{\partial \mathrm{V}_{t+h}(\xi_t; \eta)}{\partial \eta^\top} &= \frac{\partial \operatorname{vec}\left(\left(\tilde{A} + \tilde{B}\mathbb{1}_{\{h>1\}}\right) \mathrm{V}_{t+h-1}(\xi_t; \eta)\right)}{\partial \eta^\top} \\
&= \left(\mathrm{V}_{t+h-1}(\xi_t; \eta)^\top \otimes I_{\frac{n(n+1)}{2}}\right) \frac{\partial \operatorname{vec}\left(\tilde{A} + \tilde{B}\mathbb{1}_{\{h>1\}}\right)}{\eta^\top} \\
&+ \left(\tilde{A} + \tilde{B}\mathbb{1}_{\{h>1\}}\right) \frac{\partial \mathrm{V}_{t+h-1}(\xi_t; \eta)}{\partial \eta^\top}.
\end{aligned}$$

In this case, we have to calculate $\frac{\partial \operatorname{vec}\left(\tilde{A}+\tilde{B}\mathbb{1}_{\{h>1\}}\right)}{\eta^\top}$ only once to establish the recursion for $\frac{\partial \mathrm{V}_{t+h}(\xi_t;\eta)}{\partial \eta^\top}$. This completes the proof. □

2.A.4 Causality of the VIRF

Proof of Corollary 2.2.1.

$$
\begin{aligned}
\mathrm{V}_{t+h}(\mathcal{T}_t) &= \mathrm{E}[\mathrm{vech}(H_{t+h}(\mathcal{T}_t))|\tilde{\mathcal{F}}_t] - \mathrm{E}[\mathrm{vech}(H_{t+h})|\mathcal{F}_{t-1}] \\
&= \mathrm{E}[\mathrm{vech}(\mathcal{H}_{t+h})|\mathcal{F}_{t-1}, \mathcal{T}_t] - \mathrm{E}[\mathrm{vech}(H_{t+h})|\mathcal{F}_{t-1}] \\
&= \mathrm{E}[\mathrm{vech}(\mathcal{X}_{t+h})|\mathcal{F}_{t-1}, \mathcal{T}_t] - \mathrm{E}[\mathrm{vech}(X_{t+h})|\mathcal{F}_{t-1}] \\
&= \frac{\mathrm{E}[\mathrm{vech}(X_{t+h}(\mathcal{T}_t))\mathbb{1}_{\{\xi_t \in \mathcal{T}_t\}}|\mathcal{F}_{t-1}]}{\mathrm{E}\left[\mathbb{1}_{\{\xi_t \in \mathcal{T}_t\}}|\mathcal{F}_{t-1}\right]} - \mathrm{E}[\mathrm{vech}(X_{t+h})|\mathcal{F}_{t-1}] \\
&= \frac{\mathrm{E}\left[\mathrm{vech}(X_{t+h}(\mathcal{T}_t)|\mathcal{F}_{t-1}\right]\mathrm{E}\left[\mathbb{1}_{\{\xi_t \in \mathcal{T}_t\}}|\mathcal{F}_{t-1}\right] + \mathrm{cov}(\mathrm{vech}(X_{t+h}(\mathcal{T}_t)), \mathbb{1}_{\{\xi_t \in \mathcal{T}_t\}}|\mathcal{F}_{t-1})}{\mathrm{E}\left[\mathbb{1}_{\{\xi_t \in \mathcal{T}_t\}}|\mathcal{F}_{t-1}\right]} \\
&\quad - \mathrm{E}[\mathrm{vech}(X_{t+h})|\mathcal{F}_{t-1}] \\
&= \mathrm{E}[\mathrm{vech}(X_{t+h}(\mathcal{T}_t)) - \mathrm{vech}(X_{t+h})|\mathcal{F}_{t-1}] + \underbrace{\frac{\mathrm{cov}(\mathrm{vech}(X_{t+h}(\mathcal{T}_t)), \mathbb{1}_{\{\xi_t \in \mathcal{T}_t\}}|\mathcal{F}_{t-1})}{\mathrm{E}[\mathbb{1}_{\{\xi_t \in \mathcal{T}_t\}}]}}_{:=\Delta_{t+h}(\mathcal{T}_t|\tilde{\mathcal{F}}_{t-1})}
\end{aligned}
$$

Under Assumption 2.2.2, which asserts that the contemporaneous treatment ξ_t is jointly independent of all future treatments and potential outcomes, it holds that: $\Delta_{t+h}(\mathcal{T}_t|\tilde{\mathcal{F}}_{t-1}) = 0$. Hence, the VIRF identifies the filtered impulse causal effect. □

Chapter 3

Time-varying shock transmission in proxy-identified volatility models*

Jeannine Polivka†

*Financial support from the Doc.Mobility Program of the University of St. Gallen (HSG), Grant No: 1031603, is gratefully acknowledged.

†School of Economics and Political Science, Department of Economics, University of St. Gallen, Bodanstrasse 6, 9000 St. Gallen, Switzerland. Email: jeannine.polivka@unisg.ch.

Abstract

I suggest a modeling framework allowing for dynamic shock impacts in high-frequent proxy-identified structural models with reduced form errors obeying a multivariate GARCH structure. The model captures smoothly time-varying behavior in the shock transmission mechanism due to, e.g., the financial business cycle or changes in monetary policy, by combining the proxy identification method with a nonparametric estimation approach. To simultaneously point-identify all shocks driving the system, I state the optimization problem of finding the structural matrix guaranteeing shock orthogonality given the identifying information encoded in the proxy variables as an orthogonal Procrustes problem. I investigate the impact of financial and monetary policy uncertainty shocks on daily returns in an empirical application to a system of major asset classes, which are focal components of the green energy transition. The model delivers nuanced volatility spillover patterns and indicates that it is crucial to account for time variation in structural transmission mechanisms for informed policy and financial stability analysis.

Keywords: multivariate GARCH models, proxy identification, nonparametric modeling, structural identification, sVAR, time-varying shock transmission, volatility spillovers, uncertainty

JEL: C32, C14, C51, C58, E32, E52

3.1 Introduction

Against the background of the Great Recession following the Gobal Financial Crisis (GFC) and the COVID-19 pandemic, analyzing the impact of uncertainty on financial markets has become a prime focus of policy authorities, market participants and researchers. In the quest to obtain a comprehensive understanding of uncertainty shocks and their dynamic effects (see, e.g., the seminal work by Bloom, 2009), three questions stand out: Does the transmission mechanism of financial uncertainty shocks vary with the financial business cycle? Does the transmission of monetary policy shocks change with the monetary policy stance and strategies? And what are the joint effects of financial and monetary policy uncertainty? These questions have also attracted new attention to the literature on structural models which aim at analyzing the impacts and spillover effects of perturbations on the economy for policy and financial stability analysis (see, e.g., the seminal paper by Bekaert et al., 2013). While numerous studies examine the dynamic transmission of structural shocks, analyses typically focus on low-frequent time-varying parameter (TVP) structural vector autoregression (sVAR) models of macroeconomic variables with heteroscedastic shocks as originated by Primiceri (2005), which are inferred using classical identification techniques such as ordering or sign restrictions.

In this paper, I suggest a modeling framework which can capture smoothly time-varying behavior in the impact of proxy-identified shocks and apply it to a high-frequent structural model with multivariate GARCH (MGARCH) type errors. The proposed framework contributes to the extant literature on identification in three ways: First, my model modifies the relevance condition of the proxy identification approach by Stock and Watson (2012, 2018) and Mertens and Olea (2013) to allow for smooth time variation and provides a nonparametric estimator for the structural parameter matrix. Second, targeting the point identification of several structural shocks at once over time, the model infers an optimal structural decomposition guaranteeing shock orthogonality by drawing from the literature on orthogonal Procrustes problems (see, e.g., Gower and Dijksterhuis, 2004, for an overview). Third, while extant work typically focuses on the analysis of one dimension of uncertainty at a time (see, e.g., Stock and Watson, 2012), my model allows me to analyse the simultaneous dynamic impacts of several shocks on a multivariate system and its second moments over time.

Understanding the impact of labeled structural shocks on financial systems and the change

of their transmission over time is crucial for, e.g., asset and risk management purposes. Looking beyond negative correlations of asset returns to minimize portfolio variance, it is of first-order importance to understand under which market and policy circumstances assets are affected by certain structural shocks and how. A comprehensive understanding of the dynamic impact of, e.g., financial uncertainty and monetary policy shocks on return and volatility systems helps policy authorities improve their measures and communication conditional on, e.g., the business cycle phase or the monetary policy stance, to support economic activity, preserve financial stability and bolster the green energy transition. In this context, the paper contributes to the fast-growing literature on the joint dynamic impact of financial and monetary policy uncertainty shocks on financial market returns and their (co)variances.

Besides their popularity in the empirical sVAR literature, uncertainty measures are natural instrument candidates to examine smoothly time-varying shock transmission mechanisms in structural models. They feature, e.g., countercyclical variations (Bloom, 2014) or move with the Federal Open Market Committee (FOMC) cycle (Bauer et al., 2021) and are often available at a constant high frequency which facilitates nonparametric estimation and identification. The modeling framework featuring MGARCH errors is particular attractive for the investigation of the dynamic impact of shocks on daily asset return systems (Bauwens et al., 2006). Techniques for the identification of the high-frequent latent shocks driving structural MGARCH models have been suggested by Hafner et al. (2022), whose approach is inspired by independent component analysis, and Fengler and Polivka (2022a), who employ a proxy-guided Givens orthogonalization approach building on the external instruments sVAR literature. However, like the majority of the related sVAR literature, their pioneering work on structural multivariate volatility models assumes the shock transmission mechanism to be static.

In the context of the sVAR literature, the quest for flexible structural models dates to Primiceri (2005) who extends the sVAR model to allow for time-varying parameters and multivariate stochastic volatility. Revisiting this seminal work, Koop et al. (2009) divide the potential sources of time-varying shock transmissions into heteroskedasticity of the latent exogenous shocks or a changing transmission mechanism. In an application to a standard system of macroeconomic variables, Koop et al. (2009) report evidence of changes in the transmission mechanism as well as in the covariance matrix of the structural shocks in a TVP-sVAR framework. While the TVP-sVAR model has since been extended in various directions, see, e.g., the work of Sims and Zha (2006) investigating regime-changes in the

reduced form parameters, the identifying assumptions employed are typically standard identifying restrictions, such as sign restrictions. In recent years, however, the identification based on external instruments introduced by Mertens and Ravn (2013) and Stock and Watson (2012, 2018) has gained popularity as it provides an alternative to restrictive recursive or implausible economic identifying assumptions. Their approach has spurred new research efforts in the areas of full identification and dynamic impacts of shocks. While the original proxy identification framework targets the identification of one shock at a time, Angelini and Fanelli (2019) provide conditions for the identification of the entire underlying shock system, and Fengler and Polivka (2022a) suggest a proxy-guided Givens orthogonalization approach to achieve full identification when using k external instruments to identify k shocks. Targeting dynamic shock transmission, Lütkepohl and Schlaak (2022) suggest a heteroskedastic proxy-VAR framework which – in the tradition of the literature on identification by heteroscedasticity (see, e.g., Herwartz and Lütkepohl (2014)) – can feature dynamic impact effects through regime-switching behavior in the covariance of the structural shock of interest with its instrument. Hence, the dynamics of the transmission mechanism change with the covariance regime.

This paper goes beyond the idea of regime-dependent volatility by explicitly modeling the conditional heteroscedasticity in the reduced form innovations. Hence – even when assuming the shock transmission mechanism to be static – my model captures the time variation in the shock propagation which derives from the dynamics of the MGARCH model for the reduced form errors. In addition to this time variation, my model targets the investigation of the presence of an exogenously time-varying contemporaneous transmission mechanism – a research direction recently also suggested by Mumtaz and Petrova (2022) in the context of a Bayesian proxy-sVAR model with time-varying parameters. By simultaneously allowing for the presence of a dynamic model for the conditional mean and for the multivariate conditional covariance matrix, the modeling framework aims at disentangling variations in the contemporaneous shock transmission mechanism from the dynamics of the mean equation, which may, e.g., follow a TVP-sVAR in the spirit of Primiceri (2005), and from the evolution of the conditional covariance matrix of the reduced form innovations. Following a similar objective, Hafner and Herwartz (2022), for instance, suggest an sVAR-MGARCH specification for the dynamic extension of their structural MGARCH framework. Similar to Lütkepohl and Schlaak (2022), to render the proxy identification approach flexible, my model assumes the covariance of the structural shocks with their respective instrument to be smoothly time-varying. This generalization allows for flexible nonparametric estimation of the structural transmission matrix under, e.g.,

local stationarity and continuous differentiability assumptions on the parameter evolution (Zhang and Wu, 2012). By modeling the structural parameter matrix as a smooth function of time, the model dispenses of implausible random walk assumptions (Primiceri, 2005; Koop et al., 2009) and of restrictive autoregressive assumptions (Hafner and Herwartz, 2022) to describe the evolution of the multivariate shock propagation mechanism. As the orthogonal Procrustes problem has a known analytical solution, using the proxy-guided estimate of the structural transmission matrix as input, it is computationally simple to obtain the clostest matrix in terms of the Frobenius norm which guarantees shock orthogonality.

In an empirical application, I investigate a system of major asset classes, which are focal components of the green energy transition. The model provides compelling evidence of changes in the daily shock transmission of a financial uncertainty and a joint monetary policy surprise and uncertainty shock to foreign exchange, clean energy equity and commodity markets. Empirical results furthermore emphasize the presence of time variation in the volatility reception mechanism in accordance with, e.g., the financial cycle, changes in monetary policy measures, such as the introduction of quantitative easing programs, and fluctuations in oil supply. At the same time, the model delivers a deeper understanding of the joint impact of financial and monetary policy shocks. While, e.g., monetary policy shocks are – even at the zero lower bound – the driving force of U.S. Dollar Index returns and (co)variances, the reaction of the U.S. Dollar Index to financial uncertainty shocks during market downturns is consistent with the Dollar's role as a safe-haven currency. While the static proxy-MGARCH model indicates, e.g., a negligible influence of monetary policy uncertainty and commodity-related shocks on the conditional variance of clean energy equities, the dynamic model reveals spikes in their contribution. Changes in the transmission mechanism hint at potential substitution effects between commodities and clean energy markets in crisis times and at transition effects, e.g., during the COVID-19 pandemic.

The paper is structured as follows: The next section describes the modeling framework and presents the proxy-based approach to full identification in the static as well as the dynamic setting. The data section extensively discusses the choice of proxy variables. The centerpiece of the paper is the empirical application of the novel identification procedure, featuring an investigation of the time-varying transmission mechanism, the contemporaneous impact of counterfactual shocks and the dynamic volatility spillovers. The last section concludes.

3.2 Time-varying shock transmission

3.2.1 Modeling framework and identification

Consider the system of n speculative (log) returns given by

$$r_t = \mu_t + \varepsilon_t \quad (t \in \mathbb{Z}) \tag{3.1}$$

where $\mu_t = \mathrm{E}[r_t|\mathcal{F}_{t-1}]$ and $\mathcal{F}_t = \sigma(\{\varepsilon_s : s \leq t\})$ denotes the information available up to time t, generating the filtration $(\mathcal{F}_t)_{t\in\mathbb{Z}}$. The n-dimensional innovation vector ε_t is assumed to be square-integrable, satisfies $\mathrm{E}[\varepsilon_t|\mathcal{F}_{t-1}] = 0$ and has the conditional covariance matrix $\mathrm{Var}[\varepsilon_t|\mathcal{F}_{t-1}] = H_t$. For example, ε_t can be the reduced form innovation of a stable VAR model featuring conditional heteroscedasticity. This process $(H_t)_{t\in\mathbb{Z}}$ is assumed to be covariance stationary and for every $t \in \mathbb{Z}$ the matrix H_t is almost surely symmetric and positive definite. By $H_t^{1/2} \in \mathbb{R}^{n\times n}$, I denote the principal matrix square root (see Definition D.1) of H_t which uniquely exists, for all $t \in \mathbb{Z}$, as H_t is symmetric and positive definite. Furthermore, let $\left(\tilde{R}_t\right)_{t\in\mathbb{Z}}$ be a sequence of orthogonal matrices (see Definition D.2) and $\xi = (\xi_t)_{t\in\mathbb{Z}}$ an n-dimensional real-valued white noise process of structural shocks with zero mean and identity covariance matrix, i.e., $\xi_t \sim WN(0, I_n)$. The set of latent structural shocks is assumed to be combinedly influencing the observable asset returns through the following mechanism:

Definition 3.2.1. The process $(\varepsilon_t)_{t\in\mathbb{Z}}$ follows a time-varying structural multivariate GARCH process with structural decomposition Q_t if it satisfies:

$$\varepsilon_t = Q_t\xi_t = H_t^{1/2}\tilde{R}_t\xi_t \quad (t \in \mathbb{Z}). \tag{3.2}$$

If furthermore $\xi_t \sim SWN(0, I_n)$ follows a strict white noise process, then $(\varepsilon_t)_{t\in\mathbb{Z}}$ is said to follow a strong time-varying structural multivariate GARCH process.

The orthogonal matrix $\tilde{R}_t$ in (3.2) endows the model with a structural interpretation and specifies the propagation channels of the structural shocks. By allowing $\tilde{R}_t$ to vary with time, the model can accommodate changes in the way that variables react to shocks, e.g., against the background of policy changes and monetary policy transitions or worsening economic conditions. Even in combination with a flexible VAR model for the mean

$$r_t = c_t + A_{1,t}r_{t-1} + \ldots + A_{p,t}r_{t-p} + \varepsilon_t \quad (t \in \mathbb{Z}) \tag{3.3}$$

the strong time-varying MGARCH model differs from the standard TVP-VAR with stochastic volatility suggested by Primiceri (2005) in several aspects: First, the strong MGARCH model accounts for the complex dynamics in the conditional covariance process of the demeaned returns. It allows for dependencies between the variables through the conditional covariances and captures two of the most important stylized facts of asset returns: conditional heteroscedasticity and volatility clustering. Second, by capturing the conditional time variation in the second moments of the reduced form innovation, the strong time-varying structural MGARCH model allows one to assume that the underlying structural shocks are independent and identically distributed (iid) variables. They can thus be modeled as genuine surprises to financial markets given past information. This framework stands in sharp contrast to Primiceri's (2005) modeling approach which assumes that the unobserved structural shocks are heteroscedastic and that their logarithmic variances – like the time-varying VAR parameters – follow random walks. This assumption implies that the variance exhibits non-stationary behavior and becomes unbounded in the limit, whereas asset return (co)variances are typically assumed to be stationary. Third, the strong time-varying structural MGARCH model allows for separate dynamics in the reduced form parameters of the mean, in the conditional multivariate volatility process[3] and in the structural transmission mechanism. By allowing for full covariance dynamics in the returns in combination with a structural transmission matrix, it is more flexible than the modeling approach of Primiceri (2005) who specifies (conditionally) heteroscedastic but mutually uncorrelated structural shocks which are multiplied with a structural transmission matrix B_t derived from

$$\mathrm{E}[\varepsilon_t \varepsilon_t^\top | \mathcal{F}_{t-1}] = B_t \Lambda_t B_t^\top \tag{3.4}$$

where $\Lambda_t = \mathrm{Var}(\xi_t | \mathcal{F}_{t-1})$ is a diagonal matrix. Highlighting the commonalities of the suggested model and the framework proposed by Primiceri (2005), both models allow for a dynamic contemporaneous impact matrix (B_t respectively $\tilde{R}_t$). In Primiceri's (2005) model, Λ_t is assumed to be diagonal, which implies that a perturbation in the i-th shock of interest has a time-invariant structural effect on the j-th return variable. This in turn motivates the assumption that B_t should be time-varying (Primiceri, 2005). By contrast, the strong structural multivariate GARCH allows for time-varying structural effects across shocks and variables already through the off-diagonal elements of the conditional covariance matrix evolving with the MGARCH process. While the macroeconomic VAR literature

[3] In theory, the introduction of dynamics in the conditional multivariate volatility process can be extended to the consideration of separate dynamics in the reduced form parameters of H_t. While such specifications exist (see, e.g., Silvennoinen and Teräsvirta, 2015, 2021) they are complex to estimate and rarely applied outside of bivariate systems.

mainly follows Primiceri (2005) and Del Negro and Primiceri (2015) and imposes random walk dynamics on B_t, I exploit information from outside the strong MGARCH model to identify $\tilde{R}_t$ at every point in time.

To illustrate the consequences of a static and non-structural transmission mechanism in the context of multivariate volatility models, one could consider, e.g., choosing $\tilde{R}_t$ to be the constant identity matrix. This choice implies a constant propagation mechanism, which is symmetric because the principal matrix square root preserves the symmetry of H_t. In contrast, if one chooses a mechanism which transforms the sequence of principal matrix square roots into, e.g., triangular matrices given by Cholesky decompositions, the volatility spillovers obey a recursive ordering principle imposed by the triangular decomposition. Such a cascading structure may – due to the interconnectedness of financial markets – only hold in limited scenarios. Thus, although both the principal matrix square root and the Cholesky decomposition are popular static ad hoc decompositions, neither specification for $\tilde{R}_t$ rests on solid economic grounds for general asset return systems at daily frequency (see also the discussion by Fengler and Polivka, 2022a).

Potential avenues for the identification of a constant structural matrix $\tilde{R}$ for high-frequent data include the identification by non-Gaussianity developed by Hafner et al. (2022) and the proxy-based scheme devised by Fengler and Polivka (2022a) which may additionally allow for shock labeling. Both approaches can – despite assuming the orthogonal matrix to be constant – deliver conditionally time-varying volatility spillovers through the dynamics of the multivariate process H_t and its principal matrix square root. However, assuming the structural shock transmission matrix R_t to be time-invariant precludes the structural model from capturing, e.g., exogeneous policy changes or business cycle effects, which may imply deviations from the long-run propagation mechanism, e.g., during recessions. Hafner and Herwartz (2022) motivate the extension of their statistical identification approach with the presence of time-dependent higher conditional moments of daily asset return systems. They introduce an autoregressive updating mechanism for the static rotation matrix in a bivariate VAR-MGARCH system and show that their time-varying kurtosis measure can be connected to the geopolitical risk factor of Engle and Campos-Martins (2020). Instead of intensifying the parameterization of the structural model, I suggest a dynamic nonparametric approach to identification based on external data (see Stock and Watson (2016) for a comprehensive survey on the identification of structural shocks). My approach readily extends to higher dimensional systems and provides identified shocks that can be interpreted economically in a theoretically consistent manner.

3.2.2 Identification by proxy

The proxy sVAR approach introduced by Stock and Watson (2012) and Mertens and Ravn (2013), which has gained recent popularity in structural modeling, estimates the contemporaneous impact matrix using an instrumental variable (IV) procedure. In contrast to the classical IV setting aiming at identifying a causal relationship by using the IV in the presence of latent confounders, here, the instrument acts as an exogenous proxy for the latent shock of interest. The proxy variable is usually constructed using a narrative approach (Romer and Romer, 2004). By relying on external information, the proxy sVAR methodology reduces the argumentative effort for the justification of economically motivated restrictions to achieve identification. This makes it particularly attractive for the structural modeling of high-frequent asset return systems (see also the discussion by Fengler and Polivka, 2022a). In the context of VAR models, employing the proxy variable as an instrument – instead of including it as an endogenous variable in the dynamic mean equation – alleviates the effects of measurement error in the proxy (Carriero et al., 2015).

To derive the structural decomposition of the time-varying strong MGARCH model, I consider the principal matrix square root as initial decomposition of the conditional covariance matrix, $H_t = H_t^{1/2}\left(H_t^{1/2}\right)^\top$. Following Fengler and Polivka (2022a), I define the standardized residuals $(u_t)_{t\in\mathbb{Z}}$ for every $t \in \mathbb{Z}$ via

$$\begin{aligned} \varepsilon_t &= Q_t\xi_t = H_t^{1/2}\tilde{R}_t\xi_t \\ \Leftrightarrow \quad \tilde{R}_t\xi_t &= (Q_t)^{-1}\,\varepsilon_t =: u_t \end{aligned} \tag{3.5}$$

One could equally consider the Cholesky decomposition of H_t as starting value. For example, Mumtaz and Petrova (2022) use a triangular decomposition in their Bayesian identification approach to a time-varying parameter proxy-sVAR with heteroscedastic reduced form innovations combined with a constant orthogonal transmission matrix.

Static full identification by proxy

As the static strong structural MGARCH model serves as a benchmark for the dynamic modeling approach, I give a brief overview over potential avenues for full identification of a constant structural orthogonal matrix using proxy variables. Assume, in the spirit of Stock and Watson (2012) and Mertens and Ravn (2013), that there exists a centered $(n-1)$-dimensional instrument process $Z = (Z_t)_{t\in\mathbb{Z}}$ such that, for all $i = 1, \ldots, n-1$, $t =$

$1, \ldots, T$,

$$\mathrm{E}[\xi_{it} Z_{it}] = \phi_i \in \mathbb{R} \setminus \{0\} \qquad \text{(relevance)} \tag{3.6}$$

$$\mathrm{E}[\xi_t^{-i} Z_{it}] = 0 \in \mathbb{R}^{n-1} \qquad \text{(exogeneity)} \tag{3.7}$$

where the index i relates to the i-th vector element and the superscript $-i$ denotes all vector elements apart from the i-th element. Based on assumptions (3.6) and (3.7), an individual column of $\tilde{R}$ can be estimated using moment conditions (Fengler and Polivka, 2022a):

$$\tilde{R}_{\bullet i} = \pm \mathrm{E}[u_t Z_{it}] \left(\mathrm{E}[Z_{it} u_t^\top] \, \mathrm{E}[u_t Z_{it}] \right)^{-1/2}. \tag{3.8}$$

To estimate the full orthogonal matrix, one can proceed by means of a proxy-guided Givens orthogonalization scheme (Fengler and Polivka, 2022a). This approach derives the orthogonal transmission matrix $\tilde{R}^{QR}$ from a QR decomposition of the input matrix $\tilde{R}^{\mathrm{nv}}_{n\times(n-1)}$ consisting of the $(n-1)$ individually estimated columns:

$$\tilde{R}^{\mathrm{nv}}_{n\times(n-1)} = \tilde{R}^{QR} R \Rightarrow \tilde{R}^{QR} = \tilde{R}^{\mathrm{nv}}_{n\times(n-1)} R^{-1}. \tag{3.9}$$

It enforces the orthogonality of the resulting structural shocks and the exogeneity conditions for all pairs (Z_i, ξ_j) with $j > i$, $i = 1, \ldots, n-1$. Hence, one can target full exogeneity by successive orthogonalization of the proxy variables among each other. The proxy-guided orthogonalization procedure exploits the $n-1$ instruments recursively for identification of the columns of the orthogonal matrix. In practice, it is therefore advisable to order the instruments by descending relevance. Fengler and Polivka (2022a) show that consistent estimation of the transmission matrix and asymptotic inference is possible by replacing expectations with their sample mean analogues.

While it may be tempting to estimate the first $n-1$ columns of $\tilde{R}$ jointly by

$$\tilde{R}_{n\times k} = \mathrm{E}[u_t Z_t^\top] \left(\mathrm{E}[u_t^\top \odot Z_t] \, \mathrm{E}[Z_t^\top \odot u_t] \odot I_k \right)^{-1/2} \tag{3.10}$$

where $\odot$ denotes the Hadamard product, this procedure does not generally yield a well-defined orthogonal matrix: The resulting columns may not be orthogonal to each other, and while the matrix columns are orthonormal by construction, the orthonormality of the matrix rows may not be guaranteed either.

However, it is possible to calculate the closest orthogonal matrix, in terms of the Frobenius norm, to the $n \times (n-1)$ input matrix by means of an orthogonal Procrustes approach (see, e.g., Gower and Dijksterhuis, 2004). This approach takes all instrumental variables into

account with equal weight. While the Givens orthogonalization approach, e.g., treats the first column of the input matrix as the fixed first column of the orthogonal transmission matrix, the Procrustes solution simultaneously transforms all input columns. The optimal projection $\tilde{R}^*_{n\times k}$ $(k = n-1)$ can be calculated based on the singular value decomposition of the input matrix $\tilde{R}_{n\times k} = U_{n\times n} S_{n\times k} V^\top_{k\times k}$ (Schönemann, 1966), yielding

$$\tilde{R}^*_{n\times k} = U_{n\times n} I_{n\times k} V^\top_{k\times k} \tag{3.11}$$

where $I_{n\times k}$ denotes the identity matrix. To obtain a full $(n \times n)$ orthogonal matrix $\tilde{R}^*$, the last column can be computed as the residual vector which is orthogonal to the existing $(n-1)$ columns using the adjoint of $\tilde{R}^*_{n\times k}$. Although this residual column does not have a structural interpretation a priori, it captures all remaining shocks influencing the system. Like the proxy-guided Givens orthogonalization approach, the proxy-guided Procrustes orthogonalization approach guarantees the orthogonality of the resulting structural shocks. However, the additional flexibility in comparison to the recursive approach comes at the cost of the Procrustes approach not guaranteeing that the instrument exogeneity conditions will hold. However, if assumptions (3.6) and (3.7) are fulfilled, the Procrustes approach provides the optimal solution in terms of the Frobenius norm and is therefore superior to the Givens approach. Therefore, I use the static Procrustes approach as my baseline methodology and provide solutions using the static Givens scheme for comparison.

3.2.3 Dynamic structural shock transmission

The introduction of time dependence in the structural transmission matrix can be achieved via two methodological avenues. On the one hand, one can model the evolution of the orthogonal matrix over time in a stand-alone fashion. For example, Hafner et al. (2022) impose an autoregressive structure on the rotation angle defining the orthogonal matrix of their bivariate structural model identified via non-Gaussianity. While their approach can be generalized to higher dimensions, every additional k-th dimension adds $k-1$ further autoregressive parameters to the model, hence adding further complexity to the estimation procedure. On the other hand, one can implement time variation in $\tilde{R}$ through regime-switching mechanisms or smooth transition frameworks. In the case of structural identification based on external data, these approaches can be tied directly to the identification conditions of the proxy-sVAR approach. Lütkepohl and Schlaak (2022) show how to extend the proxy-sVAR methodology to allow for regime changes in the contemporaneous impact matrix B_t in (3.4) through a time-varying relevance condition

that changes with the volatility regime. Their methodological approach can be applied in a similar fashion to identify the structural orthogonal matrix in (3.2). As specifying the conditional covariance matrix by an MGARCH model already delivers conditional dynamics of the multivariate volatility process, I present a smooth transition framework which models the time-varying orthogonal matrix as a smooth function of time.

Dynamic identification by proxy

In the constant model, the estimate of each column $\tilde{R}_{\bullet i}$ is based on the static relationship

$$\mathrm{E}[u_t Z_{it}] = \mathrm{E}[\tilde{R}_{\bullet i}\xi_{it} Z_{it} + \tilde{R}^* \xi_t^* Z_{it}] = \tilde{R}_{\bullet i}\,\mathrm{E}[\xi_{it} Z_{it}] = \tilde{R}_{\bullet i}\phi_i\,, \tag{3.12}$$

which allows one to identify $\tilde{R}_{\bullet i}$ up to the unknown relevance parameter ϕ_i. The latter can be identified up to sign by

$$\mathrm{E}[Z_{it} u_t^\top]\,\mathrm{E}[u_t Z_{it}] = \phi_i \tilde{R}_{\bullet i}^\top \tilde{R}_{\bullet i}\phi_i = \phi_i^2. \tag{3.13}$$

Hence, by combining (3.13) and (3.12), one obtains (3.8) (see Fengler and Polivka, 2022a). In the static relevance set-up, the estimate $\hat{\psi}_i$ of $\mathrm{E}[u_t Z_{it}]$ is inferred using the constant sample mean analog. In the dynamic framework, I instead make use of nonparametric estimation techniques for time-varying regressions, originated by Robinson (1989) and developed further by, among others, Cai (2007), Zhou and Wu (2010), Zhang and Wu (2012), Vogt (2012) and Zhang and Wu (2015).

In its most general form, the time-varying regression model can be expressed by

$$Y_{it} = m_t(X_t) + \eta_t, \quad (t = 1, \ldots, T) \tag{3.14}$$

where Y_{it} is the response variable, X_t the vector of explanatory variables, η_t the error term and $m : [0,1] \times \mathbb{R}^n \to \mathbb{R}^n$, $m_t(\cdot) := m(t/T, \cdot)$ a smooth, time-varying regression function operating in rescaled time (t/T), $t = 1, \ldots, T$. Within this modeling class, the nonparametric regression techniques for locally stationary time series by Vogt (2012) and the time-varying coefficient (TVC) model (see, e.g., Cai, 2007) are particularly attractive due to their flexibility to fit stationary and non-stationary data (Chan et al., 2022). While Vogt (2012) suggests a local constant estimation procedure, both constant and local linear estimators – among which the latter perform better at the boundaries (Fan and Gijbels, 1996) – have been proposed for TVC models. TVC models are of the general form (Vogt, 2012)

$$Y_t = X_t^\top \beta_t + \eta_t, \quad (t = 1, \ldots, T). \tag{3.15}$$

For the framework at hand, $Y_t = Y_{it} = u_t Z_{it} = H_t^{-1/2} \varepsilon_t Z_{it}$ where the subscript i refers to the instrument Z_{it}, $\beta_t = \beta_{it} = \beta_i \left(\frac{t}{T}\right)$ for a smooth function $\beta_i : [0,1] \to \mathbb{R}^n$ operating in rescaled time, X_t denotes the explanatory variables and η_{it} the error term. When choosing, e.g., a unit constant as explanatory variable, the model reduces to the classical local linear estimator. In its original version, the model builds on iid assumptions for explanatory variables and error terms. However, Leung (2005) shows how the model can be estimated robustly in the presence of outliers in the error terms, Cai (2007) assumes the explanatory variable to be stationary and α-mixing but allows for serial correlation and heteroscedasticity in the error terms and Zhang and Wu (2012); Zhou and Wu (2010) relax this setting to the point that the variables are allowed to be locally stationary in the sense of Zhou and Wu (2010) (see Definition D.3) and Vogt (2012) (see Definition D.4, which is inspired by Dahlhaus (1997)). Both authors call a process locally stationary if it behaves in an approximately stationary way over a short period of time (Vogt, 2012).

As I assume β_i to be smooth, a Taylor approximation of first order around $s \in [0,1]$ arbitrary but fixed, following the notation of Cai (2007), yields

$$\beta_i \left(\frac{t}{T}\right) \approx \beta_i (s) + \beta_i' (s) \left(\frac{t}{T} - s\right) \tag{3.16}$$

where β_i' denotes the derivative of β_i. Hence, the TVC model can be locally approximated by

$$Y_{it} \approx \boldsymbol{X}_t^\top \zeta_i + \eta_{it} \tag{3.17}$$

where $\boldsymbol{X}_t = \left(X_t^\top, X_t^\top \left(\frac{t}{T} - s\right)\right)^\top$ and $\zeta_i = \zeta_i (s) = \left(\beta_i (s)^\top, \beta_i' (s)^\top\right)^\top$. Thus, a possible nonparametric local estimator for the time-varying covariance between the reduced form residuals and the proxy variables and its derivative is given by minimizing the locally weighted sum of squared residuals

$$\left(\hat{\beta}_i (s), \hat{\beta}_i'(s)\right) = \operatorname{argmin}_{\zeta_i} \sum_{t=1}^{T} \left(Y_{it} - \boldsymbol{X}_t^\top \zeta_i\right)^2 K \left(\frac{\frac{t}{T} - s}{b_T}\right) \tag{3.18}$$

where K denotes a kernel function and $b_T > 0$ is the bandwidth satisfying $b_T \to 0$ and $T b_T \to \infty$ for $T \to \infty$. Define $\hat{\psi}_{i0}(s) = \hat{\beta}_i(s)$ and $\hat{\psi}_{i1}(s) = b_T \hat{\beta}_i'(s)$. The minimizer of (3.18) is given by (Cai, 2007):

$$\begin{pmatrix} \hat{\psi}_{i0}(s) \\ \hat{\psi}_{i1}(s) \end{pmatrix} = \begin{pmatrix} U_{T,0}(s) & U_{T,1}(s) \\ U_{T,1}(s) & U_{T,2}(s) \end{pmatrix}^{-1} \begin{pmatrix} V_{T,0}(s) \\ V_{T,1}(s) \end{pmatrix} = U_T^{-1}(s) V_T(s) \tag{3.19}$$

with, for $0 \leq k \leq 2$,

$$U_{T,k}(s) = \frac{1}{Tb_T} \sum_{t=1}^{T} X_t X_t^\top \left(\frac{\frac{t}{T} - s}{b_T} \right)^k K \left(\frac{\frac{t}{T} - s}{b_T} \right) \tag{3.20}$$

$$V_{T,k}(s) = \frac{1}{Tb_T} \sum_{t=1}^{T} X_t Y_{it} \left(\frac{\frac{t}{T} - s}{b_T} \right)^k K \left(\frac{\frac{t}{T} - s}{b_T} \right). \tag{3.21}$$

With these estimates at hand, the columns of the candidate structural matrix can be inferred from

$$\widehat{\tilde{R}_{\bullet i}}(s) = \pm \hat{\psi}_{i0}(s) \left(\hat{\psi}_{i0}(s)^\top \hat{\psi}_{i0}(s) \right)^{-1/2} \tag{3.22}$$

With the candidate matrix at hand at every point in time, one can then proceed to compute the sequence of closest orthogonal matrices by means of (3.11).

Kernel choice and bandwidth selection

As kernel function, I choose the Epanechnikov kernel $K(\nu) = \frac{3}{4} \max(0, 1 - \nu^2)$ and employ the Gaussian kernel to check for robustness. The Epanechnikov kernel is one of the most popular choices for nonparametric estimation because it is compactly supported – which is a common assumption for derivations of asymptotic theory and makes the Epanechnikov kernel particularly suitable for variables which are not defined on the entire real line to minimize boundary effects – and because it minimizes the mean-squared error in the iid setting (Epanechnikov, 1969). The suggested kernel functions are both symmetric. While this can be justified for describing the dynamic volatility spillovers in the historical sample, an asymmetric kernel giving weight only to past and current observations would be more natural in a forecasting context. The bandwidth selection for nonparametric smoothing of time series data is a nontrivial problem. Under strongly mixing dependence, Xia and Li (2002) have shown the asymptotic optimality of the cross validation bandwidth selector for local polynomial fitting. For dependent, nonstationary error and covariate processes, Zhang and Wu (2012) propose a generalized cross-validation procedure but recommend a rule of thumb based on their simulation results. In the context of a structural model, it is equally important that bandwidths are chosen consistent with economic theory regarding the modeled variables. Indeed, both proxy variables employed in the empirical application provide economic arguments for specific bandwidth choices. These choices additionally turn out to be backed by the results of a leave-one-out cross-validation.

3.3 Empirical Application

I illustrate the merits of the time-varying structural modeling approach by analyzing a system of daily asset returns. It comprises three asset classes which are focal components of the global decarbonization efforts and green energy transition: foreign exchange, clean energy equity and commodity markets.

3.3.1 Data

I study daily price data ranging from 22/02/2007 to 30/09/2020 taken from Thomson Reuters Eikon. My asset triple consists of the Finex U.S. Dollar Index, the S&P Global Clean Energy Index and the Bloomberg Commodity Index. The data sample starts at the launch date of the S&P Global Clean Energy Index. The Finex U.S. Dollar Index is a measure of the value of the U.S. dollar relative to a basket of U.S. trade partners' currencies which goes up when the U.S. dollar gains value compared to the other currencies. The S&P Global Clean Energy Index measures the performance of companies in global clean energy-related businesses such as solar or wind energy companies. Among all available green equity indices, it features the longest performance record and is therefore the subject of choice in analyses in energy economics (see, e.g., Elie et al., 2019). The Bloomberg Commodity Index is a commodity price index where the energy sector, reflected in oil and gas prices, represents the largest index component. As commodities are traded in U.S. dollar, it is important to include the USD Index in the system to disentangle variations in foreign exchange markets from volatilities in energy markets.

I compute daily log returns r_t for each asset, see Figure 3.1. All series exhibit the typical features of daily return data such as heteroscedasticity and volatility clustering (see also the summary statistics in Table 3.1). Using the Schwartz criterion to select an optimal autoregressive moving average (ARMA)(p, q) model for each return variable, I can conclude that – apart from the Clean Energy Index which shows weak autoregressive behavior at one lag ($\phi_1^{AR} = 0.10$) – a constant mean model delivers the lowest BIC and therefore the best fit for the mean equation. The estimation of a VAR(1) model furthermore indicates the absence of cross dynamics as the VAR coefficients are largely insignificant at conventional levels. Therefore, in the following, I treat the demeaned log returns as the reduced form model innovations and proceed with the fitting of an MGARCH model to obtain standardized residuals $\hat{u}_t$ serving as input for the identification approach. Among the large class of

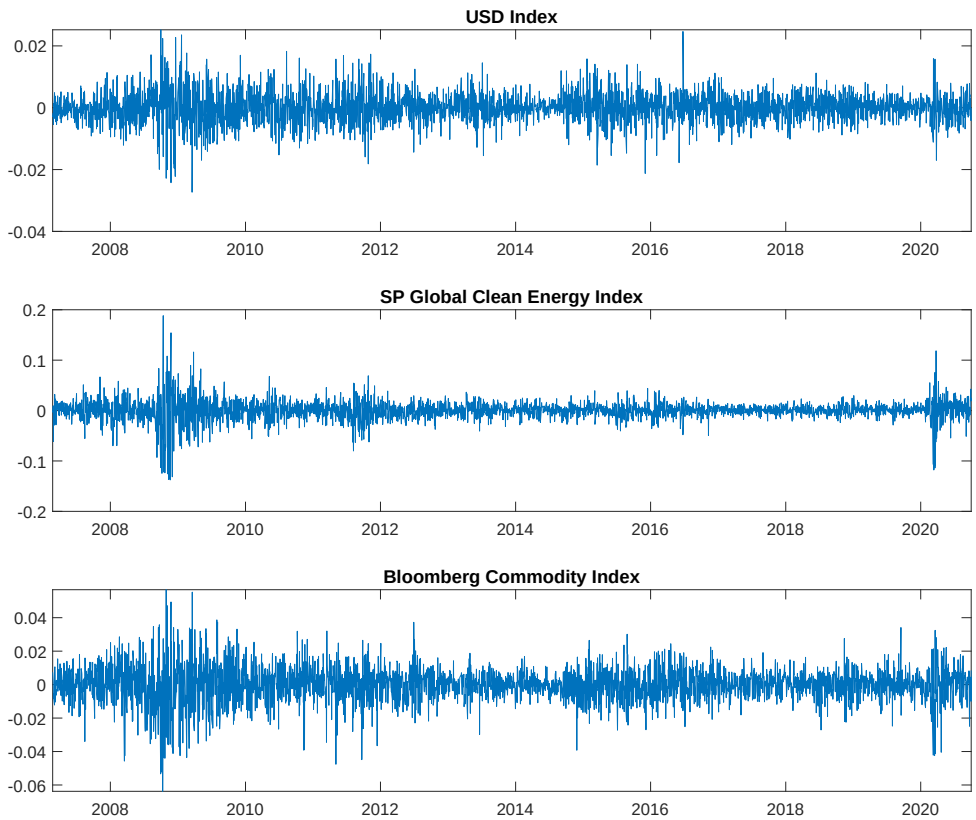

Figure 3.1: Demeaned daily log returns

Time series of the demeaned daily log returns of the Bloomberg Commodity Index, the Finex U.S. Dollar Index and the S&P Global Clean Energy Index from 23/02/2007 to 30/09/2020.

MGARCH models, the BEKK GARCH model enjoys popularity as it offers maximum flexibility for the modeling of the dynamics of the conditional covariance matrix (Bauwens et al., 2006). Therefore, I opt to fit a BEKK(1, 1) model to the reduced form innovations.

With the choice of my proxy variables, I aim at disentangling the effects of uncertainty on the asset system. While uncertainty is a multidimensional concept, it is often categorized into financial, macroeconomic and economic policy uncertainty, with each type exhibiting its own dynamics and impact effects on the economy (Blot et al., 2020). As Ludvigson et al. (2021) provide evidence that shocks to financial uncertainty, rather than macroeconomic uncertainty, are the main drivers of economic fluctuations, I pursue the goal of identifying a financial uncertainty shock as a first shock of interest to the asset return system. Investigating financial uncertainty shocks has become a prime focus of macroeconomic and financial research since the GFC triggered the Great Recession. Analyzing the impacts of

Statistic	USD Index	Clean Energy	Commodity
Minimum	-0.0273	-0.1377	-0.0638
Maximum	0.0252	0.1883	0.0567
Mean	0.0000	0.0000	-0.0000
Median	-0.0000	0.0000	0.0000
Std. Dev.	0.0049	0.0194	0.0104
Skewness	0.0144	-0.4928	-0.3553
Kurtosis	5.3972	15.2618	6.3978

Table 3.1: Descriptive statistics of the demeaned daily log returns

Descriptive statistics of the demeaned daily log returns of the Finex U.S. Dollar Index, the S&P Global Clean Energy Index and the Bloomberg Commodity Index from 23/02/2007 to 30/09/2020; $N = 3411$ observations.

financial uncertainty shocks on asset return systems in general, and clean energy equities in particular, is of practical relevance for policy makers, monetary policy authorities and financial market participants because uncertainty rises during market downturns with implications for investor behavior, financial stability and the energy transition.

Since positive monetary policy surprises and increases in monetary policy uncertainty raise credit costs and lower firm investment (Husted et al., 2020), I furthermore investigate a joint monetary policy uncertainty and monetary policy surprise shock. Simultaneously analyzing a financial and a monetary policy uncertainty shock contributes to the literature on the interaction of different types of uncertainty. For example, Aastveit et al. (2017) provide evidence that financial uncertainty dampens the effects of monetary policy shocks. The analysis of the impacts of a monetary policy shock is of further interest for the chosen asset system, because green energy and commodity markets are global and U.S. Dollar denominated, and monetary policy stance and monetary policy makers' decisions influence exchange rates. The remainder shock affecting the asset system may capture, e.g., oil and commodity supply shocks which are not reflected in the identified financial and monetary policy shocks. The remainder shocks are driving factors of commodity markets – and therefore possibly of green energy equity markets. Influences may materialize, e.g., through a substitution channel of fossil energy by clean energy.

The two chosen target shocks are among the six shocks suggested by Stock and Wat-

son (2012) to disentangle the channels of recessions, although Stock and Watson (2012) investigate their impacts in an isolated manner instead of analyzing them simultaneously in an identified system. Stock and Watson (2012) additionally consider liquidity/financial risk shocks (found to be strongly comoving with the uncertainty shock) and fiscal policy shocks. Uncertainty and monetary policy shocks are prominently featured in research on economic business cycles and are accompanied by a substantial literature to draw upon for identification. Monetary policy uncertainty has been identified as the defining characteristic of the monetary policy landscape (Greenspan, 2004). Uncertainty shocks have strong explanatory power for financial crises and asset price fluctuations (Baker et al., 2016; Bloom, 2009) and are therefore of special interest for the analysis of smoothly time-varying shock transmission mechanisms.

A natural proxy variable candidate for a financial uncertainty shock to a high-frequent asset return system are the daily returns of the Chicago Board Options Exchange Volatility Index (CBOE VIX). This choice is motivated by the influential paper by Bloom (2009), who employs VIX data to assess the impact of uncertainty shocks, and by the seminal work of Stock and Watson (2012) who introduce their proxy sVAR methodology by identifying an uncertainty shock using the VIX. The VIX is a risk-neutral measure of the expected variance of the stock market over the following 30 days and is calculated from options on the S&P 500. Using an implied volatility measure as proxy variable is a sensible fit in the context of a speculative return system because it is a forward looking indicator of financial uncertainty and a canonical measure for uncertainty in financial markets (Basu and Bundick, 2017; Bloom, 2009). However, although well known as the "fear index" for equity markets, the VIX does not only reflect stock market uncertainty but also a variance risk premium which mirrors investors' risk aversion (Bekaert and Hoerova, 2014) and liquidity issues in the market for tail risk hedging (Fan et al., 2016). Bekaert and Hoerova (2014) show that the variance risk premium has significant predictability for stock returns, but that it is the uncertainty component of the VIX which robustly predicts economic activity and has explanatory power for financial instability. Therefore, the uncertainty component can be expected to be of higher relevance for the analysis of time-varying shock transmissions in multivariate volatility models. Furthermore, the uncertainty component proves to be the dominating component of the VIX (Bekaert et al., 2020), and the variance risk premium decreases in response to monetary policy easing (Bekaert et al., 2013). Accommodative monetary policy stances prevail in the data set investigated in this paper. Due to the small relative contribution of the variance risk premium and the empirical difficulties attached to its estimation, I therefore focus on the VIX as proxy variable.

The VIX data is available at daily frequency. In the sVAR literature, proxy time series are frequently restricted to the dates of narratively identified uncertainty events (Gertler and Karadi, 2015; Piffer and Podstawski, 2017) and potentially aggregated at the low-frequent level of the underlying VAR model. To identify the financial uncertainty shock of the underlying daily MGARCH model of asset returns, I use the full set of observations of the VIX to identify the financial uncertainty shock at the daily level. This choice circumvents missing data issues and the need for a variable bandwidth selection in the nonparametric analysis and avoids censoring of proxy variables. In a long time series, censoring a proxy variable may affect its relevance adversely, while the selective consideration of proxies at certain dates may raise doubts about the global validity of the inferred shock transmission mechanism for the full-length daily shock time series.

An alternative prominent proxy variable for financial uncertainty suggested by Piffer and Podstawski (2017) are high-frequency changes in the price of gold. This choice is motivated by the notion of gold as a safe-haven asset and therefore likely connected to underlying uncertainty shocks. To mitigate noise, Piffer and Podstawski (2017) suggest using variations in gold prices tightly around narratively selected past uncertainty events. I use their updated measure for a robustness check of the empirical results of the static model (see Appendix 3.B.3). While the publicly available financial uncertainty measure of Ludvigson et al. (2021) would be an interesting measure for comparison, their index is only available at monthly level. Further popular measures of uncertainty which are available at daily frequency include the geopolitical risk index (GPR) of Caldara and Iacoviello (2022) and the economic policy uncertainty index (EPU) of Baker et al. (2016), which is also employed by Stock and Watson (2012). As the EPU is based on newspaper data, it is – in contrast to the VIX – less likely to be correlated with uncertainty measures which are constructed based on financial market data and may therefore be better suited to identify the separate propagation channels of financial and monetary policy uncertainty. However, changes in the GPR, fluctuations of the EPU and gold price variations turn out to be less relevant instruments in the empirical application (see the robustness checks in Appendix 3.B.3). For the EPU, this finding is backed by the results of Houari (2022) who finds that the effects of EPU shocks on a large panel of variables are less significant than those of VIX shocks and claims that the VIX generates the most significant impact on the U.S. economy. The relatively weak performance of the gold proxy for the asset return system aligns with the empirical finding of Hood and Malik (2013) for an earlier sample period that the VIX is a stronger safe-haven asset and superior hedging instrument for the S&P 500 compared to

gold.

As proxy variable for the second shock of interest, I combine the returns of the monetary policy uncertainty index (MPU) of Bauer et al. (2021), which is a model-free monetary policy uncertainty measure based on derivatives, with the high-frequency monetary policy shocks (MPS) put forward by Bauer and Swanson (2022). This choice is motivated historically, because the Fed used to employ the federal funds rate (FFR) as the main instrument of monetary policy but has used asset purchases and forward guidance in the last decades as an increasingly central tool, especially in the aftermath of the financial crisis and during the zero lower bound period. While the MPU captures forward guidance because it is based on Eurodollar futures and is available at the daily level, the MPS acts as a proxy for conventional policy surprises and is measured based on changes in asset prices in small windows around FOMC announcements ($n = 109$ observations). While a high level of the MPU indicates high uncertainty levels regarding monetary policy, a positive MPS corresponds to a hawkish surprise and a negative MPS implies a dovish surprise. Stock and Watson (2012, 2018) discuss the use of high-frequency monetary policy surprises as instrument in proxy VAR identification, and since Gertler and Karadi (2015) their usage is standard in the VAR literature. I combine monetary policy and monetary policy uncertainty measures because both variables exhibit pronounced effects on asset prices. Changes in monetary policy uncertainty around FOMC announcements, mainly due to forward guidance, affect asset prices such that the magnitude of financial market reactions depends on the level of uncertainty (Bauer et al., 2021). These effects are distinct from the responses to conventional policy surprises, where rate decisions can lead to substantial changes in asset prices (Gürkaynak et al., 2005). Bauer et al. (2021) show that the MPU is significantly and positively related to the target policy rate surprise and strongly positively related to the so-called path factor which reflects information about the future path of monetary policy (Gürkaynak et al., 2005). The MPU is thus a convenient measure to analyze the responses of asset prices to forward guidance. This holds especially for the time periods where the FFR is at the zero lower bound (ZLB). Here, the MPU mirrors shifts in the second moment of the perceived distribution of the future policy rate (Bauer et al., 2021). In contrast to the widely used monetary policy uncertainty measure by Husted et al. (2020), which follows the narrative directive of the EPU by Baker et al. (2016), the MPU by Bauer et al. (2021) has a very clear economic interpretation as the conditional volatility of the future short rate. Furthermore, it is available at a daily frequency, which is crucial when investigating the impact of monetary policy uncertainty on financial markets. While there are further popular alternative instruments for monetary policy shocks, e.g.,

by Romer and Romer (2004), the vast majority of them is available at the monthly level only, and therefore not suitable for the analysis of the daily asset return system.

To facilitate the identification of the underlying iid shocks of the strong structural MGARCH model, I fit flexible ARMA models to both instruments to distill the unexpected innovations to the proxy series and use the resulting innovations as proxy variables going forward. Miranda-Agrippino and Ricco (2019) suggest to regress instruments for monetary policy shocks not only on their own lags but also on central bank information contained in the Greenbook. Bauer et al. (2021) furthermore recommend to orthogonalize monetary policy shocks with respect to the macroeconomic and financial variables that are observed before the FOMC announcement to avoid the "Fed response to news channel". This strategy isolates the component of the monetary policy surprise that is due to the monetary policy shock and increases the likelihood that the resulting series is a valid instrument in a VAR: the proxy variable must be exogenous with respect to the other structural shocks and the lagged variables of the VAR (Stock and Watson, 2018). The fit of a distributed lag model to the proxy variables however shows no significant dependence of the monetary policy measure on the lagged financial uncertainty measure but reveals a significant contemporaneous correlation of the two measures of 0.1730. Therefore, I orthogonalize the monetary policy proxy with respect to the financial uncertainty proxy by means of least squares. The lack of correlation of the monetary policy instrument with the lagged financial uncertainty measure alleviates concerns that the instrument may be contaminated by feedback effects from the "Fed response to news channel" of Bauer et al. (2021). Table 3.2 shows statistical summary measures of the resulting instrumental variables which I henceforth refer to as the financial uncertainty proxy, Z_1, and the monetary policy surprise and uncertainty proxy, or monetary policy (uncertainty) proxy for short, Z_2. The large positive skewness of the financial uncertainty proxy is in line with the widely accepted notion that investors and returns react more strongly to negative compared to positive news. Figure 3.2 shows plots of the filtered and standardized proxy time series.

3.3.2 Structural model

In this section, I present the estimation results of the static and time-varying structural proxy-MGARCH model and demonstrate how shock impacts change when moving from a constant to a time-varying shock transmission framework.

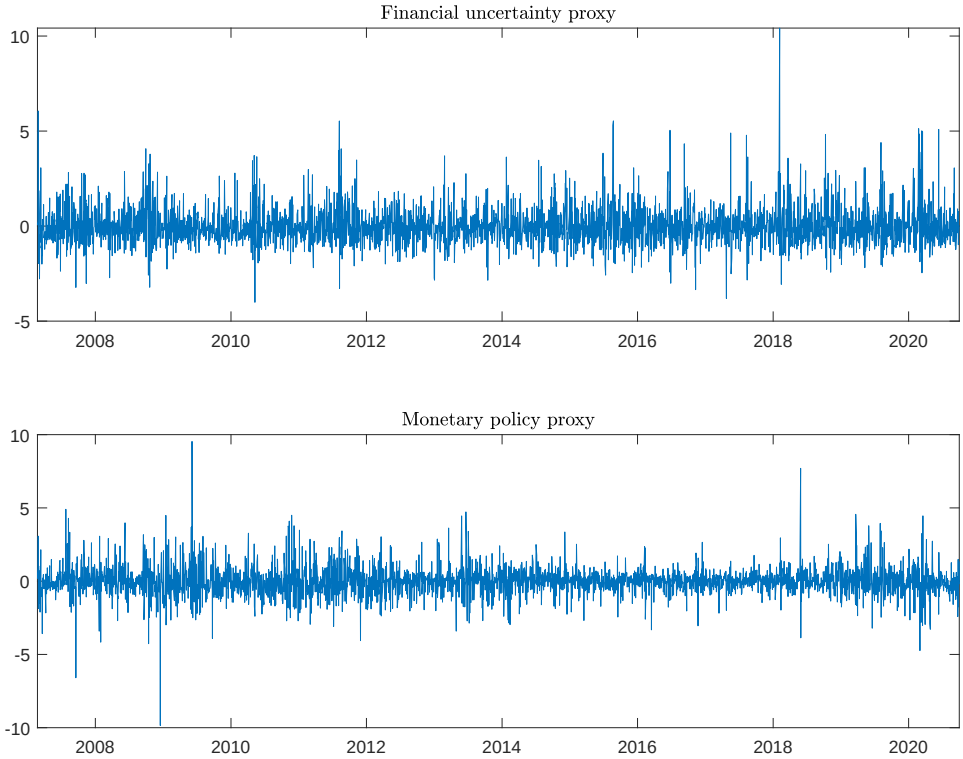

Figure 3.2: Time series of the instruments

Time series of the proxy variables from 23/02/2007 to 30/09/2020. The upper panel shows the financial uncertainty proxy based on the VIX. The lower panel shows the monetary policy proxy based on MPU and MPS.

Estimation results

Table 3.3 documents the results of the quasi maximum likelihood estimation of the BEKK(1, 1) model of the asset return system. By using the values of a diagonal BEKK specification as starting values combined with a randomization strategy for the off-diagonal elements of the coefficient matrices, I verify that the resulting estimates correspond to a maximum of the loglikelihood function. I optimize the loglikelihood numerically using the analytical derivatives provided in Hafner and Herwartz (2008). Inference about the coefficient matrices of the BEKK model is based on t-statistics derived from the analytical derivatives. The diagonal parameters and selected off-diagonal parameters of the coefficient matrices turn out to be statistically significant at conventional levels. The Schwartz

Statistic	Z_1	Z_2
Minimum	-4.0099	-9.8036
Maximum	10.4195	9.7487
Mean	-0.0000	-0.0000
Median	-0.1110	-0.0117
Std. Dev.	1.0000	1.0000
Skewness	1.3473	0.3574
Kurtosis	10.0556	11.8526

Table 3.2: Descriptive statistics of the standardized and filtered proxy variables

Descriptive statistics of the standardized and filtered proxy variables from 23/02/2007 to 30/09/2020; $N = 3411$ observations.

criterion speaks in favor of the full BEKK specification (see again Table 3.3) such that I base my further analysis on this model.

Based on the sequence of conditional covariance matrices provided by the BEKK model, I estimate the constant proxy-MGARCH model using the proxy-guided Procrustes orthogonalization as the static benchmark. The analysis of the proxy variables reveals that both instruments seem to be relevant with the VIX-based proxy being particularly strong (see Table 3.4). The structural rotation matrix clearly departs from the identity matrix. This indicates that spectral decompositions imposing symmetric spillover mechanisms are not applicable. The Wald test for symmetric spillovers of Fengler and Polivka (2022a) confirms this finding (see Table 3.4). The correlation matrix of the inferred structural shocks with the proxy variables shows a diagonal structure in agreement with the relevance (3.6) and the exogeneity condition (3.7) with p-values of zero indicating the statistical significance of the relation of the structural shocks of interest and their respective proxy variables. The inferred structural shocks are mutually and serially uncorrelated, speaking in favor of white noise properties (see Table 3.7). A robustness check based on the proxy-guided Givens rotations approach of Fengler and Polivka (2022a) delivers similar results (see Tables 3.5 and 3.8). The similarity of the two transmission matrices confirms the relative strength of the VIX-based proxy variable in identification and underlines that the chosen instruments closely adhere to the exogeneity conditions.

The values of the static rotation matrix given by the models are consistent with economic

theory (see also Table 3.6, which displays the long-run structural variance decomposition): As the second entry in the first row of $\tilde{R}$ shows, a large positive monetary policy uncertainty shock, i.e., an increase in uncertainty, channels into an increased USD Index long-run variance. Judging from the magnitude of the channeling of each shock component, the monetary policy shock is the main driver of USD Index returns among the structural shocks. On average, an increase in monetary policy uncertainty leads to an appreciation of the U.S. dollar. This also holds, albeit to a lesser extent, for growing financial uncertainty. This finding confirms recent results that U.S. financial and monetary policy uncertainty strengthens the U.S. dollar (see, e.g., Mueller et al., 2017; Bauer et al., 2021; Akinci et al., 2022). In contrast, positive financial uncertainty shocks on average exhibit downward pressure on clean energy equities and function as main drivers of their long-run variance, and the monetary policy and the remainder shock can amplify this effect. This finding aligns with empirical results that financial and monetary policy uncertainty shocks decrease asset prices (see, Bauer et al., 2021; Akinci et al., 2022, among others).

A remainder shock can increase the long-run commodity variance, with a positive shock having a potential positive effect on prices but has an average negative effect on the Finex USD Index and the S&P Global Clean Energy Index. However, the investigation of a counterfactual unit remainder shock (see section 3.3.2 for the analysis of the transmission of counterfactual shocks) reveals that during crisis times, e.g., during the onset of the GFC and the COVID-19 pandemic, a positive remainder shock can exhibit a positive impact on the S&P Global Clean Energy Index – in line with substitution effects. Negative remainder shocks, related to decreasing oil prices due to elevated supply or phases of decreased demand, like, e.g., during the global COVID-19 lockdowns, may equally have a positive effect on the S&P Global Clean Energy Index – in line with clean energy transition efforts. While financial market uncertainty and – although to a lesser extent – monetary policy uncertainty are drivers of long-run commodity market variance and seem to exhibit downward pressure on prices, shocks tied to the commodity market play a more important role according to the model. A persistent dominance of each structural shock towards one asset return component over time may however be questionable. The estimation of the dynamic strong structural MGARCH model therefore sheds light on the evolution of the structural parameters (see sections 3.3.2 and 3.3.2 for an in-depth analysis).

The optimal bandwidths for the nonparametric estimation given by a naive cross-validation[4]

[4]The employment of the leave-one-out cross-validation in contrast to a leave-k-out procedure is motivated by weak autocorrelations in the process $(\hat{u}_t Z_{it})_{t\in\mathbb{N}}$, see Figure 3.13.

based on a Gaussian kernel are approximately 25 days for the first column and approximately 60 days for the second column. The smoothing window for the column of the rotation matrix governed by the financial uncertainty proxy thus spans approximately one month, which aligns well with the fact that the VIX is a one-month forward projection of volatility: the VIX is derived from the prices of index options on the S&P 500 with near-term expiration dates. Similarly, the smoothing window for the monetary policy uncertainty proxy covers three months, which aligns well with the horizon of the underlying, the three-month U.S. dollar London Interbank Offered Rate (LIBOR), of the Eurodollar futures and options from which the MPU is derived. The selected bandwidths are thus consistent with the economic characteristics of the proxy variables. Conducting the cross-validation based on an Epanechnikov kernel, the naive optimal bandwidths are given by approximately double the Gaussian bandwidth values. As the estimation results do not visibly differ other than showing varying degrees of smoothness, see exemplarily Figure 3.14, I report in the following the results obtained with the Epanechnikov kernel. As a further robustness check of the nonparametric modeling approach, I check the estimation results with a two-step estimation approach: First, I infer the structural shocks based on the static proxy-MGARCH model. Second, I calculate a nonparametric estimate of the covariance of the model-inferred static shocks with the proxy variables $\mathrm{E}[\hat{\xi}_t Z_{it}]$. The optimal bandwidth turns out to be of similar size and the estimated relevance parameters follow similar dynamics (see Figure 3.15). The errors of the nonparametric estimation procedure (see Figures 3.16 and 3.17) do not depict any clear autocorrelation patterns but indicate a slight remaining clustering behavior and the presence of outliers. To better understand the origins of these large deviations, I investigate outlier cleaned versions of the proxy variables in Appendix 3.C.

$\hat{C}$			$\hat{A}$			$\hat{B}$		
0.0004	0.0004	0.0002	0.1676	0.1399	0.1085	0.9806	−0.0313	−0.0236
–	−0.0013	$0.0036 \times 1e^{-2}$	$0.0971 \times 1e^{-2}$	0.2685	0.0203	−0.0003	0.9582	−0.0051
–	–	0.0006	−0.0156	0.0421	0.1708	$0.0099 \times 1e^{-2}$	−0.0024	0.9820
(4.6913)	(1.2626)	(1.4096)	(7.9249)	(1.8910)	(1.9324)	(212.31)	(−1.8499)	(−1.6913)
–	(−5.0196)	(0.1911)	(0.0774)	(10.096)	(1.4703)	(−0.0921)	(133.01)	(−1.6913)
–	–	(3.3378)	(−0.6976)	(0.8795)	(7.5825)	(0.2002)	(−0.2199)	(182.73)
Loglikelihood full BEKK: 35039			Loglikelihood DBEKK: 6460					
Schwartz criterion								
full BEKK: $-69'883$			DBEKK: $-12'821$					

Table 3.3: Quasi maximum likelihood (QML) parameter estimates of the unrestricted BEKK model of the demeaned daily log returns of the Finex U.S. Index, the S&P Global Clean Energy Index and the Bloomberg Commodity Index over the period from 23/02/2007 to 30/09/2020. Entries in parentheses are the robust QML t-ratios determined with the analytical derivatives as provided by Hafner and Herwartz (2008). The Schwartz criterion speaks in favor of the full BEKK model compared to a diagonal BEKK specification.

Time-varying relevance

The nonparametric estimates of the covariance of the reduced form residual and the proxy variables which determine the dynamics of the transmission mechanism, $\hat{\beta}_{nk,t}$ $(n = 1, 2, 3;\ k = 1, 2)$, warrant a closer look. Figures 3.3 and 3.4 depict the estimates corresponding to the covariances with the first and the second proxy variable. While the first (blue) and last component (yellow) in Figure 3.3 fluctuate around the zero mean, the second component (red) of the covariance with the financial uncertainty proxy moves around a level of approximately 0.5 and exhibits downward swings which coincide with major stock market downturns. Prominent examples include the GFC, the Eurozone crisis and the COVID-19 pandemic. The plot underpins that the proposed structural model is capable of capturing the dynamics of the financial business cycle. Bloom (2014) conventionalizes the cyclical behavior of uncertainty measures, which is visible here, as a stylized fact. Moreover, the graph reveals that the instrument for the financial uncertainty shock – while featuring an average absolute relevance of approximately 0.5 – shows an even higher proxy relevance in crisis times. This behavior may be reflective of endogenous increases in uncertainty in the course of recessions (Bloom, 2014).

Figure 3.4 demonstrates that the first component of the covariance vector of the reduced form innovation with the second proxy variable (blue) exhibits time-varying behavior with swings occurring in particular during quantitative easing and following tightening periods. In the plot, especially the first two large-scale asset purchase programs (LSAPs), LSAP1 and LSAP2, and the taper tantrum accompanying the scaling back of the quantitative easing measures stand out. In contrast, in 2012 and 2013 and in 2018/2019, the time series of $\hat{\beta}_{12}$ shows noticeable decreases which result in sign switches. These periods coincide with the second recession of the double-dip Eurozone crisis from the end of 2011 to 2013[5] and with the monetary policy pivot of the Fed during the global economic slowdown, which cause changes in the direction of the transmission mechanism. Both periods are marked by diverging monetary policy stances in the U.S. versus the Eurozone (see Figure 3.5), which provides evidence for a pivotal role of global monetary policy divergence for the transmission of monetary policy shocks. The other components ($\hat{\beta}_{22}$, $\hat{\beta}_{32}$) fluctuate in a more centered manner around the zero baseline. The time alignment of the extrema of $\hat{\beta}_{12}$ with the changes in monetary policy regimes is not as sharp as the alignment of the fluctuations in $\hat{\beta}_{21}$ with financial market downturns in Figure 3.3. This may be due to the wider smoothing window used for the estimation involving the second proxy variable. Overall,

[5]See `https://eabcn.org/dc/chronology-euro-area-business-cycles`

		constant proxy-MGARCH model		
$\hat{\hat{R}}$		-0.1246	0.9920	0.0194
		-0.9428	-0.1123	-0.3138
		-0.3091	-0.0574	0.9493
		ξ_1	ξ_2	ξ_3
correlations	Z_1	0.5390	0.0111	-0.0000
	Z_2	0.0036	0.1693	-0.0000
t-statistics	Z_1	22.1238	0.4807	-0.0000
	Z_2	0.1781	7.6895	0.0000
p-values	Z_1	0.0000	0.6307	1.0000
	Z_2	0.8586	0.0000	1.0000
F-test		statistic	$b = 0.01,\ \alpha = 0.01$	$b = 0.05,\ \alpha = 0.01$
	Z_1	459.06	51.50	16.26
	Z_2	33.977	51.50	16.26
Wald test	distribution	statistic	critical value	p-value
	$\chi^2_{(4)}$	125069	9.4877	0.0000

Table 3.4: Estimation results of the constant structural MGARCH model using the proxy-guided Procrustes approach.

The table shows, from top to bottom, the estimated rotation matrix, the correlations of the proxy variables Z_1, Z_2 with the inferred structural shocks ξ_1, ξ_2 and ξ_3, followed by the corresponding heteroscedasticity and autocorrelation robust t-statistics and p-values. Furthermore, it reports the outcomes of the F-test of Lunsford (2015) for robustness under weak proxy variables and of the Wald test for symmetry of volatility spillovers by Fengler and Polivka (2022a). For the F-test, the critical values for $n = 3$ assets, an of asymptotic bias level b and a significance level α are given in (Lunsford, 2015, Table 2). The asset system consists of demeaned daily log returns of the Finex U.S. Index, the S&P Global Clean Energy Index and the Bloomberg Commodity Index over the period from 23/02/2007 to 30/09/2020. Proxy variables for identification of a financial uncertainty shock and a monetary policy uncertainty and surprise shock are returns to the VIX (Z_1) and the returns to the MPU of Bauer et al. (2021) combined with the MPS of Bauer and Swanson (2022) (Z_2). The structural orthogonal matrix is identified using a proxy-guided Procrustes projection scheme.

		constant proxy-MGARCH model		
$(\hat{\theta}_{12}, \hat{\theta}_{13}, \hat{\theta}_{23})^\top$		-1.6802	-0.3154	-0.0536
$\hat{\hat{R}}$		-0.1038	0.9944	0.0194
		-0.9450	-0.0925	-0.3138
		-0.3102	-0.0509	0.9493
		ξ_1	ξ_2	ξ_3
correlations	Z_1	0.5365	-0.0000	-0.0000
	Z_2	0.0072	0.1702	0.0000
t-statistics	Z_1	37.1166	$--$	$--$
	Z_2	0.4203	10.0840	$--$
p-values	Z_1	0.0000	$--$	$--$
	Z_2	0.6743	0.0000	$--$
F-test		statistic	$b = 0.01,\ \alpha = 0.01$	$b = 0.05,\ \alpha = 0.01$
	Z_1	459.06	51.50	16.26
	Z_2	33.977	51.50	16.26
Wald test	distribution	statistic	critical value	p-value
	$\chi^2_{(4)}$	125069	9.4877	0.0000

Table 3.5: Estimation results of the constant structural MGARCH model using the proxy-guided Givens approach.

The table shows, from top to bottom, the estimated rotation angles, the estimated rotation matrix, the correlations of the proxy variables Z_1, Z_2 with the inferred structural shocks ξ_1, ξ_2 and ξ_3, followed by the corresponding heteroscedasticity and autocorrelation robust t-statistics and p-values. Furthermore, it reports the outcomes of the F-test of Lunsford (2015) for robustness under weak proxy variables and of the Wald test for symmetry of volatility spillovers by Fengler and Polivka (2022a). For the F-test, the critical values for $n = 3$ assets, an of asymptotic bias level b and a significance level α are given in (Lunsford, 2015, Table 2). The asset system consists of demeaned daily log returns of the Finex U.S. Index, the S&P Global Clean Energy Index and the Bloomberg Commodity Index over the period from 23/02/2007 to 30/09/2020. Proxy variables for identification of a financial uncertainty shock and a monetary policy uncertainty and surprise shock are returns to the VIX (Z_1) and the returns to the MPU of Bauer et al. (2021) combined with the MPs of Bauer and Swanson (2022) (Z_2). The structural orthogonal matrix is identified using a proxy-guided Givens orthogonalization scheme.

$\bar{H}^{1/2}\tilde{R}$			$\bar{H}^{1/2}$			$\tilde{R}$		
0.0008	0.0048	−0.0006	0.0047	−0.0011	−0.0011	−0.1246	0.9920	0.0194
−0.0189	−0.0034	−0.0029	−0.0011	0.0191	0.0033	−0.9428	−0.1123	−0.3138
−0.0060	−0.0021	0.0083	−0.0011	0.0033	0.0098	−0.3091	−0.0574	0.9493

Table 3.6: Long run variance decomposition of the constant structural MGARCH model identified using the proxy-guided Procrustes approach.

The table shows from right to left the static structural transmission matrix, the principal matrix square root of the long-run covariance matrix $\bar{H}$, $\bar{H}^{1/2}$, and the structural decomposition of the long-run covariance matrix. The asset system consists of demeaned daily log returns of the Finex U.S. Index, the S&P Global Clean Energy Index and the Bloomberg Commodity Index over the period from 23/02/2007 to 30/09/2020. The inferred structural shocks are a financial uncertainty shock (ξ_1) and a monetary policy surprise and uncertainty shock (ξ_2).

both figures clearly indicate the presence of time variation in the structural transmission mechanism in line with financial market cycles and monetary policy actions and stances, illustrating the power of a dynamic structural model and the importance of allowing for time variation in the transmission mechanism for accurate policy analysis.

Narrative corroboration

A narrative corroboration of the derived structural shocks of the time-varying proxy MGARCH model (see Tables 3.10, 3.11 and 3.12) illustrates that the tail observations of the identified financial uncertainty shock indeed coincide with key uncertainty moments documented in the news, regarding, e.g., the financial and the Euro crisis, Brexit, the China slowdown and U.S.–China trade war and the global COVID-19 pandemic. A comparison with the financial uncertainty tail shocks of the static model reveals an overlap of approximately 50%. These overlaps occur mainly during steep market downturns. Regarding the monetary policy surprise and uncertainty shock, it is crucial to investigate both upper and lower percentiles of the shock distribution as reductions in uncertainty about monetary policy may be of equal interest. The tail shocks can, e.g., be tied to dovish statements as, for instance, quantitative easing announcements, as well as to hawkish announcements, such as forward guidance related to rate increases in 2014 and 2016, market worries about rate hikes and reactions to statements by Fed officials. While the

Descriptive statistics

	constant model			time-varying model		
Statistic	ξ_1	ξ_2	ξ_3	ξ_1	ξ_2	ξ_3
Mean	-0.0120	-0.0004	-0.0027	-0.0097	0.0187	-0.0040
Median	-0.0406	-0.0000	0.0302	-0.0634	0.0138	0.0129
Minimum	-4.3800	-4.7080	-5.1432	-3.6379	-5.0806	-4.6302
Maximum	5.1198	4.7197	4.9786	5.3403	5.1065	3.9003
Std. Dev.	0.9928	1.0059	0.9967	1.0117	1.0249	0.9576
Skewness	0.1727	0.0993	-0.2042	0.3580	0.0474	-0.0626
Kurtosis	4.2513	4.1492	4.3102	4.0496	4.5263	3.8730

Ljung-Box test for serial correlation

	constant model			time-varying model		
Lag order	p-value ξ_1	p-value ξ_2	p-value ξ_3	p-value ξ_1	p-value ξ_2	p-value ξ_3
$l = 5$	0.5251	0.5587	0.0556	0.3589	0.5099	0.1695
$l = 10$	0.2678	0.6870	0.1800	0.4800	0.6028	0.0686
$l = 15$	0.5220	0.5699	0.4511	0.5594	0.7959	0.1126

Correlations

	constant model			time-varying model		
ξ_1	ξ_2	ξ_3	ξ_1	ξ_2	ξ_3	
ξ_1	1.0000	-0.0087	-0.0057	1.0000	-0.0114	-0.0160
ξ_2	-0.0087	1.0000	0.0035	-0.0114	1.0000	0.0006
ξ_3	-0.0057	0.0035	1.0000	-0.0160	0.0006	1.0000

Correlation p-values

ξ_1	0	0.6410	0.7520	0	0.5041	0.3510
ξ_2	0.6410	0	0.8553	0.5041	0	0.9727
ξ_3	0.7520	0.8553	0	0.3510	0.9727	0

Table 3.7: Descriptive statistics of the inferred structural shocks of the constant (left panel) and time-varying rotation (right panel) structural MGARCH model of the demeaned daily log returns of the Finex U.S. Dollar Index, the S&P Global Clean Energy Index and the Bloomberg Commodity Index from 23/02/2007 to 30/09/2020. The structural rotations are derived by means of the proxy-guided Procrustes approach. The inferred structural shocks are a financial uncertainty shock (ξ_1) and a monetary policy surprise and uncertainty shock (ξ_2).

Descriptive statistics

	constant model			time-varying model		
Statistic	ξ_1	ξ_2	ξ_3	ξ_1	ξ_2	ξ_3
Mean	-0.0123	-0.0002	-0.0012	-0.0181	0.0232	-0.0041
Median	-0.0570	-0.0014	0.0295	-0.0793	0.0210	0.0109
Minimum	-4.2011	-4.7055	-4.9299	-4.2610	-4.7725	-4.6020
Maximum	4.9851	4.6738	4.7700	5.3209	4.9880	3.9043
Std. Dev.	0.9947	1.0061	0.9946	1.0306	1.0046	0.9587
Skewness	0.2903	0.0953	-0.1107	0.3641	0.0406	-0.0676
Kurtosis	4.1171	4.1483	4.1319	4.1353	4.3193	3.8802

Ljung-Box test for serial correlation

	constant model			time-varying model		
Lag order	p-value ξ_1	p-value ξ_2	p-value ξ_3	p-value ξ_1	p-value ξ_2	p-value ξ_3
$l = 5$	0.3125	0.5939	0.0558	0.4950	0.0550	0.1823
$l = 10$	0.2667	0.7017	0.1590	0.6124	0.1345	0.0870
$l = 15$	0.5077	0.5677	0.4182	0.7153	0.2347	0.1530

Correlations

	constant model			time-varying model		
ξ_1	ξ_2	ξ_3	ξ_1	ξ_2	ξ_3	
ξ_1	1.0000	-0.0088	-0.0067	1.0000	-0.0002	-0.0186
ξ_2	-0.0088	1.0000	0.0006	-0.0002	1.0000	0.0023
ξ_3	-0.0067	0.0006	1.0000	-0.0186	0.0023	1.0000

Table 3.8: Descriptive statistics of the inferred structural shocks under the Givens approach

Descriptive statistics of the inferred structural shocks of the constant (left panel) and time-varying rotation (right panel) structural MGARCH model of the demeaned daily log returns of the Finex U.S. Dollar Index, the S&P Global Clean Energy Index and the Bloomberg Commodity Index from 23/02/2007 to 30/09/2020. The structural rotations are derived by means of the proxy-guided Givens approach. The inferred structural shocks are a global financial uncertainty shock (ξ_1) and a monetary policy surprise and uncertainty shock (ξ_2).

third shock is a priori not identified, the observations in its 1% quantile coincide with idiosyncratic shocks to the commodity market, concerning predominately the fossil energy market. Geopolitical events and natural disasters, such as the Japanese tsunami in 2011, are also present in the list. Notable shock periods include the oil supply crisis in 2014/2015. Hence, I conclude the last structural shock to be a global commodity shock but will henceforth refer to it as remainder shock. Relating the three inferred shocks to the recent work of Engle and Campos-Martins (2023) on global volatility factors, the dates of the most extreme observations of the CoVol index[6] overlap partly with the dates of the tail events in the 99% respectively upper 1% quantiles of the structural shocks of my model (see the values printed in bold in Tables 3.10, 3.11 and 3.12) but overlap fully with the dates of tail events above the 90% respectively below the 10% shock quantile thresholds.

Time-varying structural transmission mechanism

Figure 3.6 displays the evolution of the individual matrix entries $\hat{\tilde{R}}_{i,j}(t)$, $(i, j = 1, \ldots, 3)$ of the dynamic orthogonal transmission matrix over time. The dashed line indicates the level of the matrix entry in the constant proxy-MGARCH model. Each matrix component shows clear signs of time variation – either with variations around the constant mean (see, e.g., $\hat{\tilde{R}}_{1,1}(t)$) or with strong departures from a given level in one direction (see $\hat{\tilde{R}}_{1,2}(t)$, $\hat{\tilde{R}}_{2,1}(t)$ and $\hat{\tilde{R}}_{3,3}(t)$). The corresponding plot for the dynamic model estimates based on Givens rotations is provided in Figure 3.7 and shows similar dynamics but differences in reception magnitudes. Due to the multitude of parameters in the smoothly time-varying setting, I focus on three entries of the transition matrix which show unique time variation features for a more detailed analysis.

The structural transmission matrix describes how the individual structural shock components are linearly combined into the reduced form residual $u_t = \tilde{R}\xi_t$. The plot of, e.g., $\hat{\tilde{R}}_{1,1}(t)$ illustrates how financial uncertainty shocks enter the first component of the reduced form innovation vector. Periods with a positive sign of $\hat{\tilde{R}}_{1,1}$ coincide with expansionary monetary policy and quantitative easing periods, respectively. For example, the upwards trend during the years 2008 and 2009 breaks the zero threshold in December 2008 – when the Fed cut interest rates to near zero (see Figure 3.5). In the aftermath of the financial crisis, the time series remains at positive levels. The ramp-up of the time series during the maturity extension program (MEP) in late September 2011, where the

[6]Dates are taken from `https://vlab.stern.nyu.edu/covol` on 12.12.2022.

series increases almost to one, is especially pronounced. By contrast, the taper tantrum of 2013 and the financial turmoil prior to the October 2015 FOMC meeting are visible as decreases in $\hat{\hat{R}}_{1,1}(t)$ into negative territory. Interestingly, around the FOMC announcement delaying the start of tapering (September 18, 2013)[7] the sign changes back to being positive, indicating that the transmission of the financial uncertainty shock may depend on forward guidance. Evidence for a reaction to a rate decision is, e.g., the decrease around the hawkish FOMC announcements of December 16, 2015, where the Fed raised rates for the first time since 2006, giving up the zero lower bound (ZLB). The strongest decrease in reaction to hawkish forward guidance takes place around December 20, 2016, when Janet Yellen announced a faster than expected tightening which was followed by a series of rate increases.

The plot of $\hat{\hat{R}}_{2,1}(t)$ illustrates that, in the static model, financial uncertainty shocks enter the reduced form residual of the S&P Global Clean Energy Index through a reflection that switches the shocks' signs. In the dynamic model, however, the graph indicates that the transmission mechanism changes in time periods of liquidity provision and quantitative easing measures by the Fed, during the Eurozone crisis and during periods of fiscal policy and economic policy uncertainty. For example, the time series increases during the liquidity shortage in 2007, to which the Fed responded with a liquidity injection through the repo (repurchase agreement) market, and after the announcement of the quantitative easing program LSAP1 and its extension. Furthermore, the transmission mechanism changes during the Eurozone crisis. For example, the time series spikes during the Ireland crisis in November 2010 and around the Portugal crisis in April 2011. In late September 2011, the time series increases sharply, peaking at -0.35. Although the exact kickoff date is hardly determined up to the day, because of the smoothing window of one month, the rise coincides with a statement by the U.S. president that the debt crisis in Europe poses a threat to the entire world, criticizing the European crisis management. The time series peaks with a value of approximately zero around the announcement of the LSAP2, in response to growth concerns in the U.S. Afterwards, the time series returns to the static level of -1 in April 2012. This development coincides with the decline in yields on long-term treasurys of Spain and Italy signaling an easing of the Eurozone crisis.

The deviation starting in December 2012 aligns with the U.S. fiscal cliff and debt-ceiling crisis of 2013, a period of fiscal policy uncertainty. Further departures from the negative

[7] FOMC announcements dates are extracted from `https://www.federalreserve.gov/monetarypolicy/fomc_historical_year.htm`.

unit level around November 2016 and in the second half of 2018 overlap with the election of Trump and the first episode of the U.S.–China trade war. Hence, the model also captures departures from the long-run level due to, e.g., political uncertainty. As Trump's political orientation was deemed to favor fossil energy (see Table 3.11), his surprise election leads also to a visible departure from the static zero level in the transmission mechanism of the remainder shock depicted by $\hat{\hat{R}}_{2,3}$. The fluctuation in late 2019 peaks around the new quantitative easing measures announced by the Fed in November to bring down repo rates and volatility. The described changes in the transmission mechanism indicate that quantitative easing may alleviate the negative impact of financial uncertainty shocks on clean energy equities – in line with results that QE measures boosted equity prices (see, e.g., Joyce et al., 2012). Furthermore, they provide new insights into the dynamic role of fiscal and economic policy uncertainty in influencing equity markets (see, e.g., Marfatia et al. (2020) for a review of fiscal policy shocks, Mumtaz and Theodoridis (2020) and Bonam and Konietschke (2020) for an analysis of tax shocks and Arouri et al. (2016) for evidence of the negative impact of economic policy uncertainty on stock markets especially during high volatility periods).

The graph of $\hat{\hat{R}}_{1,2}(t)$ displays two pronounced departures from an otherwise stable level close to one. By contrast, the static proxy-MGARCH model transmits monetary policy shocks almost as they are. The first downward spike occurs between autumn 2011 and spring 2013, with a short interruption in between, and the second between the end of 2018 and the start of 2020. The first fluctuation occurs during the deepening of the European sovereign debt crisis, which is at the time spreading to Italy and Spain, and a divergence in the monetary policy between the U.S. and the Eurozone. Specifically, the time series starts its steep decline in September 2011. In this month, the Fed announced the maturity extension program (MEP), while the ECB was following a hawkish monetary policy stance, including rate increases. Furthermore, during this month, dollar swap agreements were put in place between the Fed and major central banks to guarantee dollar liquidity as a reaction to U.S. money market funds reducing their exposure to the Eurozone amid fears of a Greek default (De Marco, 2019). The liquidity provision was aimed at preventing a European credit crunch with regard to dollar funding which ultimately proved crucial in stabilizing the financial system in the Eurozone (Mody and Nedeljkovic, 2018). With the EU member states agreeing on bailout measures and the ECB cutting rates in November 2011, the drop in the time series becomes less sharp. The time series hits a local minimum in April 2012 amid news of rising borrowing costs for Spain and Italy, before a steep reversal takes place which lasts until May 2012 when the Spanish crisis intensifies. Stress

in the U.S. dollar lending market at the end of 2012 accompanies a further decrease in the time series. The turning point is reached in December 2012, when the series starts to rise slowly to its previous level.

The described fluctuations coincide not only with periods of monetary policy divergence between the U.S. and the Eurozone, but also with increases in two other uncertainty measures. Both the uncertainty index of Scotti (2016) for the Euro area and the composite indicator of systemic stress (CISS) of the ECB (Holló et al., 2012) spike between the end of 2011 and the start of 2012. Scotti's (2016) index measures the degree of uncertainty of agents about realized real activity conditions, and, in these specific periods, the index heavily differs from the CBOE VIX (Scotti, 2016). The sign change in the transmission mechanism may thus be evidence of Eurozone-related uncertainty affecting the USD Index in a different fashion compared to uncertainty related to domestic monetary policy developments. This interpretation is backed by the fact that the USD Index measures the strength of the U.S. dollar against, in particular, the Euro, and that the proxy for monetary policy uncertainty shocks is based on the implied volatility of Euro-USD derivatives.

The second drop occurs during repeated rate hikes and a hawkish policy stance by the Fed during the end of 2018, when concerns regarding global growth and the U.S.–China trade war rose simultaneously. The decline of the time series starts with the FOMC meeting on June 14, 2018, where the Fed decided on a +25bps rate change – a decision it repeated at its September and December meetings. The decrease reaches its turning point at the end of January 2019 after Fed chairman Powell signaled to the markets that the Fed would be flexible on policy and would not hurry further rate hikes. This statement marks the Fed monetary policy pivot indicating a more dovish policy stance going forward. From the Fed announcement of a rate cut due to global economic slowdown and inflation in July 2019 onwards, the curve slopes upwards towards the long-term unit mean – a development which is only reversed by the global pandemic. The common feature of both departures in the time series may thus be a divergence between monetary policy actions and market participants' perception of the economic conditions. This highlights the importance of financial market participants' trust in central banks' actions for the transmission of uncertainty shocks to the USD Index. The analysis of the time variation in the transmission mechanism thus provides new evidence for the pivotal role played by monetary policy institutions in the propagation of financial uncertainty and monetary policy uncertainty shocks.

As the impact of the changes in the transmission mechanism on the daily returns and their (co)variances is a priori not clear, because a transformed shock $\tilde{R}_t \xi_t$ will additionally be mapped through $H_t^{1/2}$, section 3.3.2 provides an analysis of the volatility spillovers in the system. In the spirit of the VAR literature, the following section additionally provides an investigation of the transmission of counterfactual unit shocks under the dynamic model.

Transmission of counterfactual shocks

Figures 3.8 to 3.10 offer a joint multidimensional perspective of the structural transmission mechanism by illustrating how it contemporaneously transforms counterfactual unit shocks in the financial uncertainty, the monetary policy and the remainder component.[8] I denote the outcome vectors as shocks to the USD Index (x-axis), to the Clean Energy Index (y-axis) and the Commodity Index (z-axis).

Figure 3.8 emphasizes the relative stability of the transformation of the unit financial uncertainty shock over time compared to the mapping of the other counterfactual shocks. The positive unit shock in the financial uncertainty component is without exception mapped into the $(\pm, -, \pm)$ octant of the right-handed coordinate system. The time-varying outcomes fluctuate in an environment around the static model outcome (marked with a green star), and the images at the starting (marked in with a black star wit a blue dot) and at the end point (marked with a yellow star) of the time series lie close to each other and to the image under the constant model. However, the points in the point cloud differ in the shock outcome to the Finex USD Index. While the static model outcome yields a positive first vector entry, the starting and end point mappings yield a negative first vector entry. This is representative of the entire plot, with mapped values being distributed in the $(-, +, \pm)$ and the $(+, +, \pm)$ octant. Hence, the counterfactual unit financial uncertainty shock has an effect on the Finex USD Index which varies in sign and magnitude over time. This is consistent with the notion that – in addition to economic fundamentals and interest rate differentials through divergences in monetary policy stances and pace – the U.S. dollar reacts to changes in economic market uncertainty due to its role as safe-haven currency (Fratzscher, 2009; Hofmann et al., 2022). While macroeconomic and financial uncertainty do not necessarily coincide, Figure 3.8 confirms this finding for financial market uncertainty shocks.

[8] Interactive graphics are available for download under `https://github.com/JeanninePolivka/Structural-Volatility-Modeling/blob/main/InteractiveGraphics.pdf`.

Figure 3.9 shows that the structural transmission mechanism transforms the unit monetary policy uncertainty shock visibly differently over time: At the beginning and at the end of the time series, the shock is transformed such that its image has a negative first vector entry. In contrast, the image of the constant transmission mechanism, around which a bulk of time series observations cluster, features a positive first vector entry close to unity, implying that monetary policy uncertainty shocks in expectation drive U.S. dollar appreciation. The shock impact change in magnitude and sign can be seen as traverses and swings in the time series from octant $(-,-,\pm)$ to octant $(+,-,\pm)$. The majority of the traverses cross sides near the south pole of the globe, where the transformed shock exhibits almost no impact on either the USD Index or the Clean Energy Index, but a large negative impact on the Commodity Index. These observations are indicative of a pronounced monetary policy transmission channel, possibly through foreign exchange markets, towards commodity markets (see, e.g., Akram (2009) and Anzuini et al. (2013) for a documentation of this channel). The observed dynamic pattern aligns with Taylor's (2009) analysis of the impact of monetary policy decisions by the Fed on commodity prices during the global financial crisis (GFC). The first traverse between the two states takes place during the first year of the global financial crisis (GFC) and is visible as a black U-shape in Figure 3.9. The shock transformation during the second year of the GFC is marked by a unique upward swing in the third component (shock to Commodity Index) of the image vector (see the black upwards loop in Figure 3.10 for a better perspective) accompanied by a negative value in the second component. However, the introduction of quantitative easing measures (LSAP1, LSAP2) marks the change in the in the second entry of the image vector (shock to Clean Energy Index) from negative to positive – indicating that quantitative easing measures fuel positive equity market developments, in line with the results of, e.g., Fratzscher et al. (2018). Still, the majority of the monetary policy shock is positively mapped to the first image vector component, indicating that the transmission mechanism channels the monetary policy uncertainty shock strongly towards the USD Index, confirming the findings of Bauer et al. (2021) and emphasizing the existence of the transmission channel even at the ZLB when monetary policy was based on forward guidance and unconventional measures as, e.g., quantitative easing. While Rogers et al. (2018) also present evidence for such a transmission channel, they consistently report that U.S. rate, forward guidance and easing surprises lead to dollar depreciation. During the MEP, the image time series indeed swings back to a negative value in the first vector component, which turns however positive again during the MEP extension and the LSAP3, before going into deeper negative territory combined with an upwards swing in the shock to the Commodity Index. The

turn of the year 2012/2013 then reveals a prominent traverse back to the status quo of the constant model image. From autumn 2018 to winter 2019, in the phase of the Fed monetary policy pivot from a hawkish stance including rate hikes to a dovish one which led to an increase in short-term rates but a decline in long-term yields, one can observe again a swing pattern, similar to the one during the MEP. The swinging behavior of the transformed unit monetary policy surprise shock may thus mirror a flattening or inversion of the yield curve due to monetary policy measures.

With the start of the COVID-19 pandemic, the shock impact is channeled again more heavily towards the first image vector component. Following the Fed COVID-19 easing announcements, the majority of the shock impact spreads positively to the second image vector component, accompanied by a negative impact on the third component. The pattern of this impact change is unique in the course time series overall. This may be reflective of the decline in energy demand during lockdown measures and an orientation towards clean energy sources as a result of favorable policy work in the past, declining costs through innovation and rising sustainability awareness of investors (Kuzemko et al., 2020). This development lasts to the point where, at the end of 2020, the impact concentrates again fully and negatively on the first image vector component – which may be consistent with the depreciation of the U.S. dollar towards the end of the year amid weak economic data. On a more general note, the observed changes in the mapping of the counterfactual unit monetary policy shock complement the results of, e.g., Miranda-Agrippino and Rey (2020) and Miranda-Agrippino and Ricco (2021) who find that contractionary monetary policy causes the dollar to appreciate and of, e.g., Rogers et al. (2018) and Inoue and Rossi (2019) who report that accommodative monetary policy causes the dollar to depreciate (independent of the measures being conventional or unconventional), by painting a nuanced picture of the impact of a counterfactual monetary policy uncertainty shock over time.

Volatility spillovers

Because the defining features of high-frequent asset return systems are their conditional (co)variance dynamics, the analysis of volatility spillovers in the empirical asset return system is of central interest. To analyze the volatility spillovers and how they change under a time-varying transmission mechanism compared to a static framework, I rely on the measure for volatility reception defined in Fengler and Polivka (2022a): Let $i, j \in \{1, \ldots, n\}$.

Then volatility reception between i and j is measured by

$$VR_{t,i\leftarrow j} = \frac{q_{t,ij}^2}{\sum_{l=1}^{k} q_{t,il}^2} \quad \text{(volatility reception)} \tag{3.23}$$

where $q_{t,ij}$ denote the matrix entries of the identified $Q_t = H_t^{1/2}\tilde{R}_t$. Volatility reception measures the share of the impact of the j-th structural shock on the i-th return in relation to the impact of all other shocks on this component. The suggested measure is a contemporaneous analogon of the forecast error variance decomposition (FEVD) which is used in the contexts of VAR models to assess the driving forces of business cycles. Figure 3.11 shows the volatility reception mechanisms implied by the constant and the time-varying structural model under the Procrustes approach. Figure 3.12 delivers the same plots under the Givens orthogonalization approach. A comparison indicates that the two approaches deliver similar volatility reception patterns for the asset return system – although the reception magnitudes can vary strongly. Considering, e.g., the first plot of Figure 3.12, the Givens approach – which weights Z_1 stronger than Z_2 in the shock derivation – delivers a more gradual increase in the contribution of financial uncertainty to the USD Index volatility in the course of the financial and Eurozone crisis. In contrast, the Procrustes approach shows the contribution of the monetary policy shock during the Eurozone crisis more clearly. The volatility reception patterns of the Finex USD Index and the S&P Global Clean Energy Index concerning the financial uncertainty shock devised under the Givens scheme are very similar to the graphs of the volatility reception of the S&P 500 and the Finex USD Index volatility concerning equity market shocks provided by Fengler and Polivka (2022a).

Turning to the analysis of the volatility reception patterns under the static and the dynamic Procrustes approach, the first row of Figure 3.11 shows the volatility reception of the USD Index from the financial uncertainty, monetary policy and the remainder shock. Figure 3.11a reveals that, although the volatility reception from the financial uncertainty shock shows a similar base pattern in the constant and time-varying model, the dynamic model depicts magnified responses: The magnitude of the impact of financial uncertainty shocks ramps up during peaks of the financial and especially the second part of the Eurozone crisis. The largest surge in financial uncertainty over 2011/2012 coincides as well with the fiscal cliff. After the European debt crisis, the impact of the financial uncertainty shock on USD Index volatility rapidly decreases towards a level below 20%. Instead, monetary policy uncertainty takes over in driving the variation in USD Index returns with a level close to 100% from 2013 to the first half of 2018 (see Figure 3.11b). Spikes in volatility

reception from the financial uncertainty shock occur during the Brexit vote, the election of Trump, the U.S.–China trade war and the COVID-19 pandemic. Thus, the USD Index shows a weaker volatility reception from monetary policy surprise and uncertainty shocks in phases of high financial uncertainty – an observation that the static proxy MGARCH model hardly reflects, even less after the financial and Eurozone crisis. The volatility reception of the USD Index from the remainder shock (see Figure 3.11c) is characterized by a series of upwards swings during periods in which the oil price peaked. Figure 3.11h, depicting the volatility reception of the Commodity Index from the monetary policy shock, displays a similar pattern. While it is widely documented that changes in oil prices can affect exchange rates and vice versa (see Kilian and Zhou (2022) for an overview of the transmission channels between the U.S. dollar and oil prices), the similarity of the plots provides evidence that monetary policy uncertainty can affect commodity price volatility – extending, among others, Anzuini et al. (2013) who find that accommodative U.S. monetary policy shocks increase commodity indices but are not the main driver of price variations.

Zooming in on the volatility reception of the USD Index from the monetary policy surprise and uncertainty shock in Figure 3.11b, the first two pronounced ramp-ups occur during the Greek debt crisis and the Eurozone crisis, with a slight dip in November 2009. This may indicate magnifying effects between financial and monetary policy uncertainty. Before the LSAP2 announcement, the volatility reception then ramps up with a spike in November 2011. However, the USD Index receives less volatility from monetary policy uncertainty shocks during quantitative easing periods: after the LSAP2 announcement, the influence of the monetary policy uncertainty shock even falls briefly to zero. While it increases again afterwards, the MEP and MEP extension bring its influence down again, indicating that quantitative easing and unconventional monetary policy may have the potential to calm foreign exchange markets. This empirical finding adds to the results of Neely (2015) who claims that unconventional monetary policy can reduce long-term yields and the value of the dollar – even at the ZLB. The static model does not capture the following downward spikes in volatility reception, of which especially the decline in late 2019 during the accommodative monetary policy stance of the Fed catches the eye, and the following rapid increase before fiscal and monetary policy measures are taken to alleviate the COVID-19 crisis. These observations extend the claim by Dornbusch (1976) that monetary policy may be a major driver of exchange rate volatility to monetary policy uncertainty being another important driving force. At the same time, they do not contradict the argument of, e.g., Gabaix and Maggiori (2015) that risk factors and financial frictions are the dominant

drivers of foreign exchange volatility, since financial uncertainty – possibly rising with risk factors and frictions – visibly contributes to USD Index volatility. Ilzetzki et al. (2020) claim that the reintroduction of the ZLB during the start of the pandemic reduces financial risks, such that forward guidance and the long-term consequences of monetary policy actions, such as, e.g., QE measures, may be more relevant drivers.

Focusing on Figure 3.11d, one can observe the same time variation pattern in the volatility reception of the Clean Energy Index from the financial uncertainty shocks in the dynamic model as foreshadowed in Figure 3.6. By contrast, the static model indicates a constant volatility reception of approximately 95%. Figure 3.11e reveals that – although the volatility reception of the equity index is mainly driven by financial uncertainty – monetary policy uncertainty can contribute up to approximately 75%. The observation that equity volatility reacts to monetary policy uncertainty complements recent findings of Gürkaynak et al. (2022) who show that stock prices react to monetary policy announcements and forward guidance of the Fed both at and away from the ZLB depending on their debt maturities. As clean energy projects are typically characterized by high initial investments with long-term financing structures, the results of Gürkaynak et al. (2022) imply that they react to forward guidance – which is in turn strongly related to the MPU. The driving role of financial uncertainty as proxied by the VIX for the dynamics of clean energy stocks is also documented in Ji et al. (2018) using time-varying copulas. Figure 3.11f furthermore documents volatility reception in the form of regular spikes in the contribution of the remainder commodity shock.

Figure 3.11i reveals another explanatory potential of the dynamic model: it can capture the effects of shortages and surpluses in oil supply through the remainder shock. For example, the pronounced volatility reception of the Commodity Index from the remainder shock during the years 2013 to 2015 peaks during the oil price collapse in late November 2014, when Saudi Arabia left an Opec meeting prematurely, stating that they would not cut oil production as had been expected amid the rise of U.S. shale oil production. Similarly, the spike on October 10, 2018 aligns with high market volatility caused by the Iran sanctions causing Iranian oil exports to decrease. This provides evidence that supply-side oil shocks encoded in the remainder shock may be strong drivers of daily commodity volatility. While the static proxy-MGARCH model is able to capture commodity volatility being being driven to approximately 25% by financial uncertainty shocks and 75% by remainder shocks, the time-varying model detects additional variation in these patterns and reveals the contemporaneous impact of the monetary policy shock.

3.4 Conclusion

To account for smooth changes in the impacts of structural shocks on high-frequent asset returns over time, I propose a strong dynamic proxy-MGARCH model. Modifying the static relevance condition of the identification approach using external instruments, I assume the covariances of the structural shocks with their respective proxy variables to be smoothly time-varying to infer a nonparametric estimator to identify the columns of a candidate structural matrix. Drawing on the literature on orthogonal Procrustes problems, I derive the closest orthogonal matrix to this input matrix. In an investigation of the effects of a financial uncertainty and a joint monetary policy surprise and uncertainty shock on a system of daily foreign exchange, clean energy equity and commodity returns, I find compelling evidence of smoothly time-varying behavior in the contemporaneous transmission of shocks and the volatility spillovers. The transmission mechanism evolves, e.g., with the financial business cycle and with monetary policy actions such as quantitative easing measures.

My results illustrate the explanatory power of dynamic structural models and the importance of allowing for time variation in the transmission mechanism for accurate monetary policy analysis. For example, the time variation in the relevance parameters provides evidence for the pivotal role of global monetary policy divergence in the propagation of monetary policy shocks to the foreign exchange market. At the same time, the model delivers a deeper understanding of the contemporaneous impact of financial and monetary policy shocks. While, e.g., monetary policy shocks are – even at the zero lower bound – the driving force of U.S. Dollar Index returns and (co)variances, the reaction of the U.S. Dollar Index to financial uncertainty shocks during market downturns is consistent with the Dollar's role as a safe-haven currency. Furthermore, the evolution of the transmission mechanism indicates, e.g., that quantitative easing measures may alleviate the negative impact of financial uncertainty shocks on clean energy equities. Concerning the green energy transition, changes in the propagation mechanism hint at potential substitution effects between commodities and clean energy markets in crisis times and at transition effects, e.g., during the COVID-19 pandemic.

Moreover, the suggested approach deepens the understanding of volatility spillovers. For example, financial uncertainty shocks amplify the volatility of the USD Index during market downturns, whereas the influence of monetary policy shocks diminishes. Similarly,

quantitative easing may decrease the impact of monetary policy shocks on USD Index volatility. While the static proxy-MGARCH model indicates, e.g., a negligible influence of monetary policy uncertainty and commodity-related shocks on the conditional variance of clean energy equities and identifies financial uncertainty shocks as their main drivers, my model reveals their time-varying exposure to monetary policy uncertainty, possibly through forward guidance. My findings thus emphasize the importance of accounting for time variation in structural models for informed and effective policy and financial stability analysis.

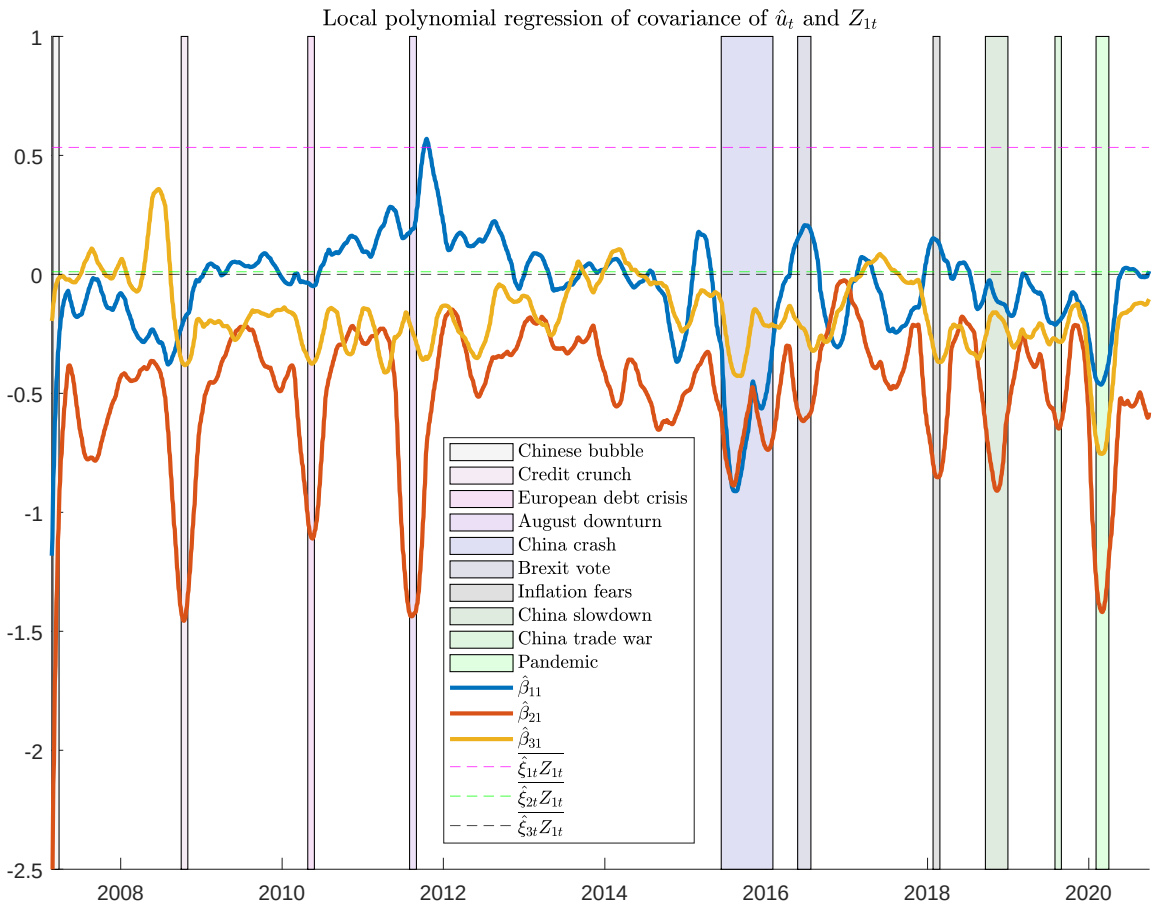

Figure 3.3: Nonparametric estimate of the covariance of the reduced form residual vector $\hat{u}_t$ and the instrument Z_1.

The dashed lines indicate the static covariance levels of the three shocks with the proxy, $\overline{\hat{\xi}_{it}Z_{1t}}$ $(i = 1, \ldots, 3)$. Shaded bars indicate periods with major stock market downturns. The periods (from left to right) correspond to: Chinese stock bubble of 2007, Credit crunch of the global financial crisis 2008, European debt crisis 2010 with focus on Greece, August 2011 stock markets fall during the European sovereign debt crisis, Chinese stock market turbulence of 2015/2016, Brexit vote in June 2016, U.S. inflation fears in February 2018, China's economic slow-down and the first episode of the U.S.–China trade war of 2018, U.S.–China trade war escalations in 2019, Global COVID-19 pandemic starting in February 2020.

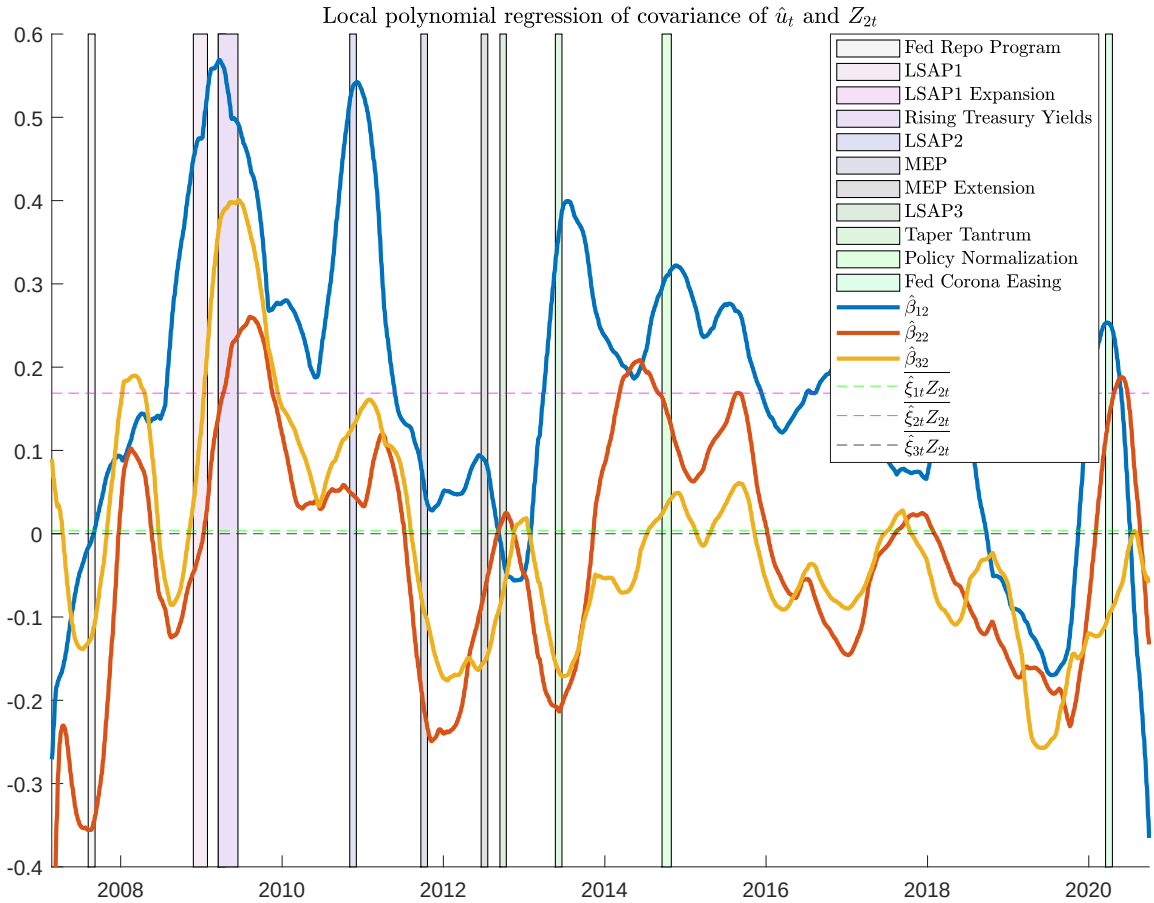

Figure 3.4: Nonparametric estimate of the covariance of the reduced form residual vector $\hat{u}_t$ and the instrument Z_2.

The dashed lines indicate the static covariance levels of the three shocks with the proxy, $\overline{\hat{\xi}_{it} Z_{2t}}$ $(i = 1, \ldots, 3)$. Shaded bars indicate periods with monetary policy changes. Periods correspond to (from left to right): Fed Repo Agreement (Fed liquidity injection in repurchase agreement (repo) market, August 10, 2007), LSAP1 (Large-Scale Asset Purchase program, November 25, 2008), LSAP1 expansion (March 18, 2009), Maturity Extension Program (MEP, September 21, 2011), MEP Extension (June 20, 2012), LSAP3 (September 13, 2012), Taper Tantrum (reactionary panic after announcement of QE tapering, May 22, 2013), Policy Normalization (FOMC statement on policy normalization principles and plans, September 17, 2014), Fed Corona Easing (Monetary policy and fiscal stimulus reactions to COVID-19 pandemic, March 17, 2020).

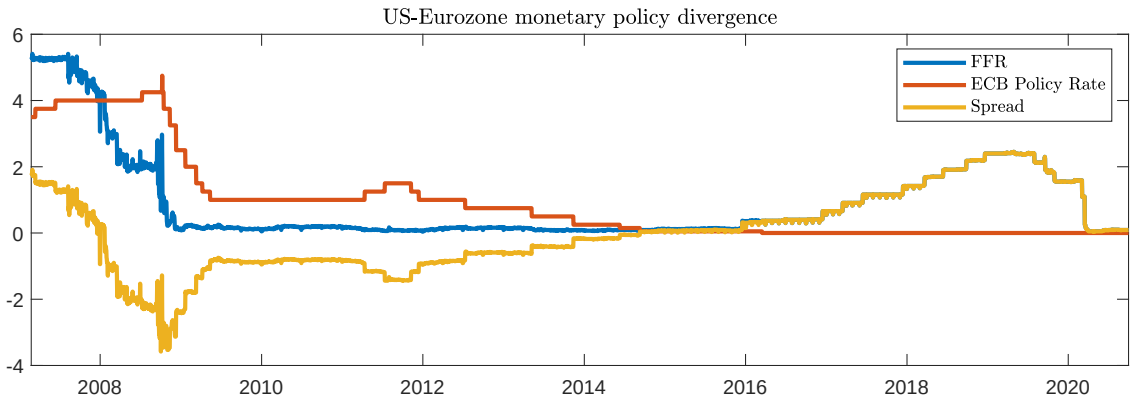

Figure 3.5: Monetary policy divergence between the U.S. and the Eurozone.

Evolution of the daily U.S. federal funds effective rate (FFER) (blue), the ECB policy rate (red) and their spread (yellow). The data is extracted from the FRED database (series: DFF, ECBMRRFR) and changes in the policy rate are sourced from the ECB (`https://www.ecb.europa.eu/stats/policy_and_exchange_rates/key_ecb_interest_rates/html/index.en.html`).

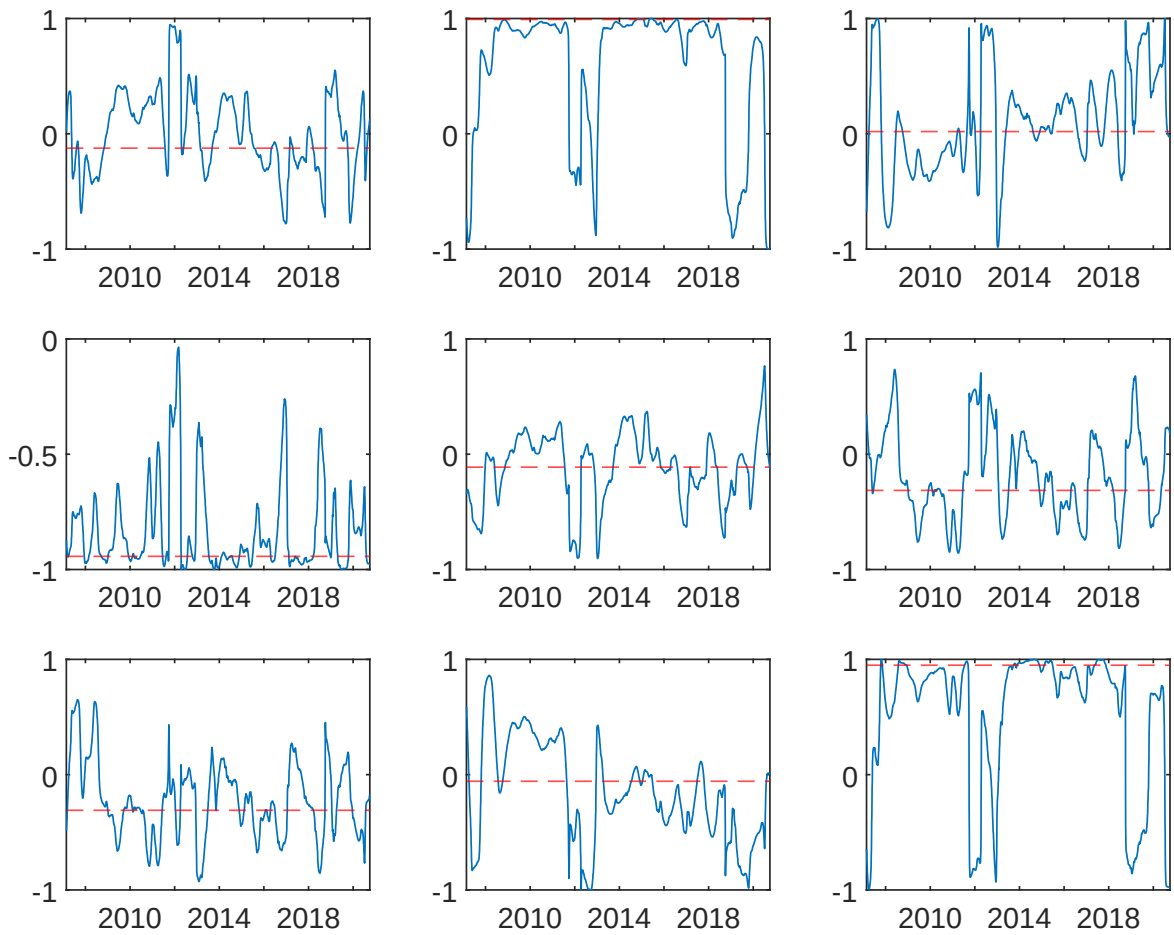

Figure 3.6: Time series of rotation matrix entries under the Procrustes approach.

The graph displays the evolution of the individual matrix entries of the structural transmission matrix, $\hat{\hat{R}}_{i,j}(t)$, $(i, j = 1, \ldots, 3)$, derived from the proxy-guided Procrustes approach over time.

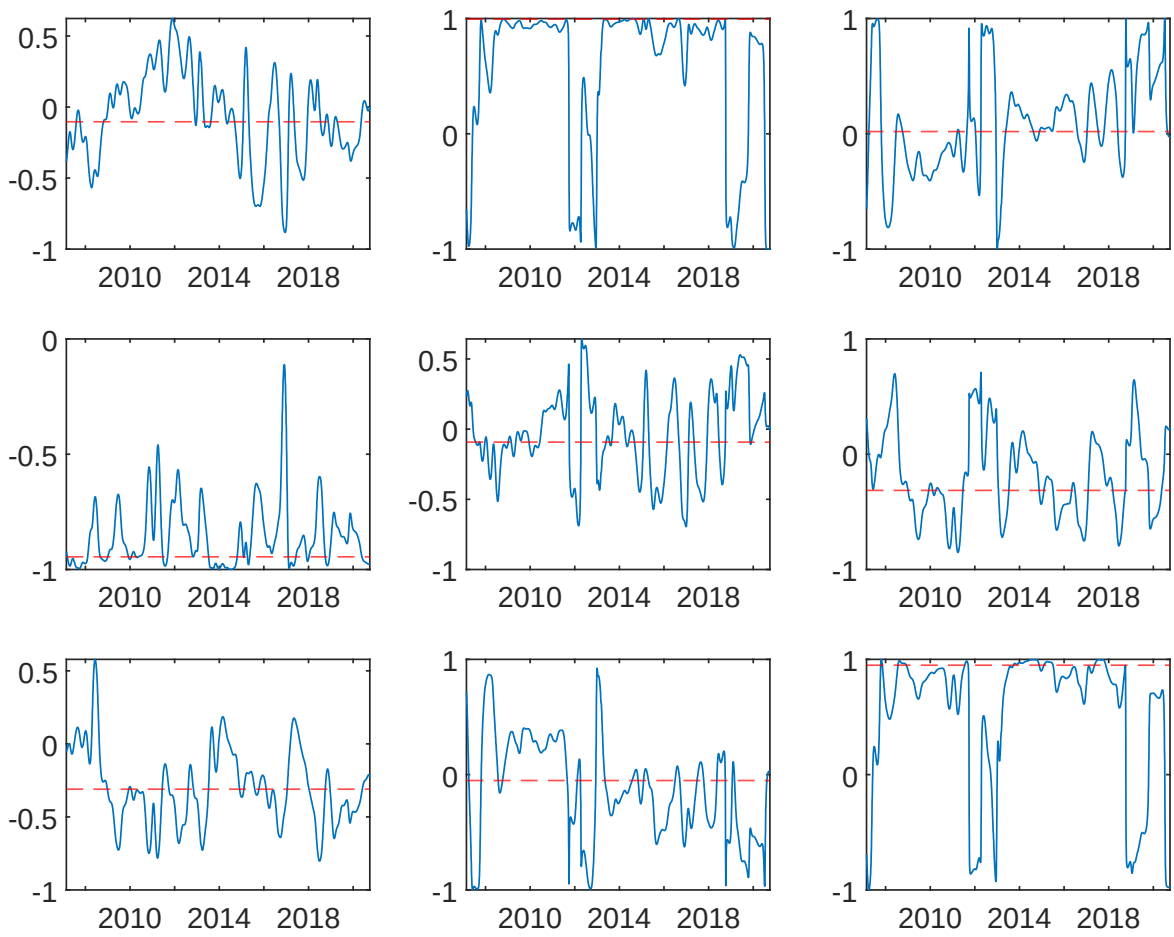

Figure 3.7: Time series of rotation matrix entries under the Givens approach.

The graph displays the evolution of the individual matrix entries of the structural transmission matrix, $\hat{\hat{R}}_{i,j}(t)$, $(i, j = 1, \ldots, 3)$, derived from the proxy-guided Givens approach over time.

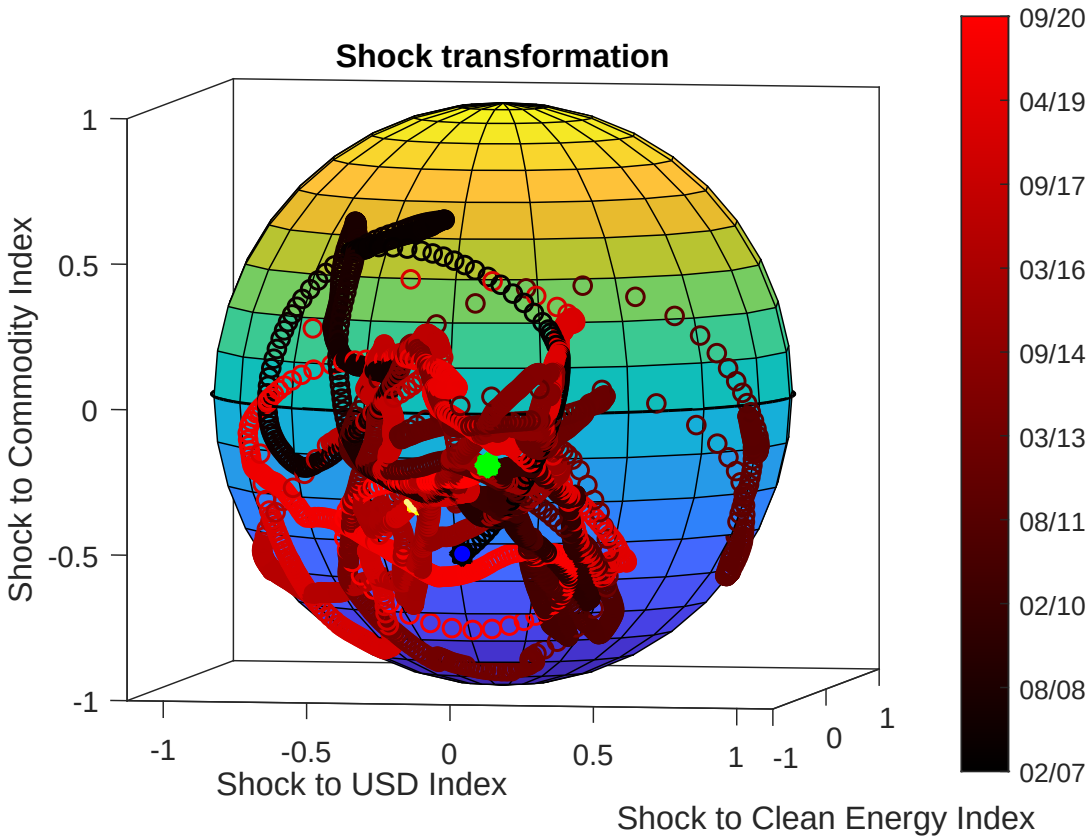

Figure 3.8: Time-varying transformation of a unit financial uncertainty shock.

This plot displays the mapping of a unit shock in the financial uncertainty component through the structural transmission matrix. The yellow star indicates the mapping of the shock vector based on the static structural model. The black star with a blue dot indicates the first mapping of the time series of structural transmission matrices, the green star indicates the final mapping of the same time series.

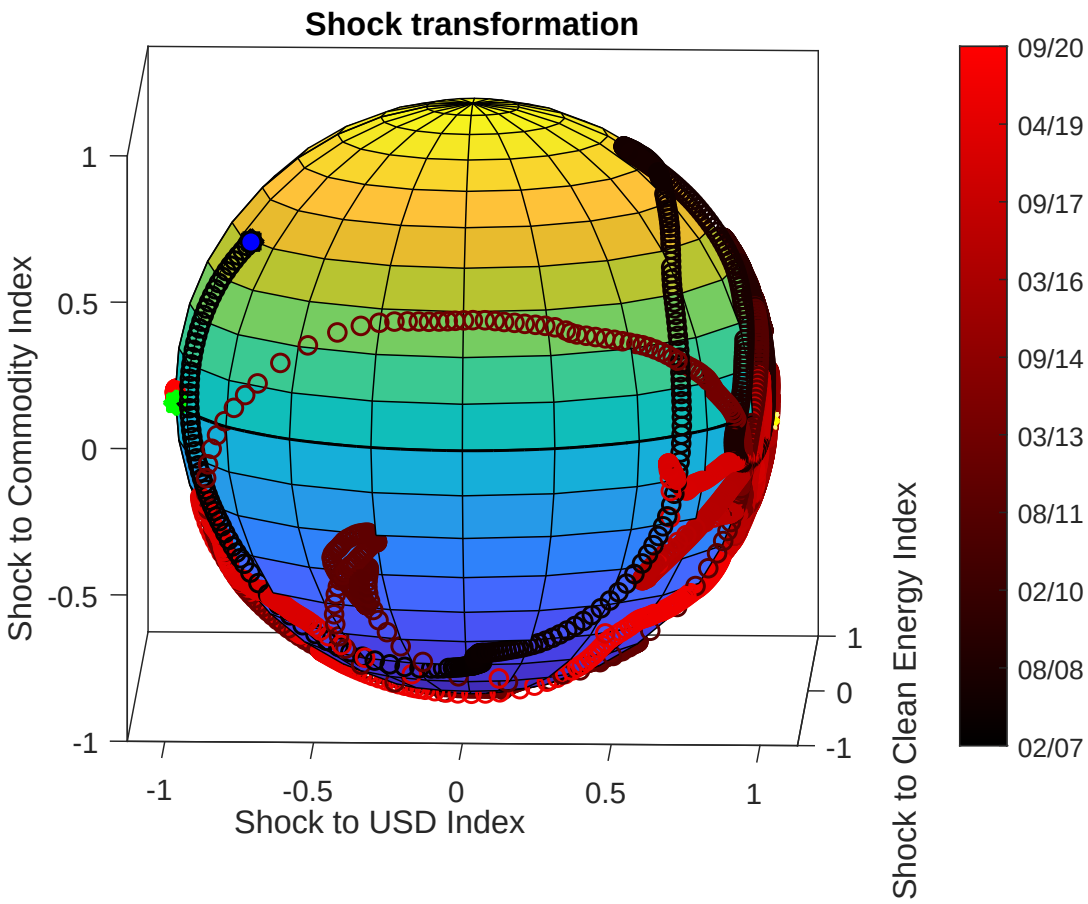

Figure 3.9: Time-varying transformation of a unit monetary policy uncertainty shock.

This plot displays the mapping of a unit shock in the financial uncertainty component through the structural transmission matrix. The yellow star indicates the mapping of the shock vector based on the static structural model. The black star with a blue dot indicates the first mapping of the time series of structural transmission matrices, the green star indicates the final mapping of the same time series.

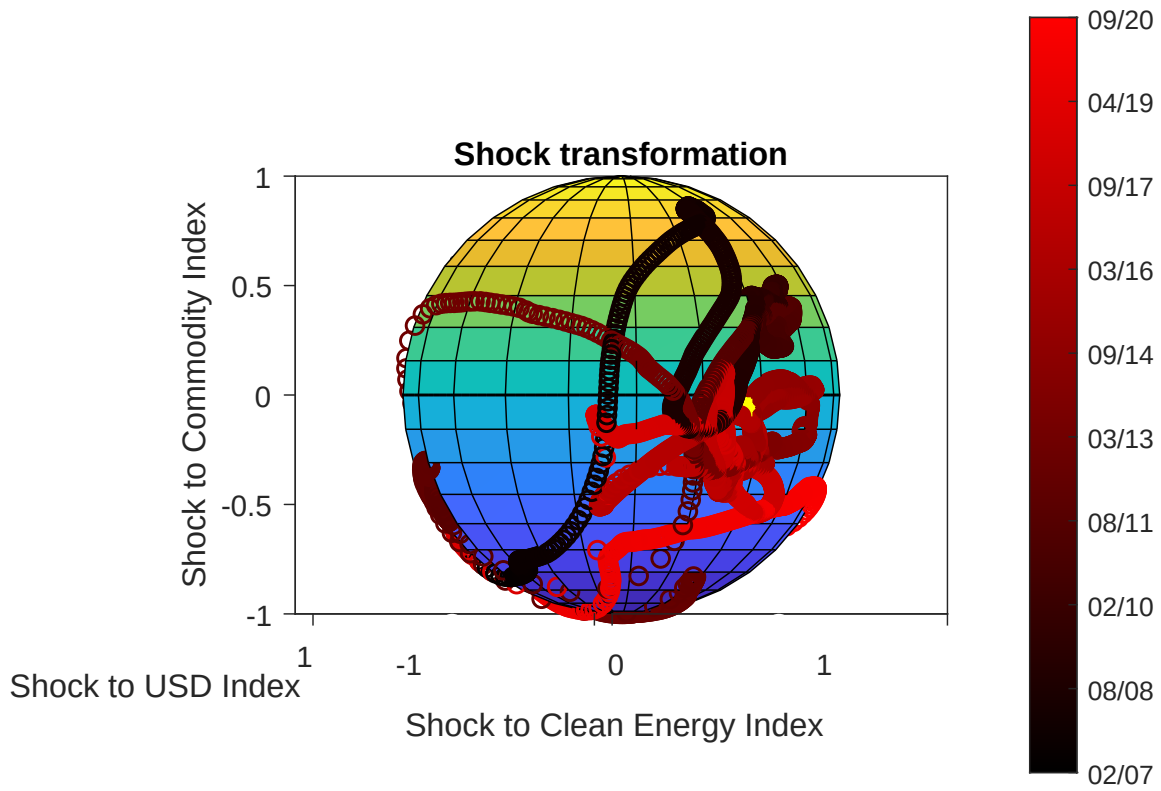

Figure 3.10: Second view on the time-varying transformation of a unit monetary policy uncertainty shock.

This plot displays the mapping of a unit shock in the financial uncertainty component through the structural transmission matrix. The yellow dot indicates the mapping of the shock vector based on the static structural model. The black dot indicates the first mapping of the time series of structural transmission matrices, the green dot indicates the final mapping of the same time series. The picture presents a front view where the shock to the USD index is positive.

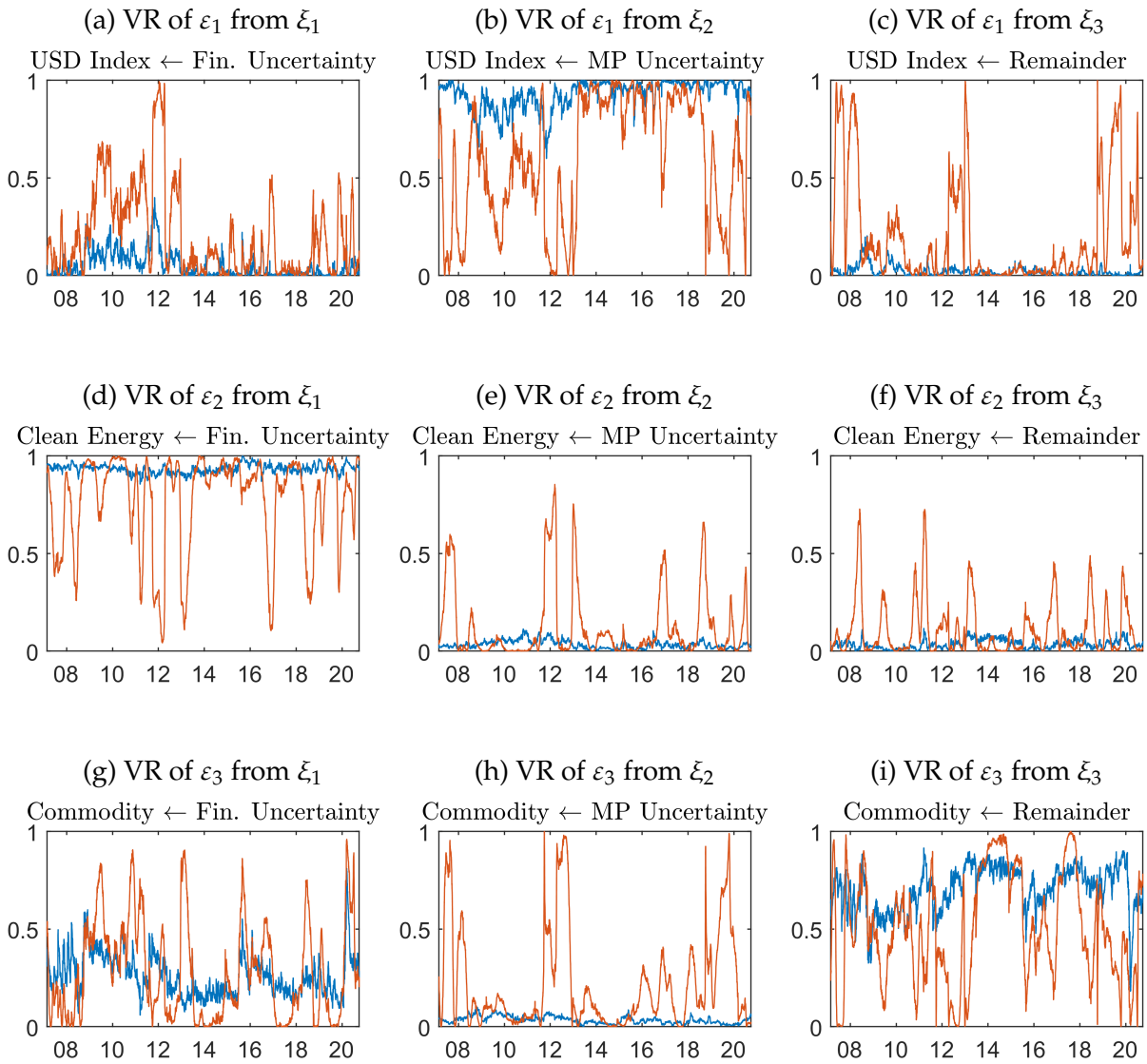

Figure 3.11: Volatility reception in the constant (blue) and the time-varying (red) structural MGARCH model identified using the proxy-guided Procrustes projection.

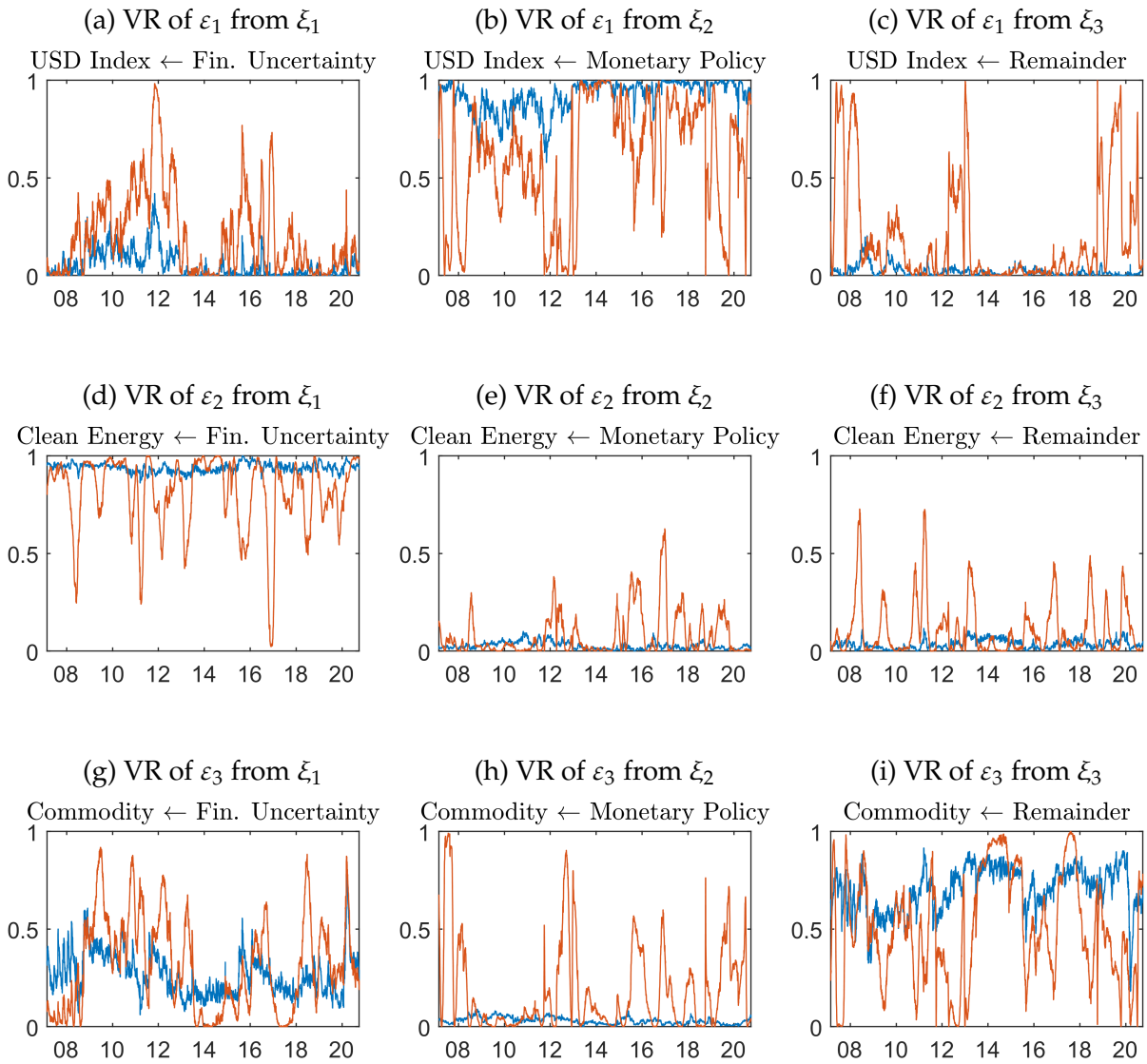

Figure 3.12: Volatility reception in the constant (blue) and the time-varying (red) structural MGARCH model identified using proxy-guided Givens rotations.

3.A Mathematical prerequisites

Definition D.1. Principal matrix square root. Any real symmetric $(n \times n)$ matrix M can be factorized as $M = \Gamma\Lambda\Gamma^\top$ where Γ is an orthogonal $(n \times n)$ matrix with the normalized eigenvectors of M as columns and Λ the diagonal matrix of the eigenvalues. The principal matrix square root of M is defined as $\Gamma\Lambda^{1/2}\Gamma^\top$ where $\Lambda^{1/2}$ denotes the diagonal matrix of the square root of the eigenvalues of M. It is the unique matrix square root which has non-negative eigenvalues, see Horn and Johnson (2012, Theorem 7.2.6).

Definition D.2. Orthogonal matrix. An orthogonal matrix R is a real $(n \times n)$ matrix satisfying $R^\top R = RR^\top = I_n$.

Definition D.3. Local stationarity (Zhou and Wu, 2009). Let $(\zeta_t)_{t\in\mathbb{Z}}$ be a sequence of iid random variables and define $y_t := (\zeta_s : s \leq t)$. The sequence of time series $(X_{t,T})_{t=1,\ldots,T}$, $(T \in \mathbb{N})$ is locally stationary if there exists a measurable function $G : [0,1] \times \mathbb{R}^\infty \mapsto \mathbb{R}$ such that $G(s, y_t)$ is a well-defined random variable for all $s \in [0,1]$ and $X_{t,T} = G(t/T, y_t)$, $(t = 1, \ldots, T)$.

Remark. In Definition D.3 the data generating mechanism G changes smoothly with the time index t such that a subsequence $(X_t, ..., X_{t+j-1})$ is approximately stationary if its length j is sufficiently small compared to T (Zhou and Wu, 2009).

Definition D.4. Local stationarity (Vogt, 2012). A sequence of time series $(X_{t,T})$, $t \in \mathbb{Z}$ with index $T \in \mathbb{N}$ in a normed vector space $(\mathbb{R}^d, |\cdot|)$, is locally stationary of order p if for each time point $s \in [0,1]$ in rescaled time there exists an associated strictly stationary time series $X_t^{(s)} : t \in \mathbb{Z}$ and a process of positive variables $S_{t,T}(s)$ satisfying $\mathrm{E}[(S_{t,T}(s))^p] < C$ for some $p > 0$ and $C < \infty$ independent of s, t and T such that it holds that

$$|X_{t,T} - X_t(s)| \leq \left(\left| \frac{t}{T} - s \right| + \frac{1}{T} \right) S_{t,T}(s) \quad \text{a.s.}$$

Remark. In Definition D.4 the process $X_{t,T} : t = 1, \ldots, T_{T=1,\ldots\infty}$ can be approximated by a stationary process $X_t(s)_{t\in\mathbb{Z}}$ locally in time with the approximation being of order $\mathcal{O}_p\left(\left|\frac{t}{T} - s\right| + \frac{1}{T}\right)$ (Vogt, 2012).

		constant model			time-varying model		
correlations		ξ_1	ξ_2	ξ_3	ξ_1	ξ_2	ξ_3
	ξ_1	1.0000	-0.0088	-0.0067	1.0000	-0.0002	-0.0186
	ξ_2	-0.0088	1.0000	0.0006	-0.0002	1.0000	0.0023
	ξ_3	-0.0067	0.0006	1.0000	-0.0186	0.0023	1.0000
p-values	ξ_1	0	0.6069	0.6939	0	0.9913	0.2773
	ξ_2	0.6069	0	0.9704	0.9913	0	0.8923
	ξ_3	0.6939	0.9704	0	0.2773	0.8923	0

Table 3.9: Correlations of the inferred structural financial uncertainty and monetary policy uncertainty and surprise shocks of the constant (left panel) and time-varying (right panel) structural MGARCH model identified using the proxy-guided Givens approach. The asset system consists of demeaned daily log returns of the Finex U.S. Index, the S&P Global Clean Energy Index and the Bloomberg Commodity Index over the period from 23/02/2007 to 30/09/2020. The inferred structural shocks are a financial uncertainty shock (ξ_1) and a monetary policy surprise and uncertainty shock (ξ_2).

3.B Choice of proxy variables

3.B.1 Narrative corroboration

Tables 3.10 to 3.12 show that the interpretation of the model-implied structural shocks can be narratively corroborated as in Fengler and Polivka (2022a).

Financial Uncertainty Shocks		
Date	Shock	Event
27-Feb-2007*	3.0439	Federal home loan mortgage corporation (Freddie Mac) announces that it will no longer buy the riskiest subprime mortgages and mortgage-related securities;
		Rumors of a Chinese crackdown on market speculation; Alan Greenspan warns of possible impending recession; Dick Cheney assassination attempt; Drop in durable goods orders.
15-Jan-2008*	3.6457	Citi plumbs, Merrill gets USD 6.6 billion infusion and Fed auctions credit below main rate; Dollar slumps versus the Yen and Euro upon rate outlook, gold surges.
06-Jun-2008	3.3860	Crude prices' largest one-day advance ever and the biggest one-month surge in over 20 years in the unemployment rate.
26-Jun-2008	3.3861	Dow tumbles as crude hits record high; Goldman Sachs downgrades investment banks; Dollar falls against both the Euro and the Yen; Day before bear market declaration.
09-Sep-2008*	5.3403	Stocks tumble upon worries about Lehman Brothers and AIG; Financials slump after rescue of Fannie Mae and Freddie Mac; Falling oil prices add to worries about the slowing global economy.
29-Sep-2008*	3.3149	U.S. House of Representatives rejects the Emergency Economic Stabilization Act of 2008 (bailout plan); Stock market crash.
04-Feb-2010*	3.1546	U.S. stock markets decline amid China curbing lending and sovereign debt issues in Greece, Portugal, and Spain.
16-Apr-2010*	2.9601	Goldman Sachs charged with fraud by SEC; Treasurys rally, stocks and oil tumble; Euro slumps on Greece jitters; ECB worries about U.S. debt.
04-May-2010	3.0471	Stocks decline on worries about Greece's debt; Treasury prices rally.
19-Oct-2010	3.0040	Stock markets fall amid efforts to force Bank of America to repurchase bad mortgages; Investors weigh a surprise rate hike by the Chinese government, and mixed data on the housing market and corporate results.
12-Nov-2010	3.0874	Sell-off in U.S. stocks following a volatile trading session in Asian markets; Concerns about a Europeans sovereign debt crisis, potential tightening of China's monetary policy, and tepid U.S. growth.
16-Nov-2010	3.1698	U.S. stocks tumble as investors cast a worried eye at economic developments in Europe (Ireland) and China; The Dollar Index rises weakening commodity prices.
05-May-2011	4.3107	Dollar rallies as Euro slumps upon Greece rumors; Falling commodity prices, crude slumps.
04-Aug-2011*	3.6440	Global stock markets decline due to continuing high foreclosure rates in the U.S and the European debt crisis (Italy, Spain).
08-Aug-2011*	4.2764	Global stock markets decline due to the widening eurozone government debt crisis and Friday's U.S. rating downgrade.
09-Sep-2011	2.8268	Deepening fears about Europe sink stocks as Greek default fears return.
16-Apr-2013	3.1598	Stocks rebound from year's worst sell-off, commodities mixed.
20-Jun-2013*	3.1613	Worst day of the year for Dow and S&P one day after Fed raised fears it may be preparing to wind down its stimulus policies this year; Strong dollar weighs on commodities.
07-Nov-2013*	3.1370	Stocks take a big dive, but Twitter surges; ECB unexpectedly cuts rates.
24-Jan-2014	3.3616	Global stock market slump amid concerns about an economic slowdown in China.
09-Sep-2014*	2.8420	Stock markets slump amid concerns about rate hikes.
28-Nov-2014	3.9390	Energy prices slip due to concerns about sluggish demand out of Europe and an economic slowdown in China.
20-May-2015	3.0025	Gold Prices spike on dovish FOMC, U.S. oil prices rise as U.S. data show large drops in supplies of crude oil; Liquidity-starved markets fear worst in Europe.
		Five banks pay penalties; Skies darken for China's solar industry; China manufacturing index below expectations.
29-Jun-2015	2.8665	Global stock market sell-offs among Greek default fears and announcement of referendum on bailout terms increasing Grexit chances; U.S. stocks suffer their worst plunge in 2015.
06-Jul-2015	3.2313	Global stocks and oil drop on concerns about Greece, China, as China's bazooka fails to overwhelm; Gold gains.
07-Jan-2016*	3.0744	Oil prices hit 12-year low as fears about China grow; China stock market crash causes world markets to slide; Devaluation of Yuan.
10-Jun-2016*	3.3790	U.S. stocks slide as German, U.K., Japan bond yields hit fresh lows; Treasury yields fall to three-year lows; Concerns about low rates; Central banks explore response to possible turbulence from Brexit vote.
15-Jun-2018	2.7297	China: 'The US has launched a trade war'; Trump approves USD 50 billion tariffs on Chinese goods.
24-Jun-2016	2.6089	Global stock market fall due to Brexit vote results; British pound crashes.
11-Jul-2018	2.9710	US stocks retreat after announcement of new US steps in China trade war amid fear of derailing of global economy due to denting business confidence, jacking up prices and paralyzing supply chains.
05-Aug-2019*	3.9307	Escalating US China trade war; US stocks post worst day of the year after China devalues its currency.
27-Jan-2020*	3.2937	Coronavirus outbreak sends ripples through markets; Oil prices fall 10% as Coronavirus raises fears for global growth.
09-Mar-2020*	4.9037	US stocks plummet on Coronavirus fears; Italy lockdown; Dow has its worst day since 2008; Oil crash amid Saudi Arabia / Russia oil price war.
11-Jun-2020*	2.7669	Stocks plunge as new Coronavirus cases rise and economic outlook from the US Fed is somber; Crude prices drop 8%.
03-Sep-2020*	3.6087	VIX hits its highest level ever at an all-time high for the S&P 500 amid the upcoming elections; Increasing worries about a correction.

Table 3.10: Narrative corroboration of the upper first percentile of the financial uncertainty shock corresponding to large increases in uncertainty. The underlying asset return system consists of the daily log returns of the Finex U.S. Index, the S&P Global Clean Energy Index and the Bloomberg Commodity Index over the period from 23/02/2007 to 30/09/2020. It is identified using the time-varying proxy MGARCH model. Proxy variables for identification of a financial uncertainty shock and a monetary policy shock are returns to the VIX (Z_1) and the returns to the MPU of Bauer et al. (2021) combined with the MPS of Bauer and Swanson (2022) (Z_2). News headlines are extracted from the Wall Street Journal news archive on wsj.com and from CNNMoney.com Market Report. Shocks marked with an asterisk fall as well into the upper first percentile of the structural shocks identified by the static proxy MGARCH model.

Monetary Policy Shocks		
Date	Shock	Event
16-Aug-2007	4.4016	Stocks erase most losses after panic about credit and mortgage markets; Treasury prices rally as investors search safety; The dollar slumps versus the Yen and falls versus the Euro. Oil and gold prices tumble.
08-Aug-2008*	3.4983	Stocks soar as oil prices slump and the dollar rallies in response to ECB's economic outlook.
30-Sep-2008*	4.4941	Stocks rally upon bets that Congress will pass a version of the government's bailout package; Credit markets remain frozen.
04-Dec-2009*	3.6664	Gold and oil futures end lower after stronger-than-expected economic data boosts the U.S. Dollar and sparks fears Fed might begin to lift interest rates.
22-Sep-2011	3.7206	Renewed fears of a global economic slowdown cause investors to dump stocks and retreat to U.S. Treasurys, pushing 10-year yields to 1940s levels; Fed stimulus plan to buy USD 400 billion longer-dated Treasurys; VIX finishes high as U.S. stocks and oil prices decline sharply on economic growth concerns. Money-fund assets drop; EU banks cut dollar exposure; Dollar soars.
13-Mar-2013*	3.7745	U.S. Dollar is powering higher against the world's major currencies, a reversal driven by the relative health of the U.S. economy; Discussion of deficit reduction package in Congress; 10-year note auction fuels price rebound in Treasurys; Retail data boost dollar; Dollar correlations fall; Oil drillers boost efforts to coax more from shale; Italy's bond sale meets tepid demand.
20-Jun-2013	3.3459	Euro group agrees on rules for bailout fund; Fed chairman Bernanke sees a slightly better economy, but stimulus will continue; China credit crunch; Gold falls, Treasurys retreat after soft TIPS sale; Concerns about the Fed's exit from its bond-buying program; 10-year Treasury yield hits the highest level in 22 months; Dollar rises sharply as investors sell other currencies to prepare for a pullback in the Fed's easy-money policies after Bernanke comment; Crude settles sharply lower; U.S. jobless claims rise, but labor-market growth chugs on; Spanish and Italian bond markets feel fallout from the Fed; China banks warn of loan woes.
04-Sep-2014*	4.3559	Companies step up bond sales as rates remain low; Bondholders meet with Argentina officials; ECB surprisingly cuts rates, plans stimulus, aims at Euro; Euro drops to 14-month low against dollar; Gold and oil prices fall on dollar strength; Bundesbank chief opposes ECB moves.
03-Oct-2014*	3.3977	Dollar and stocks rally bolstered by U.S.'s strong September jobs growth, bolstering expectations for an interest-rate increase; Oil prices extend losses; Gold prices fall to four-year low.
22-Jan-2015*	3.6307	China's Yuan slides; Aggressive ECB stimulus ushers in new era for Europe; ECB to purchase Euro 60 billion in assets each month starting in March. Dollar rises against Euro; Oil plunges as supplies grow; Gold rises on ECB move; U.S. jobless claims flash some warning signs; China injects USD 8 Billion into banking system to boost liquidity.
24-Jun-2016*	4.4188	Global stock market fall due to Brexit vote results; British pound crashes while dollar, Yen soar; Treasury yields plummet after vote; U.S. grain prices drop after Brexit.
09-Nov-2016*	3.6118	Trump's surprise victory spurs speculations about responses of and political pressure on Fed; Volatile commodity prices; Oil prices lower, gold higher; Overhang and OPEC uncertainty weigh; Bank stocks surge on hope Trump lightens regulatory load; Stocks rally after overnight tumult; Treasury prices fall, coal and copper win with Trump; On energy and climate, Trump to chart a new course; COVID: ban on European visitors.
20-Dec-2018	3.3660	House passes funding bill with wall, setting stage for shutdown; Dollar falls upon Fed guidance: Slowdown in rate increases expected; Treasurys fall ahead of government bond auction after Fed decision; Interest rate concerns and concerns about slowing global demand drive oil to 17-Month Low; Saudis to cut more oil than planned as OPEC drums up pact; Treasury Secretary says market has overreacted to Fed.
31-May-2019	3.5045	Dallas Fed's gauge showed underlying inflation rose to 2% in April; Oil falls sharply on trade tensions and China fears, gold hits high; Trump's Mexico threats will cause Fed to cut rates, JP Morgan says.
01-Aug-2019	3.5020	Stocks, bond yields, oil fall on new China tariffs, expected surge in oil supply and tariffs add to glut concern; Treasury yield hits lowest level since 2016 vote upon Fed rate cut; Weak economic data and decline in oil prices raise concerns on global growth outlook and Fed's ability to stimulate inflation after rate-cut announcement; U.S. manufacturing slips; U.S. jobless claims increased.
13-Mar-2020*	5.1065	U.S. policy makers weigh next stage of stimulus in response to Coronavirus; Central banks struggle with response as there is no scope for cutting interests to stimulate growth; Markets central to financial system remain jittery despite Fed injection; Fed accelerates previously announced purchases of treasury securities on Friday; Consumer views on economy slip.
17-Mar-2020*	4.4061	Trump administration seeks to send checks to Americans as part of stimulus package; Fed to relaunch primary dealer credit facility; U.S. Delays April 15 Tax payments for 90 days for most Americans; Dollar surges as investors seek shelter from market disruption; U.S. February retail spending drop shows Coronavirus concerns started to take hold.
17-Mar-2008	-4.0488	Dollar continues plunge, heightened fears of further credit turmoil in the U.S. amid sale of Bear to J.P. Morgan Chase amid credit crunch; Global stock market downturn; Central bank offers loans to brokers, cuts key rate, more rate cuts expected; Broadest expansions of Fed's lending authority since the 1930s.
12-Sep-2008*	-3.1169	Lehman slides, fixed-rate 30-year mortgages fall on bailout news of Fannie Mae and Freddy Mac; Rate-cut speculation douses dollar's advance.
25-Nov-2008*	-2.8991	OECD foresees worst recession since 1980s; Fed expands stimulus to consumer credit and MBS market; U.S. government's rescue plan for Citigroup; USD down; Treasurys down due to prospect of record offering.
18-Mar-2009*	-4.6357	Fed's USD 300B pledge to purchase long-term Treasurys over the next six months.
19-May-2010	-2.9184	USD sinks against Euro upon speculation ECB will act to stop Euro's drop; German short-selling ban may back ECB into corner and worries stock markets.
01-Jul-2010*	-3.5797	USD sinks against Euro upon disappointing US jobs data leading investors to question pace of US recovery.
09-Feb-2012	-3.09	NY Fed AIG bond sale; Treasury explores final exit from bank bailouts; Greece signs economic reform deal; Gold rallies on Greek debt deal; US jobless claims sink; US trade deficit low; OPEC cuts oil-demand view.
29-Jun-2012*	-4.0514	Germany approves bailout fund; U.S. Treasurys sell off on EU deal, boosts Euro and oil, pressure from Italy and Spain helps secure pact as Germany cedes on key debt issues.
11-Jul-2013*	-3.2371	U.S., China to pursue investment treaty; Dow surges to new high on Bernanke remarks that the Fed will maintain its easy-money policies for the long run; Dollar loses ground, Treasurys push higher after Bernanke.
15-Oct-2014*	-2.9414	Treasury issued its semiannual report to Congress on exchange-rate policies of its major trading policies, calls on core Eurozone economies to do more for growth; Europe fears send rates tumbling; Greek financial markets slump amid fears over political instability; Worries about global growth push back expectations for higher U.S. interest rates.
03-Dec-2015*	-4.6894	ECB's stimulus efforts fell short of expectations and weakens USD; U.S. non-farm payroll data may signal slow pace at Fed; Crude oil prices edge higher ahead of OPEC meeting and due to weak dollar; Fed's Stanley Fischer sees financial system far less vulnerable than before 2008 crisis.
03-Feb-2016*	-3.7426	Investors cast wary eye on Fed rate increases; Broad decline in the dollar and a sharp drop this year in U.S. Treasury yields; Oil prices higher upon weak dollar but glut to keep prices lower for longer; U.S. to cut back issuance of longer-term debt.
03-Jun-2016*	-4.5054	Fed's Brainard makes case for "Watchful Waiting"; Fed's Dudley raises questions about rate increases; U.S. Treasury increasing issuance of short-term debt; Gold prices rise on weaker dollar, broader market concerns.
06-Sep-2016	-2.8926	Fed's Williams argues for "earlier," gradual rate increases; Oil prices waver on weaker Dollar, OPEC uncertainty; Gold and U.S. government-bond prices higher on doubts of a Fed rate increase on weak business data; Stocks and bonds are moving together.
24-Jan-2018	-3.3506	Powell confirmed as Fed Chairman; Gold surges, dollar slides after Treasury Secretary Mnuchin comments that a weaker dollar was good for trade and decision on new tariffs in trade war; Fresh 3-year high for oil futures as data shows drop in supplies; Treasurys weaken on global growth.
16-Sep-2019	-5.0806	Oil prices log historic rally after Saudi attack; inflation bonds gain; Trump again pressures the Fed to lower interest rates in wake of Saudi attacks and strong dollar.
02-Mar-2020*	-3.5171	Long-term U.S. Treasury yields hit record lows; Futures market expects rate cut by Fed in March to combat pandemic; Coronavirus is hammering China's economic outlook, hits once-isolated U.S. natural gas market.

Table 3.11: Narrative corroboration of the upper and lower first percentile of the monetary policy shock. News items are extracted from market reports on money.cnn.com and news articles from the Wall Street Journal news archive on wsj.com. Shocks marked with an asterisk fall as well into the upper first percentile of the structural shocks identified by the static proxy MGARCH model.

Remainder Shocks		
Date	Shock	Event
02-Jul-2007	-2.3923	Most commodity prices soar despite economic woes; Fear of inflation lurks in U.S. recovery; US housing market sagging.
28-Sep-2007	-2.5809	Historic surge in grain prices and demand roils markets: biggest changes in global food markets in 30 years. Congress grants rise in public-debt ceiling due to Iraq war;
		USD sinks to an all-time low as U.S. housing data is weaker than expected; Gold high amid fears of US recession.
19-Mar-2008	-2.5549	Slumping oil and gold prices as worry about credit crisis returns; Fed three-quarter-point cut in interest rate. Bush's delivers speech on Iraq. ECB pumps funds into money markets, housing starts slip.
29-May-2008	-2.9406	Stocks gain amid sliding oil prices, a rallying dollar and a report that GDP growth was better than initially reported; Jobless claims rise; Dollar increases as U.S. data suggest no imminent rate cut.
		Oil decline due to short-term delays in unloading Gulf Coast tankers; Gas hits record high, Gold slumps. Corn prices under pressure amid USDA land move.JP Morgan-Bear Stearns deal closes.
15-Jul-2008	-2.3956	Biggest oil price drop in 17 years as Fed chief indicates inflation and high fuel prices will cut into U.S. demand for oil. OPEC lowers demand forecast. Gas continues record high.
		Fannie Mae and Freddie Mac continued to tumble, one session after the news of the government's rescue plan failed to soothe investors.
04-Aug-2008	-3.0641	Stocks stumble on economic jitters; Fear about Tuesday's Fed rate decision, drop in oil prices after reports that a tropical storm in the Gulf of Mexico is losing steam and signs of softening demand.
16-Sep-2008*	-2.7449	Stocks rise on Fed; Investors relieved that Fed's outlook was not more bearish; Oil prices plunge as investors continue to bet on a global economic slowdown amid Wall Street's meltdown.
10-Oct-2008*	-3.0347	Panic grips financial markets amid credit crunch; Ted spread at all-time high; Oil, gas and gold prices slump on slowdown fears; USD gains against Euro and Yen; Global stock market crash.
30-Oct-2008*	-3.3057	Stocks get a boost after Fed and other central banks cut rates, lending improves, and GDP shrinks at a slower-than-expected pace. Credit crunch loosens.
10-Mar-2009	-2.5683	Stocks stumble on recession fears; Oil hits record; USD touches a fresh record low against the euro Friday on the weak jobs report; Gold prices, along with other dollar-traded commodities, surge.
26-Mar-2009	-3.1587	Successful Treasury debt auction. Treasury Secretary Geithner outlines overhaul of regulatory system. Biggest drop in GDP since 1982 but economic data bolster oil prices. PetroChina profit drops; Output curbs expected.
14-Mar-2011	-3.2256	Japan's earthquake and tsunami. Oil slips amid concerns about the fallout from Japan's earthquake.
15-Mar-2011*	-4.6302	Japan's devastating earthquake and nuclear crisis. Oil price falls nearly 4%.
05-May-2011*	-3.2292	Stocks tumble on job report worries and amid oil price plunging 8% below USD 100 a barrel.
22-Sep-2011*	-2.7153	Stocks and commodities plunge worldwide on fear factor of crisis September.
12-Apr-2013	-3.0542	Bitcoin bubble may have burst, Treasurys lifted by growth worries, commodities rout. Yen rebounds as safe haven. Crude oil settles lower on weak demand. metal tumbles, rising food grain prices.
31-Dec-2013*	-2.9464	Stocks end year on a high note after a rally year. China manufacturing growth slows, U.S. oil inventories seen falling again, year's worst-performing commodity: corn, due to droughts. Gold falls.
28-Nov-2014*	-4.0996	Oil price plummets as OPEC starts price war with the US
02-Dec-2014	-2.3945	Oil price slide due to several supply shocks as Iraq government agrees on Kurdistan oil deal; Natural gas falls on mild winter and Russia decides to drop southstream pipeline
08-Apr-2015*	-2.6812	Dollar rises after Fed's rate signals zero yield, or less; Oil slides as supplies soar: largest one-week build in U.S. crude supplies since 2001. Saudi oil output at record high. Gold declines after Fed minutes.
02-Dec-2015*	-2.6545	Gold hits six-year low, OPEC-U.S. market share battle leaves flood of oil, oil price falls below 40 USD. Natural gas falling on mild weather. Yellen signals Fed on track to raise rates sending dollar to 13-year high.
16-Dec-2015	-2.6970	Fed raises rates after seven years near zero, U.S. businesses worry stronger dollar may weigh on growth and exports; Wind, solar companies get boost from tax-credit extension;
		Natural gas falls to all-time inflation-adjusted low as US natural-gas inventories at high level; Oil prices fall on record supplies. Gold prices slide after Fed decision.
01-Feb-2016	-2.7447	Volatile oil and stock prices boost demand for safe-haven bonds; Oil prices drop as chances fade for output cuts. Natural gas retreats on warm weather forecasts.
09-Feb-2016*	-3.1583	Oil settles below $28 a barrel and natural gas falls with stockpiles still high. Global energy monitor says oversupply grew worse in January with surge in production from OPEC. U.S. 10-year yield drops to year low.
		S&P downgrades junk-level ratings on 25 oil-and-gas producers. President proposes new taxes on oil industry, boost to clean-energy funding,
		Copper prices fall amid global equity weakness, growth fears as U.S. weekly chain-store sales fall.
07-Jul-2016*	-2.6350	Stocks slip, along with oil prices; Brexit aftermath may stem oil recovery; Natural gas falls on supply concerns; Crude-oil prices dropped Thursday on growing concerns that a glut of gasoline is due to persist;
		Fed extends deadline for banks to shed certain investments under Volcker Rule; ECB Minutes show concerns over Brexit spillover in Eurozone;
		China flooding roils soybean meal market; Gold trades around two-year high on safe-haven buying.
03-Jan-2017	-2.7767	Gold edges up despite dollar strength, dollar soars on manufacturing data; Natural gas falls on warmer weather forecast; Bonds end lower as economic reports sap demand;
		Oil futures tumbled Tuesday as the dollar rose and doubts about whether major producers will be able to follow through on an agreement to cut production continued to weigh on the market.
04-May-2017	-3.3544	Russia, Turkey, Iran sign deal on Syria de-escalation zones; Commodity sell-off damps U.S. stocks; Dollar slips as traders weigh economic data, Natural gas falls on larger-than-expected inventory build;
		Deepening gasoline glut pushes oil to a five-month low; investors skeptical of OPEC's abilities to ease a global supply glut amid elevated U.S. crude production and inventories;
		Metals slide on global growth concerns; Treasuries extend declines after Fed comments.
19-Mar-2018	-2.6203	U.S. stocks plummet amid tech selloff; Volatility gauge rises most since last month's market rout; Oil edges lower as stocks fall.
14-Nov-2018	-3.9449	Bitcoin plunges below $6,000, hits new lows for the year; Fed tracking world growth worries, Powell says; Libya's oil production has more than doubled since June, oil chief says; Global economy shows strain
		as U.S. steams ahead: China, Japan and Germany show signs of stress; U.S. oil prices rise from 2018 lows; Investors weigh concerns that global output could outstrip demand as OPEC and its allies signal supply cuts;
		USD lower after consumer price data; Shipping industry sends a trade warning; Global oil supply to outstrip demand on record U.S., Russia, Saudi Production; More signs of trouble in China's auto market.
20-Jun-2019	-2.4491	EU threatens sanctions amid Turkey-Cyprus drilling spat; Gold surges to highest price since 2013 after fed hints at rate cut; S&P 500 hits record close after fed hints of interest-rate cut;
		Middle East clashes send oil sharply higher: oil prices climbed sharply Thursday as tensions mounted in the Middle East and the dollar fell, extending a period of high volatility for crude. 10-year yield falls below 2%.
04-Sep-2019	-2.8855	U.S. stocks rise after global rally, U.K. lawmakers vote to delay Brexit and bar snap election, foiling Johnson; Volatility continues to jolt oil market; Signs of easing tensions in Hong Kong fuel another big move in crude;
		Fed's beige book reports modest growth despite trade uncertainty: U.S. trade gap narrowed as imports fell; Democrats propose climate spending plans; Carbon-emissions credits slide over Brexit fears.
28-Feb-2020*	-2.9134	China purchasing indexes drop to record lows as epidemic stalls output; Fed: Will act as appropriate to support the economy; Stocks suffer biggest weekly losses since 2008;
		Oil logs its worst week since the financial crisis as Coronavirus-driven sell-off in risky assets accelerates; Treasury yields hit new lows.
06-Mar-2020	-2.7090	Dollar slides upon rate cuts; Oil prices plunge after Russia-Saudi split: oil producers fail to agree on whether to reduce global supply amid Coronavirus's devastating effect on demand.
		Coronavirus risk rises for U.S., global economies; Fed stores dollars arriving from Asia as Coronavirus precaution; Berkshire backs away from Canadian gas project; U.S. Trade gap narrowed in January as flows slowed.
26-Mar-2020	-2.6587	Dow rallies after stimulus vote; ECB begins new bond purchases; Short-term Treasury yields go negative in scramble for cash; Oil slides on renewed demand woes due to Coronavirus.

Table 3.12: Narrative corroboration of the first percentile of the remainder shock of the time-varying proxy MGARCH model. News items are extracted from market reports on money.cnn.com and news articles from the Wall Street Journal news archive on wsj.com. Shocks marked with an asterisk fall as well into the upper first percentile of the structural shocks identified by the static proxy MGARCH model.

3.B.2 MPU versus MPS

Alternative proxy variable choices for identification are given by exploiting only the MPU or only the MPS. The correlation of the two time series is 0.2927, and the correlation of the orthogonalized final instrument Z_2 with MPS is 0.2796, the proxies deliver similar structural models. Even though the model identified using the MPS instrument shows a much stronger correlation with the monetary policy shock of 0.4843 under the Givens identification approach (see Table 3.19), the model violates the exogeneity condition through a small but statistically significant correlation between Z_2 and ξ_1. Furthermore, the F-test of Lunsford (2015) indicates that the MPS instrument may be more prone to be a weak instrument. When identifying the model using the Procrustes approach, the correlation of the MPS instrument with the monetary policy shock remains at a similar level but the model-implied shocks fulfill the exogeneity conditions (see Table 3.17). These promising results emphasize the need to extend the time-varying modeling approach to account for non-equidistantly spaced, sparse proxy variables in further research. The model identified using the orthogonalized MPU instrument shows slightly smaller values in terms of correlation with the monetary policy uncertainty shock and in terms of the F-statistics for weak instrument testing compared to the main model. This indicates that monetary policy surprises at FOMC meetings contain structural information which differs from monetary policy uncertainty and that adding this information may improve full identification of the transmission channels of the structural model.

3.B.3 Alternative proxy choices

Tables 3.21 - 3.23 display the estimation results of the constant proxy-MGARCH model based on the Procrustes approach when employing the EPU, the GPR and variations in the gold price as proxy variables. Table 3.21 reveals that economic policy uncertainty is – in contrast the financial uncertainty as proxied by the VIX – not a main driver of variations in the asset return system and that the financial uncertainty shock identified using the VIX already contains information on economic policy uncertainty. Białkowski et al. (2022) provide a discussion of the differences in the evolution of the VIX and the EPU and the informational disconnect of the two uncertainty measures. Table 3.22 indicates that the GPR may be a weak instrument as well but employing GPR as second proxy variable has a visible effect on the last column of the transmission matrix, which differs from the other models: the impact matrix assigns a larger weight to a unit geopolitical uncertainty shock

		constant proxy-MGARCH model		
$\hat{\hat{R}}$		-0.1464	0.9892	-0.0061
		-0.9398	-0.1410	-0.3113
		-0.3088	-0.0398	0.9503
		ξ_1	ξ_2	ξ_3
correlations	Z_1	0.5358	0.0228	0.0000
	Z_2	0.0069	0.1596	-0.0000
t-statistics	Z_1	37.0472	1.3296	0.0000
	Z_2	0.4044	9.4381	-0.0000
p-values	Z_1	0.0000	0.1838	1.0000
	Z_2	0.6859	0.0000	1.0000
F-test		statistic	$b = 0.01$, $\alpha = 0.01$	$b = 0.05$, $\alpha = 0.01$
	Z_1	459.06	51.50	16.26
	Z_2	29.770	51.50	16.26

Table 3.13: Estimation results of the constant structural MGARCH model using the MPU as second proxy under the Procrustes approach.

The table shows, from top to bottom, the estimated rotation angles, the estimated rotation matrix, the correlations of the proxy variables Z_1, Z_2 with the inferred structural shocks ξ_1, ξ_2 and ξ_3, followed by the corresponding t-statistics and p-values. Furthermore, it reports the outcomes of the F-test of Lunsford (2015) for robustness under weak proxy variables and of the Wald test for symmetry of volatility spillovers by Fengler and Polivka (2022a). For the F-test, the critical values for $n = 3$ assets, an of asymptotic bias level b and a significance level α are given in (Lunsford, 2015, Table 2). The asset system consists of demeaned daily log returns of the Finex U.S. Index, the S&P Global Clean Energy Index and the Bloomberg Commodity Index over the period from 22/02/2007 to 30/09/2020. Proxy variables for identification of a global financial uncertainty shock and a monetary policy uncertainty shock are returns to the VIX (Z_1) and the returns to the MPU of Bauer et al. (2021) (Z_2).

		constant model		
correlations		ξ_1	ξ_2	ξ_3
	ξ_1	1.0000	-0.0099	-0.0065
	ξ_2	-0.0099	1.0000	0.0002
	ξ_3	-0.0065	0.0002	1.0000
p-values	ξ_1	0	0.5621	0.7042
	ξ_2	0.5621	0	0.9892
	ξ_3	0.7042	0.9892	0

Table 3.14: Correlations of the inferred structural global financial uncertainty and monetary policy uncertainty shocks of the constant and time-varying structural MGARCH model under the Procrustes approach. The asset system consists of demeaned daily log returns of the Finex U.S. Index, the S&P Global Clean Energy Index and the Bloomberg Commodity Index over the period from 22/02/2007 to 30/09/2020. The inferred structural shocks are a financial uncertainty shock (ξ_1) and a monetary policy uncertainty shock (ξ_2).

than to a unit remainder shock to the Commodity Index. This finding reflects the notion that commodity dynamics respond to geopolitical events (see, e.g., the recent analysis of Wang et al. (2022)). From Table 3.23 it is apparent that gold price variations satisfy the exogeneity conditions but constitute only a weakly relevant proxy variable for financial uncertainty in the asset return system.

3.C Robustness of estimation

Choosing $k = 1$ in the naive leave-k-out cross-validation procedure to infer optimal bandwidths for both covariances is motivated by the weak correlation in the product of the reduced form error and the instrument of interest, see Figure 3.13.

The plot of the proxy variables in Figure 3.2 and the graphs of the error terms of the nonparametric estimation procedure in Figures 3.16 and 3.17 indicate the presence of several extreme observations in the instrument data. Removing potential outliers, e.g., by clipping the data at the lower and upper five percentiles and re-estimating the benchmark

		constant proxy-MGARCH model		
$(\hat{\theta}_{12}, \hat{\theta}_{13}, \hat{\theta}_{23})^\top$		-1.6802	-0.3154	-0.0536
$\hat{\hat{R}}$		-0.1038	0.9946	-0.0061
		-0.9450	-0.1005	-0.3113
		-0.3102	-0.0265	0.9503
		ξ_1	ξ_2	ξ_3
correlations	Z_1	0.5365	-0.0000	-0.0000
	Z_2	0.0138	0.1591	-0.0000
t-statistics	Z_1	37.1166	$--$	$--$
	Z_2	0.8085	9.4074	$--$
p-values	Z_1	0.0000	$--$	$--$
	Z_2	0.4189	0.0000	$--$
F-test		statistic	$b = 0.01$, $\alpha = 0.01$	$b = 0.05$, $\alpha = 0.01$
	Z_1	459.06	51.50	16.26
	Z_2	29.770	51.50	16.26

Table 3.15: Estimation results of the constant structural MGARCH model using the MPU as second proxy under the Givens approach.

The table shows, from top to bottom, the estimated rotation angles, the estimated rotation matrix, the correlations of the proxy variables Z_1, Z_2 with the inferred structural shocks ξ_1, ξ_2 and ξ_3, followed by the corresponding t-statistics and p-values. Furthermore, it reports the outcomes of the F-test of Lunsford (2015) for robustness under weak proxy variables and of the Wald test for symmetry of volatility spillovers by Fengler and Polivka (2022a). For the F-test, the critical values for $n = 3$ assets, an of asymptotic bias level b and a significance level α are given in (Lunsford, 2015, Table 2). The asset system consists of demeaned daily log returns of the Finex U.S. Index, the S&P Global Clean Energy Index and the Bloomberg Commodity Index over the period from 22/02/2007 to 30/09/2020. Proxy variables for identification of a financial uncertainty shock and a monetary policy uncertainty shock are returns to the VIX (Z_1) and the returns to the MPU of Bauer et al. (2021) (Z_2).

		constant model		
correlations		ξ_1	ξ_2	ξ_3
	ξ_1	1.0000	-0.0090	-0.0065
	ξ_2	-0.0090	1.0000	0.0006
	ξ_3	-0.0065	0.0006	1.0000
p-values	ξ_1	0	0.6001	0.7039
	ξ_2	0.6001	0	0.9979
	ξ_3	0.7039	0.9979	0

Table 3.16: Correlations of the inferred structural financial uncertainty and monetary policy uncertainty shocks of the constant and time-varying structural MGARCH model under the Givens approach. The asset system consists of demeaned daily log returns of the Finex U.S. Index, the S&P Global Clean Energy Index and the Bloomberg Commodity Index over the period from 22/02/2007 to 30/09/2020. The inferred structural shocks are a financial uncertainty shock (ξ_1) and a monetary policy uncertainty shock (ξ_2).

constant proxy MGARCH model, results in decreases in the correlation of instrumental variables and structural shocks (see Table 3.24). Hence, the removal of extreme observations is slightly detrimental for the properties of the static model, respectively, the extreme observations increase the covariance of the reduced form residuals and the instrument. The naive optimal bandwidth for the trimmed instruments is approximately three times as large as the original bandwidth but gives rise to outliers at the same points in time in the residuals of the nonparametric estimation, however with smaller magnitude and slightly lower autocorrelations in the residuals (see exemplarily Figure 3.18). However, the wide smoothing window renders a visual alignment of the movements of the resulting nonparametric estimators with market downturns and stimulus programs infeasible and is therefore not reasonable for the structural analysis of the asset return system.

		constant proxy-MGARCH model		
$\hat{\hat{R}}$		-0.0628	0.9971	-0.0434
		-0.9488	-0.0731	-0.3073
		-0.3096	0.0219	0.9506
		ξ_1	ξ_2	ξ_3
correlations	Z_1	0.5362	-0.0218	-0.0000
	Z_2	-0.0299	0.4839	-0.0000
t-statistics	Z_1	37.0913	-1.2760	-0.0000
	Z_2	-1.7482	32.2842	-0.0000
p-values	Z_1	0.0000	0.2021	1.0000
	Z_2	0.0805	0.0000	1.0000
F-test		statistic	$b = 0.01$, $\alpha = 0.01$	$b = 0.05$, $\alpha = 0.01$
	Z_1	459.06	51.50	16.26
	Z_2	10.411	51.50	16.26

Table 3.17: Estimation results of the constant structural MGARCH model under the Procrustes approach using the MPS as second proxy.

The table shows, from top to bottom, the estimated rotation angles, the estimated rotation matrix, the correlations of the proxy variables Z_1, Z_2 with the inferred structural shocks ξ_1, ξ_2 and ξ_3, followed by the corresponding t-statistics and p-values. Furthermore, it reports the outcomes of the F-test of Lunsford (2015) for robustness under weak proxy variables and of the Wald test for symmetry of volatility spillovers by Fengler and Polivka (2022a). For the F-test, the critical values for $n = 3$ assets, an of asymptotic bias level b and a significance level α are given in (Lunsford, 2015, Table 2). The asset system consists of demeaned daily log returns of the Finex U.S. Index, the S&P Global Clean Energy Index and the Bloomberg Commodity Index over the period from 22/02/2007 to 30/09/2020. Proxy variables for identification of a financial uncertainty shock and a monetary policy shock are returns to the VIX (Z_1) and the MPS of Bauer et al. (2021) (Z_2).

		constant model		
correlations		ξ_1	ξ_2	ξ_3
	ξ_1	1.0000	-0.0082	-0.0062
	ξ_2	-0.0082	1.0000	-0.0006
	ξ_3	-0.0062	-0.0006	1.0000
p-values	ξ_1	0	0.6304	0.7175
	ξ_2	0.6304	0	0.9735
	ξ_3	0.7175	0.9735	0

Table 3.18: Correlations of the inferred structural financial uncertainty and monetary policy uncertainty shocks of the constant and time-varying structural MGARCH model under the Procrustes approach using the MPS as second proxy. The asset system consists of demeaned daily log returns of the Finex U.S. Index, the S&P Global Clean Energy Index and the Bloomberg Commodity Index over the period from 22/02/2007 to 30/09/2020. The inferred structural shocks are a financial uncertainty shock (ξ_1) and a monetary policy shock (ξ_2).

			constant proxy-MGARCH model	
$(\hat{\theta}_{12}, \hat{\theta}_{13}, \hat{\theta}_{23})^\top$		-1.6802	-0.3154	-0.0536
$\hat{\hat{R}}$		-0.1038	0.9936	-0.0434
		-0.9450	-0.1122	-0.3073
		-0.3102	0.0092	0.9506
		ξ_1	ξ_2	ξ_3
correlations	Z_1	0.5365	-0.0000	-0.0000
	Z_2	$\mathbf{-0.0594}$	0.4843	0.0000
t-statistics	Z_1	37.1166	$--$	$--$
	Z_2	-3.4714	32.3210	$--$
p-values	Z_1	0.0000	$--$	$--$
	Z_2	0.0005	0.0000	$--$
F-test		statistic	$b = 0.01,\ \alpha = 0.01$	$b = 0.05,\ \alpha = 0.01$
	Z_1	459.06	51.50	16.26
	Z_2	10.411	51.50	16.26

Table 3.19: Estimation results of the constant structural MGARCH model under the Givens approach using the MPS as second proxy.

The table shows, from top to bottom, the estimated rotation angles, the estimated rotation matrix, the correlations of the proxy variables Z_1, Z_2 with the inferred structural shocks ξ_1, ξ_2 and ξ_3, followed by the corresponding t-statistics and p-values. Furthermore, it reports the outcomes of the F-test of Lunsford (2015) for robustness under weak proxy variables and of the Wald test for symmetry of volatility spillovers by Fengler and Polivka (2022a). For the F-test, the critical values for $n = 3$ assets, an of asymptotic bias level b and a significance level α are given in (Lunsford, 2015, Table 2). The asset system consists of demeaned daily log returns of the Finex U.S. Index, the S&P Global Clean Energy Index and the Bloomberg Commodity Index over the period from 22/02/2007 to 30/09/2020. Proxy variables for identification of a financial uncertainty shock and a monetary policy shock are returns to the VIX (Z_1) and the MPS of Bauer et al. (2021) (Z_2).

		constant model		
correlations		ξ_1	ξ_2	ξ_3
	ξ_1	1.0000	-0.0092	-0.0061
	ξ_2	-0.0092	1.0000	-0.0008
	ξ_3	-0.0061	-0.0008	1.0000
p-values	ξ_1	0	0.5906	0.7189
	ξ_2	0.5906	0	0.9618
	ξ_3	0.7189	0.9618	0

Table 3.20: Correlations of the inferred structural financial uncertainty and monetary policy uncertainty shocks of the constant and time-varying structural MGARCH model under the Givens approach using the MPS as second proxy. The asset system consists of demeaned daily log returns of the Finex U.S. Index, the S&P Global Clean Energy Index and the Bloomberg Commodity Index over the period from 22/02/2007 to 30/09/2020. The inferred structural shocks are a financial uncertainty shock (ξ_1) and a monetary policy shock (ξ_2).

		constant proxy-MGARCH model		
$\hat{\hat{R}}$		0.4641	0.8856	−0.0157
		0.8362	−0.4323	0.3374
		0.2921	−0.1698	−0.9412
		ξ_1	ξ_2	ξ_3
correlations	Z_1	0.0251	0.0088	0.0000
	Z_2	0.0566	0.1615	0.0000
$\hat{\hat{R}}$		0.3182	0.9480	−0.0106
		−0.9021	0.2993	0.3108
		−0.2915	0.1085	0.9504
		ξ_1	ξ_2	ξ_3
correlations	Z_1	0.4888	0.2197	0.0000
	Z_2	−0.0111	0.0240	0.0000

Table 3.21: Estimation results of the constant structural MGARCH model under the Procrustes approach using the EPU as first proxy variable (first two paragraphs) respectively as second proxy variable (third and fourth paragraph).

		constant proxy-MGARCH model		
$\hat{\hat{R}}$		-0.1325	0.9831	-0.1265
		0.8348	0.0419	-0.5489
		-0.5343	-0.1784	-0.8263
		ξ_1	ξ_2	ξ_3
correlations	Z_1	0.0433	-0.0090	0.0000
	Z_2	-0.0358	0.1666	0.0000
$\hat{\hat{R}}$		-0.2452	-0.4279	0.8699
		-0.8031	0.5923	0.0649
		-0.5430	-0.6828	-0.4888
		ξ_1	ξ_2	ξ_3
correlations	Z_1	0.5096	-0.1629	0.0000
	Z_2	-0.0133	0.0420	0.0000

Table 3.22: Estimation results of the constant structural MGARCH model under the Procrustes approach using the GPR as first proxy variable (first two paragraphs) respectively as second proxy variable (third and fourth paragraph).

		constant proxy-MGARCH model		
$\hat{\hat{R}}$		-0.0075	0.9892	0.1464
		0.5129	-0.1319	0.8483
		0.8584	-0.0638	0.5089
		ξ_1	ξ_2	ξ_3
correlations	Z_1	0.0440	-0.0028	0.0000
	Z_2	-0.0112	0.1700	0.0000

Table 3.23: Estimation results of the constant structural MGARCH model under the Procrustes approach using variations in Gold prices as first proxy variable.

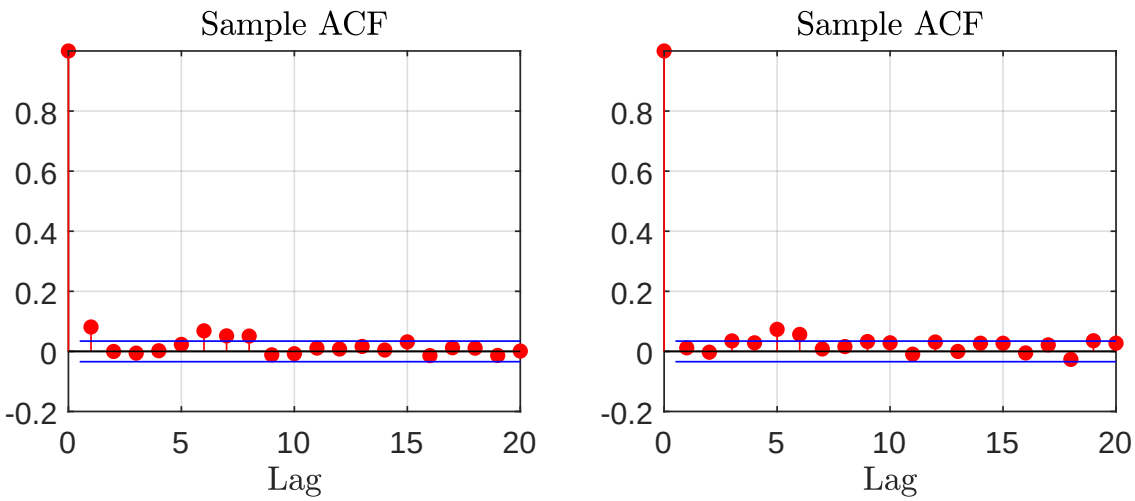

Figure 3.13: Autocorrelation of $\hat{u}_{1t}Z_{1t}$ (left) and $\hat{u}_{2t}Z_{2t}$ (right).

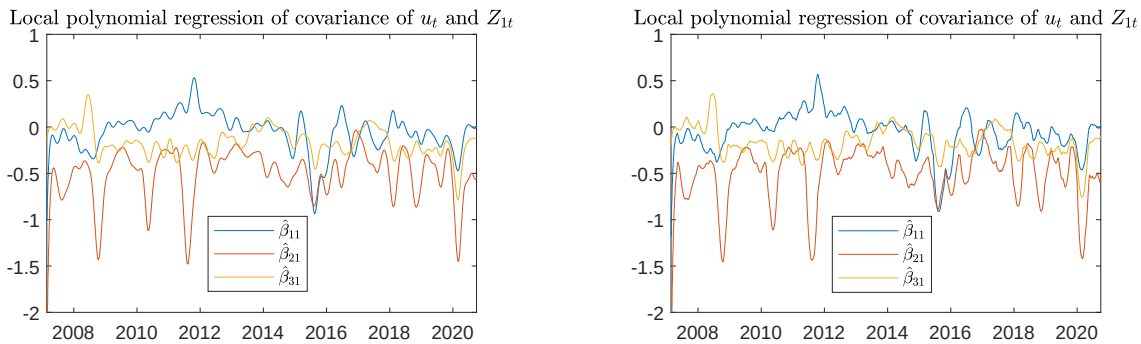

Figure 3.14: Nonparametric estimators of $\hat{\psi}$ for the Gaussian (left) and the Epanechnikov (right) kernel.

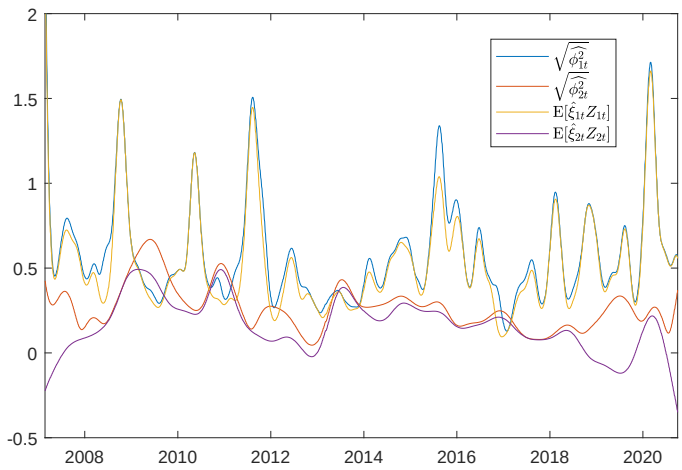

Figure 3.15: Time series of relevance parameters using (3.19) and a two-step estimation procedure.

The plot shows the time series of the nonparametrically estimated relevance parameters using the estimator (3.19) (blue and red line) and using a two-step estimation procedure based on the static model (yellow and violet line) where the expectation of the structural shocks and the proxy variables is calculated using a sample mean estimator.

		constant proxy-MGARCH model		
$\hat{\hat{R}}$		-0.1027	0.9947	-0.0057
		-0.9451	-0.0958	-0.3125
		-0.3103	-0.0375	0.9499
		ξ_1	ξ_2	ξ_3
correlations	Z_1	0.5257	-0.0013	0.0000
	Z_2	-0.0004	0.1494	0.0000

Table 3.24: Estimation results of the constant structural MGARCH model under the Procrustes approach using outlier cleaned proxy variables (clipping of variables at the 5% and the 95% quantile thresholds).

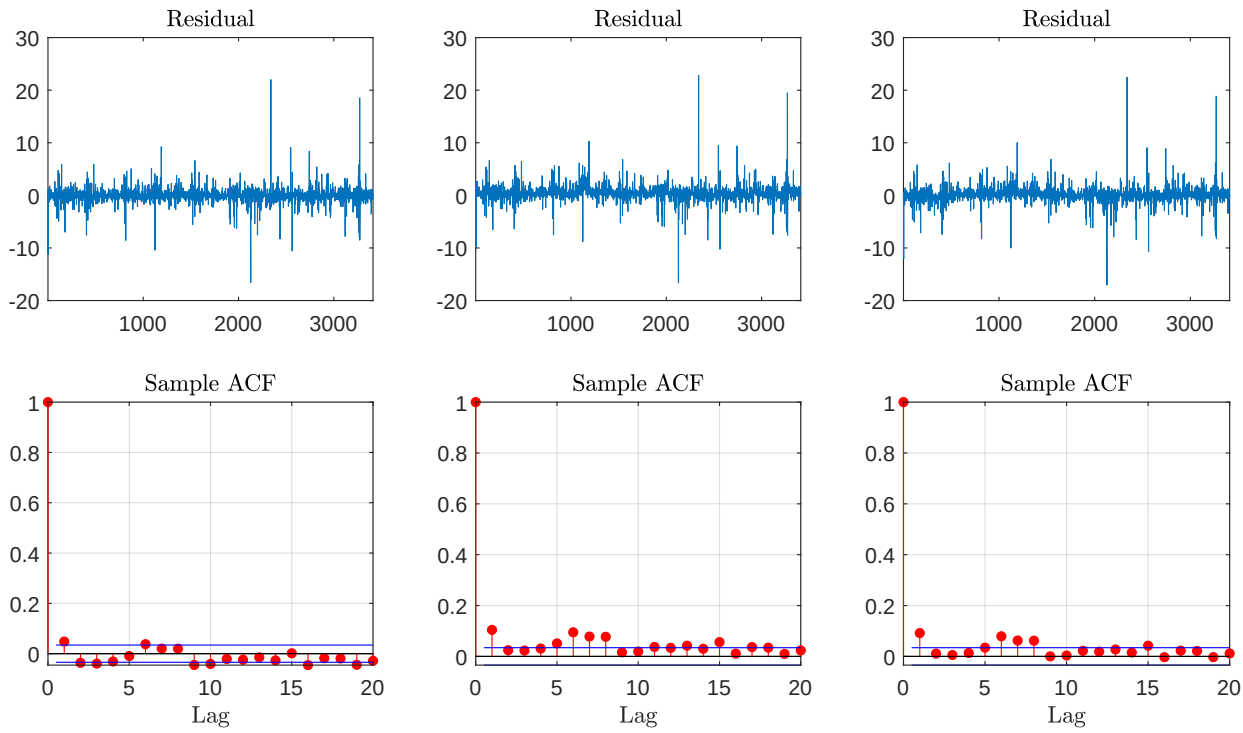

Figure 3.16: Residuals $\hat{\eta}_{1t}$ of the nonparametric estimation of the covariance of $\hat{u}_t$ and Z_{1t} in the order $\hat{\eta}_{11,t}$, $\hat{\eta}_{21,t}$ and $\hat{\eta}_{31,t}$, from left to right, and their sample ACFs.

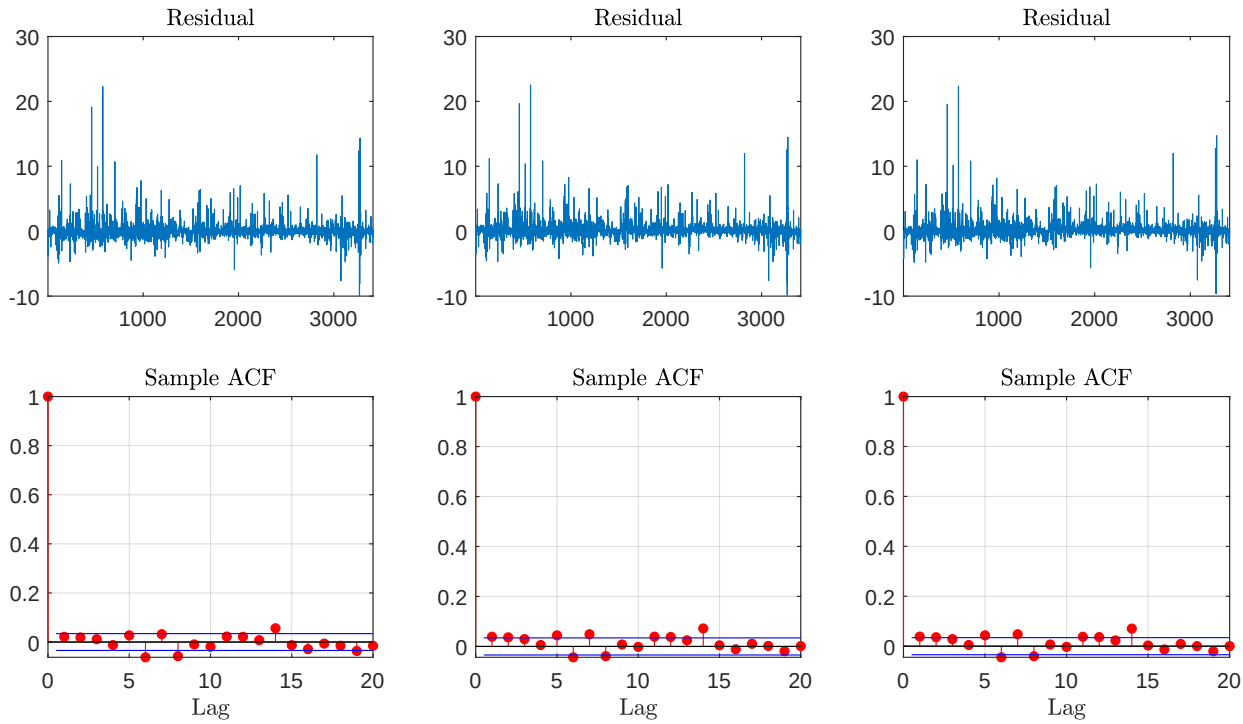

Figure 3.17: Residuals $\hat{\eta}_{2t}$ of the nonparametric estimation of the covariance of $\hat{u}_t$ and Z_{2t} in the order $\hat{\eta}_{21,t}$, $\hat{\eta}_{22,t}$ and $\hat{\eta}_{32,t}$, from left to right, and their sample ACFs.

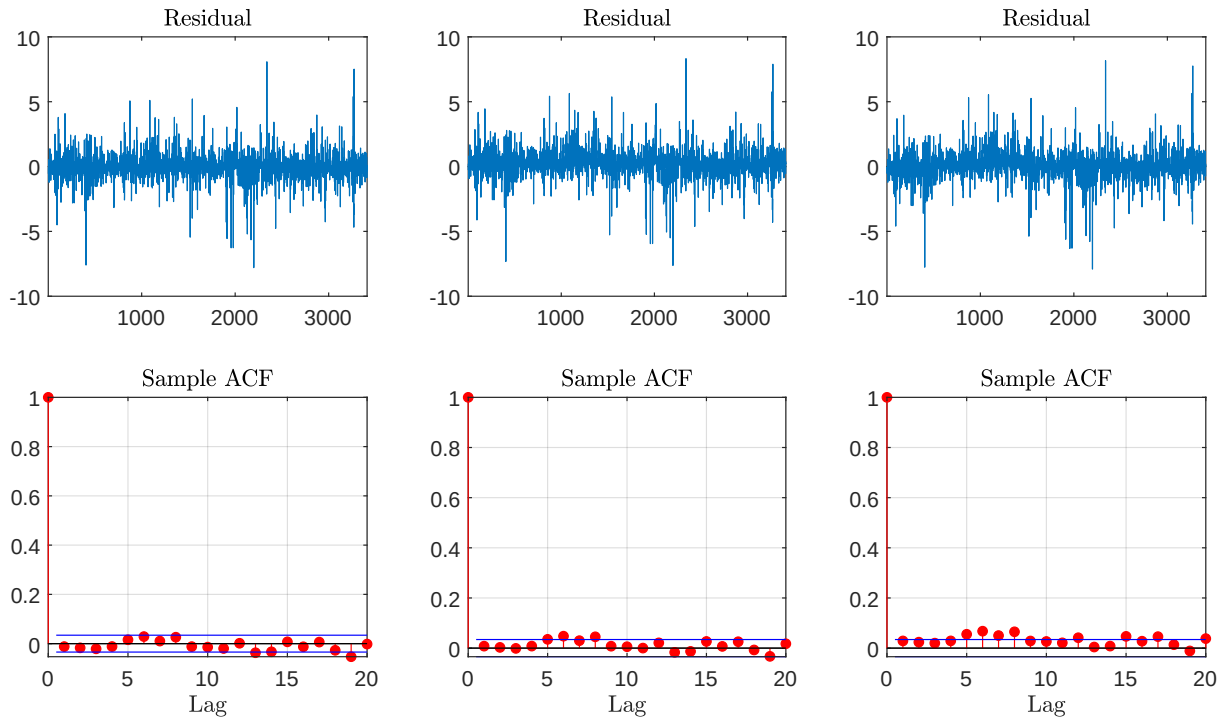

Figure 3.18: Residuals of the nonparametric estimation of the covariance of $\hat{u}_t$ and the clipped instrument Z_1 in the order $\hat{\eta}_1$, $\hat{\eta}_2$ and $\hat{\eta}_3$ from left to right, and their sample ACFs.

References

Aastveit, K. A., Natvik, G. J. and Sola, S. (2017). Economic uncertainty and the influence of monetary policy, *Journal of International Money and Finance* **76**: 50–67.

Akinci, O., Kalemli-Özcan, S. and Queralto, A. (2022). Uncertainty shocks, capital flows, and international risk spillovers, *NBER Working Paper 30026*, National Bureau of Economic Research.

Akram, Q. F. (2009). Commodity prices, interest rates and the dollar, *Energy Economics* **31**(6): 838–851.

Amisano, G. and Giannini, C. (2012). *Topics in Structural VAR Econometrics*, Springer Science & Business Media.

Andersen, T., Bollerslev, T. and Diebold, F. (2003). Micro effects of macro announcements: Real-time price discovery in foreign exchange, *American Economic Review* **93**: 38–62.

Andersen, T. G., Davis, R. A., Kreiß, J.-P. and Mikosch, T. V. (2009). *Handbook of Financial Time Series*, Springer Science & Business Media.

Angelini, G. and Fanelli, L. (2019). Exogenous uncertainty and the identification of structural vector autoregressions with external instruments, *Journal of Applied Econometrics* **34**(6): 951–971.

Anzuini, A., Lombardi, M. J. and Pagano, P. (2013). The impact of monetary policy shocks on commodity prices, *International Journal of Central Banking* **9**(3): 125–150.

Arias, J. E., Rubio-Ramírez, J. F. and Waggoner, D. F. (2021). Inference in Bayesian proxy-SVARs, *Journal of Econometrics* **225**(1): 88–106.

Arouri, M., Estay, C., Rault, C. and Roubaud, D. (2016). Economic policy uncertainty and stock markets: Long-run evidence from the US, *Finance Research Letters* **18**: 136–141.

Baker, S. R., Bloom, N. and Davis, S. J. (2016). Measuring economic policy uncertainty, *The Quarterly Journal of Economics* **131**(4): 1593–1636.

Basu, S. and Bundick, B. (2017). Uncertainty shocks in a model of effective demand, *Econometrica* **85**(3): 937–958.

Bauer, M. D., Lakdawala, A. and Mueller, P. (2021). Market-based monetary policy uncertainty, *The Economic Journal* **132**(644): 1290–1308.

Bauer, M. D. and Swanson, E. T. (2022). A reassessment of monetary policy surprises and high-frequency identification, *CESifo Working Paper Series 9642*, CESifo.

Bauwens, L., Hafner, C. and Laurent, S. (2012). *Handbook of Volatility Models and Their Applications*, John Wiley & Sons, Ltd.

Bauwens, L., Laurent, S. and Rombouts, J. V. K. (2006). Multivariate GARCH models: A survey, *Journal of Applied Econometrics* **21**(1): 79–109.

Bekaert, G., Engstrom, E. and Ermolov, A. (2020). The variance risk premium in equilibrium models, *NBER Working Paper 27108*, National Bureau of Economic Research.

Bekaert, G. and Hoerova, M. (2014). The VIX, the variance premium and stock market volatility, *Journal of Econometrics* **183**(2): 181–192.

Bekaert, G., Hoerova, M. and Duca, M. L. (2013). Risk, uncertainty and monetary policy, *Journal of Monetary Economics* **60**(7): 771–788.

Białkowski, J., Dang, H. D. and Wei, X. (2022). High policy uncertainty and low implied market volatility: An academic puzzle?, *Journal of Financial Economics* **143**(3): 1185–1208.

Bloom, N. (2009). The impact of uncertainty shocks, *Econometrica* **77**(3): 623–685.

Bloom, N. (2014). Fluctuations in uncertainty, *Journal of Economic Perspectives* **28**(2): 153–76.

Blot, C., Hubert, P. and Labondance, F. (2020). Uncertainty and monetary policy in the euro area, *Monetary dialogue papers*, Publications Office of the European Union.

Bollerslev, T., Li, J. and Xue, Y. (2018). Volume, volatility, and public news announcements, *The Review of Economic Studies* **85**(4): 2005–2041.

Bomfim, A. N. (2003). Pre-announcement effects, news effects, and volatility: Monetary policy and the stock market, *Journal of Banking and Finance* **27**(1): 133–151.

Bonam, D. and Konietschke, P. (2020). Tax multipliers across the business cycle, *De Nederlandsche Bank Working Paper 699*, De Nederlandsche Bank.

Boudoukh, J., Feldman, R., Kogan, S. and Richardson, M. (2018). Information, trading and volatility: Evidence from firm-specific news, *The Review of Financial Studies* **32**(3): 992–1033.

Boussama, F., Fuchs, F. and Stelzer, R. (2011). Stationarity and geometric ergodicity of BEKK multivariate GARCH models, *Stochastic Processes and their Applications* **121**(10): 2331–2360.

Boyd, J. H., Hu, J. and Jagannathan, R. (2005). The stock market's reaction to unemployment news: Why bad news is usually good for stocks, *Journal of Finance* **60**(2): 649–672.

Brüggemann, R., Jentsch, C. and Trenkler, C. (2014). Inference in VARs with conditional heteroskedasticity of unknown form. Working Paper 2014-13, Department of Economics, University of Konstanz.

Brüggemann, R., Jentsch, C. and Trenkler, C. (2016). Inference in VARs with conditional heteroskedasticity of unknown form, *Journal of Econometrics* **191**(1): 69–85.

Cai, Z. (2007). Trending time-varying coefficient time series models with serially correlated errors, *Journal of Econometrics* **136**(1): 163–188.

Caldara, D. and Iacoviello, M. (2022). Measuring geopolitical risk, *American Economic Review* **112**(4): 1194–1225.

Carriero, A., Mumtaz, H., Theodoridis, K. and Theophilopoulou, A. (2015). The impact of uncertainty shocks under measurement error: A proxy SVAR approach, *Journal of Money, Credit and Banking* **47**(6): 1223–1238.

Cavicchioli, M. (2019). Fourth moment structure of Markov switching multivariate GARCH models, *Journal of Financial Econometrics* **19**(4): 565–582.

Cenedese, G. and Mallucci, E. (2016). What moves international stock and bond markets?, *Journal of International Money and Finance* **60**(1): 94–113.

Chan, N. H., Gao, L. and Palma, W. (2022). Simultaneous variable selection and structural identification for time-varying coefficient models, *Journal of Time Series Analysis* **43**(4): 511–531.

Clark, P. K. (1973). A subordinated stochastic process model with finite variance for speculative prices, *Econometrica* **41**(1): 135–155.

Cox, D. R. (1958). *Planning of Experiments*, Wiley.

Dahlhaus, R. (1997). Fitting time series models to nonstationary processes, *The Annals of Statistics* **25**(1): 1–37.

Davidson, J. (1994). *Stochastic Limit Theory: An Introduction for Econometricians*, Oxford University Press.

De Marco, F. (2019). Bank lending and the European sovereign debt crisis, *Journal of Financial and Quantitative Analysis* **54**(1): 155–182.

Del Negro, M. and Primiceri, G. E. (2015). Time varying structural vector autoregressions and monetary policy: A corrigendum, *The Review of Economic Studies* **82**(4): 1342–1345.

Diebold, F. X. and Yilmaz, K. (2012). Better to give than to receive: Predictive directional measurement of volatility spillovers, *International Journal of Forecasting* **28**(1): 57–66.

Dornbusch, R. (1976). Expectations and exchange rate dynamics, *Journal of Political Economy* **84**(6): 1161–1176.

Ehrmann, M., Fratzscher, M. and Rigobon, R. (2011). Stocks, bonds, money markets and exchange rates: measuring international financial transmission, *Journal of Applied Econometrics* **26**(6): 948–974.

Elie, B., Naji, J., Dutta, A. and Uddin, G. S. (2019). Gold and crude oil as safe-haven assets for clean energy stock indices: Blended copulas approach, *Energy* **178**: 544–553.

Engle, R. F. and Campos-Martins, S. (2020). Measuring and hedging geopolitical risk, *NIPE Working Papers 08/2020*, NIPE - Universidade do Minho.

Engle, R. F. and Campos-Martins, S. (2023). What are the events that shake our world? Measuring and hedging global COVOL, *Journal of Financial Economics* **147**(1): 221–242.

Engle, R. F. and Ng, V. K. (1993). Measuring and testing the impact of news on volatility, *The Journal of Finance* **48**(5): 1749–1778.

Engle, R. and Kroner, K. F. (1995). Multivariate simultaneous generalized ARCH, *Econometric Theory* **11**(1): 122–150.

Epanechnikov, V. A. (1969). Non-parametric estimation of a multivariate probability density, *Theory of Probability & Its Applications* **14**(1): 153–158.

Fan, J. and Gijbels, I. (1996). *Local Polynomial Modelling and Its Applications: Monographs on Statistics and Applied Probability 66*, Chapman & Hall/CRC Monographs on Statistics & Applied Probability, Taylor & Francis.

Fan, J., Imerman, M. B. and Dai, W. (2016). What does the volatility risk premium say about liquidity provision and demand for hedging tail risk?, *Journal of Business & Economic Statistics* **34**(4): 519–535.

Fengler, M. and Herwartz, H. (2018). Measuring spotvariance spillovers when (co)variances are time-varying – the case of multivariate GARCH models, *Oxford Bulletin of Economics and Statistics* **80**(1): 135–159.

Fengler, M. R. and Polivka, J. (2022a). Identifying structural shocks to volatility through a proxy-MGARCH model, *Economics Working Paper Series 2103*, University of St. Gallen, School of Economics and Political Science.
URL: *https://ideas.repec.org/p/usg/econwp/202103.html*

Fengler, M. R. and Polivka, J. (2022b). Structural volatility impulse response analysis, *Economics Working Paper Series 2211*, University of St.Gallen, School of Economics and Political Science.
URL: *https://ideas.repec.org/p/usg/econwp/202211.html*

Fisher, L. and Huh, H. S. (2019). Combining sign and parametric restrictions in SVARs by utilising Givens rotations, *Studies in Nonlinear Dynamics and Econometrics* **24**(3): 1–19.

Francq, C. and Zakoïan, J. (2010). *GARCH Models: Structure, Statistical Inference and Financial Applications*, John Wiley & Sons Ltd.

Fratzscher, M. (2009). What explains global exchange rate movements during the financial crisis?, *Journal of International Money and Finance* **28**(8): 1390–1407.

Fratzscher, M., Lo Duca, M. and Straub, R. (2018). On the international spillovers of US quantitative easing, *The Economic Journal* **128**(608): 330–377.

Fry, R. and Pagan, A. (2011). Sign restrictions in structural vector autoregressions: A critical review, *Journal of Economic Literature* **49**(4): 938–960.

Gabaix, X. and Maggiori, M. (2015). International liquidity and exchange rate dynamics, *The Quarterly Journal of Economics* **130**(3): 1369–1420.

Gallant, A., Rossi, P. and Tauchen, G. (1993). Nonlinear dynamic structures, *Econometrica* **61**(4): 871–907.

Gertler, M. and Karadi, P. (2015). Monetary policy surprises, credit costs, and economic activity, *American Economic Journal: Macroeconomics* **7**(1): 44–76.

Giacomini, R., Kitagawa, T. and Read, M. (2021). Robust Bayesian inference in proxy SVARs, *Journal of Econometrics* **228**(1).

Givens, W. (1958). Computation of plain unitary rotations transforming a general matrix to triangular form, *SIAM Journal* **6**(1): 26–50.

Gower, J. C. and Dijksterhuis, G. B. (2004). *Procrustes problems*, Vol. 30, Oxford University Press.

Granger, C. W. J. (1969). Investigating causal relations by econometric models and cross-spectral methods, *Econometrica* **37**(3): 424–438.

Greenspan, A. (2004). Risk and uncertainty in monetary policy. Remarks by Chairman Alan Greenspan at the Meeting of the American Economic Association, San Diego, California.
URL: *https://www.federalreserve.gov/boarddocs/speeches/2004/20040103/default.htm*

Grobys, K. (2015). Are volatility spillovers between currency and equity market driven by economic states? Evidence from the US economy, *Economics Letters* **127**: 72–75.

Groß-Klußmann, A. and Hautsch, N. (2011). When machines read the news: Using automated text analytics to quantify high frequency news-implied market reactions, *Journal of Empirical Finance* **18**(2): 321–340.

Gürkaynak, R., Karasoy-Can, H. G. and Lee, S. S. (2022). Stock market's assessment of monetary policy transmission: The cash flow effect, *Journal of Finance* **77**(4): 2375–2421.

Gürkaynak, R. S., Sack, B. and Swanson, E. (2005). Do actions speak louder than words? The response of asset prices to monetary policy actions and statements, *International Journal of Central Banking* **1**(1): 55–93.

Hafner, C. and Herwartz, H. (2008). Analytical quasi maximum likelihood inference in multivariate volatility models, *Metrika: International Journal for Theoretical and Applied Statistics* **67**(2): 219–239.

Hafner, C. M. and Herwartz, H. (2006). Volatility impulse responses for multivariate GARCH models: An exchange rate illustration, *Journal of International Money and Finance* **25**(5): 719–740.

Hafner, C. M. and Herwartz, H. (2022). Dynamic score-driven independent component analysis, *Journal of Business & Economic Statistics* (forthcoming): 1–11.
URL: *https://www.tandfonline.com/doi/abs/10.1080/07350015.2021.2013244?journalCode=ubes20*

Hafner, C. M., Herwartz, H. and Maxand, S. (2022). Identification of structural multivariate GARCH models, *Journal of Econometrics* **227**(1): 212–227. Annals Issue: Time Series Analysis of Higher Moments and Distributions of Financial Data.

Hafner, C. and Preminger, A. (2009). On asymptotic theory for multivariate GARCH models, *Journal of Multivariate Analysis* **100**(9): 2044–2054.

Hemingway, E. G. and O'Reilly, O. M. (2018). Perspectives on Euler angle singularities, Gimbal lock, and the orthogonality of applied forces and applied moments, *Multibody System Dynamics* **44**: 31–56.

Herrndorf, N. (1984). A functional central limit theorem for weakly dependent sequences of random variables, *Annals of Probability* **12**(1): 141–153.

Herwartz, H. and Lütkepohl, H. (2014). Structural vector autoregressions with Markov switching: Combining conventional with statistical identification of shocks, *Journal of Econometrics* **183**(1): 104–116.

Hoffman, D. K., Raffenetti, R. C. and Ruedenberg, K. (1972). Generalization of Euler angles to n-dimensional orthogonal matrices, *Journal of Mathematical Physics* **13**(4): 528–533.

Hofmann, B., Mehrotra, A. and Sandri, D. (2022). Global exchange rate adjustments: drivers, impacts and policy implications, *BIS Bulletin 62*, Bank for International Settlements.

Hofmann, B., Shim, I. and Shin, H. S. (2020). Bond risk premia and the exchange rate, *Journal of Money, Credit and Banking* **52**(S2): 497–520.

Holló, D., Kremer, M. and Duca, M. L. (2012). CISS - a composite indicator of systemic stress in the financial system, *ECB Working Paper 1426*, ECB.

Hood, M. and Malik, F. (2013). Is gold the best hedge and a safe haven under changing stock market volatility?, *Review of Financial Economics* **22**(2): 47–52.

Horn, R. A. and Johnson, C. R. (2012). *Matrix Analysis, 2nd Edition*, Cambridge University Press.

Houari, O. (2022). Uncertainty shocks and business cycles in the US: New insights from the last three decades, *Economic Modelling* **109**: 105762.

Husted, L., Rogers, J. and Sun, B. (2020). Monetary policy uncertainty, *Journal of Monetary Economics* **115**: 20–36.

Ilzetzki, E., Reinhart, C. M. and Rogoff, K. S. (2020). Will the secular decline in exchange rate and inflation volatility survive COVID-19?, *Brookings Papers on Economic Activity* pp. 279–316.

Inoue, A. and Kilian, L. (2013). Inference on impulse response functions in structural VAR models, *Journal of Econometrics* **177**(1): 1–13.

Inoue, A. and Rossi, B. (2019). The effects of conventional and unconventional monetary policy on exchange rates, *Journal of International Economics* **118**(C): 419–447.

Jentsch, C. and Lunsford, K. G. (2022). Asymptotically valid bootstrap inference for proxy SVARs, *Journal of Business & Economic Statistics* **40**(4): 1876–1891.

Jeon, Y., McCurdy, T. H. and Zhao, X. (2021). News as sources of jumps in stock returns: Evidence from 21 million news articles for 9000 companies, *Journal of Financial Economics* **145**(2): 1–17.

Ji, Q., Liu, B.-Y., Nehler, H. and Uddin, G. S. (2018). Uncertainties and extreme risk spillover in the energy markets: A time-varying copula-based CoVaR approach, *Energy Economics* **76**: 115–126.

Jin, X., Lin, S. X. and Tamvakis, M. (2012). Volatility transmission and volatility impulse response functions in crude oil markets, *Energy Economics* **34**(6): 2125–2134.

Jones, C. M., Lamont, O. and Lumsdaine, R. L. (1998). Macroeconomic news and bond market volatility, *Journal of Financial Economics* **47**(3): 315–337.

Joyce, M., Miles, D., Scott, A. and Vayanos, D. (2012). Quantitative easing and unconventional monetary policy – an introduction, *The Economic Journal* **122**(564): 271–288.

Kilian, L. (2013). Structural vector autoregressions, *Handbook of research methods and applications in empirical macroeconomics*, Edward Elgar Publishing.

Kilian, L. and Lütkepohl, H. (2017). *Identification by Sign Restrictions*, Themes in Modern Econometrics, Cambridge University Press, pp. 421–490.

Kilian, L. and Zhou, X. (2022). Oil prices, exchange rates and interest rates, *Journal of International Money and Finance* **126**((forthcoming)).

Koop, G., Leon-Gonzalez, R. and Strachan, R. (2009). On the evolution of the monetary policy transmission mechanism, *Journal of Economic Dynamics and Control* **33**(4): 997–1017.

Koop, G., Pesaran, M. H. and Potter, S. M. (1996). Impulse response analysis in nonlinear multivariate models, *Journal of Econometrics* **74**(1): 119–147.

Kremer, M., Lo Duca, M. and Holló, D. (2012). CISS - a composite indicator of systemic stress in the financial system, *Working Paper Series 1426*, European Central Bank.
URL: *https://ideas.repec.org/p/ecb/ecbwps/20121426.html*

Kuzemko, C., Bradshaw, M., Bridge, G., Goldthau, A., Jewell, J., Overland, I., Scholten, D., Van de Graaf, T. and Westphal, K. (2020). COVID-19 and the politics of sustainable energy transitions, *Energy Research & Social Science* **68**.

Lanne, M., Lütkepohl, H. and Maciejowska, K. (2010). Structural vector autoregressions with Markov switching, *Journal of Economic Dynamics and Control* **34**(2): 121–131.

Lechner, M. (2010). The relation of different concepts of causality used in time series and microeconometrics, *Econometric Reviews* **30**(1): 109–127.

Leung, D. H.-Y. (2005). Cross-validation in nonparametric regression with outliers, *The Annals of Statistics* **33**(5): 2291–2310.

Lin, W.-L. (1997). Impulse response function for conditional volatility in GARCH models, *Journal of Business & Economic Statistics* **15**(1): 15–25.

Liu, X. (2018). Structural volatility impulse response function and asymptotic inference, *Journal of Financial Econometrics* **16**(2): 316–339.

Luati, A. and Proietti, T. (2010). Hyper-spherical and elliptical stochastic cycles, *Journal of Time Series Analysis* **31**(3): 169–181.

Ludvigson, S. C., Ma, S. and Ng, S. (2021). Uncertainty and business cycles: Exogenous impulse or endogenous response?, *American Economic Journal: Macroeconomics* **13**(4): 369–410.

Lunsford, K. G. (2015). Identifying structural VARs with a proxy variable and a test for a weak proxy, *Working Paper No. 15-28*, Federal Reserve Bank of Cleveland.
URL: *https://doi.org/10.26509/frbc-wp-201528*

Lütkepohl, H. (2010). Impulse response function, *Macroeconometrics and time series analysis*, Springer, pp. 145–150.

Lütkepohl, H. (2005). *New Introduction to Multiple Time Series Analysis*, Springer.

Lütkepohl, H. and Schlaak, T. (2021). Heteroscedastic proxy vector autoregressions, *Journal of Business & Economic Statistics* **40**(3): 1–14.

Lütkepohl, H. and Schlaak, T. (2022). Heteroscedastic proxy vector autoregressions, *Journal of Business & Economic Statistics* **40**(3): 1268–1281.

Lütkepohl, H., Staszewska-Bystrova, A. and Winker, P. (2015). Confidence bands for impulse responses: Bonferroni vs. Wald, *Oxford Bulletin of Economics and Statistics* **77**(6): 800–821.

Magnus, J. R. and Neudecker, H. (1988). *Matrix Differential Calculus with Applications in Statistics and Econometrics*, John Wiley & Sons Ltd.

Marfatia, H. A., Gupta, R. and Miller, S. (2020). 125 years of time-varying effects of fiscal policy on financial markets, *International Review of Economics & Finance* **70**: 303–320.

Mertens, K. and Olea, J. L. M. (2013). Marginal tax rates and income: New time series evidence, *Working Paper 19171*, National Bureau of Economic Research.

Mertens, K. and Ravn, M. O. (2013). The dynamic effects of personal and corporate income tax changes in the United States, *American Economic Review* **103**(4): 1212–1247.

Miranda-Agrippino, S. and Rey, H. (2020). U.S. monetary policy and the global financial cycle, *The Review of Economic Studies* **87**(6): 2754–2776.

Miranda-Agrippino, S. and Ricco, G. (2019). Identification with external instruments in structural VARs under partial invertibility, *CEPR Discussion Papers 13853*, CEPR.

Miranda-Agrippino, S. and Ricco, G. (2021). The transmission of monetary policy shocks, *American Economic Journal: Macroeconomics* **13**(3): 74–107.

Mody, A. and Nedeljkovic, M. (2018). Central bank policies and financial markets: Lessons from the Euro crisis, *CESifo Working Paper Series 7400*, CESifo.

Mueller, P., Tahbaz-Salehi, A. and Vedolin, A. (2017). Exchange rates and monetary policy uncertainty, *Journal of Finance* **72**(3): 1213–1252.

Mumtaz, H. and Petrova, K. (2022). Changing impact of shocks: A time-varying proxy SVAR approach, *Journal of Money, Credit and Banking* (forthcoming).

Mumtaz, H. and Theodoridis, K. (2020). Fiscal policy shocks and stock prices in the United States, *European Economic Review* **129**: 1–25.

Neely, C. J. (2015). Unconventional monetary policy had large international effects, *Journal of Banking & Finance* **52**: 101–111.

Olson, E., Vivian, A. J. and Wohar, M. E. (2014). The relationship between energy and equity markets: Evidence from volatility impulse response functions, *Energy Economics* **43**: 297–305.

Piffer, M. and Podstawski, M. (2017). Identifying uncertainty shocks using the price of gold, *The Economic Journal* **128**(616): 3266–3284.

Primiceri, G. (2005). Time varying structural vector autoregressions and monetary policy, *The Review of Economic Studies* **72**(3): 821–852.

Rambachan, A. and Shephard, N. (2020). Econometric analysis of potential outcomes time series: instruments, shocks, linearity and the causal response function. arXiv:1903.01637.
URL: *https://ideas.repec.org/p/arx/papers/1903.01637.html*

Rambachan, A. and Shephard, N. (2021). When do common time series estimands have nonparametric causal meaning? Working Paper.
URL: *https://scholar.harvard.edu/shephard/publications/nonparametric-dynamic-causal-model-macroeconometrics*

Rigobon, R. (2003). Identification through heteroskedasticity, *Review of Economics and Statistics* **85**(4): 777–792.

Rigobon, R. and Sack, B. (2003). Measuring the reaction of monetary policy to the stock market, *The Quarterly Journal of Economics* **118**(2): 639–669.

Robinson, P. M. (1989). *Nonparametric Estimation of Time-Varying Parameters*, Springer Berlin Heidelberg, pp. 253–264.

Rogers, J. H., Scotti, C. and Wright, J. H. (2018). Unconventional monetary policy and international risk premia, *Journal of Money, Credit and Banking* **50**(8): 1827–1850.

Romer, C. D. and Romer, D. H. (2004). A new measure of monetary shocks: Derivation and implications, *American Economic Review* **94**(4): 1055–1084.

Romer, C. D. and Romer, D. H. (2010). The macroeconomic effects of tax changes: Estimates based on a new measure of fiscal shocks, *American Economic Review* **100**(3): 763–801.

Rosa, C. (2013). The financial market effect of FOMC minutes, *Economic Policy Review* (December Issue, Federal Reserve Bank of New York): pp. 67–81.

Rubin, D. B. (1980). Randomization analysis of experimental data: The Fisher randomization test, *Journal of the American Statistical Association* **75**(371): 591–593.

Schönemann, P. H. (1966). A generalized solution of the orthogonal Procrustes problem, *Psychometrika* **31**: 1–10.

Scotti, C. (2016). Surprise and uncertainty indexes: Real-time aggregation of real-activity macro-surprises, *Journal of Monetary Economics* **82**: 1–19.

Silvennoinen, A. and Teräsvirta, T. (2015). Modeling conditional correlations of asset returns: A smooth transition approach, *Econometric Reviews* **34**(1-2): 174–197.

Silvennoinen, A. and Teräsvirta, T. (2021). Consistency and asymptotic normality of maximum likelihood estimators of a multiplicative time-varying smooth transition correlation GARCH model, *Econometrics and Statistics* (in press).

Sims, C. A. (1972). Money, income, and causality, *American Economic Review* **62**(4): 540–552.

Sims, C. A. and Zha, T. (1999). Error bands for impulse responses, *Econometrica* **67**(5): 1113–1155.

Sims, C. A. and Zha, T. (2006). Were there regime switches in U.S. monetary policy?, *American Economic Review* **96**(1): 54–81.

Sornette, D., Cauwels, P. and Smilyanov, G. (2018). Can we use volatility to diagnose financial bubbles? Lessons from 40 historical bubbles, *Quantitative Finance and Economics* **2**(1): 486–590.

Stock, J. H. and Watson, M. (2012). Disentangling the channels of the 2007-09 recession, *Brookings Papers on Economic Activity* **43**(1): 81–156.

Stock, J. H. and Watson, M. (2016). Dynamic factor models, factor-augmented vector autoregressions, and structural vector autoregressions in macroeconomics, *Handbook of Macroeconomics*, Vol. 2, Elsevier, chapter 8, pp. 415–525.

Stock, J. H. and Watson, M. W. (2018). Identification and estimation of dynamic causal effects in macroeconomics using external instruments, *The Economic Journal* **128**(610): 917–948.

Taylor, J. B. (2009). The financial crisis and the policy responses: An empirical analysis of what went wrong, *Working Paper 14631*, National Bureau of Economic Research.

Taylor, J. B. and Uhlig, H. (eds) (2016). *Handbook of Macroeconomics*, Vol. 2, Elsevier.

Vogt, M. (2012). Nonparametric regression for locally stationary time series, *The Annals of Statistics* **40**(5): 2601–2633.

Wang, Y., Bouri, E., Fareed, Z. and Dai, Y. (2022). Geopolitical risk and the systemic risk in the commodity markets under the war in Ukraine, *Finance Research Letters* **49**: 1–20.

Weber, E. (2010). Structural conditional correlation, *Journal of Financial Econometrics* **8**(3): 392–407.

Xia, Y. and Li, W. (2002). Asymptotic behavior of bandwidth selected by the cross-validation method for local polynomial fitting, *Journal of Multivariate Analysis* **83**(2): 265–287.

Zhang, T. and Wu, W. B. (2012). Inference of time-varying regression models, *The Annals of Statistics* **40**(3): 1376–1402.

Zhang, T. and Wu, W. B. (2015). Time-varying nonlinear regression models: nonparametric estimation and model selection, *The Annals of Statistics* **43**(2): 741–768.

Zhou, Z. and Wu, W. B. (2009). Local linear quantile estimation for nonstationary time series, *The Annals of Statistics* **37**(5B): 2696–2729.

Zhou, Z. and Wu, W. B. (2010). Simultaneous inference of linear models with time varying coefficients, *Journal of the Royal Statistical Society. Series B (Statistical Methodology)* **72**(4): 513–531.